# High Resolution Terahertz Spectroscopy on Small Molecules of Astrophysical Importance

Inaugural-Dissertation
zur
Erlangung des Doktorgrades
der Mathematisch-Naturwissenschaftlichen Fakultät
der Universität zu Köln

vorgelegt von

Sandra Brünken
aus Sevelen

Köln 2005

Cover Illustration:

False color image of ionisation fronts in a DC glow discharge.

Berichterstatter: Privatdozent Dr. T. Giesen
Prof. Dr. J. Jolie
Prof. Dr. P. Jensen

Tag der mündlichen Prüfung: 25. Mai 2005

*“We are all made of stars”*

Richard Melville Hall / Moby

# Abstract

In this work the results of rotational spectroscopic investigations of selected molecular species with both astrophysical and purely spectroscopical importance are presented.

The rotational spectra of the deuterium cyanide isotopomers DCN, D$^{13}$CN, DC$^{15}$N, and D$^{13}$C$^{15}$N were recorded in the vibrational ground and first excited bending state ($v_2 = 1$) up to 2 THz. $R$-branch transitions up to 1 THz were measured with sub-Doppler resolution. These very high resolution saturation dip measurements allowed for resolving the underlying hyperfine structure due to the nuclear spin of $^{14}$N in DCN and D$^{13}$CN. Accuracies of about 3 kHz were achieved for sub-Doppler measurements of isolated lines. Additionally, high $J$ $R$-branch transitions around 2 THz and direct $l$-type transitions ($\Delta J = 0$) between 66 and 118 GHz were recorded in Doppler-limited resolution. These new experimental data, together with available infrared rovibrational data, were subjected to a global least squares analysis for each isotopomer. This yielded precise sets of molecular constants for the ground and first excited vibrational states, including the nuclear quadrupole and magnetic spin-rotation coupling constants of the $^{14}$N nucleus for DCN and D$^{13}$CN.
Two astrophysically important rotational transitions between energetically low lying levels of methylene ($CH_2$) have been measured with high accuracy near 2 THz for the first time. For the *in-situ* synthesis of this unstable radical and the recording of its gas-phase rotational spectrum a new absorption cell has been designed and the technique of Zeeman modulation has been introduced to the Cologne laser sideband system. A non-standard Euler expansion of the effective Hamiltonian was employed for the analysis of a global dataset, yielding precise spectroscopic parameters with improved predictive capability for astrophysical important transitions.
More than 170 rotational transitions of the two water isotopomers HDO and $D_2O$ were measured up to high energies in the frequency range between $700 - 1000$ GHz and around 2 THz in the vibrational ground and first excited states. The global analysis of this data together with other available rotational and rovibrational transition frequencies by means of the Euler approach resulted in an improved spectroscopic parameter set on these molecules. The analysis provides highly accurate transition frequency predictions which are valuable both for atmospheric and astrophysical science.

# Kurzzusammenfassung

In dieser Arbeit werden die Ergebnisse von Untersuchungen der Rotationsspektren ausgewählter molekularer Spezies vorgestellt, welche von sowohl astrophysikalischem als auch rein spektroskopischem Interesse sind.

Die Rotationsspektren im Vibrationsgrundzustand und innerhalb der ersten angeregten Knickschwingung ($v_2 = 1$) der deuterierten Blausäure-Isotopomere DCN, D$^{13}$CN, DC$^{15}$N und D$^{13}$C$^{15}$N wurden im Frequenzbereich bis $2$ THz gemessen. $R$-Zweig - Übergänge unterhalb von $1$ THz wurden mit sub-Doppler-Auflösung aufgenommen. Mit dieser hochauflösenden Sättigungsspektroskopie konnte die durch den Kernspin des $^{14}$N hervorgerufene Hyperfeinstruktur im Fall von DCN und D$^{13}$CN spektral aufgelöst werden. Für isolierte Spektrallinien kann mit dieser Methode die Übergangsfrequenz auf bis zu $3$ kHz bestimmt werden. Zusätzlich wurden mit Doppler-begrenzter Auflösung $R$-Zweig Linien mit hoher Rotations-Quantenzahl $J$ im Bereich um $2$ THz aufgenommen, sowie einige direkte $\ell$-Typ Übergänge mit $\Delta J = 0$ im Frequenzbereich $66 - 118$ GHz. Die neugewonnenen Daten wurden zusammen mit zur Verfügung stehenden Infrarot-Daten der Vibrationsbande einer globalen Analyse unterzogen, die hochpräzise Molekülkonstanten für den Vibrationsgrundzustand und den ersten angeregten Knickzustand lieferte. Unter anderem konnten die Kernquadrupol-Wechselwirkungs- und die Kopplungskonstante der magnetischen Kernspin-Rotation-Wechselwirkung des $^{14}$N Kerns bestimmt werden.
Zum ersten Mal konnten zwei astrophysikalisch relevante Rotationsübergänge zwischen energetisch niedrig liegenden Niveaus von Methylen ($CH_2$) mit hoher Genauigkeit im Frequenzbereich um $2$ THz gemessen werden. Zur *in situ*-Erzeugung dieses höchst instabilen Radikals wurde eine neue Absorptionszelle entwickelt. Außerdem wurde die Methode der Zeeman-Modulation zum ersten Mal am Kölner Seitenband-Spektrometer angewandt. Zur Analyse der zur Verfügung stehenden Rotationsdaten wurde statt des standardmäßig angewandten Modells eine Euler-Entwicklung des Hamilton-Operators verwendet. Es konnten präzise spektroskopische Parameter ermittelt werden, die eine verbesserte Vorhersage von astrophysikalisch relevanten Labor-Übergangsfrequenzen erlauben.
Im Frequenzbereich zwischen $700 - 1000$ GHz und um $2$ THz wurden mehr als 170 energetisch hochliegende Rotationsübergänge im Grund- und angeregten Knickschwingungs-Zustand der Wasser-Isotopomere HDO und $D_2O$ gemessen. Deutlich verbesserte spektroskopische Parameter konnten für beide Moleküle durch den Euler-Ansatz, angewandt auf einen umfangreichen, globalen Datensatz reiner Rotations-, sowie Rotations-Schwingungsübergänge, gewonnen werden. Die auf diesem Parametersatz basierenden Frequenzvorhersagen liefern wertvolle Informationen sowohl für die Atmosphären- als auch die Astrophysik.

# Zusammenfassung

In naher Zukunft beginnt die Erschließung des Terahertz-Frequenzbereichs für die Astrophysik durch zum Beispiel das Stratosphären-Observatorium SOFIA[1] oder die Satelliten-Mission Herschel. Dadurch stellt sich für die Spektroskopie die Aufgabe, in diesem Frequenzbereich zuverlässige Rotations-Übergangsfrequenzen astrophysikalisch relevanter Moleküle zur Verfügung zu stellen. Dies geschieht einerseits durch direkte Labormessungen im Terahertz-Bereich und andererseits durch Extra- und Interpolation basierend auf geeigneten theoretischen Modellen.
Im Rahmen dieser Arbeit wurden Untersuchungen an einer Vielzahl von astrophysikalisch interessanten Molekülen durchgeführt, von denen drei in dieser Dissertation näher beschrieben werden.
Die Messungen wurden hauptsächlich am Kölner Terahertz Spektrometer, basierend auf phasenstabilisierten Rückwärtswellengeneratoren[2], und am Kölner Laser-Seitenband-Spektrometer[3] durchgeführt, die Frequenzbereiche zwischen $130 - 1000$, beziehungsweise $1750 - 2010$ GHz abdecken. Es zeigte sich, daß zur Analyse der Rotationsspektren im Fall von leichten, quasilinearen Molekülen wie z.B. Wasser-Isotopomeren oder des Methylen, das standardmäßig verwendete Modell eines effektiven Hamilton-Operators als Potenzreihe der Drehimpulsoperatoren nicht angewandt werden kann. Stattdessen wurde ein neuartiger, von H. Pickett [1] vorgeschlagener Ansatz einer Euler-Entwicklung des Hamilton-Operators verwendet.

Die Ergebnisse der einzelnen Teilprojekte können folgendermaßen zusammengefaßt werden.

Die Rotationsspektren von vier Isotopomeren deuterierter Blausäure, DCN, D$^{13}$CN, DC$^{15}$N und D$^{13}$C$^{15}$N, wurden im Frequenzbereich zwischen 66-2000 GHz sowohl im Schwingungs-Grundzustand als auch im ersten angeregten Zustand der Knickschwingung ($v_2 = 1$) gemessen. Für $R$-Zweig Übergänge von $J = 3 \leftarrow 2$ bis $J = 13 \leftarrow 12$, entsprechend dem Frequenzbereich unterhalb $1$ THz, wurde höchstauflösende Sättigungsspektroskopie durchgeführt. Die resultierenden Linienbreiten liegen mit ca. $70$ kHz deutlich unterhalb der thermischen Dopplerbreite, so daß mit dieser Technik die vom Kernspin des $^{14}$N-Kerns verursachte Hyperfein-Struktur in DCN und D$^{13}$CN für Übergänge bis $J = 10 \leftarrow 9$ aufgelöst werden konnte. Die Frequenzgenauigkeit dieser Methode liegt bei etwa 3 kHz für isolierte Linien. Zusätzlich wurden $R$-Zweig Linien mit hohen Rotations-Quantenzahlen ($J = 25 \leftarrow 24$ bis $J = 28 \leftarrow 27$) im Bereich um $2$ THz, sowie direkte $\ell$-Typ Übergänge mit $\Delta J = 0$ ($v_2 = 1$, $J = 19$ bis $25$) im niederfrequenten Bereich zwischen $66$ und $118$ GHz in Doppler-limitierter Auflösung gemessen, um die

[1] Stratospheric Observatory for Infrared Astronomy
[2] BWOs - Backward Wave Oscillators
[3] COSSTA - Cologne Sideband Spectrometer for Terahertz Applications

Bestimmung der Molekülparameter höherer Ordnung zu verbessern. Die neu gewonnenen Daten wurden zusammen mit zur Verfügung stehenden Rotations-Schwingungs-Daten der Knickschwingungs-Bande analysiert und es konnte in allen Fällen ein deutlich verbesserter Molekül-Parametersatz gewonnen werden. Unter anderem konnten die Parameter der Kernspin-Wechselwirkung mit hoher Präzision bestimmt werden. Basierend auf dem vorliegenden Datensatz können Übergangsfrequenzen im gesamten Frequenzbereich bis zu 2.5 THz höchstpräzise inter- und extrapoliert werden. Diese Daten stehen zur Analyse von astrophysikalischen Beobachtungen im Ferninfrarot-Bereich zur Verfügung.

Die energetisch niedrigsten Rotationsübergänge des Methylen-Radikals $CH_2$ liegen vornehmlich im Terahertz-Bereich. Diese Übergänge sind von besonderer Bedeutung für die Beobachtung von $CH_2$ im kalten interstellaren Medium. Im Rahmen dieser Arbeit konnten erstmals zwei energetisch tiefliegende Übergänge von Methylen im elektronischen und Vibrations-Grundzustand mit hoher Präzision im Bereich um 2 THz gemessen werden. Ein Übergang, das $N_{KaKc} = 2_{11} \leftarrow 2_{02}$ Multiplett, gehört zu ortho-$CH_2$ und liegt bei $1.954$ THz, während der andere, das $N_{KaKc} = 1_{10} \leftarrow 1_{01}$ Multiplett, zu para-$CH_2$ gehört und bei $1.915$ THz liegt. Methylen zeigt im elektronischen Grundzustand $^3B_1$ sowohl Fein-, als auch, im Falle von ortho-$CH_2$, Hyperfein-Wechselwirkungen, was zu den beobachteten Aufspaltungen der reinen Rotationsübergänge in Multipletts führt, von denen insgesamt 29 Komponenten gemessen werden konnten. Zur *in situ* Erzeugung des extrem instabilen Radikals wurde eine spezielle Absorptionszelle konstruiert, bestehend aus einer Pyrolyse-Einheit, einer Gleichspannungs-Entladung und einem Kühlkreislauf mit flüssigem Stickstoff. Methylen besitzt ein permanentes magnetisches Moment, so daß zu seiner Detektion eine Zeeman-Modulation am Laser-Seitenband-Spektrometer integriert wurde.
Die neuen Messungen erweitern den sehr spärlichen Datensatz dieses Moleküls erheblich. Um die Vorhersage weiterer, bisher noch nicht gemessener, Übergänge zu ermöglichen, wurde ein globaler Datensatz erstellt und mit Hilfe des Euler-Ansatzes analysiert. Die dadurch gewonnenen spektroskopischen Parameter ermöglichen eine deutlich verbesserte Vorhersage von vor allem für die Astrophysik relevanten niederenergetischen Rotationsübergängen des Methylen. Basierend auf diesen Vorhersagen konnte $CH_2$ in kalten Molekülwolken in der Sichtlinie in Richtung des galaktischen Zentrums detektiert werden. Desweiteren konnte gezeigt werden, daß die hier erstmals für die Analyse von $CH_2$ verwendete Euler-Entwicklung des Hamilton-Operators sehr viel besser geeignet ist, Moleküle mit großen Zentrifugalverzerrungs-Wechselwirkungen theoretisch zu beschreiben, als der Standard-Ansatz des Watson Hamilton-Operators.

Im verschiedenen Frequenzbändern zwischen $5$ GHz und $2$ THz wurden mehr als $170$ energetisch hochliegende Rotationsübergänge der Wasser-Isotopomere HDO und $D_2O$ im Grund- und angeregten Knickschwingungs-Zustand gemessen. Hierzu wurde neben dem Kölner Terahertz Spektrometer und dem Laser-Seitenband System auch ein Fourier-Transform Mikrowellen-Spektrometer in der Gruppe von Prof. H. Mäder an der Universität Kiel verwendet. Speziell im Fall des einfach deuterierten Wassermoleküls HDO fehlten hochpräzise Rotationsdaten zu höheren Energieniveaus und im ersten angeregten Knickschwingungs-Zustand. Im Grundzustand konnten Übergänge mit Rotationsquantenzahlen bis $J = 14$ und $K_a = 8$, im ersten angeregten Schwingungs-Zustand bis

$J = 11$ und $K_a = 5$ gemessen werden. Die Energie des absorbierenden Niveaus liegt in diesem Fall bei $\sim 2700$ cm$^{-1}$. Für $D_2O$ gehörten die höchsten Zustände zu $J = 16$, $K_a = 10$, beziehungsweise $J = 15$, $K_a = 7$. Dieser Datensatz wurde kombiniert mit neuen Daten der Spektroskopie-Gruppe des Jet Propulsion Laboratory (JPL, Pasadena, USA), sowie mit allen anderen zur Verfügung stehenden reinen Rotations-, sowie Rotations-Schwingungsübergängen. Eine Analyse dieses umfangreichen, globalen Datensatzes mit dem Euler-Ansatz lieferte deutlich verbesserte spektroskopische Parameter für beide Moleküle. Die auf diesem Parametersatz basierenden Frequenzvorhersagen liefern wertvolle Informationen sowohl für die Atmosphären- als auch die Astrophysik. Im Fall von HDO kann die erstellte Linienliste der Fundamentalbande der Knickschwingung $\nu_2$ als hochpräziser Sekundärstandard zur Kalibrierung von Infrarot-Daten dienen.

Frequenzvorhersagen aller vorgestellten Moleküle werden in der Kölner Datenbank für Molekülspektroskopie (CDMS - Cologne Database for Molecular Spectroscopy) zur Verfügung gestellt, wo sie kostenlos online unter *www.cdms.de* abrufbar sind.

# Contents

**Abstract** i

**Kurzzusammenfassung** ii

**Zusammenfassung** iii

**1 Introduction** 1

**2 Experimental Setup - Spectroscopy in the Terahertz Domain** 7

2.1 The Cologne Terahertz Spectrometer . . . . . 8

2.1.1 Sub-Doppler Spectroscopy . . . . . 11

2.1.2 Terahertz Radiation from Multiplier Sources . . . . . 13

2.2 COSSTA - Cologne Sideband Spectrometer for Terahertz Applications . . . . . 16

2.2.1 Zeeman Modulation . . . . . 21

2.3 Sub-Terahertz Spectrometers . . . . . 26

2.3.1 The AMC Spectrometer . . . . . 26

2.3.2 The Kiel FTMW Spectrometer . . . . . 27

**3 Theoretical Considerations** 31

3.1 Fitting Spectra and Calculating Transition Frequencies . . . . . 32

3.2 Linear Molecules - Hydrogen Cyanide Isotopomers . . . . . 33

3.2.1 Rovibrational Interactions for the First Excited Bending State 33

3.2.2 Hyperfine Structure . . . . . 34

3.3 Asymmetric Rotor Molecules - Water and Methylene . . . . . 37

3.3.1 The Pure Rotational Hamiltonian . . . . . 38
3.3.2 The Euler Approach . . . . . 40
3.3.3 Asymmetric Rotors with Electronic and Nuclear Spin - Methylene . . . . . 46
3.3.4 The Hyperfine Structure of Water . . . . . 48

**4 Deuterium Cyanide and its Isotopomers 51**
4.1 Previous Laboratory Work . . . . . 52
4.2 Experimental Setup . . . . . 53
4.3 Measurements . . . . . 53
4.4 Analysis . . . . . 62
4.5 Conclusions . . . . . 65

**5 The Methylene Radical - $CH_2$ 67**
5.1 Previous Work . . . . . 69
5.2 Measurement of Low $N$ Pure Rotational Transitions of $CH_2$ in the Terahertz Regime . . . . . 72
5.2.1 *In-situ* Production of Methylene . . . . . 72
5.2.2 Zeeman Modulated $CH_2$ - Exemplary Spectra . . . . . 74
5.3 Global Analysis of the Data . . . . . 77
5.3.1 Standard $A$-reduced Hamiltonian . . . . . 77
5.3.2 The Euler Approach . . . . . 80
5.4 Interstellar Detection of Cold $CH_2$ . . . . . 87
5.5 Conclusions . . . . . 93

**6 The Water Molecule: Measurements and Analysis of Terahertz Data 95**
6.1 $D_2O$ . . . . . 99
6.1.1 Previous Work . . . . . 100
6.1.2 New Dataset . . . . . 101
6.1.3 Analysis and Results . . . . . 104
6.2 HDO . . . . . 112
6.2.1 Previous Work . . . . . 113
6.2.2 New Dataset . . . . . 115

6.2.3 Analysis and Results . . . . . 119
6.2.4 HDO as a Secondary Frequency Standard for IR Measurements . . . . . 123
6.3 Conclusions . . . . . 127

**A Experimental Data - Deuterium Cyanide** **129**
A.1 DCN . . . . . 130
A.2 $D^{13}CN$ . . . . . 136
A.3 $DC^{15}N$ . . . . . 144
A.4 $D^{13}C^{15}N$ . . . . . 146

**B Experimental Data - Methylene** **149**

**C Experimental Data - Water** **159**
C.1 $D_2O$ . . . . . 159
C.2 HDO . . . . . 168

**Bibliography** **177**

# List of Figures


1.1 The electromagnetic spectrum. . . . . 2

1.2 The Cologne terahertz spectrometers. . . . . 3

2.1 Schematical Drawing of the Cologne Terahertz Spectrometer. . . . . 9

2.2 Principle of the backward wave oscillator (BWO). . . . . 10

2.3 Simulated Doppler and sub-Doppler spectrum. . . . . 12

2.4 The JPL 1.9 THz MoMeD tripler. . . . . 15

2.5 Principle of sideband generation. . . . . 16

2.6 Schematic Drawing of the Cologne Sideband Spectrometer for Terahertz Applications (COSSTA). . . . . 17

2.7 Block diagram of the FIR laser stabilisation realised at COSSTA. . . . . 18

2.8 Voltage response of the AFC unit. . . . . 19

2.9 Atmospheric transmission. . . . . 20

2.10 Principle of recording of Zeeman-modulated spectra. . . . . 24

2.11 Simulated Zeeman-spectrum of two closely neighboured lines. . . . . 25

2.12 Experimental relationship between applied voltage, coil current and resultant magnetic field measured in non-pulsed mode. . . . . 26

2.13 Response curve of the Zeeman coil. . . . . 27

2.14 Experimental Setup of the AMC spectrometer. . . . . 28

2.15 Pressure induced line-shift $\nu_p - \nu_{P_0}$ (relative to $p_0 = 0.07$ Pa) and broadening $\Delta\nu$ of a HDO line measured with the FTMW. . . . . 29

3.1 Energy level scheme of the asymmetric rotor molecule $H_2O$. . . . . 38

3.2 3D plots of the Euler transformation of the momentum operators. . . . . 42

3.3 Coupling scheme for $CH_2$ in Hund's case (b). . . . . 46

4.1 Energy level scheme of the $J = 4 \leftarrow 3$ rotational transition of DCN ($v_2$=0). 55
4.2 Calculated frequency shift of each DCN hyperfine transition. . . . . 55
4.3 The $J = 1 \leftarrow 0$ rotational transition of $D^{13}CN$ in the ground vibrational state. . . . . 57
4.4 The $J = 3 \leftarrow 2$ rotational transition of $D^{13}CN$ in the vibrational ground state. . . . . 58
4.5 The $J = 4 \leftarrow 3$ rotational transition of DCN in the first excited bending state (010). . . . . 58
4.6 The $J = 7 \leftarrow 6$ rotational transition of $D^{13}CN$ in the vibrational ground state. . . . . 59
4.7 The $J = 9 \leftarrow 8$ rotational transition of DCN in the vibrational ground state. 59
4.8 The $J = 13 \leftarrow 12$ rotational transition of DCN in the $v_2 = 1^e$ state. . . . 60
4.9 The $J = 8 \leftarrow 7$ rotational transition of $DC^{15}N$ in the $v_2 = 1^f$ state. . . . . 60
4.10 The $J = 11 \leftarrow 10$ rotational transition of the rare isotopomer $D^{13}C^{15}N$ in the $v_2 = 1^f$ state. . . . . 61
4.11 Exemplary spectrum recorded with COSSTA around 2 THz of the $J = 28 \leftarrow 27$ rotational transition of $D^{13}CN$ in the $v_2 = 1^f$ vibrational state. . 61
4.12 Exemplary spectrum of a direct $\ell$-type transition ($\Delta J = 0$, $J = 25$) of $D^{13}C^{15}N$. . . . . 62

5.1 Calculated energy level scheme of $CH_2$. . . . . 69
5.2 Potential energy curve of $CH_2$ and its geometry. . . . . 70
5.3 Energy level scheme of the para-$CH_2$ $N_{KaKc} = 1_{10} - 1_{01}$ multiplet measured with COSSTA. . . . . 73
5.4 Energy level scheme of the ortho-$CH_2$ $N_{KaKc} = 2_{11} - 2_{02}$ multiplet measured with COSSTA. . . . . 74
5.5 Experimental setup for the in-situ production of $CH_2$ at COSSTA. . . . . 75
5.6 Influence of the magnetic field strength on Zeeman-spectra. . . . . 76
5.7 Calculated stick spectrum of the measured para-$CH_2$ transitions. . . . . 76
5.8 Calculated stick spectrum of the measured ortho-$CH_2$ transitions. . . . . 77
5.9 Plot of the $K_a$ dependent terms in the $A$-reduced form of the Hamiltonian. 81
5.10 Fine structure components of the $N_{Ka,Kc} = 5_{0,5} - 4_{1,4}$ transition of $CH_2$. 84
5.11 Data and fit of $CH_2$ transitions towards SgrB2. . . . . 91

5.12 Data and fit of $CH_2$ transitions towards W 49 N. . . . . 92

6.1 Geometrical structure and vibrational modes of $D_2O$. . . . . 99

6.2 Two low frequency transitions of $D_2O$ measured with the Kiel FTMW spectrometer. . . . . 103

6.3 Exemplary spectra of a strong and a weak $D_2O$ transition measured both with COSSTA and the JPL tripler. . . . . 104

6.4 Energy levels of the $v_2 = 1$ and 2 states of $D_2O$. . . . . 106

6.5 Comparison of calculated energy levels of the $v_2 = 0$ and $v_2 = 1$ states of $D_2O$ with experimental levels. . . . . 109

6.6 Geometrical structure and vibrational modes of HDO. . . . . 112

6.7 Two high frequency transitions of HDO as measured with the JPL frequency multiplier chain in Cologne and by the JPL group. . . . . 116

6.8 Two rotational transitions of HDO measured with COSSTA in the 2 THz region. . . . . 117

6.9 A weak rotational transition of HDO in the first excited vibrational bending state, measured with the Cologne Terahertz Spectrometer. . . . . 118

6.10 Two low frequency transitions of HDO measured with the Kiel FTMW spectrometer. . . . . 119

6.11 Excerpt from the energy level scheme of HDO with measured rotational transitions. . . . . 125

# List of Tables


3.1 Standard names of the expansion coefficients of the power series Hamiltonian. . . . 41

3.2 Transformation from $A$-reduction to Euler. . . . 44

3.3 Transformation from Euler to $A$-reduction. . . . 44

4.1 Summary of measurements on DCN isotopomers. . . . 57

4.2 High precision rotational and hyperfine constants of DCN in the vibrational ground and first excited bending state. . . . 63

4.3 High precision rotational and hyperfine constants of $D^{13}CN$ in the vibrational ground and first excited bending state. . . . 63

4.4 High precision rotational and hyperfine constants of $DC^{15}N$ in the vibrational ground and first excited bending state. . . . 64

4.5 High precision rotational and hyperfine constants of $D^{13}C^{15}N$ in the vibrational ground and first excited bending state. . . . 64

5.1 The available dataset on $CH_2$. . . . 71

5.2 Compilation of new experimental data used in the analysis of $CH_2$. . . . 78

5.3 Analysis of $CH_2$ data with the standard $A$-reduced Hamiltonian. . . . 79

5.4 Coefficients of the Euler expansion of the Hamiltonian for $CH_2$. . . . 82

5.5 Comparison between Watson parameters converted from Euler series coefficients and from the direct fit. . . . 85

5.6 Comparison between transition frequencies either measured in Cologne or predicted with the Euler parameter set and LMR data by Sears. . . . 86

5.7 The low-lying transitions of $CH_2$ in the frequency range covered by the ISO LWS. . . . 89

6.1 Available rovibrational and rotational data on the ground and first excited bending state ($v_2 = 1$) of $D_2O$. . . . . 102

6.2 Coefficients of the Euler expansion for $D_2O$ for both the vibrational ground and first excited bending state $v_2 = 1$. . . . . 107

6.3 The weighted root mean square (wrms) of each separate dataset of $D_2O$. . 111

6.4 Available rovibrational and rotational data on the ground and first excited bending state ($v_2 = 1$) of HDO. . . . . 114

6.5 Coefficients of the Euler expansion for HDO for both the vibrational ground and first excited bending state $v_2 = 1$. . . . . 120

6.6 The weighted root mean square (wrms) of each separate dataset of HDO. 122

6.7 Hyperfine interaction constants of HDO in the vibrational ground state in kHz. . . . . 123

A.1 Rotational spectrum of DCN in the vibrational ground state. . . . . 130

A.2 Rotational spectrum of DCN in the first excited vibrational state $v_2 = 1^{e,f}$. 132

A.3 Table of the experimental direct $\ell$-type transitions in the first excited bending state of DCN used in the fit. . . . . 135

A.4 Rotational spectrum of $D^{13}CN$ in the vibrational ground state. . . . . 136

A.5 Rotational spectrum of $D^{13}CN$ in the first excited vibrational state $v_2 = 1^{e,f}$.138

A.6 Table of the experimental direct $\ell$-type transitions in the first excited bending state of $D^{13}CN$ used in the fit. . . . . 142

A.7 Rotational spectrum of $DC^{15}N$ in the vibrational ground state (000). . . . 144

A.8 Rotational spectrum of $DC^{15}N$ in the first excited bending state ($01^{e,f}0$). . 145

A.9 Rotational spectrum of $D^{13}C^{15}N$ in the vibrational ground state (000). . . 146

A.10 Rotational spectrum of $D^{13}C^{15}N$ in the first excited bending state ($01^{e,f}0$). 147

B.1 Compilation of experimental data used in the analysis of $CH_2$. . . . . 149

B.2 Transition frequency predictions for $CH_2$ calculated for $J \leq 6$ and $K_a = 0, 1$. . . . . 152

C.1 Rotational transitions of $D_2O$ in the ground and first excited bending mode. 159

C.2 Pure rotational transitions of HDO in the ground and first excited bending mode. . . . . 168

C.3 Rotational transitions of HDO in the ground vibrational state with partially resolved hyperfine structure. . . . . 173

# 1

# Introduction

Electromagnetic radiation is the main carrier of information about space. Its generation by and interaction with cosmic matter is used to gain insights into the formation and evolution of stars and galaxies. Both the birthplaces and graveyards of stars are populated by a plethora of interstellar molecules. To date approximately 140 molecular species have been detected in the interstellar medium (ISM) and circumstellar shells. The temperatures found in these objects are typically ranging from below 10 to 200 K for dense molecular clouds and star-forming regions up to a few hundred K for circumstellar shells. Consequently, radiation from the low energy part of the electromagnetic spectrum, i.e. from the microwave to far infrared region, where most molecules interact via rotational transitions, is best suited for diagnostics of these sources (see Figure 1.1). The accurate knowledge of laboratory transition frequencies of the molecules used as diagnostic tools is the prerequisite for the analysis of astronomical observations, and ever since the first detection of an interstellar molecule by radio waves [2], laboratory spectroscopy and radio astronomy have worked hand in hand.

The submillimeter wavelength and terahertz frequency regime has been opened up by extensive technical developments both for laboratory spectroscopy and for radio astronomy during the last decade.
Among the submillimeter wavelength telescopes that have been or are operated are high-altitude observatories like the Kölner Observatorium für SubMillimeter Astronomie (KOSMA), the Caltech Submillimeter Observatory (CSO), the James Clark Maxwell Telescope (JCMT), the SubMillimeter Array (SMA) and satellite based facilities like the Submillimeter-Wave Astronomy Satellite (SWAS) and the Infrared Space Observatory (ISO). Further improvements in receiver technology will enable future projects such as the Atacama Large Millimeter Array (ALMA) and its pathfinder experiment APEX, the Herschel Space Telescope, and the airborne Stratospheric Observatory for Infrared Astronomy (SOFIA) to extend the accessible frequency range further into the terahertz region.

This progress is accompanied in the field of laboratory spectroscopy by the development of very accurate and sensitive spectrometers. The experiments carried out in

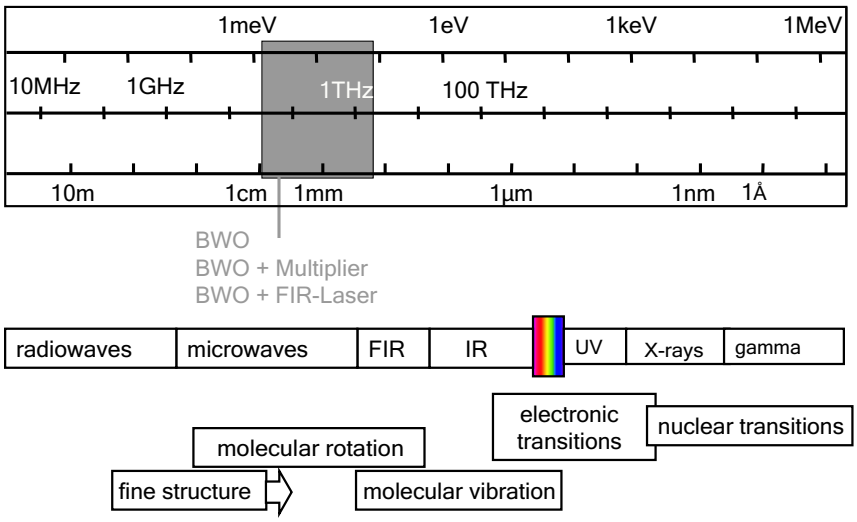


Figure 1.1: The electromagnetic spectrum and the main interaction processes of radiation with matter.

the course of this work employed spectrometers with phase-stabilised backward wave oscillators (BWOs) as key element. These radiation generators can be used either as direct sources as in the Cologne Terahertz Spectrometer [3, 4], as fundamental sources in combination with harmonic mixers operating as frequency multipliers [5], or as sideband sources in combination with a fixed frequency far infrared laser as in the Cologne Sideband Spectrometer for Terahertz Applications (COSSTA) [6, 7]. The frequency coverage of the Cologne spectrometers is summarised in Figure 1.2 and compared to that of major future radio telescopes.

Transitions between energetically low lying rotational levels of very light molecules, e.g. mono- and dihydrides, and between higher excited rotational states of medium-sized molecules, e.g. $CH_3OH$ or $SO_2$, fall predominantly in the terahertz region. In other words, terahertz transitions of the first class of molecules can be used to probe the cold interstellar medium like dark molecular clouds, whereas the latter probe the denser, warmer regimes like hot cores in star-forming regions or excited gas in the vicinity of old stars. Especially these comparatively small molecules up to 4-5 atoms are found with high abundances in the interstellar medium. Most of them, such as water, $OH^+$, CH, $CH_2$, $NH_3$, $HCO^+$, $H_3^+$, HCN, $H_2CO$ etc., are important reagents in interstellar chemistry reactions and thought to be the building blocks of larger molecules. Relative abundances and physical parameters obtained from the astronomical observation of these species give valuable information about the underlying chemical pathways for molecule formation as well as the physical and chemical evolution of the sources.

In the course of this work a large variety of molecular species have been investigated by means of rotational spectroscopy in the terahertz region. Among these are fully deuter-

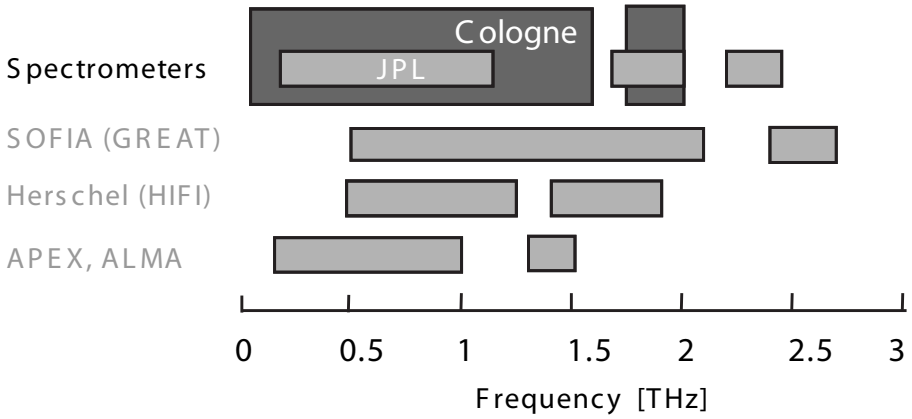


Figure 1.2: Frequency coverage of the terahertz spectrometers in Cologne compared to the operation range of future major telescope projects.

ated phosphine ($PD_3$), formaldehyde ($H_2CO$), oxadisulfane (HSOH, DSOD), molecular oxygen ($O_2$), sulphur dioxide ($SO_2$), deuterium isocyanide (DNC), hydrogen cyanide (HCN) and its isotopomers, methylene ($CH_2$) and water ($H_2O$) and its isotopomers. This thesis will concentrate on the three latter molecular species in detail, since their measurement and analysis account for the most extensive studies. They serve the astrophysical and spectroscopic community in different ways.

## Deuterium Cyanide and its Isotopomers

Hydrogen cyanide (HCN) was one of the first molecules detected in the interstellar medium [8]. It is very abundant in a variety of interstellar environments and commonly used as a high density gas tracer. Moreover, it has been observed in very highly excited rotational and vibrational states [9]. Since the main isotopomer often exhibits opacity effects, the less abundant isotopically substituted species are frequently used as an alternative to obtain information on the physical conditions in an interstellar source. Furthermore, isotopic enrichment in the interstellar medium is subject of prevailing scientific discussion. In particular in the cold interstellar medium, deuterated species are found to be much more abundant than expected from the cosmic D/H ratio. Molecular isotopic ratios, deduced from chemical calculations, have been shown to be highly dependent upon the underlying chemical reaction network (e.g. [10] for deuterated species). Therefore, observationally deduced ratios are a test of the chemical models employed, for example gas-phase or grain-surface reaction pathways. Moreover, there is a need for highly accurate laboratory data for the analysis of the extremely narrow molecular lines observed in quiescent dark clouds, where hyperfine components of cyanide species can be used to gain insight into cloud dynamics [11].

In order to provide accurate laboratory data for these investigations, the rotational spectra of the deuterated cyanide species DCN, $D^{13}CN$, $DC^{15}N$, and $D^{13}C^{15}N$ in their vibrational ground and first excited bending state have been recorded up to 2 THz. The

technique of sub-Doppler spectroscopy has been applied to be able to resolve the underlying hyperfine structure due to the nitrogen nucleus. The subsequent analysis yielded considerably improved spectroscopic parameters, which in turn are used to obtain highly accurate transition frequency predictions up to 2.5 THz.

## The Methylene Radical

The methylene radical ($CH_2$) is of high interest for both astrophysical and spectroscopic reasons. It is an important reactant in gas-phase chemical models of interstellar molecular clouds and has already been observed in the hot cores of star-forming regions [12]. Furthermore, combined gas-phase and grain-surface models predict it to have high abundances in the cold interstellar medium [13]. However, transitions involving the energetically lowest rotational levels of $CH_2$ are located in the terahertz domain due to the extreme lightness of the molecule, and are not accessible with ground-based telescopes. Moreover, the methylene radical is also challenging for laboratory spectroscopy, since it is, on the one hand, difficult to produce in sufficient amounts to perform absorption spectroscopy, and, on the other hand, it cannot be described easily by standard theoretical models. This is reflected in the very sparse experimental dataset on this molecule and large uncertainties for transition frequency predictions, respectively.

This work reports on highly accurate measurements of two energetically low-lying rotational transitions of methylene near 2 THz. Furthermore, a global analysis of all published data on this molecule with a non-standard approach is presented, which enables the prediction of further transition frequencies relevant for astrophysical searches. A successful search in the ISO database for terahertz methylene absorption lines in cold interstellar gas in the line of sight towards the galactic center source Sagittarius B2 was triggered by this new analysis [14].

## Water and its Isotopomers

Water is the third most abundant molecule in the interstellar medium. It has been detected in a wide variety of galactic and even extragalactic sources. Whereas its observation from the ground is hampered by strong absorption of atmospheric water vapour, the search of rotational water lines, which are the major cooling lines of star-forming regions, is one of the main scientific projects of the future submillimeter wavelength and terahertz satellite and airborne missions Herschel and SOFIA [15]. Most of its energetically low lying transitions appear in the submillimeter wavelength and terahertz regimes. Moreover, in the warmer interstellar medium, particularly in shock regions or circumstellar shells of late type stars, higher rotational and vibrational levels of water are likely to be populated considerably [16, 17], giving rise to additional transitions in this frequency domain. The knowledge of accurate transition rest frequencies is, therefore, mandatory up to notable high energies. Also, the observation of deuterated water species is important to increase the knowledge about isotopic fractionation and, thereby, to gain insight into molecular

formation processes [10].
Furthermore, water is the main absorbant in the earth's atmosphere, and accurate transition frequencies and intensities of its abundant isotopomers are demanded for atmospheric modelling.

As in the case of methylene, there is also a great purely spectroscopic interest in water and its isotopomers. It is the prototypical asymmetric rotor molecule, exhibiting large centrifugal distortion interactions, and many theoretical investigations employing different models to describe its rotational and rovibrational energy level structure have been carried out (see a recent review by Bernath [18]). Highly accurate laboratory data is needed to test these models.

Whereas for the main isotopomer new far infrared measurements and a thorough analysis of the eight lowest vibrational states has been recently published [19], the dataset on the deuterated species HDO and $D_2O$ is considerably smaller, in particular highly accurate rotational data on higher excited rotational levels and in vibrationally excited states was missing. During the course of this work, this dataset has been extended significantly on both isotopic species in the vibrational ground and first excited bending state by measurements performed in the terahertz domain. Furthermore, a global analysis with a non-standard model is described, capable of providing reliable rotational transition frequency predictions of HDO and $D_2O$ up to the far-infrared region and also of their fundamental vibrational bending mode in the IR.

## Outline of this thesis

The experimental measurements and spectroscopic analyses of three molecular species are reported in this thesis. Although each of these species requires the introduction of certain experimental methods and theoretical models to some extent, they have in common that their rotational spectra were recorded mainly in the terahertz domain and that their rovibrational spectra were analysed with the aid of an effective Hamiltonian. Both the description of the experimental setup used for the measurements and the available theoretical armamentarium is, therefore, summarised for all three classes of molecules in Chapter 2 and 3, respectively. In Chapter 2, the sub-Doppler technique employed for the DCN isotopomers and the implementation of a Zeeman modulation at the laser sideband spectrometer necessary for the methylene measurements, are elucidated to some extent. A more thorough introduction of the Euler expansion of the Hamiltonian, applied for the analysis of water and methylene, is given in Chapter 3, together with a compilation of standard theoretical approaches for the class of linear and asymmetric rotor molecules with varying interactions. The following chapters deal with the spectroscopic investigations in detail. Chapter 4 contains information on the measurement and analysis of the deuterium cyanide isotopomers DCN, $D^{13}CN$, $DC^{15}N$, and $D^{13}C^{15}N$. The investigation of the methylene radical is described in Chapter 5, together with a discussion of the applicability of standard models for its analysis and a report of the detection of cold interstellar $CH_2$. In the last chapter (Chapter 6), new measurements on the two water isotopomers

$D_2O$ and HDO are presented, in combination with the results of a thorough literature research on available published data and a global analysis of the extensive purely rotational and rovibrational dataset.

# 2

# Experimental Setup - Spectroscopy in the Terahertz Domain

Performing spectroscopy in the terahertz domain is still a technically challenging task. Whereas commercially available microwave synthesizers based on field-effect transistors have a maximum output frequency of only $60$ GHz, another solid-state source, the Gunn oscillator, reaches frequencies of up to $150$ GHz. It is a common approach to use frequency-multiplier devices, such as Schottky diodes, to extent the frequency range, but the conversion efficiency decreases fast for higher harmonics. Even with cascaded multiplier chains much effort has to be made to reach frequencies higher than 1 THz with sufficient output power. Moreover, contributions from lower harmonics have to be carefully filtered to obtain monochromatic radiation.

Backward wave oscillators, belonging to the group of vacuum tube generators, can produce monochromatic radiation up to $1200$ GHz, with typical levels of output power of several tens of mW to a few mW for the highest frequencies. This is sufficient to measure even extremely weak absorption lines. These sources have been successfully used for laboratory spectroscopy in Cologne for several years now and are the principal elements of the Cologne Terahertz Spectrometer, which will be described in more detail in Section 2.1. Successful attempts have been undertaken in the past and at present to use frequency multiplier devices in combination with BWOs as pumping sources.

In the frequency range between $\sim 1 - 5$ THz, no tunable solid-state or vacuum tube sources are available. Therefore, this domain is often called the terahertz gap. Quantum cascade lasers (QCLs) are promising candidates for closing this gap in the future, since fast developments are underway at the moment to tune their output frequency [20] towards terahertz frequencies. However, no cw-devices below $5$ THz are commercially available at the moment, and the problem of frequency stabilisation and tunability of these sources in the terahertz region has not been addressed properly. Several alternative methods have been used to explore the terahertz or far infrared region. The method of Fourier transform spectroscopy, very successful in the IR region, can also be applied to the FIR, but the transition frequency accuracy achievable is around a few MHz only. Another approach is

frequency mixing, either of the output of two optical diode lasers on a nonlinear optical crystal (photonic mixing) or of that of two IR gas lasers on a metal-insulator-metal (MIM) diode (Tunable Far Infrared spectroscopy - TuFIR). In both cases a difference frequency in the THz region is generated. Whereas the first method is limited by usually very small output powers, the second one is technically very elaborate.

The Cologne Terahertz Spectrometer is a typical absorption spectrometer with a tunable frequency source, an absorption cell, and a broadband detector. A schematical drawing of the spectrometer is presented in Figure 2.1. The Cologne Terahertz Spectrometer will be described in Section 2.1; details on this spectrometer can also be found in [3, 4].

The technique of sideband mixing has been successfully implemented in Cologne and will be described in more detail in Section 2.2. With this method, two radiation sources, in the FIR and millimeter-wavelength region, are mixed on a non-linear device to produce radiation at the sum frequency. Conversion losses are considerably smaller than in the case of photonic mixing and TuFIR, and a broadband tunability can be reached by using backward wave oscillators as sideband sources.

## 2.1 The Cologne Terahertz Spectrometer

As radiation sources, frequency stabilised backward wave oscillators (ISTOK RPC, Fryazino, Moscow Region, Russia) are used. Each of these vacuum tube devices is tunable by about 30 % of its nominal frequency. In Cologne BWOs ranging from $130 - 1200$ GHz are available with variable output power between $0.5$ and $100$ mW. A sketch of a BWO is shown in Figure 2.2. In these sources, an electron beam, emitted from a cathode (1) and accelerated by a high voltage ($1 - 6$ kV) to non-relativistic velocities, is de- and accelerated by a periodic slow-wave structure (2), thereby emitting coherent terahertz radiation in direction opposite to its flight direction. The electrons are focussed by a strong magnetic field (3), generated by an electromagnet. The radiation is coupled out by a small monomode aperture. In most cases, a conical horn antenna is directly mounted on the output flange of the BWO (4). The output frequency is dependent upon the accelerating voltage applied, which allows for pure electronic tuning of the device.

A free running BWO will display frequency fluctuations of several MHz on a timescale of $\sim$1 minute, generally more than the Doppler linewidth of molecular transitions and much more than the desired precision of the spectrometer. Therefore, a phase-stabilisation of the BWO is realised in Cologne to improve the frequency stability of the system. For this purpose, a small part of the radiation (around 10%) is coupled via for example a polarisation selective beam splitter onto a harmonic mixer device, where it is mixed with the output of a commercial frequency synthesizer (KVARZ, Russia) operating between $78 - 118$ GHz. The harmonic mixer will generate harmonics (IF) of the two input frequencies

$$\nu_{\mathrm{IF}} = \pm m \cdot \nu_{\mathrm{BWO}} \pm n \cdot \nu_{\mathrm{Synth.}}$$

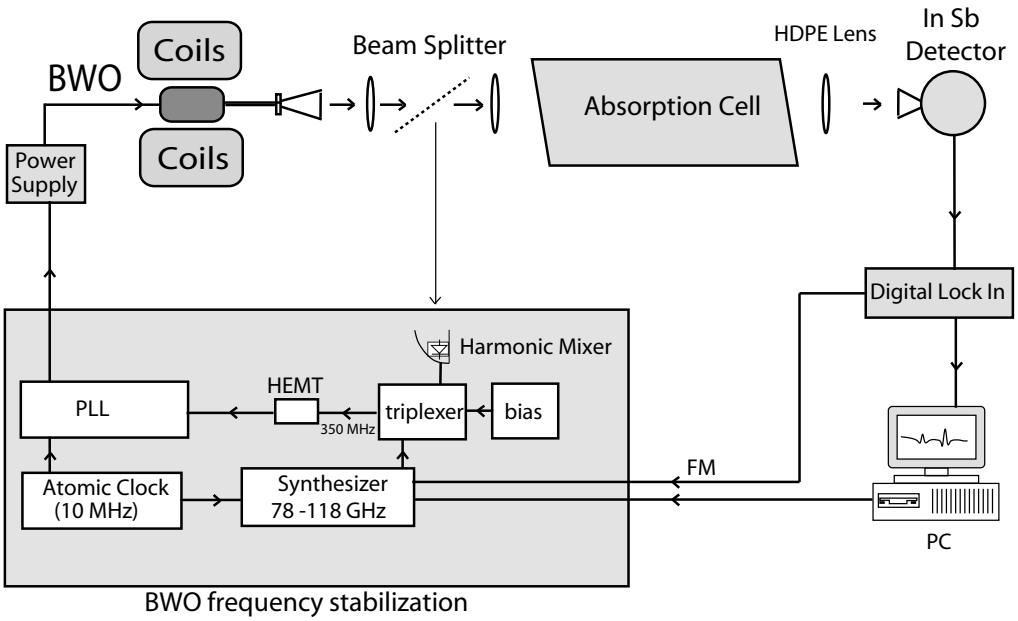


Figure 2.1: Schematical Drawing of the Cologne Terahertz Spectrometer.

For the stabilisation of the BWO, $n$ and $\nu_{\text{Synth.}}$ are choosen in a way to obtain a $\nu_{\text{IF}}$ of 350 MHz for the desired BWO frequency $\nu_{\text{BWO}}$ ($m = +1$). This IF signal is compared in phase to a reference signal that is delivered by an atomic clock (rubidium reference, $\Delta\nu/\nu = 10^{-11}$). Any change in phase is converted into a voltage error signal applied to the BWO (see Figure 2.2 (5)) by the phase lock loop circuit (PLL). With this method, a frequency stability in the range of a few Hz can be achieved, reflecting the frequency accuracy of the atomic clock.

Pyrex glass tubes, typically between 1 and 3 m in length, are used as absorption cells. The radiation passes through Teflon or HDPE (high density polyethylene) windows which have low absorption coefficients in the terahertz region. The pumping system consists in general of a rotary vane pump followed by a turbo molecular pump and pressures of $8 \cdot 10^{-3}$ Pa can be reached.

A fast (relaxation time $\sim$1 $\mu$s) InSb hot electron Bolometer (QMC Instruments, Cardiff, UK) is used for the detection. This allows for a frequency-modulation of the BWO radiation up to $500$ kHz, where $7 - 20$ kHz are typically used for the measurements. Measurements at the Cologne Terahertz Spectrometer are usually performed in 2f-modulation mode, resulting in recording of the second derivative of the absorption signal. A lock-in amplifier is used for demodulation of the signal. The amplitude of the frequency modulation can be optimised depending upon the expected linewidth and -strength.

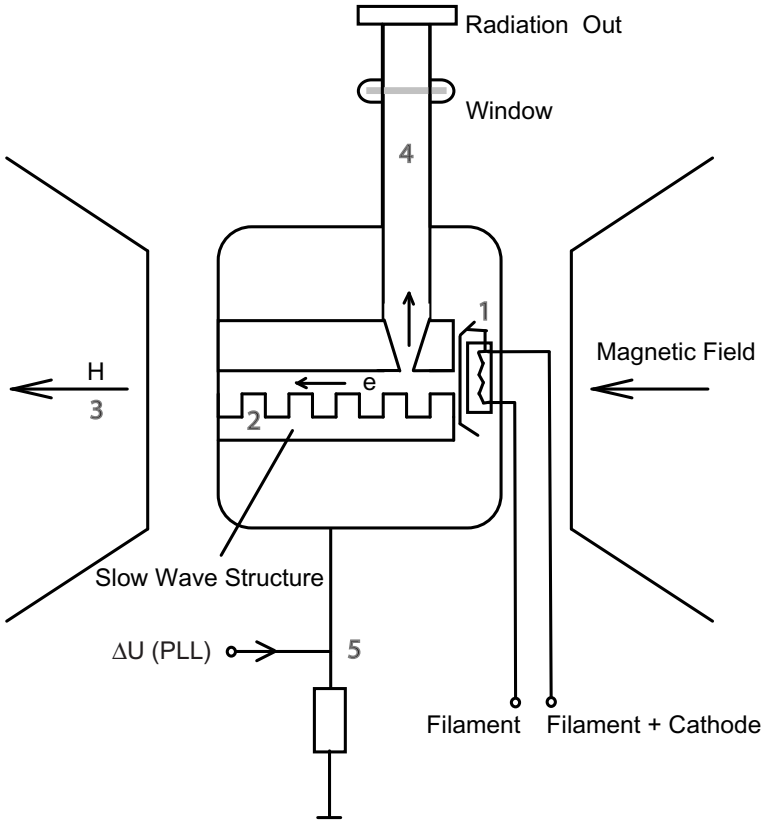


Figure 2.2: Principle of the backward wave oscillator (BWO).

### 2.1.1 Sub-Doppler Spectroscopy

Whereas the frequency stability of the terahertz spectrometer is with a few Hz extremely accurate, the limiting factor for the accuracy with which transition frequencies can be measured is the broadening of the lines by their thermal velocity. In this Doppler-limited mode, frequency accuracies between $10 - 200$ kHz can be achieved, depending upon the linewidth, lineshape and signal-to-noise ratio of the recorded lines. The Doppler width of a transition $2 \leftarrow 1$ is given by

$$\Delta\nu_D[\text{MHz}] = 7.15 \cdot 10^{-4} \nu_0[\text{GHz}] \sqrt{\frac{T\,[\text{K}]}{M\,[\text{amu}]}} \tag{2.1}$$

for a transition center frequency $\nu_0$ of a molecule with atomic mass $M$ at a temperature $T$, and for example 0.7 MHz for the DCN molecule at 300 K and 300 GHz. The natural linewidth of a transition, in contrast, is determined by its spontaneous emission probability or Einstein coefficient $A_i$

$$\Delta\nu_n[\text{Hz}] = \frac{A_i}{2\pi} = 1.16 \cdot 10^{-11} (\nu_0[\text{GHz}])^3 |\boldsymbol{\mu_{12}}[\text{D}]|^2 \tag{2.2}$$

where $\boldsymbol{\mu_{12}}$ is the transition matrix element. For a hypothetic transition with $\boldsymbol{\mu_{12}} = \mathbf{1}$ D at $300$ GHz a value of $\Delta_n = 3 \cdot 10^{-4}$ Hz can be calculated, several orders of magnitude smaller than the Doppler width.

With the Cologne Terahertz Spectrometer, measurements with sub-Doppler resolution can be performed by saturation or Lamb-dip spectroscopy [21]. The principle of this technique is the following. Typically, a pump and a probe beam of the same frequency are guided in opposite directions through the absorbing gas, consisting of particles following a Maxwell velocity distribution. Let the direction of the pump beam define a positive direction. At a specific frequency $\nu_1 = \nu_0 + \Delta\nu$ well within the Doppler width of the transition, molecules with a velocity component $v = -\Delta\nu \frac{c}{\nu_0}$ will interact with the pump beam, whereas those with $v = +\Delta\nu \frac{c}{\nu_0}$ do interact with the probe beam. Both beams will depopulate the lower energy level in the velocity class of molecules they interact with. If the frequency is tuned to the center frequency $\nu_0$, both beams do interact with the same class of molecules. A spectrum recorded with the probe beam will, therefore, show a narrow dip, the so-called Lamb-dip at the center of the Doppler-broadened profile. The line profile can be described by [22]

$$\alpha_s(\nu) = \alpha_{\text{Doppler}}(\nu) \left[ 1 - \frac{S_0}{2} \left( 1 + \frac{(\Delta\nu_S/2)^2}{(\nu - \nu_0)^2 + (\Delta\nu_S/2)^2} \right) \right] \tag{2.3}$$

with $\alpha_{\text{Doppler}}(\nu)$ the Gaussian Doppler lineshape and

$$\Delta\nu_S = 2\,\Delta\nu_H \sqrt{1 + S_0} \tag{2.4}$$

the linewidth of the saturation dip. The factor two in Equation 2.4 is only valid under the assumption that both participating levels have the same homogeneously broadened relaxation rate $\gamma_{iH} = \Delta\nu_{iH}/2$, otherwise $2\Delta\nu_H$ has to be replaced by $(\Delta\nu_{1H} + \Delta\nu_{2H})$.

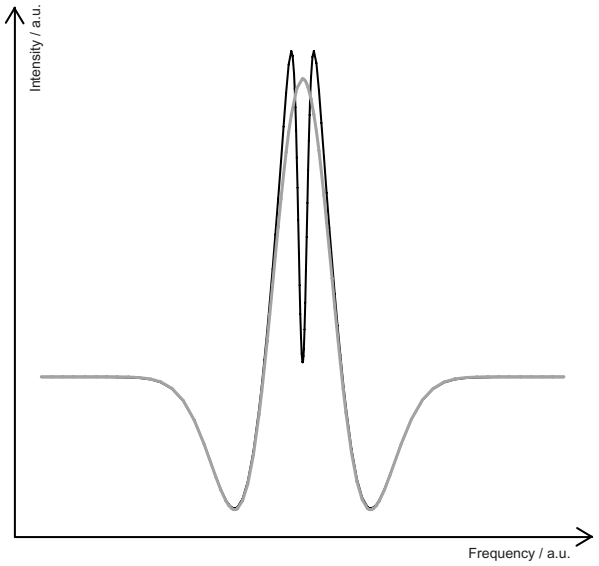


Figure 2.3: Simulated Doppler (grey) and sub-Doppler (black) spectrum of a line measured in second derivative mode. In this example, the linewidth of the saturation dip is one sixth of the Doppler linewidth, and $S_0 = 0.1$.

$S_0$ is a measure for the saturation of the line at the center frequency $\nu_0$, depending upon the transition matrix element and the radiation power $I = E^2$

$$S_0 = \frac{\boldsymbol{\mu_{12}^2} I}{(\Delta\nu_H/2)^2}. \tag{2.5}$$

It is obvious, that with increasing saturation, that is, increasing radiation power, the saturation dip gets broader, an effect called power broadening. Furthermore, the natural linewidth $\Delta\nu_n$ is homogeneously broadened by pressure effects to [23]

$$\Delta\nu_H = b\,p \tag{2.6}$$

where $p$ is the pressure in the absorption cell and $b$ is a pressure broadening parameter with typical values of $\sim 10$ MHz/mbar. The actual linewidth of the saturation dip will, therefore, be considerably larger than the natural linewidth. Additionally, flight time effects and misaligned optics might cause additional broadening of the lines. A simulated sub-Doppler spectrum is shown in Figure 2.3, the lineshape is not exactly as given in equation 2.3 since the 2f-detection mode was taken into account.

At the Cologne Terahertz Spectrometer, pump and probe beams are realised by making use of radiation reflected at the detector surface. By careful optical alignment a standing wave is generated by the incident and reflected beam, and equation 2.3 applies. The gas pressure in the absorption cell and the power of the BWO have to be adjusted according to the linestrength and the desired resolution, for the reasons outlined above. Furthermore, the frequency modulation might cause additional broadening effects and its amplitude has to be chosen as small as possible. Taking into account all these effects, a linewidth of the saturation dips of $30$ kHz can be obtained, and the line positions can be determined experimentally to an accuracy in excess of $500$ Hz [24, 25].

### Crossover Dips

The situation gets more complicated in the case of two transitions with a frequency separation $\Delta\nu_{12} = \nu_2 - \nu_1$ less than the Doppler width and a common upper or lower energy level. The transition intensities are influenced by each other, since both transitions can be responsible for depopulation of the same velocity class of molecules at a certain frequency. If $\nu = (\nu_1 + \nu_2)/2$, molecules in the velocity class with $v = \pm\frac{c}{2\nu}(\nu_2 - \nu_1)$ will interact with both the incoming and the reflected electromagnetic wave via the transition at $\nu_1$ and $\nu_2$, respectively. Consider $\nu_1$ and $\nu_2$ as belonging to the transitions $1 \leftarrow 0$ and $2 \leftarrow 0$, respectively, and $\nu_{12}$ being the frequency of the $2 \leftarrow 1$ transition. For the sake of clarity, the same homogeneous linewidth $\Delta\nu$ is assumed for all transitions. It can be shown that [26]

$$\begin{aligned}\alpha_s \;=\; & \alpha_{\text{Doppler}}\left[1 - \frac{S_{01}}{2}\left(1 + \frac{(\Delta\nu/2)^2}{(\Delta\nu/2)^2 + (\nu-\nu_1)^2}\right)\right. \\ & -\frac{S_{02}}{4}\frac{(\Delta\nu/2)^2}{(\Delta\nu/2)^2 + \nu_{12}^2}\left(\frac{(\Delta\nu/2)^2 - \nu_{12}^2}{(\Delta\nu/2)^2 + (\nu_{12}/2)^2} + \frac{(\Delta\nu/2)^2 - \nu_{12}(\nu-\nu_1)}{(\Delta\nu/2)^2 + (\nu-\nu_1)^2}\right) \\ & \left.-\frac{S_{02}}{4}\left(\frac{(\Delta\nu/2)^2}{(\Delta\nu/2)^2 + (\nu_{12}/2)^2} + \frac{(\Delta\nu/2)^2}{(\Delta\nu/2)^2 + (\nu-(\nu_1+\nu_2)/2)^2}\right)\right] \\ & +(1 \rightleftharpoons 2).\end{aligned} \tag{2.7}$$

The first term represents the Lamb dip at the frequency $\nu_1$ (or $\nu_2$, respectively), whereas the third term is responsible for the appearance of a so-called crossover dip or resonance at the frequency $(\nu_1 + \nu_2)/2$, at the arithmetic mean of the Lamb dip frequencies. The second term in equation 2.7 is a dispersion term which influences the lineshape at the frequency of the Lamb dip. This will shift the apparent center frequency of the Lamb dips. For the measurements performed on DCN isotopomers presented in this work, the influence of this term has shown to be negligible due to the relatively large separation of the two participating transitions. Crossover terms, however, have been observed for several transitions and were included in the analysis. They provide useful additional information in the case of overlapped transitions, since not all of these participate in crossover transitions.

## 2.1.2 Terahertz Radiation from Multiplier Sources

A common approach to extend the frequency range of radiation sources to higher values is by frequency multiplication of a high power fundamental source by means of a non-linear device. By illuminating for example a Schottky diode with monochromatic light, the non-linearity in its I-V-characteristic will cause the generation of radiation with frequencies at higher harmonics of the fundamental.

In the course of the work on the water isotopomers, I had the opportunity to use a frequency multiplier designed for an output frequency of $1.9$ THz for spectroscopic measurements. This device was fabricated by the workgroup of P. Siegel at the JPL (Jet

Propulsion Laboratory, Pasadena, USA) to work as a frequency tripler in a solid-state-chain designated as local oscillator (LO) for the HIFI/Herschel space project. Since to that date no high power solid-state-chain with an output frequency of above $600$ GHz existed, the device was in Cologne for test measurements with a BWO as pumping source. The results of these tests and a schematic drawing of the device are shown in Figure 2.4 [27]. Two diodes are mounted in balanced mode in a mixer block with appropriately designed filters and waveguides. The balanced mode suppresses the propagation of the second harmonic. The diodes were manufactured in substrateless membrane technology (MoMeD - Monolithic Membrane Diodes). As can be seen in Figure 2.4 c) and d), the output power is between $0.2 - 1.0\,\mu$W in the frequency range from $1.78 - 1.94$ THz, with a slight frequency and large input power dependance.

For the spectroscopic measurements, the radiation of the BWO was quasi-optically focussed on the input horn antenna of the mixer block with a HDPE lens. An additional lens was used for the generation of a parallel beam that passed the absorption cell of $1$ m length, and a third after the absorption cell to focus the radiation onto the detector. Very thin ($\sim 2$ mm) HDPE windows were utilised. Care was taken to minimise the optical path for the frequency-tripled radiation, since the absorption of water in the laboratory air is high at frequencies of around $2$ THz (see also the next Section). Although optical adjustment was complicated by the fact that the balanced diodes are unbiased, that is the quality of the input coupling could not be optimised directly by observing a diode bias change, the THz radiation generated had enough power to be detected in chopped mode at the hot electron bolometer.

A comparison of lines measured both with the tripler setup and with the sideband system introduced in Section 2.2 is shown in Figure 6.3 of Section 6.1.

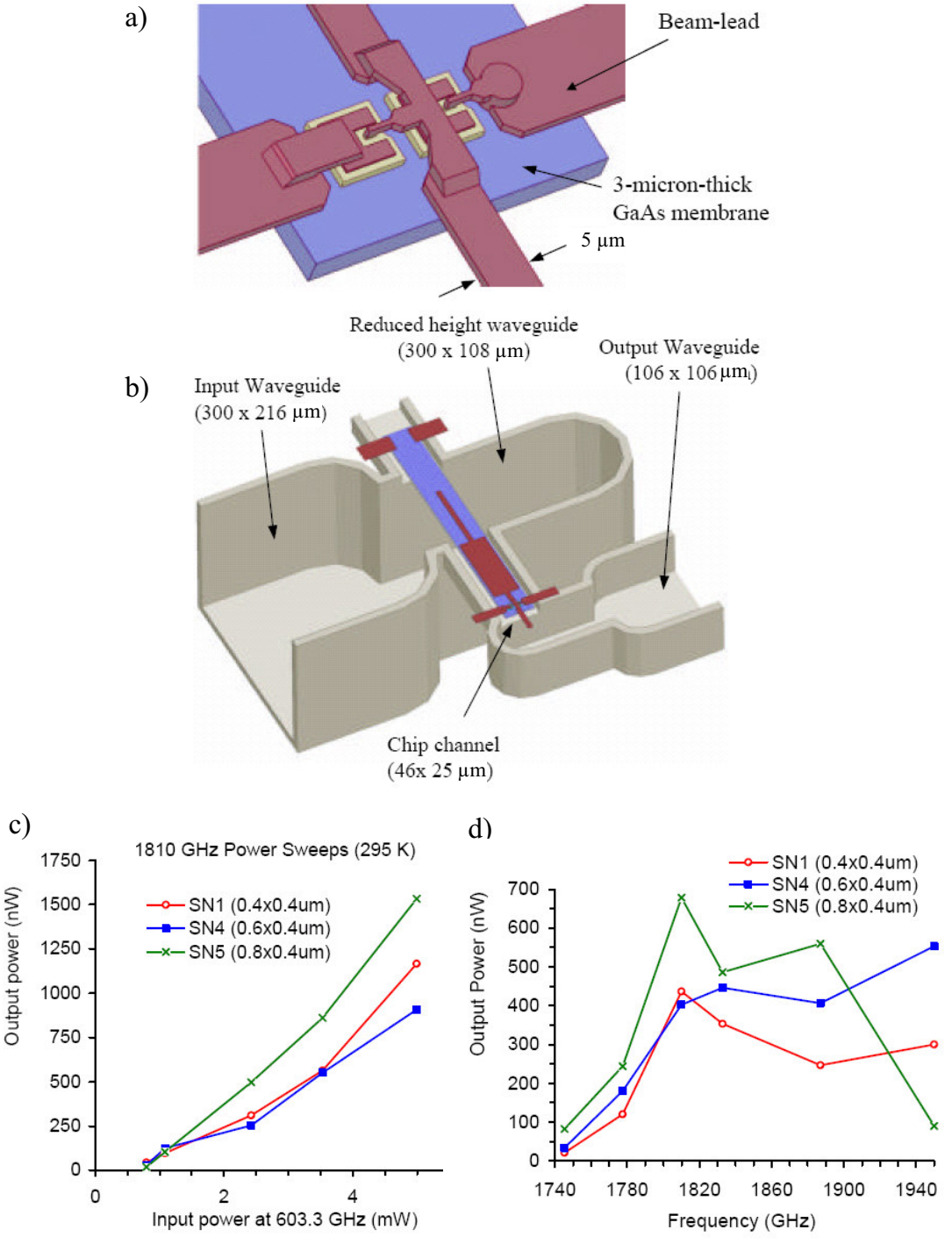


Figure 2.4: a) Detail of the anode area of the 1.9 THz JPL MoMeD tripler with two balanced diodes, b) Mounting of the diode in the mixer block with input and output waveguide, c) Frequency response of the three test triplers at room temperature with 3 mW input power provided by a BWO, d) Dependence of the output power from input power at 1810 GHz. All figures are taken from [27].

## 2.2 COSSTA - Cologne Sideband Spectrometer for Terahertz Applications

An alternate approach to generate terahertz radiation is the sideband technique. In principle, radiation from two sources, a high frequency carrier, and a broadband tunable microwave or sub-mm-wavelength source, is mixed by means of a non-linear device, such as a fast Schottky-diode. The generated sideband radiation with the sum or difference frequency of the two incident sources is then filtered out and used for spectroscopy.

The Cologne Sideband Spectrometer for Terahertz Application uses two high power

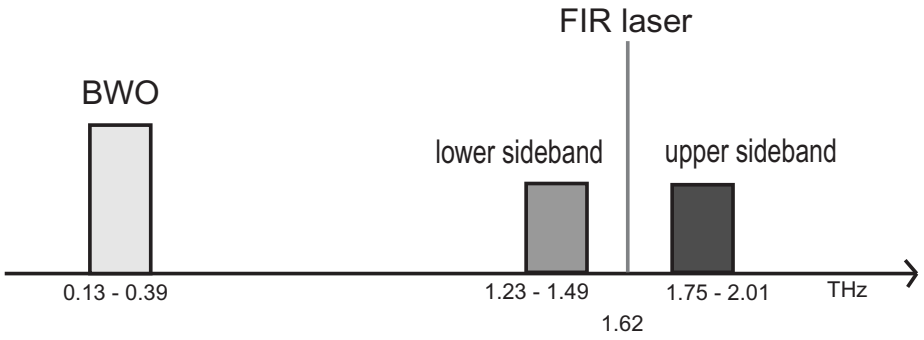


Figure 2.5: Principle of sideband generation.

Backward Wave Oscillators ($20 - 100$ mW) covering in total a frequency range from $130 - 385$ GHz as broadband tunable and a far-infrared (FIR) gas laser as fixed carrier frequency source at $1.623$ THz. This results in upper sideband radiation with frequencies between $1.75 - 2.01$ THz (see Figure 2.5). A schematical drawing of the whole setup is shown in Figure 2.6. The system has been described in some detail in [6, 7].

To the left, the BWO part is shown. The BWOs are phase-stabilised in the same manner as described in Section 2.1. A Hewlett-Packard microwave synthesizer providing $2 - 18$ GHz instead of the high frequency KVARZ synthesizer is used to down-convert the sub-mm-wavelength radiation and also to tune the frequency. Consequently, harmonics as high as the 21st have to be used for stabilisation. A small step size for recording the spectra is guaranteed by utilising a second low frequency HP synthesizer. It provides the reference frequency of $350$ MHz and can additionally be tuned by steps in excess of $10$ Hz, which results in a minimum stepsize of $10$ Hz at $2$ THz as well. Typically, step sizes of $10 - 50$ kHz are adjusted. The frequency accuracy achieved by the phase-lock-loop is better than $1$ Hz.

The greater part of the BWO radiation is reflected at the beam splitter and guided into the vacuum box containing the optics and to the sideband mixer.

The right part of Figure 2.6 shows the FIR laser system, developed originally by E. Michael [28]. A $CO_2$ gas laser serves as pumping source for a FIR ring laser. All experiments presented in this work were performed with laser emission of a rotational line of $CH_2F_2$, difluormethane, at $\sim 1.623$ THz. This line was pumped with the ${}^9R_{32}$ $CO_2$

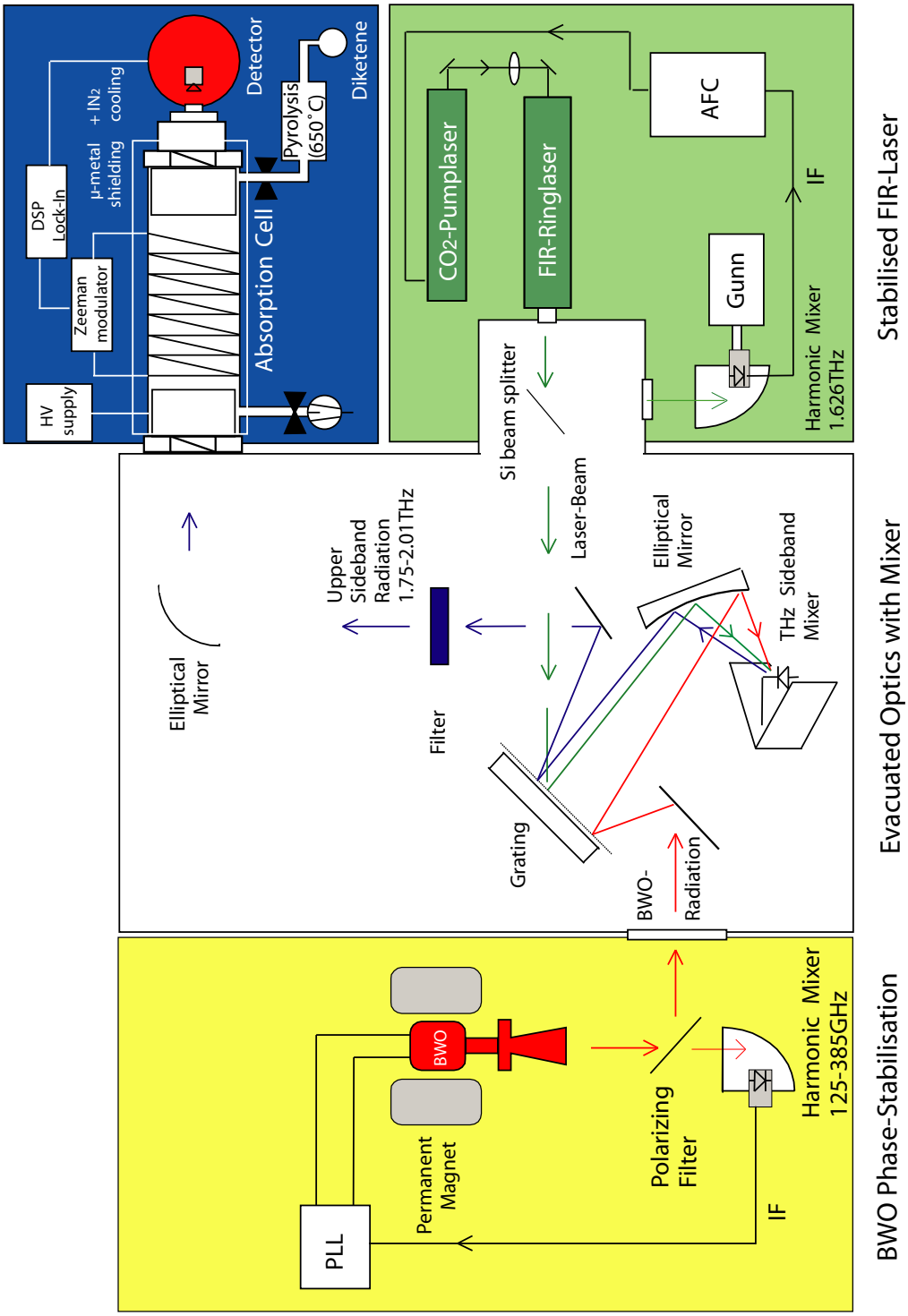


Figure 2.6: Schematic Drawing of the Cologne Sideband Spectrometer for Terahertz Applications (COSSTA).

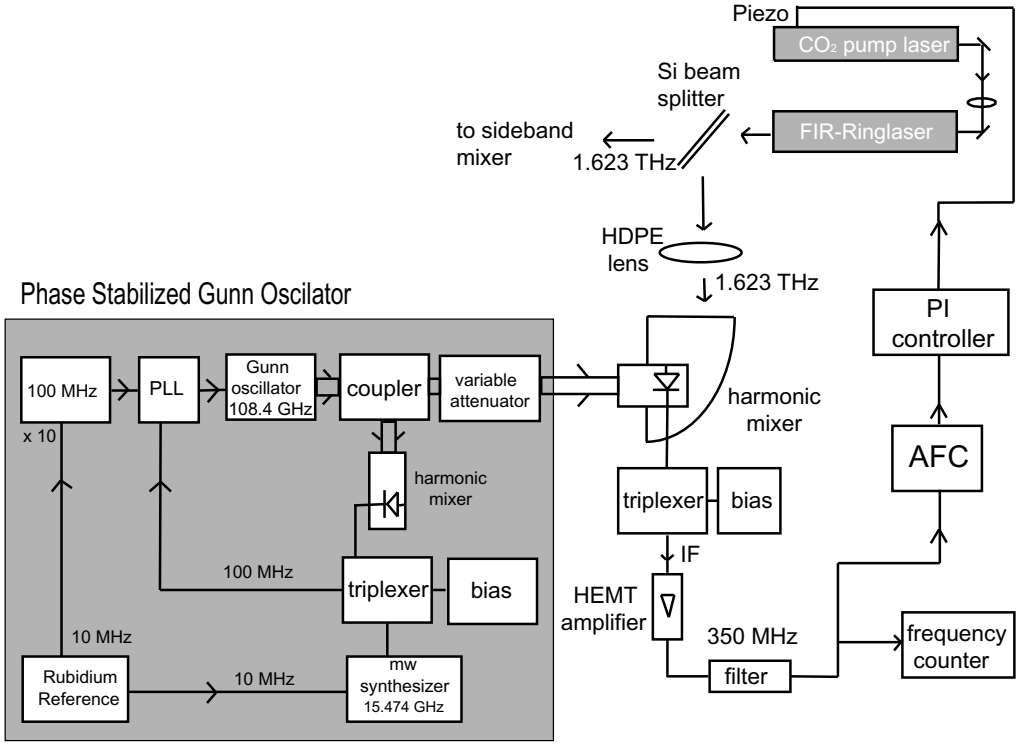


Figure 2.7: Block diagram of the FIR laser stabilisation realised at COSSTA.

laser line ($J = 33 \leftarrow 32$ at $9.2$ $\mu$m). With optimal optical adjustment the output power of the $CO_2$ laser was 7 W at this line, and the corresponding power for the FIR line was measured to be $\sim 3$ mW.

The gain profiles of the $CO_2$ and also the FIR laser are rather broad. Due to slow thermal drifts the output frequency can vary by around $2$ MHz, and vibrations, induced for example by the vacuum pumps, might give rise to additional fast variations in the frequency. To increase the frequency accuracy of the system, an active frequency stabilisation has to be employed [29].

This frequency stabilisation is shown schematically in Figure 2.7. A small fraction of the laser radiation ($\sim$ 5 %) is coupled out by a silicon beam splitter into a quasi-optical terahertz harmonic mixer with an implemented planar Schottky diode. A HDPE lens and a parabolic mirror are used to focus the beam onto the harmonic mixer. To down-convert the signal to a frequency that can be processed by the following frequency discriminator, the signal is mixed with the output of a phase-stabilised Gunn oscillator. The difference between the 15th harmonic of the Gunn oscillator ($108.4$ GHz) and the FIR laser frequency results in an intermediate frequency (IF) of $\sim 350$ MHz. After amplifying this signal by an ultralow noise HEMT (high electron mobility transistor), and filtering it with a narrow bandpass filter, it is processed by a frequency discriminator circuit (AFC - *A*utomatic *F*requency *C*ontrol in the figure). This device delivers a voltage proportional to the IF frequency of the FIR laser, which contains all frequency shift information. A plot of the voltage response of the frequency discriminator is given in Figure 2.8. The output of a frequency synthesizer with variable power was used for testing the AFC performance

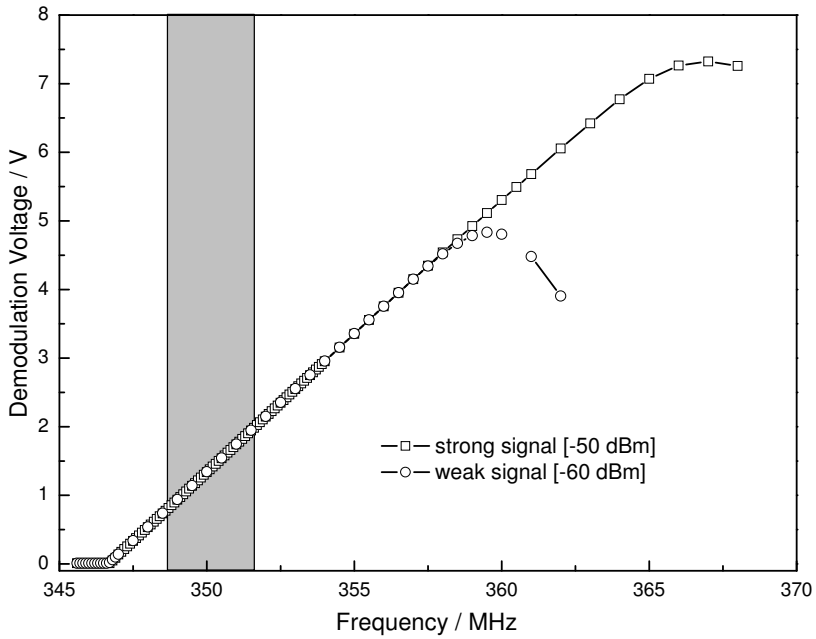


Figure 2.8: Voltage response characteristic of the frequency discriminator used in the FIR laser stabilisation circuit.

instead of the signal from the harmonic mixer. The excellent linearity of the device is shown. Deviations for low and high frequencies are due to the integrated bandpass filter, but do not affect the frequency range of the IF, shown in grey in the diagram.

Even small deviations from the selected FIR laser frequency result in a voltage change at the AFC output, which drives via a PI (*P*roportional *I*ntegral) controller a piezo actuator to move the grating of the $CO_2$ pump laser. Mode locking of the two lasers results in the stabilisation of the FIR laser. The FIR laser frequency is corrected within the gain profile of the IR laser. Judged by frequency counting of the IF signal, a frequency stability (AFC loop error signal) of $< 5$ kHz is achieved. This enables us to calibrate the FIR laser in absolute frequency.

To obtain an overall high frequency precision, the Gunn oscillator, used to stabilise the FIR laser, has to be frequency stabilised also. Since the Gunn frequency is in the order of $100$ GHz, its signal has to be down-converted to a lower intermediate frequency ($100$ MHz) for signal processing. Therefore, a part of the Gunn radiation is coupled via a waveguide to a second planar Schottky diode and mixed with the 7th harmonic of a HP microwave synthesizer (at $15.474$ GHz). The intermediate frequency of $100$ MHz is amplified and processed by a PLL unit, where its phase is compared to a $100$ MHz reference signal. Phase deviations are converted to a voltage error signal which is applied to the Gunn, thereby controlling its phase. The microwave synthesizer and the $100$ MHz reference for the PLL are coupled to a rubidium reference. The overall stability of the Gunn is therefore equivalent to the stability of the rubidium reference, i.e. $\frac{\Delta\nu}{\nu} = 10^{-11}$.

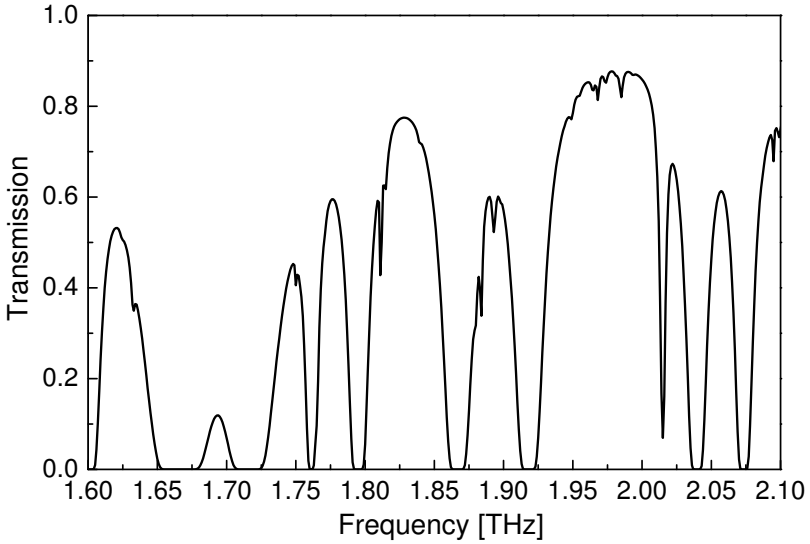


Figure 2.9: Transmission through 1 m of laboratory air (80 % humidity) in the frequency range relevant for COSSTA [7].

As can be seen in Figure 2.6, the radiation of the BWO and FIR laser are focussed on a whisker-contacted corner-cube Schottky diode (Type IT6, Virginia Diodes Inc.), acting as non-linear device. The generated upper sideband radiation is separated from the incoming light by means of an Echelette grating, additionally filtered by a Fabry-Perot cavity, and quasi optically guided through the absorption cell to a broadband InSb hot electron bolometer detector. The detector is cooled to $4.2$ K and magnetically tuned to operate with maximum sensitivity (NEP = $3.5$ pW$\sqrt{\text{Hz}^{-1}}$) in the frequency range between $1.8 - 2.4$ THz.

The whole high-frequency optics is contained in a vacuum box that can be evacuated to pressures of a few Pa. Furthermore, the space between absorption cell and detector is evacuated. This is necessary due to high absorption of mainly water vapour in the laboratory air, as demonstrated in Figure 2.9.

The sensitivity of the spectrometer can be estimated from the measurement of a weak line. For lines with known intensity $I(T)$ [nm$^2$MHz] at a temperature $T$, the peak absorption coefficient $\alpha_{\text{max}}$ [cm$^{-1}$] can be evaluated in the thermal Doppler limit at the same temperature $T$ to be [30]

$$\alpha_{\text{max}} = \frac{I(T)p[\text{Pa}]}{(\Delta\nu_D/2)} \cdot 1.13405 \text{ cm}^{-1} \tag{2.8}$$

where $p$ is the partial pressure of the molecule in Pa, $\Delta\nu_D$ is the Doppler full-width at half-maximum (FWHM) of the line (see equation 2.1). One of the weakest lines measured with COSSTA in the course of the present investigation was a rotational transition

of HDO with $\alpha_{\text{max}} = 1.3 \cdot 10^{-4}$ cm$^{-1}$ over an absorption path of 1 m.

### 2.2.1 Zeeman Modulation

For molecules with a permanent magnetic dipole moment, induced by a resulting non-zero orbital angular momentum or electronic spin, the method of Zeeman modulation can be applied to record molecular spectra. This method, explained in more detail in the following paragraphs, can in principle be applied to molecules with zero electronic angular momentum or spin ($^1\Sigma$ state molecules) also, provided that a magnetic moment is introduced by the molecular rotation or by the nuclei. These effects are much weaker and thus require a much higher (by a factor $10^4$) external magnetic field, which cannot be achieved by the experimental setup used in this work.

The principle of the Zeeman modulation is the following. An applied magnetic field will cause a splitting of each rotational transition into a doublet. If the magnetic field is switched on and off, one can record the difference signal between the unsplit and split line. Under appropriate conditions, this will yield a spectrum with a line centered at the unperturbed transition frequency.
The advantage of this method compared to frequency modulation is on the one hand the elimination of baseline effects in the spectrum, since the baseline is present in both cases, with magnetic field switched on and off. The COSSTA experiment is particularly baseline limited in its sensitivity, due to standing waves introduced in the optics of the spectrometer.
On the other hand, transitions from non-magnetic species, contaminations resulting from the production mechanism, are not apparent in the spectrum, making an unambiguous identification of the species under investigation easier.

First, I want to give a short summary of the underlying theory of the Zeeman effect. The following formulae are based on the standard textbook by Gordy and Cook [31]. The interaction of the molecule with an external magnetic field will introduce an additional term to the molecular Hamiltonian, which looks the following for weak fields:

$$H = H_{mol} + H_{Zee} = H_{mol} + \mu_{\mathbf{F}} \cdot \mathbf{H} = H_{mol} + g_F \, \mu_B \, \mathbf{H} \cdot \mathbf{F}, \tag{2.9}$$

where $\mu_F$ is the magnetic moment of the molecule (depending on the quantum state), $\mathbf{H}$ the applied magnetic field strength, $g_F$ the state dependent $g$-factor, and $\mu_B$ the Bohr magneton.

This extra term will lead to a splitting of each rotational transition into a $\pi$ and, with the assumption made below, two $\sigma$ components. The $\pi$ component will only be observable with light polarised parallel, the $\sigma$ transitions with light polarised perpendicular to the direction of the applied magnetic field, as it is realized in this experiment. The transition frequencies can be derived to be:

$$\nu_{\sigma^\pm} = \nu_0 + [(g_{F''} - g_{F'}) m_{F''} \pm g_{F'}] \frac{\mu_B}{h} H, \tag{2.10}$$

where $\nu_0$ is the transition frequency without applied field, $g_{F''}$ and $g_{F'}$ the resultant $g$-factors of the lower and upper energy level, respectively, and $m_{F''}$ the magnetic quantum number ($m_F = -F, -F+1, \ldots, F-1, F$). To simplify, we assume in the following $g_{F''} = g_{F'}$, the total amount of the splitting can then be calculated to be[1]:

$$\Delta\nu_\sigma[\text{MHz}] = 2g_{F'}\frac{\mu_B}{h}H \sim 2.8 \cdot g_{F'} \cdot H[G]. \tag{2.11}$$

In the case, where no hyperfine structure is present, $g_{J'}$ has to be used instead of $g_{F'}$. The $g$-factor of an asymmetric rotor molecule is generally a rather complex function of the quantum numbers $J$, $K_a$ and $K_c$. In the case of a $^3\Sigma$ state, however, the magnetic interaction is dominated by the electronic spin of the molecule and $g_J$ simplifies to:

$$g_J = \frac{g_s}{2}\frac{J(J+1)+S(S+1)-N(N+1)}{J(J+1)} \sim \frac{J(J+1)+S(S+1)-N(N+1)}{J(J+1)}, \tag{2.12}$$

with $g_s \sim 2$ the $g$-factor of the electron[2]. The $g_F$ value can be derived in the case of a weak magnetic field from the nuclear $g$-factors of the two hydrogen nuclei ($I_1$, $I_2$), the appropriate quantum numbers for the level under consideration ($J$, $F_1$, $F_2$) and the $g_J$ value. Here we consider a sequential coupling of the two nuclear spins, although their coupling strength is naturally of the same size.

$$g_F = g_{F_1}\alpha_{F_1} + g_{I_2}\alpha_{I_2} \tag{2.13}$$

$$g_{F_1} = g_J\alpha_J + g_{I_1}\alpha_{I_1} \tag{2.14}$$

and

$$\alpha_J = \frac{F_1(F_1+1)+J(J+1)-I_1(I_1+1)}{2F_1(F_1+1)} \tag{2.15}$$

$$\alpha_{F_1} = \frac{F(F+1)+F_1(F_1+1)-I_2(I_2+1)}{2F(F+1)} \tag{2.16}$$

$$\alpha_{I_2} = \frac{F(F+1)+I_2(I_2+1)-F_1(F_1+1)}{2F(F+1)} \tag{2.17}$$

$$\alpha_{I_1} = \frac{F(F+1)+I_1(I_1+1)-J(J+1)}{2F(F+1)} \tag{2.18}$$

On the other hand, the contribution of the nuclear $g$-factors will be negligible, due to their much smaller ($\sim 10^{-3}$) value compared to $g_J$, which is dominated by the electronic interaction. Therefore, it follows:

$$g_F = g_J\,\alpha_J \tag{2.19}$$

with

$$\alpha_J = \frac{F(F+1)+J(J+1)-I(I+1)}{2F(F+1)} \tag{2.20}$$

[1]Otherwise, the two components would each show a $m_F$ dependent sub-structure. Usually, this is not resolved but leads to a state dependent broadening of the transitions.

[2]In comparison, the rotational $g$-factor is usually $g_r \sim 10^{-4}$.

and $I$ is the total nuclear spin quantum number.

The consequences of this behaviour for the recording of rotational transition lines in the presence of a magnetic field, are simulated in Figure 2.10. Let us assume to measure a line in total power mode with the magnetic field switched off, then the line shape in the Doppler limit will look as in the upper panel. With the magnetic field switched on, perpendicular to the polarisation of the radiation, the line will split into two $\sigma$-components, as in the middle panel. If we now switch the field on and off with a high repetition rate, we can use a lock-in amplifier to record the difference signal between magnetic field on and magnetic field off (or *vice versa*). The resulting signal will look as shown in the lower panel, very similar to a typical 2f - frequency modulated line, if the intensity of the magnetic field is properly chosen.

As follows from Equation 2.11, the splitting is proportional to the applied magnetic field and also to the $g_F$-factor of the upper energy level of the individual line under inspection. The observed intensity of the line varies with the splitting and the optimum conditions have to be found experimentally for each line. Typically, the $g_F$-factor is of order of magnitude $\sim 0.1 - 1$, and magnetic fields of a few Gauss are sufficient to reach a splitting of a few MHz, comparable to the Doppler line width. Some lines, however, might have such a low $g_F$-factor that they appear almost non-magnetic. In these cases they cannot be observed by the technique of Zeeman-modulation described here.

The signal intensities observed do, for the reasons outlined above, not reflect directly the transition strength. This might cause irritation for the line assignment, since the actual intensity ratio of different transitions is not as expected. As an example, Figure 2.11 demonstrates the situation for two closely spaced lines with the same transition strength, but different $g$-factors of the upper energy level. The ratio of the $g$-factor is $3/5$, the smaller value belonging to the left line. With the magnetic field switched off (upper panel), a total power spectrum would yield two lines with the same intensity. By applying the magnetic field, both lines split into doublets, but the splitting is different for each line and the resulting blended total power spectrum looks like the middle panel of Figure 2.11. The recorded signal in Zeeman mode is the difference between both absorption signals and the result is shown in the lower panel. The line with lower $g$-factor has an apparent lower intensity.

Furthermore, in the preceding considerations the effect of varying $g$-factors for the lower and upper energy levels was neglected. Especially for transitions with higher $F$ values, certain combinations of quantum numbers can yield a comparatively small value for $g'_F$, but a rather high difference $g_{F''} - g_{F'}$, which causes, following equation 2.10, a broadening of the Zeeman splitted lines according to their magnetic quantum number $m''_F$. This will, of course, affect the observed line shape.

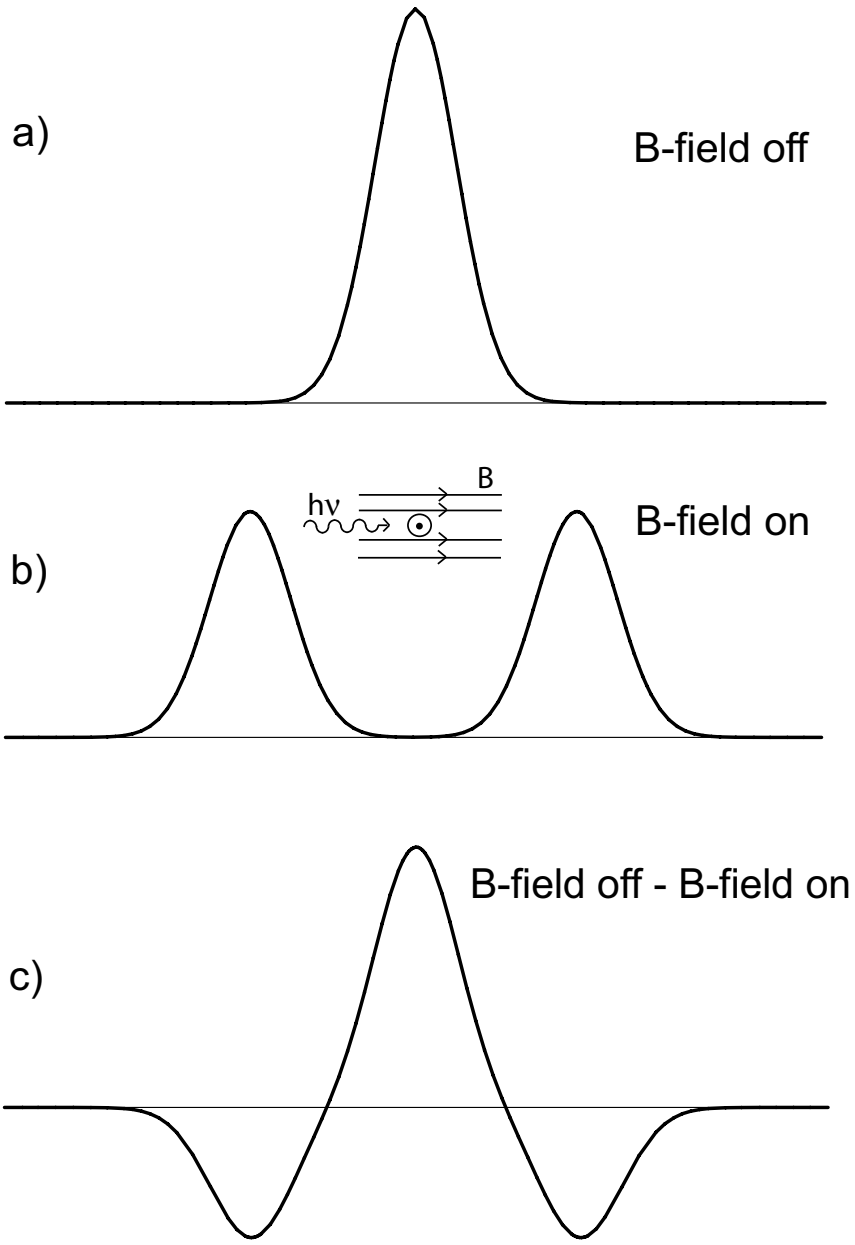


Figure 2.10: Principle of recording of Zeeman-modulated spectra: a) Total power line shape without applied magnetic field. b) Splitting of the lines due to the magnetic field B applied in direction parallel to the radiation and perpendicular to the polarisation. c) The difference signal is the actual recording.

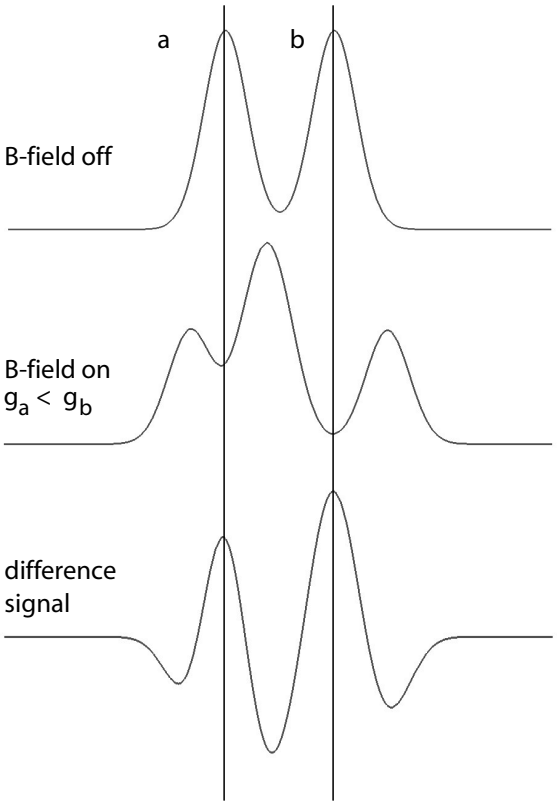


Figure 2.11: Simulated Zeeman-spectrum of two closely neighboured lines of identical transition strength, but different magnetic $g$ values.

### Experimental Details

An axial magnetic field was generated by attaching a flexible copper wire coil, able to withstand $30$ A of continuous current, directly to the absorption glass cell. The magnetic field in non-pulsed mode has been measured inside the cell with a very sensitive fluxgate magnetometer. The homogeneity over the whole active region was excellent with deviations of only $\sim 5\%$. Magnetic fields up to $6$ G can easily be applied.

The linearity of both the coil current and the resultant magnetic field with the voltage applied to the square wave modulator is demonstrated in Figure 2.12. These measurements were performed in non-pulsed mode. From the relation $H = \mu_0 \, I \, \frac{n}{l}$ and the experimental relation between $H$ and $I$, the number of coil turns per length $\frac{n}{l} = 38.7(4)$ m$^{-1}$ can be deduced, which is in excellent agreement with the intended spacing of 2.5 cm. The inductivity can then be calculated to be $\sim$15 $\mu$H.

The modulation of the magnetic field was implemented by applying a fast square wave modulation of the voltage with a frequency of around $4 - 5$ kHz. The modulation source, capable of switching high currents at high speed, has been described earlier [32],

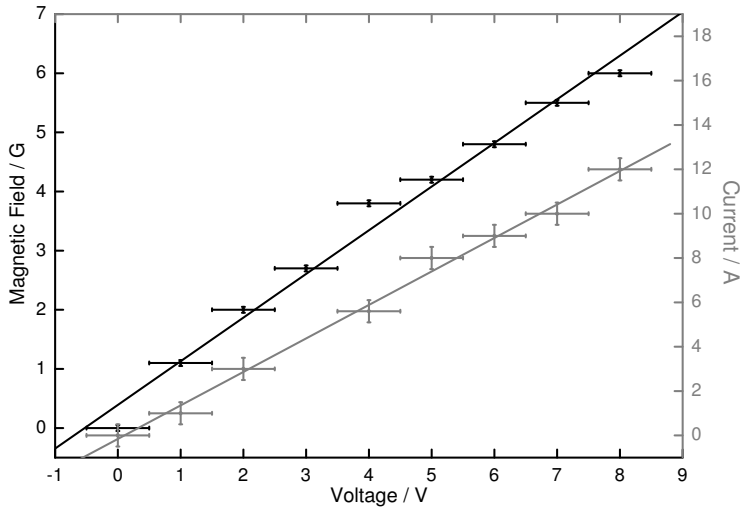


Figure 2.12: Experimental relationship between applied voltage, coil current and resultant magnetic field measured in non-pulsed mode.

but this method was adapted for the first time with COSSTA. The demodulation of the signal was achieved with a digital lock-in amplifier. A sketch of the setup is given in Figure 2.6.

The fluxgate magnetometer was also used to measure the present earth-magnetic field inside the absorption cell. A component parallel to the incident radiation will cause a broadening of the observed lines due to the earlier described $\sigma$-splitting, and a component perpendicular to the radiation and parallel to the polarisation will give rise to an additional $\pi$-transition, which might affect the observed line-shape. Values measured were around $300 - 400$ mG in axial, $300 - 500$ mG in vertical, and $100$ mG in horizontal direction, and thus not negligible compared to the applied magnetic fields of typically 2-4 G.

Therefore, I constructed a shielding of the earth-magnetic field, consisting of high permeable mu-metal (Ni containing alloy, 1 mm thick), covering the whole active region. The repeated measurement of the remnant magnetic field yielded values of below $10$ mG in all directions and over the complete active region. Care was taken to avoid induced eddy currents in the shielding box that arise from the Zeeman modulation and may cause field inhomogeneities.

## 2.3 Sub-Terahertz Spectrometers

### 2.3.1 The AMC Spectrometer

The AMC Millimeter Wave Spectrometer (Analytik und Messtechnik GmbH, Chemnitz) has been used for several measurements of DCN isotopomers. It is a conventional mil-

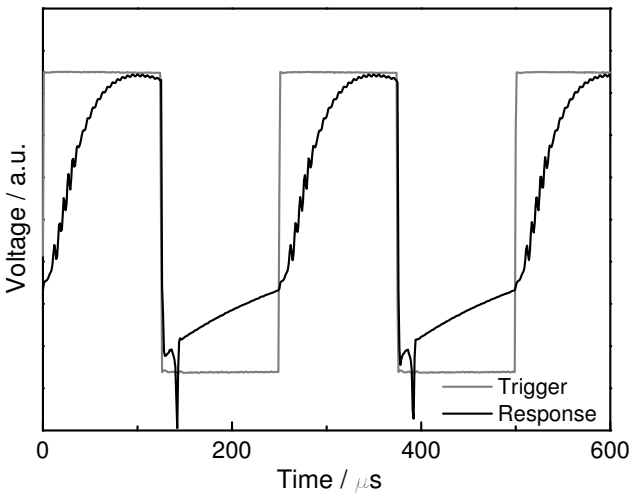


Figure 2.13: Measured response curve of the Zeeman coil in pulsed mode ($4$ kHz). The trigger voltage is shown in grey, whereas the current response is drawn in black. The intensity scale of the latter signal has been scaled for clarity purposes.

limeter wave spectrometer utilising frequency modulation. Its major components are a millimeter wave synthesizer, a modulation unit, and a receiver module. Millimeter wave power is generated by continuously tunable backward wave oscillator tubes (ISTOK, Moscow region, Russia), delivering an output power of a few mW throughout the entire frequency range. A schematical setup is shown in Figure 2.14. Three synthesizers are available in Cologne, covering the $4$-, $3$-, and $2$ millimeter wavelength range ($54 - 178$ GHz, respectively). The BWOs are phase locked internally, which yields a frequency stability of a few Hz, as has been outlined earlier. Standard Schottky diodes operated at room temperature are used as detectors in general. Optionally, InSb hot electron bolometers can be used for detection.

### 2.3.2 The Kiel FTMW Spectrometer

Fourier Transform MicroWave (FTMW) spectroscopy is conceptionally different from the "classical" absorption spectroscopy described up to this point. In FTMW experiments an ensemble of molecules is excited by a strong microwave pulse and the resulting transient emission signal of the relaxing particles is subsequently measured versus time. Only a Fourier transformation of this time-domain spectrum will yield the typical power spectrum in the frequency domain.

A strong, short and coherent microwave pulse near the resonance frequency of a molecular transition $2 \leftarrow 1$ is used to polarise the molecular sample. After the field is switched off, the molecules return to their level population at thermal equilibrium, thereby

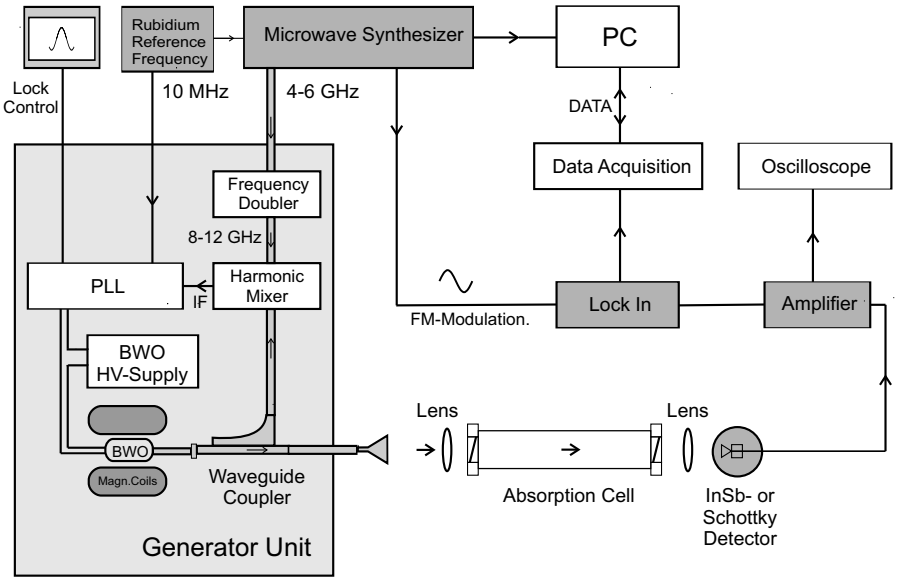


Figure 2.14: Experimental Setup of the AMC spectrometer.

emitting coherent radiation at the transition frequency $\nu_{12}$. The emission is damped due to pressure-induced collisions with a relaxation time $T$ and the resulting emission signal $S(t)$ can be written as [33]

$$S(t) = S_0 \exp\left(-\frac{t}{T}\right) \cos\left(\frac{\nu_{12} t}{2\pi} + \phi_{12}\right) \tag{2.21}$$

where $S_0$ is the amplitude of the observed signal after the electric field is switched off and is proportional to the population difference, the transition frequency, the transition dipole moment, the length of the sample cell and dependent upon the length of the applied electromagnetic pulse. In the case of several rotational transitions excited by the same microwave pulse, the total signal is a sum of terms in the form of equation 2.21. The Fourier transformation of this signal will result in a power spectrum with lines at the transition frequencies $\nu_{ij}$. A direct analysis of the time domain signal by fitting phase, frequency and amplitude is also possible.

The first FTMW has been presented by Ekkers and Flygare [34]. In Kiel, in the group of H. Mäder, two FTMW spectrometers cover the frequency range from $4 - 18$ (X-band) and $18 - 26$ GHz (K-band). They both consist of a phase-stabilised microwave synthesizer, which can be power-switched for the generation of pulses of durations in the range of several tens to hundreds of nanoseconds. The pulses are amplified and guided in a waveguide containing the gas sample. Typical gas pressures are below 1 Pa. The transient signal is down-converted with local oscillators to intermediate frequencies in the range of $30$ MHz, digitised and further processed by a PC. The waveguide of the K-band spectrometer is circular and has a length of $36$ m. Its sensitivity is excellent, even lines with an absorption coefficient of $4 \cdot 10^{-11}$ cm$^{-1}$ have been measured with this instrument [35].

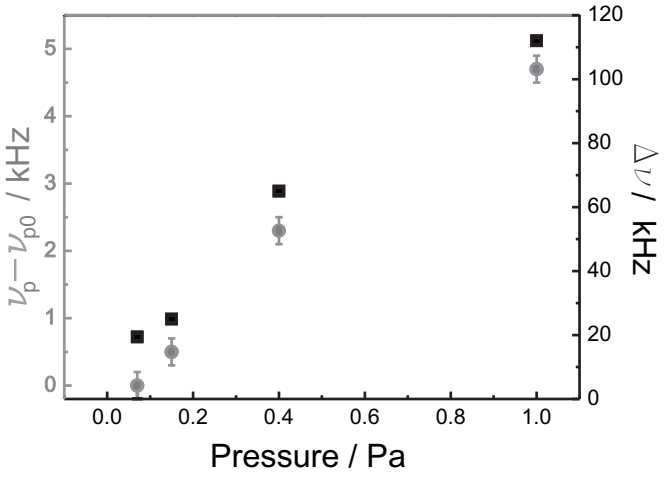


Figure 2.15: Pressure induced line-shift $\nu_p - \nu_{P_0}$ (relative to $p_0 = 0.07$ Pa) and broadening $\Delta\nu$ of a HDO line measured with the FTMW.

Depending upon the linestrength of the transition, the duration and strength of the microwave pulse have to be adjusted for each line. Furthermore, pressure broadening is the dominant factor determining the linewidth and, therefore, the resolution relevant for separating closely spaced lines. During the measurements on water isotopomers in Kiel, pressure broadening and shift effects of the $J_{Ka,Kc} = 10_{5,5} - 10_{5,6}$ $a$-type transition of HDO at 8.8 GHz have been investigated. The result is shown in Figure 2.15, even at the highest pressure of $1$ Pa, typically the upper limit used in FTMW experiments, the lineshift is only $4$ kHz, whereas the increase in linewidth certainly has to be considered.

# 3

# Theoretical Considerations

In this work, highly accurate transition frequencies of a variety of molecules have been derived experimentally. This data is then subsequently used to derive spectroscopic parameters of the molecule in the framework of an appropriate model.
In the following, the theoretical background is presented for analysing the rotational spectra of three classes of molecules that were investigated in some detail in this work.

Most linear molecules neither possess electronic angular momentum nor electronic spin. The three-atomic deuterium cyanide isotopomers presented in this work belong to this group of $^1\Sigma$ molecules. Their purely rotational energy eigenvalues can be calculated with the inclusion of rotational-vibrational interactions. Furthermore, the influence of the coupling of existing nuclear spins and quadrupole moments to the rotation has to be taken into account.

The standard model describing asymmetric rotor molecules with three non-identical principal moments of inertia will be presented, as well as an approach better suited for the group of light and floppy molecules, to which the investigated water isotopomers ($D_2O$ and HDO) and the methylene molecule ($CH_2$) belong.

The methylene molecule is a radical, with a resulting electron spin of 1. The interaction of the electronic spins of the two unpaired electrons, as well as that of the resulting total electronic spin with both the rotation of the molecule and the nuclear spins of the hydrogen atoms has a strong effect on the rotational energy levels and has to be considered to accurately reproduce the experimental spectra.

## 3.1 Fitting Spectra and Calculating Transition Frequencies

A quantum mechanical system, such as a molecule, is described by its Hamilton operator or Hamiltonian $\mathbf{H}$ representing its energy. The quantised energy levels $E$ of this system, from which transition frequencies can be derived, are obtained by solving the stationary Schrödinger equation:

$$\mathbf{H}\Psi = E\Psi \tag{3.1}$$

Electronic, vibrational and rotational contributions to the Hamiltonian can in general be uncoupled and in the following we are only dealing with the rotational Hamiltonian and its corresponding rotational energy levels. Contributions to vibrational motion will be included in a parametric form to the energy expression if necessary.

The purely rotational Hamilton operator for a rigid rotor without any interactions can be expressed through rotational angular momentum operators $\mathbf{N_i}$ along its principal axes $i = x, y, z$:

$$H_{rr} = \frac{\mathbf{N_x^2}}{2I_x} + \frac{\mathbf{N_y^2}}{2I_y} + \frac{\mathbf{N_z^2}}{2I_z}. \tag{3.2}$$

where $I_i$ is the moment of inertia along $i$. In the case of a linear ($I_a = 0$, $I_b = I_c = I$)[1] or symmetric (oblate: $I_a = I_b < I_c$, prolate: $I_a < I_b = I_c$) molecule, the Schrödinger equation can be solved directly and analytical expressions for the energy eigenvalues can be derived.
In the case of asymmetric rotor molecules ($I_a < I_b < I_c$), the Schrödinger equation cannot be solved directly. Instead, the asymmetric rotor wavefunctions are expanded in a basis set of symmetric rotor wavefunctions and the Hamiltonian matrix has to be diagonalised.

For the analysis of the asymmetric rotor spectra obtained in this work, and also for that of the linear species, the computer program SPFIT by H. Pickett [30] was employed. The input of this program is a line catalogue containing assigned experimental transition frequencies or energy levels, and a parameter file with the individual terms of the Hamiltonian. The experimental data is then subjected to a least squares analysis to the calculated energy expression. With the SPCAT program, also contained in Pickett's program suite, it is then in turn possible to calculate transition frequency predictions based on the parameter set obtained.

[1] $a$, $b$, and $c$ denote the principal axes of the moment of inertia with $I_a \leq I_b \leq Ic$

Centrifugal distortion terms in the rotational Hamilton operator, mediated via higher order angular momentum operators, as will be outlined in more detail in the next sections, are treated as small perturbations to the rigid rotor Hamiltonian and result in a correction to the rotational energy eigenvalues. Additionally, the coupling of electronic angular and spin momenta, as well as of nuclear quadrupole and spin momenta, is accounted for, and appropriate interaction terms can be considered in the Hamiltonian. Pickett's program also allows to analyse several vibrational states simultaneously by adding a vibrational energy term $E = G(v') - G(v'')$ to the energy expression. This enables the inclusion of experimental rovibrational data.

## 3.2 Linear Molecules - Hydrogen Cyanide Isotopomers

For a linear molecule with no electronic angular momentum or spin, the rotational Hamiltonian in the vibrational ground state including centrifugal distortion terms can be written [31]:

$$H_{rot} = H_{rr} + H_d^{(4)} + H_d^{(6)} + \quad \text{higher order terms} \tag{3.3}$$

$$= \frac{\mathbf{N^2}}{2I} - \frac{h}{\hbar^4} D\mathbf{N^4} + \frac{h}{\hbar^6} H\mathbf{N^6} + \quad \text{higher order terms} \tag{3.4}$$

where the centrifugal distortion constants $D$, $H$, etc. depend upon the vibrational potential function. $\mathbf{N^2} = \mathbf{N_x^2} + \mathbf{N_y^2} + \mathbf{N_z^2}$ is the total angular momentum operator. A first order perturbation treatment yields an energy expression depending upon the rotational quantum number $J$[2]:

$$E_{rot} = hB_0 J(J+1) - hD_0 J^2(J+1)^2 + hH_0 J^3(J+1)^3 + \quad \text{higher order terms} \tag{3.5}$$

where the subscript denotes the vibrational ground state.

### 3.2.1 Rovibrational Interactions for the First Excited Bending State

A $n$-atomic linear molecule has $(3n-5)$ vibrational modes. For the triatomic hydrogen cyanide isotopomers they are the symmetric stretching mode $\nu_1$, the asymmetric stretching mode $\nu_3$, and the doubly degenerate bending state $\nu_2$. The rotational constants in each of these vibrational states will be different from that of the ground state due to different effective bond lengths in the vibrationally excited states

$$E_{rot,v} = hB_v J(J+1) - hD_v J^2(J+1)^2 + hH_v J^3(J+1)^3 + \text{higher order terms} \tag{3.6}$$

where for example the rotational constant can be expressed as $B_v = B_e - \sum_i \alpha_i (v_i + \frac{d_i}{2})$ with $B_e$ the equilibrium rotational constant, $v_i$ the vibrational quantum number of the $i$-th excited state and $d_i$ the degeneracy of that state. The centrifugal distortion terms can be

[2] For molecules with no electronic angular momentum or spin, the pure rotational quantum number $N$ is identical to $J$, the total angular momentum quantum number, exclusive of nuclear spin.

expanded in a similar way.

For the degenerate bending state, one has to take into account an interaction between the rotation and the vibrational angular momentum $\mathbf{n_z}$ along the figure axis, generated by the simultaneous vibration of the molecule in two orthogonal planes. This will result in a splitting of each rotational energy level. The Hamiltonian can be expressed as

$$H_{rot,v} = \frac{\mathbf{N^2}}{2I_b} + \frac{1}{2}(\frac{1}{I_a} - \frac{1}{I_b})\mathbf{n_z^2} + CI + \text{centr. distort. terms.} \tag{3.7}$$

The effective moment of inertia $I_a$ about the figure axis $a$ is produced by the bending of the molecule. $CI$ denotes the Coriolis interaction term between rotation and vibration. For a linear molecule in the $v_2 = 1$ bending state, each rotational energy level is split into a doublet by the interaction. The energy expression has been worked out to be [31]

$$\begin{aligned} \frac{E^{\pm}_{rot,v_2=1}}{h} &= E + B_1[J(J+1) - \ell^2] - D_1[J(J+1) - \ell^2]^2 && (3.8)\\ &\quad + H_1[J(J+1) - \ell^2]^3 && (3.9)\\ &\quad \pm\frac{q_1}{2}J(J+1) \mp \frac{q_1 J}{2}J^2(J+1)^2 \pm \frac{q_{1JJ}}{2}J^3(J+1)^3 \end{aligned}$$

with the rotational constant $B_v$ defined in a slightly different way, including several interaction constants, $\ell$ is the quantum number belonging to the vibrational angular momentum and has the values $\pm 1$, $J = |\ell|, |\ell|+1, |\ell|+2, ...$ is the total angular momentum quantum number including vibrational angular momentum, and $q$ is the Coriolis coupling or $\ell$-type doubling constant. Several centrifugal distortion corrections have been added for the $\ell$-type doubling interaction.
According to the scheme proposed by Brown *et al.* [36], the rotational levels are labelled according to their energy ordering by $e$ and $f$, i.e. there exist two vibrational states ($01^{e,f}0$), the rotational energy levels in the ($01^e0$) state corresponding to $E^-$, those in the ($01^f0$) state to $E^+$. Both states have different parity, the $e$ states have the same parity as the vibrational ground state belonging to the same $J$ levels.
From this, the selection rules for electric dipole transitions can be deduced for the vibrational ground and first excited bending state:

| | | | |
|---|---|---|---|
| $v_2 = 0$: | $\Delta J = +1$ | $e \leftrightarrow e$, $f \leftrightarrow f$ | (rotational transition) |
| $v_2 = 1$: | $\Delta J = +1$ | $e \leftrightarrow e$, $f \leftrightarrow f$ | (rotational transition) |
| | $\Delta J = 0$ | $e \leftrightarrow f$ | (direct $\ell$-type transition) |

### 3.2.2 Hyperfine Structure

Nuclei with non-zero nuclear spin can interact magnetically or electrically with the fields generated by the rotating molecule. In the following, the interaction of the nuclear electric quadrupole moment of a nucleus with $I \geq 1$ with the electric field gradient of the molecule and the magnetic nuclear spin-rotation interaction of any nucleus with $I > 0$ is

summarised.

Classically, the interaction of an electric quadrupole moment with an electric field gradient is given by the scalar product of two symmetric dyadics

$$H_Q = \frac{1}{6}\mathbf{Q} : \mathbf{V} \equiv \frac{1}{6}\sum_{ij} V_{ij}Q_{ij}, \qquad i,j = \{X,Y,Z\}, \tag{3.10}$$

with the electric field gradient dyadic

$$\mathbf{V} = \boldsymbol{\nabla}\boldsymbol{E} = \mathbf{e_X}\frac{\partial \mathbf{E}}{\partial X} + \mathbf{e_Y}\frac{\partial \mathbf{E}}{\partial Y} + \mathbf{e_Z}\frac{\partial \mathbf{E}}{\partial Z} \tag{3.11}$$

and the electric quadrupole moment dyadic

$$Q_{ij} = \int \rho\{3R_iR_j - R^2\delta_{ij}\}dV. \tag{3.12}$$

The $\mathbf{e}_i$ are unit vectors along the space-fixed reference axes $i = X$, $Y$, and $Z$ and the $R_i$ are the components of the vector locating points of the nuclear volume with charge density $\rho$ in this reference system.

The corresponding Hamilton operator in the quantum mechanical description can be deduced to be [31]

$$H_Q = \frac{eQq_J}{2J(2J-1)I(2I-1)}\left[3(\mathbf{I}\cdot\mathbf{J})^2 + \frac{3}{2}\mathbf{I}\cdot\mathbf{J} - \mathbf{I^2J^2}\right]. \tag{3.13}$$

Here, $eQ$ corresponds to the electric quadrupole moment of the nucleus and $q_J$ is the expectation value of the component of the electric field gradient along the space-fixed $Z$-axis. This quantity depends on the molecular structure. For linear molecules

$$q_J = -q\frac{J}{2J+3} \tag{3.14}$$

where $q$ is independent of $J$.

The rotational angular momentum $\mathbf{J}$ and nuclear spin $\mathbf{I}$ couple to give the resultant angular momentum $\mathbf{F} = \mathbf{I} + \mathbf{J}$. For nuclei with $I = 1$ each rotational level splits into a triplet according to $F = J-1$, $J$, $J+1$. The energy expression of the quadrupole interaction can finally be written as

$$\frac{E_Q}{h} = -eQq \cdot Y(J,I,F) \tag{3.15}$$

where

$$Y(J,I,F) = \frac{\frac{3}{4}C(C+1) - I(I+1)J(J+1)}{2(2J-1)(2J+3)I(2I-1)}$$

and $C = F(F+1) - J(J+1) - I(I+1)$ is Casimir's function. The quantity $eQq$ is known as the electric nuclear quadrupole coupling constant.

In the $v_2 = 1$ state, the bending motion of the molecule and its interaction with the rotation will give raise to a small asymmetry of the electric field gradient, introducing components in directions perpendicular to the molecular axis. The whole problem can be treated in analogy to that of a slightly asymmetric rotor molecule, where the $K$ quantum number of the symmetric rotor is replaced by the $\ell$ quantum number of the vibrational angular momentum and an asymmetry parameter $\eta$ is introduced. Calculating the $q_J$ value in this case yields the following expression for the quadrupole interaction energy

$$\frac{E_Q}{h} = eQq \cdot Y(J, I, F) \left( \frac{3\ell^2}{J(J+1)} - 1 \pm \frac{\eta}{2} \right) \tag{3.16}$$

where $\eta = \frac{V_{yy} - V_{xx}}{V_{yy}}$ is the asymmetry parameter of the electric field gradient. Furthermore, a centrifugal distortion term can be introduced to the electric quadrupole moment in the form [3]

$$\frac{E_{QD}}{h} = -eQq_J J(J+1) Y(J, I, F) \left[ \frac{3\ell^2}{J(J+1)} - 1 \right]. \tag{3.17}$$

A much smaller contribution to the hyperfine splitting is attributed to an interaction between the magnetic moment $\mu_\mathbf{I} = g_I \mu_N \mathbf{I}$ of the nucleus with spin $\mathbf{I}$ and the magnetic field $\mathbf{H}$ generated by the rotating molecule. Here $g_I$ denotes the gyromagnetic ratio or $g$-factor of the nucleus and $\mu_N$ is the nuclear magneton. Under the assumption that $\mu_\mathbf{I}$ interacts only with an effective magnetic field $\mathbf{H_{eff}}$ in the direction of $\mathbf{J}$ and $J$ stays a good quantum number, the interaction can be written as

$$\begin{aligned} H_{mag} &= -\mu \cdot \mathbf{H_{eff}} \\ &= -\frac{g_I \mu_N \langle H_J \rangle}{[J(J+1)]^{1/2}} \mathbf{I} \cdot \mathbf{J} \end{aligned} \tag{3.18}$$

For linear molecules the magnetic hyperfine energies can be expressed as [31]

$$E_{mag} = \frac{C_I}{2}[F(F+1) - I(I+1) - J(J+1)] \tag{3.19}$$

where $C_I$ is the nuclear magnetic coupling constant and independent of the rotational state. In principle, there will be additional asymmetry terms to the magnetic hyperfine interaction in the first excited bending state. However, they could not be determined experimentally and are, therefore, not considered here.

Only the hyperfine interaction of the $^{14}$N nucleus has to be taken into account for the analysis of the deuterium cyanide isotopomers, since only the splitting according to this interaction could be resolved.

The overall energy expression used in the analysis is of the following form

[3] The $eQq_J$ defined here has only by coincidence the same name as the constant defined in equation 3.13

$$\begin{aligned}\frac{E_v^{\pm}}{h} &= \frac{E_{vib}}{h} + \frac{E_{v,rot}}{h} + \frac{E_{v,HFS}}{h} \\ &= G_v + B_v[J(J+1) - \ell^2] - D_v[J(J+1) - \ell^2]^2 + H_v[J(J+1) - \ell^2]^3 \\ &\quad \pm \frac{q_1}{2} J(J+1) \mp \frac{q_{1J}}{2} J^2(J+1)^2 \pm \frac{q_{1JJ}}{2} J^3(J+1)^3 \\ &\quad + eQq_v Y(J,I,F) \left[ \frac{3\ell^2}{J(J+1)} - 1 \pm \frac{\eta}{2} \right] \\ &\quad - eQq_{J,v} J(J+1) Y(J,I,F) \left[ \frac{3\ell^2}{J(J+1)} - 1 \right] \\ &\quad + \frac{C_{I,v}}{2} C.\end{aligned} \tag{3.20}$$

The subscript $v$ denotes the vibrational bending quantum number. In the vibrational ground state $\ell$, $q$, and $\eta$ are zero.[4]

## 3.3 Asymmetric Rotor Molecules - Water and Methylene

Both water and methylene are asymmetric rotor molecules, characterised by three different principal moments of inertia, and this complicates their rotational energy level scheme and also the observed spectra. The theoretical description of this class of molecules is considerably more elaborate, and a full treatment goes beyond the scope of this work. In the following, results and definitions relevant for the analysis of the experimental spectra obtained in this work will be stated. For more details the reader is referred to standard textbooks, for example [23, 38, 31].

The energy level labelling of asymmetric rotor molecules is typically done in the way $N_{KaKc}$, where $N$ is as a good quantum number associated with the rotational angular momentum operator $\mathbf{N}$, and $K_a$, $K_c$ are the $K$ quantum numbers of the limiting prolate and oblate symmetric top energy levels, respectively. They correspond to the projection of the total angular momentum onto the axis with the least and largest moment of inertia, respectively. For each rotational level belonging to one $N$ quantum number, $(2N+1)$ rotational sublevels can be found according to the allowed combinations of $K_a$ and $K_c$ with $K_a + K_c = N$ and $K_a + K_c = N + 1$.

The ladder structure of the energy levels with increasing $K$ quantum numbers for each value of $J = N$ [5] is demonstrated in Figure 3.1 with the water molecule as example.

[4] The sign of the $\ell$-type doubling constants $q$ and $eQq\eta$ depends upon the arbitrary choice of the phases of the wavefunctions [37]. In our case and with the $\pm$ designation as given in equation (3.21), both $q$ and $eQq\eta$ are positive. Since $eQq_1$ is negative, this results in the observed bigger hyperfine splitting in the $v_2 = 1^e$ compared to that in the $v_2 = 1^f$ state (see Chapter 4).

[5] In cases where no electronic spin or angular momentum is present, $N$ is replaced by $J$.

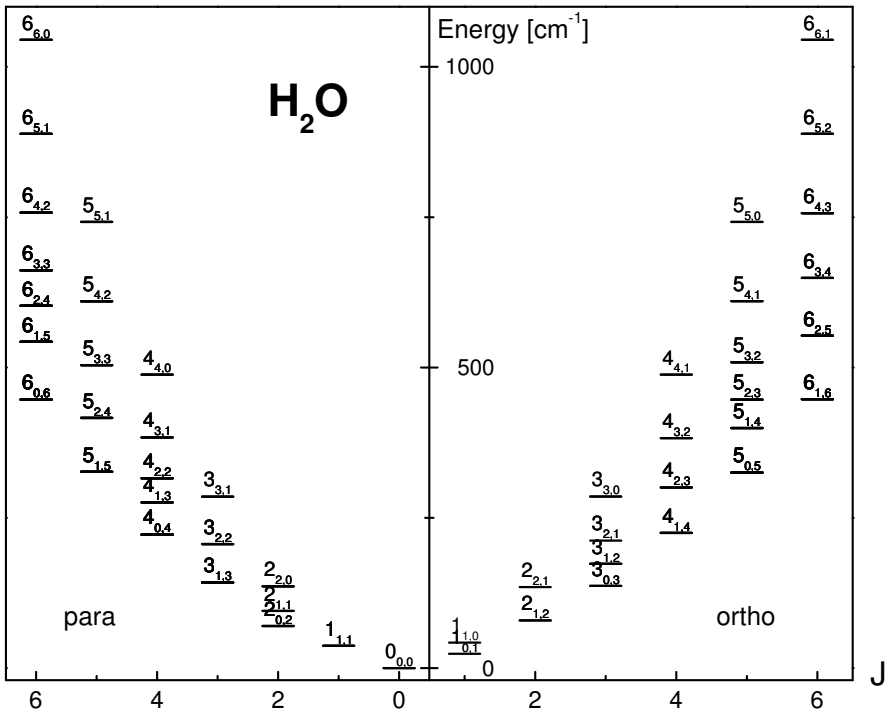


Figure 3.1: Energy level scheme of the asymmetric rotor molecule $H_2O$. For each $N$ the rotational level is split into $(2N + 1)$ sublevels. The level scheme is separated into para and ortho-levels, according to spin-statistics.

The separation into para and ortho levels is due to the two indistinguishable H nuclei. By symmetry considerations, rotational levels with $K_a + K_c$ even are allowed for $I_H = 0$, or para-$H_2O$ only, whereas those with $K_a + K_c$ odd belong to ortho-$H_2O$ with $I_H = 1$.

In addition to the selection rule $\Delta J = 0, \pm 1$, constrains on changes in the pseudo quantum numbers $K_a$ and $K_c$ can be derived by symmetry considerations. They depend upon the direction of the permanent electric dipole moment $\boldsymbol{\mu}$. Each projection of $\boldsymbol{\mu}$ along one of the principal axes of the moment of inertia will give rise to a certain kind of transitions:

| dipole component | $\Delta K_a$ | $\Delta K_c$ | |
|---|---|---|---|
| $\mu_a \neq 0$ | 0, $\pm 2$, ... | $\pm 1$, $\pm 3$, ... | $a$-type |
| $\mu_b \neq 0$ | $\pm 1$, $\pm 3$, ... | $\pm 1$, $\pm 3$, ... | $b$-type |
| $\mu_c \neq 0$ | $\pm 1$, $\pm 3$, ... | 0, $\pm 2$, ... | $c$-type |

### 3.3.1 The Pure Rotational Hamiltonian

The two asymmetric rotor molecules investigated in this work, water and methylene, are both very light and have small barriers to linearity. Consequently, they exhibit very strong

centrifugal distortion interactions. The rigid rotor Hamiltonian

$$H_{rr} = \sum_{\alpha=a,b,c} B_\alpha \mathbf{N}_\alpha^{\mathbf{2}} \tag{3.21}$$

where the $B_\alpha = \frac{\hbar^2}{2I_\alpha}$ denote the rotational constants associated with the principal axes of the moment of inertia is, therefore, not sufficient to describe these molecules.

A standard form of the rotational Hamiltonian for asymmetric rotors, including higher order terms in the angular momentum operators, has been introduced by Watson [39]

$$H_{st} = \sum_{p,q,r} h_{pqr}(\mathbf{N}_x^p \mathbf{N}_y^q \mathbf{N}_z^r + \mathbf{N}_z^r \mathbf{N}_y^q \mathbf{N}_x^p) \tag{3.22}$$

where only even values of $n = p + q + r$ are allowed. From symmetry considerations follows that for $n = 2,\ 4$, and 6, there are 3, 6 and 10 terms in the expansion, respectively, corresponding to the 3 rotational parameters, 6 quartic centrifugal distortion parameters and 10 sextic centrifugal distortion parameters.

As has been found by Watson and others, not all centrifugal distortion parameters in this expansion can be determined experimentally. He proposed, therefore, a reduced form of the Hamiltonian, containing only determinable parameters. Without going into any detail, the reduction is performed by unitary transformations acting on the Hamiltonian and an appropriate choice of boundary conditions to eliminate indeterminacies in the parameters. For further reading please refer to [40].

The most widely used form of the Hamiltonian is the asymmetric top reduction, also known as Watson's standard $A$-reduction, which can be written in the following form

$$H^{(A)} = H_{rr} + H_d^{(4)} + H_d^{(6)} + \text{higher order terms} \tag{3.23}$$

where

$$\begin{aligned} H_{rr} &= B_x \mathbf{N}_x^2 + B_y \mathbf{N}_y^2 + B_z \mathbf{N}_z^2 \qquad (3.24)\\ &= \frac{1}{2}(B_x + B_y)\mathbf{N}^2 + (B_z - \frac{1}{2}(B_x + B_y))\mathbf{N}_z^2 + \frac{1}{2}(B_x - B_y)(\mathbf{N}_x^2 - \mathbf{N}_y^2), \end{aligned}$$

$$\begin{aligned} H_d^{(4)} &= \Delta_N \mathbf{N}^4 - \Delta_{NK}\mathbf{N}^2\mathbf{N}_z^2 - \Delta_K \mathbf{N}_z^4 - 2\delta_N \mathbf{N}^2(\mathbf{N}_x^2 - \mathbf{N}_y^2) \qquad (3.25)\\ &\quad -\delta_K\{\mathbf{N}_z^2, (\mathbf{N}_x^2 - \mathbf{N}_y^2)\}, \end{aligned}$$

and

$$\begin{aligned} H_d^{(6)} &= \Phi_N \mathbf{N}^6 + \Phi_{NK} P^4 \mathbf{N}_z^2 + \Phi_{KN}\mathbf{N}^2\mathbf{N}_z^4 + \Phi_K \mathbf{N}_z^6 \qquad (3.26)\\ &\quad +2\phi_N \mathbf{N}^4(\mathbf{N}_x^2 - \mathbf{N}_y^2) + \phi_{NK}\mathbf{N}^2\{\mathbf{N}_z^2, (\mathbf{N}_x^2 - \mathbf{N}_y^2)\}\\ &\quad \phi_K\{\mathbf{N}_z^4, (\mathbf{N}_x^2 - \mathbf{N}_y^2)\}. \end{aligned}$$

The five determinable quartic distortion coefficients are $\Delta_N$, $\Delta_{NK}$, $\Delta_K$, $\delta_N$, and $\delta_K$, and $\Phi_N$, $\Phi_{NK}$, $\Phi_{KN}$, $\Phi_K$, $\phi_N$, $\phi_{NK}$, and $\phi_K$ are the seven sextic distortion coefficients. The expansion can readily be generalised to contain higher order terms, belonging to octic, decic, etc. distortion terms.

In general, the centrifugal distortion terms depend on the representation chosen to identify the molecular axes $x$, $y$, and $z$ with the principal axes of the moment of inertia $a$, $b$, and $c$. Since both water and methylene are closer to the prolate than oblate limit, the so-called $I^r$ representation was employed, where $x = b$, $y = c$, and $z = a$. With this representation, the Hamiltonian can be written in a more compact notation as a power series

$$H_{rot}^A = \sum_{m,n} f_{m,n} \cdot \left(\mathbf{N}_a^2\right)^m \cdot \left(\mathbf{N}^2\right)^n \tag{3.27}$$

$$+ \sum_{m,n} \frac{1}{2} g_{m,n} \cdot \left\{ \left(\mathbf{N}_a^2\right)^m \cdot \left(\mathbf{N}^2\right)^n, \mathbf{N}_b^2 - \mathbf{N}_c^2 \right\}. \tag{3.28}$$

The bracket $\{\mathbf{A}, \mathbf{B}\} = (\mathbf{AB} + \mathbf{BA})$ in the second row defines the anticommutator of the two operators $\mathbf{A}$ and $\mathbf{B}$. The expansion coefficients $f_{m,n}$ and $g_{m,n}$ correspond to the more general known parameters in a way that is given in Table 3.1 for comparison.

### 3.3.2 The Euler Approach

Whereas the standard $A$-reduced effective Hamiltonian has been used successfully for the analysis of a plethora of asymmetric rotor molecules in the past, it shows poor convergence or even divergence in the case of molecules exhibiting large centrifugal distortion interactions. The perturbation method cannot account for these strong interactions and the standard power series approach fails for high values of the rotational quantum numbers.

To test the convergence behaviour of a power series, one can make use of the quotient criterion (d'Alembert's criterion). If we look for example only at the first three $K_a$-dependent diagonal terms in the energy expression, we can estimate the convergence radius with respect to the $K_a$ quantum number (i.e. the projection of the total angular momentum onto the $a$ principal axis):

$$\left| \frac{A - (B+C)/2}{\Delta_K} \right| > K_{a1}^2 \tag{3.29}$$

$$\left| \frac{\Delta_K}{\Phi_K} \right| > K_{a2}^2 \tag{3.30}$$

This means, for a given rotational parameter set one can estimate a maximum value $K_{a,max} = \max(K_{a1}, K_{a2})$ so that the power series will diverge for values of $K_a > K_{a,max}$.

In the case of very light and floppy molecules, the standard model is likely to fail even for moderate values of $N$ and $K_a$ due to their large centrifugal distortion effects.

Table 3.1: Standard names of the expansion coefficients of the power series Hamiltonian.

| Expansion Coefficient | Standard Name |
|---|---|
| $f_{0,1}$ | $\frac{1}{2}(B+C)$ |
| $f_{1,0}$ | $A-\frac{1}{2}(B-C)$ |
| $f_{0,2}$ | $-\Delta_N$ |
| $f_{1,1}$ | $-\Delta_{NK}$ |
| $f_{2,0}$ | $-\Delta_K$ |
| $f_{0,3}$ | $\Phi_N$ |
| $f_{1,2}$ | $\Phi_{NK}$ |
| $f_{2,1}$ | $\Phi_{KN}$ |
| $f_{3,0}$ | $\Phi_K$ |
| $f_{0,4}$ | $L_N$ |
| $f_{1,3}$ | $L_{NNK}$ |
| $f_{2,2}$ | $L_{NK}$ |
| $f_{3,1}$ | $L_{KKN}$ |
| $f_{4,0}$ | $L_K$ |
| $g_{0,0}$ | $\frac{1}{2}(B-C)$ |
| $g_{0,1}$ | $-\delta_N$ |
| $g_{1,0}$ | $-\delta_K$ |
| $g_{0,2}$ | $\phi_N$ |
| $g_{1,1}$ | $\phi_{NK}$ |
| $g_{2,0}$ | $\phi_K$ |
| $g_{0,3}$ | $l_N$ |
| $g_{1,2}$ | $l_{NK}$ |
| $g_{2,1}$ | $l_{KN}$ |
| $g_{3,0}$ | $l_K$ |

The effect is predominant for $K_a$ dependent terms, since the $A$ rotational constant is usually extremely large for these types of molecules and the rotational energies increase very fast with increasing $K_a$ quantum number.

The two asymmetric rotor molecules investigated in this work, methylene ($CH_2$) and water ($H_2O$), certainly belong to this group of light and floppy molecules. The $K_a$ dependent convergence radii for several dihydrides and one considerably more rigidly bound molecule ($SO_2$) are found to be

| | $SH_2$ | $NH_2$ | $D_2O$ | $H_2O$ | $CH_2$ | $SO_2$ |
|---|---|---|---|---|---|---|
| Ref. | [31] | [41] | this work | [31] | this work | [42] |
| $K_{max}$ | 23 | 18 | 19 | 16 | 4 | 85 |

With the aim of increasing the convergence radius of a power series representation of the Hamiltonian for such an asymmetric rotor, H. Pickett introduced an Euler transforma-

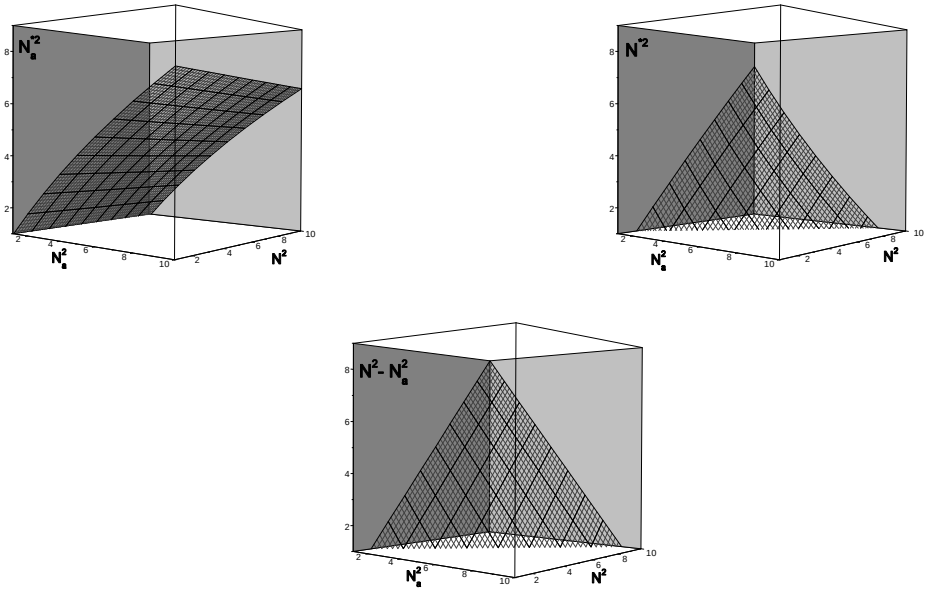


Figure 3.2: 3D plots of the absolute values of the transformed momentum operators $\mathbf{N}_a^{2*}$ and $\mathbf{N}^{2*}$ over $\mathbf{N}_a^2$ and $\mathbf{N}^2$ for arbitrary values a=0.05 and b=0.01. The bottom graph shows the sub-transformation of $\mathbf{N}^2$ to $\mathbf{N}^2 - \mathbf{N}_a^2$.

tion of the angular momentum operators to his program package SPFIT [1].
The transformation is defined in the following way:

$$\begin{aligned} (\mathbf{N}_i^2, \mathbf{N}^2) &\rightarrow (\mathbf{N}_i^{2*}, \mathbf{N}^{2*}) \qquad\qquad i = a,\, b,\, c \\ \mathbf{N}_i^{2*} &= \frac{\mathbf{N}_i^2}{1 + a\mathbf{N}_a^2 + b(\mathbf{N}^2 - \mathbf{N}_a^2)}, \\ \mathbf{N}^{2*} &= \frac{\mathbf{N}^2 - \mathbf{N}_a^2}{1 + a\mathbf{N}_a^2 + b(\mathbf{N}^2 - \mathbf{N}_a^2)} \end{aligned} \tag{3.31}$$

The result of this one-to-one mapping for a given range of values $N_i^2, N^2$ is a compression to a smaller range of values. In one dimension and with $a = 1$, the function $x \rightarrow z = f(x) := \frac{x}{1+x}$ will map the whole set of natural numbers into the interval [0..1] , $f : \mathbb{N} \rightarrow \{0..1\}$. For $N^{2*}$ an additional sub-transformation $N^2 \rightarrow N^2 - N_a^2$ is done, which naturally accounts for the constraint $N_a^2 \leq N^2$ and yields better decorrelation of the parameters. The results of both the overall transformation (Equation 3.31) and the sub-transformation alone is visualised in Figure 3.2 with arbitrary chosen values for $a$ and $b$. In the actual fitting procedure, the scaling parameters $a$ and $b$ can vary for the diagonal and the off-diagonal terms. In this case the parameters are denoted $a$, $b$ and $a_{off}$, $b_{off}$, respectively.

The expansion of the Hamiltonian (in the following called Euler expansion) can then be written in analogy to the standard A-reduction as:

$$\begin{aligned} H_{rot}^E &= \sum_{P,Q} X_{P,Q} \cdot \left(\mathbf{N}_a^{2*}\right)^P \cdot \left(\mathbf{N}^{2*}\right)^Q \\ &+ \sum_{P,Q} \frac{1}{2}\, Y_{P,Q} \cdot \left\{ \left(\mathbf{N}_a^{2*}\right)^P \cdot \left(\mathbf{N}^{2*}\right)^Q, \mathbf{N}_b^{2*} - \mathbf{N}_c^{2*} \right\} \end{aligned} \tag{3.32}$$

When employing any expansion of the Hamiltonian for fitting a rotational spectrum, the power series have to be truncated at an appropriate term. However, let us stay, for the moment, with the infinite sums. From the transformation rules 3.31 it is straightforward to find an expression of the new expansion coefficients $X_{P,Q}$ and $Y_{P,Q}$ with respect to the former ones $f_{m,n}$ and $g_{m,n}$:

$$X_{P,Q} = \sum_{r=0}^{P} \sum_{m=0}^{P-r} \sum_{n=r}^{Q+r} f_{m,n} \frac{n!\,(P+Q-1)!\,a_K^{P-m-r}\,b_J^{Q-n+r}}{r!(n-r)!(m+n-1)!(P-m-r)!(Q-n+r)!} \tag{3.33}$$

$$Y_{P,Q} = \sum_{r=0}^{P} \sum_{m=0}^{P-r} \sum_{n=r}^{Q+r} g_{m,n} \frac{n!\,(P+Q)!\,a_K^{P-m-r}\,b_J^{Q-n+r}}{r!(n-r)!(m+n)!(P-m-r)!(Q-n+r)!} \tag{3.34}$$

and vice versa:

$$f_{m,n} = \sum_{r=0}^{m} \sum_{P=0}^{m-r} \sum_{Q=r}^{n+r} X_{P,Q} \frac{Q!\,(m+n-1)!\;(a_K-b_J)^{m-P-r}\;b_J^{n-Q+r}\,(-1)^{r+P+Q-m-n}}{r!(Q-r)!(P+Q-1)!(m-P-r)!(n-Q+r)!} \tag{3.35}$$

$$g_{m,n} = \sum_{r=0}^{m} \sum_{P=0}^{m-r} \sum_{Q=r}^{n+r} Y_{P,Q} \frac{Q!\,(m+n)!\;(a_K-b_J)^{m-P-r}\;b_J^{n-Q+r}\,(-1)^{r+P+Q-m-n}}{r!(Q-r)!(P+Q)!(m-P-r)!(n-Q+r)!} \tag{3.36}$$

If we define an order $k$ of the expansion coefficients in a way that $k = m + n$ for the diagonal and $k = m+n+1$ for the off-diagonal terms (resp. $l = P+Q$ and $l = P+Q+1$ in the Euler expansion), it is important to note that for the calculation of a parameter of the order $k$ in the A-reduction no Euler terms with $l > k$ are participating, and vice versa.

The conversion formulae for the lowest terms are given explicitly in Tables 3.2 and 3.3.

Table 3.2: Explicit formulae to transform expansion coefficients of the $A$-reduced Watson-type Hamiltonian into Euler coefficients.

| Euler | Watson |
|---|---|
| $X_{0,1}$ | $f_{0,1}$ |
| $X_{1,0}$ | $f_{0,1} + f_{1,0}$ |
| $X_{0,2}$ | $f_{0,1}b_J + f_{0,2}$ |
| $X_{1,1}$ | $f_{0,1}b_J + 2f_{0,2} + f_{1,0}b_J + f_{1,1} + f_{0,1}a_K$ |
| $X_{2,0}$ | $f_{0,1}a_K + f_{1,1} + f_{0,2} + f_{1,0}a_K + f_{2,0}$ |
| $X_{0,3}$ | $f_{0,1}b_J^2 + 2f_{0,2}b_J + f_{0,3}$ |
| $X_{1,2}$ | $f_{0,1}b_J^2 + 4f_{0,2}b_J + 3f_{0,3} + f_{1,0}b_J^2 + 2f_{1,1}b_J + f_{1,2} + 2f_{0,1}a_Kb_J + 2f_{0,2}a_K$ |
| $X_{2,1}$ | $2f_{0,1}a_Kb_J + 4f_{0,2}a_K + 2f_{1,1}b_J + 2f_{1,2} + 2f_{0,2}b_J + 3f_{0,3} + 2f_{1,0}a_Kb_J$ $+2f_{1,1}a_K + 2f_{2,0}b_J + f_{2,1} + f_{0,1}a_K^2$ |
| $X_{3,0}$ | $f_{0,1}a_K^2 + 2f_{1,1}a_K + f_{2,1} + 2f_{0,2}a_K + f_{1,2} + f_{0,3} + f_{1,0}a_K^2 + 2f_{2,0}a_K + f_{3,0}$ |
| $Y_{0,0}$ | $g_{0,0}$ |
| $Y_{0,1}$ | $g_{0,0}b_J + g_{0,1}$ |
| $Y_{1,0}$ | $g_{0,1} + g_{1,0} + g_{0,0}a_K$ |
| $Y_{0,2}$ | $g_{0,0}b_J^2 + 2g_{0,1}b_J + g_{0,2}$ |
| $Y_{1,1}$ | $2g_{0,1}b_J + 2g_{0,2} + 2g_{1,0}b_J + g_{1,1} + 2g_{0,0}a_Kb_J + 2g_{0,1}a_K$ |
| $Y_{2,0}$ | $2g_{0,1}a_K + g_{1,1} + g_{0,2} + 2g_{1,0}a_K + g_{2,0} + g_{0,0}a_K^2$ |

Table 3.3: Explicit formulae for the conversion from Euler expansion coefficients to Watson rotational parameters in the $A$-reduction

| Watson | Euler |
|---|---|
| $f_{0,1}$ | $X_{0,1}$ |
| $f_{1,0}$ | $-X_{0,1} + X_{1,0}$ |
| $f_{0,2}$ | $-X_{0,1}b_J + X_{0,2}$ |
| $f_{1,1}$ | $X_{0,1}b_J - 2X_{0,2} - X_{1,0}b_J + X_{1,1} - X_{0,1}(a_K - b_J)$ |
| $f_{2,0}$ | $X_{0,1}(a_K - b_J) - X_{1,1} + X_{0,2} - X_{1,0}(a_K - b_J) + X_{2,0}$ |
| $f_{0,3}$ | $X_{0,1}b_J^2 - 2X_{0,2}b_J + X_{0,3}$ |
| $f_{1,2}$ | $-X_{0,1}b_J^2 + 4X_{0,2}b_J - 3X_{0,3} + X_{1,0}b_J^2 - 2X_{1,1}b_J + X_{1,2}$ $+2X_{0,1}(a_K - b_J)b_J - 2X_{0,2}(a_K - b_J)$ |
| $f_{2,1}$ | $-2X_{0,1}(a_K - b_J)b_J + 4X_{0,2}(a_K - b_J) + 2X_{1,1}b_J - 2X_{1,2} - 2X_{0,2}b_J$ $+3X_{0,3} + 2X_{1,0}(a_K - b_J)b_J - 2X_{1,1}(a_K - b_J) - 2X_{2,0}b_J$ $+X_{2,1} + X_{0,1}(a_K - b_J)^2$ |
| $f_{3,0}$ | $-X_{0,1}(a_K - b_J)^2 + 2X_{1,1}(a_K - b_J) - X_{2,1} - 2X_{0,2}(a_K - b_J) + X_{1,2}$ $-X_{0,3} + X_{1,0}(a_K - b_J)^2 - 2X_{2,0}(a_K - b_J) + X_{3,0}$ |
| $g_{0,0}$ | $Y_{0,0}$ |
| $g_{0,1}$ | $Y_{0,1} - Y_{0,0}b_J$ |
| $g_{1,0}$ | $-Y_{0,1} + Y_{1,0} - Y_{0,0}(a_K - b_J)$ |
| $g_{0,2}$ | $-2Y_{0,1}b_J + Y_{0,2} + Y_{0,0}b_J^2$ |
| $g_{1,1}$ | $2Y_{0,1}b_J - 2Y_{0,2} - 2Y_{1,0}b_J + Y_{1,1} - 2Y_{0,1}(a_K - b_J) + 2Y_{0,0}(a_K - b_J)b_J$ |
| $g_{2,0}$ | $2Y_{0,1}(a_K - b_J) - Y_{1,1} + Y_{0,2} - 2Y_{1,0}(a_K - b_J) + Y_{2,0} + Y_{0,0}(a_K - b_J)^2$ |

### Quartic and Sextic Planarity Conditions

There exist additional restrictions on the spectroscopic parameters for planar molecules. For a rigid rotor, one would expect, for example, the following relation between the principal moments of inertia $I_i$

$$I_c = I_a + I_b. \tag{3.37}$$

Due to vibrational interaction, however, this condition is not fulfilled in those cases where the moments of inertia are obtained from effective ground state rotational parameters $A_0$, $B_0$, $C_0$ instead of equilibrium parameters, and the inertial defect is defined in the way

$$\Delta = I_c - I_a - I_b. \tag{3.38}$$

Similarly, planarity relations and their defects can be found for the centrifugal distortion parameters.

The quartic and sextic planarity conditions for an asymmetric rotor in the standard $A$-reduction of the Hamiltonian ($I^r$ representation, prolate limit) can be written in the following form [31]:

$$4\,C\Delta_J - (B-C)\,\Delta_{JK} - 2\,(2\,A+B+C)\,\delta_J + 2\,(B-C)\,\delta_K = \Delta_Q = 0 \tag{3.39}$$

$$\begin{aligned} & 6\,C\,\Phi_J - (B-C)\,\Phi_{JK} - 2\,(2\,A+B+3\,C)\,\phi_J \\ + \;& 2\,(B-C)\,\phi_{JK} + 4\,\Delta_J^2 - 4\,\delta_J\,(4\,\Delta_J + \Delta_{JK} - 2\,\delta_J - 2\,\delta_K) \\ = \;& \Delta_S = 0 \end{aligned} \tag{3.40}$$

where $\Delta_Q$ and $\Delta_S$ are the quartic and sextic centrifugal defects.

These conditions can be expressed with corresponding parameters of the Euler expansion of the Hamiltonian, making use of the conversion formulae given in the previous section:

$$\begin{aligned} - \;& 4\,(X_{0,1} - 2\,Y_{0,0})\,(-X_{0,1}\,b_J + X_{0,2}) \\ + \;& 4\,Y_{0,0}\,(X_{0,1}\,b_J - 2\,X_{0,2} - X_{1,0}\,b_J + X_{1,1} - X_{0,1}\,(a_K - b_J)) \\ + \;& 4\,(X_{0,1} + X_{1,0})\,(Y_{0,1} - Y_{0,0}\,b_J) - 8\,Y_{0,0}\,(-Y_{0,1} + Y_{1,0} - Y_{0,0}\,(a_K - b_J)) \\ = \;& \Delta_Q^E = 0 \end{aligned} \tag{3.41}$$

$$\begin{aligned} & 6\,(X_{0,1} - 2\,Y_{0,0})\left(X_{0,1}\,{b_J}^2 - 2\,X_{0,2}\,b_J + X_{0,3}\right) \\ - \;& 4\,Y_{0,0}\left(-3\,X_{0,1}\,{b_J}^2 + 6\,X_{0,2}\,b_J - 3\,X_{0,3} + X_{1,0}\,{b_J}^2 - 2\,X_{1,1}\,b_J + X_{1,2}\right. \\ + \;& \left. 2\,X_{0,1}\,a_K\,b_J - 2\,X_{0,2}\,a_K\right) \\ - \;& 2\,(4\,X_{0,1} + 2\,X_{1,0} - 4\,Y_{0,0})\left(-2\,Y_{0,1}\,b_J + Y_{0,2} + Y_{0,0}\,{b_J}^2\right) \\ + \;& 8\,Y_{0,0}\,(4\,Y_{0,1}\,b_J - 2\,Y_{0,2} - 2\,Y_{1,0}\,b_J + Y_{1,1} - 2\,Y_{0,1}\,a_K + 2\,Y_{0,0}\,(a_K - b_J)\,b_J) \\ + \;& 4\,(-X_{0,1}\,b_J + X_{0,2})^2 \\ + \;& 4\,(Y_{0,1} - Y_{0,0}\,b_J)\,(2\,X_{0,1}\,b_J - 2\,X_{0,2} + X_{1,0}\,b_J - X_{1,1} + X_{0,1}\,a_K \\ + \;& 2\,Y_{1,0} - 2\,Y_{0,0}\,a_K) \\ = \;& \Delta_S^E = 0 \end{aligned} \tag{3.42}$$

where the superscript $E$ denotes parameters in the Euler expansion.

### 3.3.3 Asymmetric Rotors with Electronic and Nuclear Spin - Methylene

For molecules with unpaired electrons, interaction terms originating from resultant electronic angular momentum $\mathbf{L}$, as well as electronic spin $\mathbf{S}$ have to be included in the Hamiltonian [31]:

$$H = H_{vib,rot} + H_{fs} + H_{hfs}$$

The first term denotes the rotational or rovibrational part, described earlier in this Chapter, the second term is the fine structure term summarising all contributions of the electronic angular momentum and spin, and the last term represents the hyperfine contribution due to nuclear interactions. Each of the fine and hyperfine structure terms itself consists of individual contributions. The general appearance of these terms is manifold and depends upon the utilised coupling scheme, the strength of the individual interaction and the molecular symmetry. For reasons of clarity, I will in the following only concentrate on the special case of methylene in its electronic ground state.

The methylene radical $CH_2$ possesses a $X\ ^3B_1$ electronic ground state with a total electron spin $S = |\mathbf{S}| = 1$ from its two unpaired electrons with $s = 1/2$. The spin couples to the rotational angular momentum $\mathbf{N}$ via the weak magnetic field generated by the rotation of the molecule, to give the resultant angular momentum $\mathbf{J} = \mathbf{N} + \mathbf{S}$. This coupling is formally known as Hund's case (b) and yields a fine structure splitting of each rotational level into a triplet with $J = N - 1,\ N,\ N + 1$. $N$ is in a strict sense not a good quantum number anymore, but will be used to designate the rotational energy levels. Furthermore, the nuclear spins $\mathbf{I}$, $I = 1/2$ of the two H-atoms have to be considered.

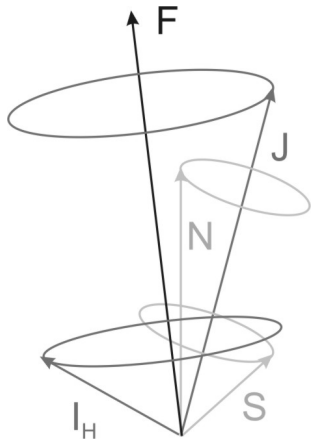


Figure 3.3: Coupling scheme for $CH_2$ in Hund's case (b).

Since they are equivalent, it is most appropriate to employ a coupling scheme, where in a first step the nuclear spins are coupled to give a resultant $\mathbf{I_H}$ of either 1 or 0. This total nuclear spin then couples to $\mathbf{J}$ to form the resultant angular momentum $\mathbf{F} = \mathbf{I_H} + \mathbf{J}$. It is obvious that in the case of para-$CH_2$, i.e. in the case of $I_H = 0$, the coupling vanishes and $J$ stays a good quantum number. For ortho-$CH_2$, with $I_H = 1$, each fine structure level will further split into a hyperfine triplet with quantum numbers $F = J - 1,\ J,\ J + 1$.

The analysis follows the work by Sears [43] and references therein.
The fine structure interaction consists of spin-spin and spin-rotation interaction terms

$$H_{fs} \;=\; H_{spin-spin} \;+\; H_{spin-rot} \tag{3.43}$$

$$\begin{aligned} H_{spin-spin} &= \alpha(3S_z^2 - \mathbf{S}^2) + \beta(\mathbf{S_x^2} - \mathbf{S_y^2}) && (3.44)\\ H_{spin-rot} &= \frac{1}{2}\sum_{\alpha,\beta}\epsilon_{\alpha,\beta}(\mathbf{N}_\alpha\mathbf{S}_\beta + \mathbf{S}_\beta\mathbf{N}_\alpha), && (3.45) \end{aligned}$$

where the subscripts $\alpha$, $\beta$ and $x$, $y$, $z$ both refer to the molecule-fixed axes. Centrifugal distortion terms depending on the rotational angular momentum operator $\mathbf{N}$ and its projection along the $a$-axis ,$\mathbf{N_a}$, can be included for the spin-spin interaction term:

$$\begin{aligned} \alpha_{eff} &= \alpha + \alpha_{SN}\mathbf{N^2} + \alpha_{SK}\mathbf{N_a^2} && (3.46)\\ \beta_{eff} &= \beta + \beta_{SN}\mathbf{N^2} + \beta_{SK}\mathbf{N_a^2}. && (3.47) \end{aligned}$$

For the spin-rotation interaction, one can also include centrifugal distortion terms. This has been worked out for an asymmetric rotor molecule in the $A$-reduction by Brown and Sears [44]:

$$\begin{aligned} H^{cf}_{spin-rot} &= \Delta_N^S\mathbf{N^2}(\mathbf{N}\cdot\mathbf{S}) \;+\; 1/2\Delta_{NK}^S\{\mathbf{N^2N_zS_z} \;+\; \mathbf{N_zS_zN^2}\} && (3.48)\\ &+\; \Delta_{KN}^S N_z^2(\mathbf{N}\cdot\mathbf{S}) \;+\; \Delta_K^S N_z^3\mathbf{S_z} \;+\; \delta_N^S(\mathbf{N_+^2} \;+\; \mathbf{N_-^2})(\mathbf{N}\cdot\mathbf{S})\\ &+\; 1/2\delta_K^S\{(\mathbf{N_+^2} \;+\; \mathbf{N_-^2})\mathbf{N_zS_z} \;+\; \mathbf{N_zS_z}(\mathbf{N_+^2} + \mathbf{N_-^2})\} \end{aligned}$$

The largest contributions to the hyperfine interaction are caused by magnetic interaction between the electron spin $\mathbf{S}$, $S = 1$, and the nuclear spin $I_H$. Hyperfine structure is, therefore, only present in the case of ortho-$CH_2$ with the hydrogen nuclear spins coupled to give $I_H = 1$.

$$H_{hfs} \;=\; H_F \;+\; H_{DD} \;=\; a_F(H)\mathbf{I}\cdot\mathbf{S} \;+\; \mathbf{S}\cdot\mathbf{T}\cdot\mathbf{I}. \tag{3.49}$$

The first term takes account of the isotropic Fermi contact interaction, and the second term represents the dipole-dipole interaction of the protons with the unpaired electron spins. This coupling is mediated via the second-rank traceless tensor $\mathbf{T}$, in general, only the two independent diagonal elements, for example $T_{aa}$ and $T_{bb}$, are determined in the fit. The off-diagonal $T_{ab}$ element causes a mixing of ortho and para states, but can only be determined by its effect on accidental nearly degenerate states with $\Delta K_a = 1$ and $\Delta K_c = 0,\ 2,\ ...$, which are not likely to be found for light dihydrides. Effective centrifugal distortion terms of the form

$$a_{Feff} \;=\; a_F \;+ a_{FN}\mathbf{N^2} \;+ a_{FK}\mathbf{K_a^2}, \tag{3.50}$$

can be defined. Direct nuclear spin-rotation and nuclear spin-spin interaction terms are usually some orders of magnitude weaker and have not been included in the analysis. The form of this interactions is discussed in the next section for the water molecule.

Since for the laboratory measurements of $CH_2$ a Zeeman-modulation was applied, the general expression for the Hamiltonian has to include an interaction term due to the external magnetic field. The form of this term has been discussed in some detail in Section 2.2.1. However, the experiment yields the field-free transition frequencies. For the global analysis of methylene, presented in Chapter 5, Section 5.3, this term has, therefore, been omitted from the Hamiltonian.

### 3.3.4 The Hyperfine Structure of Water

Water, in contrast to methylene, does not possess any resulting electronic spin. Hyperfine interactions of the deuterated water species HDO and $D_2O$ are caused by the magnetic coupling of the nuclear spins of the H and D nuclei to the molecular rotation and by spin-spin coupling of the two nuclear spins. Additionally, in the case of deuterium, the coupling of the nuclear electric quadrupole moment to the electric field gradient has to be taken into account.

The general form of the quadrupole interaction 3.13 in Section 3.2.2 applies to asymmetric rotor molecules also. However, there exist no analytical expression for $q_J$. The most general form, which has been used in the analysis, is

$$E_Q = \frac{2}{J(J+1)} Y(J,\, I,\, F) \sum_{g=a,b,c} \chi_{gg} \langle J_g^2 \rangle \tag{3.51}$$

where $\chi_{gg} = eQ\, q_{gg}$ is the diagonal element of the quadrupole coupling tensor in direction of the principal axis of the moment of inertia $g$, and $\langle J_g^2 \rangle$ is the average value of $J_g^2$ with respect to the asymmetric rotor wavefunctions. The quadrupole coupling tensor is traceless and only two elements can be deduced from experiment.

Similarly, starting from expression 3.19, the magnetic spin-rotation interaction of a nucleus in an asymmetric rotor is found to be

$$E_{mag} = \frac{1}{2J(J+1)} [F(F+1) - I(I+1) - J(J+1)] \sum_{g=a,b,c} C_{gg} \langle J_g^2 \rangle \tag{3.52}$$

where $C_{gg}$ are the diagonal elements of the magnetic coupling tensor in the principal system of the moment of inertia.

In the case of two nuclei with non-zero spin $I_1$ and $I_2$, a direct spin-spin coupling term has to be included to the Hamiltonian

$$H_{ss} = \mathbf{I_1} \cdot \mathbf{D} \cdot \mathbf{I_2} \tag{3.53}$$

where the diagonal elements of the second rank traceless coupling tensor $D$ can be calculated from geometry via (see e.g. [45])

$$D_{gg} = \frac{\mu_0}{4\pi} \frac{\mu_N^2 g_1 g_2}{r_{12}^3} (1 - 3\cos^2(\mathbf{r_{12}} \cdot \mathbf{g})) \tag{3.54}$$

with $\mathbf{r_{12}}$ the coordinate vector connecting nucleus 1 and 2, $\mu_N$ the nuclear magneton, and $\mathbf{g}$ the coordinate vector representing the principal axis $g = a, b, c$ of the moment of inertia. The $g$-factors of hydrogen and deuterium are $g_H = 5.585340$ and $g_D = 0.857392$, respectively [38]. The geometrical structure of HDO and $D_2O$ is given in Figures 6.2, and 6.1.

In general, for $H_2O$ and $D_2O$ a coupling scheme is used where the two nuclear spins of the identical particles are summed first to give a resultant $\mathbf{I_{tot}}$ which is then coupled to the rotational angular momentum $\mathbf{J}$ to give the resultant angular momentum $\mathbf{F}$. For HDO, the coupling of the deuterium nucleus to the rotation will be stronger due to the electric quadrupole interaction, and a coupling scheme with $\mathbf{F_1} = \mathbf{J} + \mathbf{I_D}$ and $\mathbf{F} = \mathbf{F_1} + \mathbf{I_H}$ is better suited to analyse the spectrum. The interactions terms have to be altered accordingly.

# 4

# Deuterium Cyanide and its Isotopomers

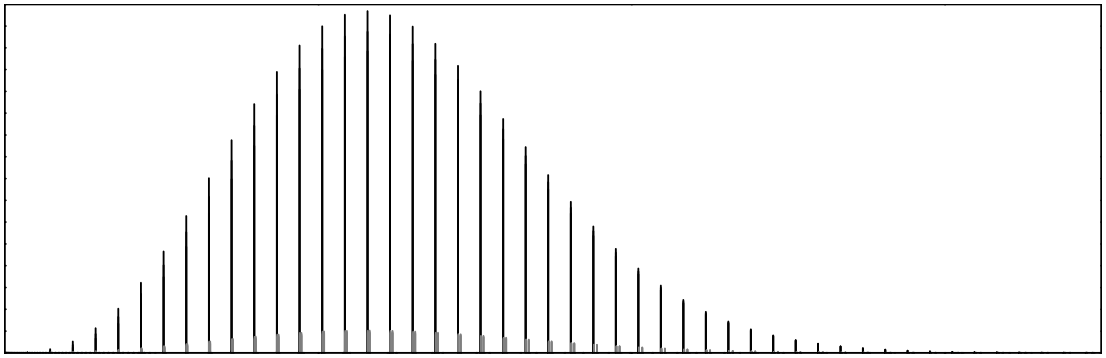

Hydrogen cyanide has been of great astrophysical interest since its first detection (of HCN and H$^{13}$CN) in the interstellar medium in 1971 [8]. The deuterated species DCN[1] and its hyperfine structure were observed soon afterwards towards the Orion star-forming region [46, 47]. In the paper presenting this first astrophysical detection of a deuterated species ever, the authors already discussed the overabundance of the D- to the H-containing isotope (DCN/HCN $\simeq 10^{-3}$) compared to terrestrial values (atomic ratio D/H $\simeq 3 - 5 \cdot 10^{-5}$). Isotopic abundance ratios provide insight into the chemical and physical evolution of the interstellar medium. In the case of deuterium-bearing species this has been theoretically discussed in detail in [48] and been applied to the HCN/DCN ratio by Roberts *et al.* [49] and Hatchell *et al.* [50]. Although the doubly and triply substituted HCN species D$^{13}$CN, DC$^{15}$N and D$^{13}$C$^{15}$N have not yet been detected in the interstellar medium, this might be feasible in the future with the aid of new, sensitive millimeter- and submillimeter-wavelength telescopes (e.g. APEX) and in consideration of the recent detection of several multi-substituted molecules like $ND_3$ [51] or $^{13}C^{17}O$ [52].

As was pointed out by Boonman *et al.* [53], energetically high-lying rotational transitions of HCN isotopes are well suited to probe the warmer, inner part of molecular cores

[1] Isotopoes not carrying a superscript are corresponding to $^{12}$C and $^{14}$N respectively

in star-forming regions with respect to the determination of molecular abundances and thereby for evolutionary effects. In the circumstellar envelope of the prototypical carbon rich star IRC+10216, Cernicharo *et al.* [9] detected rotational lines of the main isotopomer HCN as high as the $J = 48 \rightarrow 47$ transition of the $v_2 = 0$ vibrational state and the $J = 19 \rightarrow 18$ transition of several excited vibrational states. He concluded that HCN, via its strong emission lines in the FIR, is the main coolant in the case of IRC+10216. Furthermore, very recently Thorwirth *et al.* [54] were able to observe direct $\ell$-type transitions of HCN connecting energetically high-lying levels (up to $J = 14$) at relative low frequencies ($< 50$ GHz).

## 4.1 Previous Laboratory Work

The first laboratory microwave spectra of hydrogen cyanide isotopes have been reported as early as 1950 by Simmons *et al.* [55]. The pure rotational spectra of the linear triatomic HCN isotopomers exhibit both widely spaced ($B_{\mathrm{DCN}} = 36207.4622$ MHz) $R$-branch transitions with $\Delta J = 1$ and, in the first excited bending state, so-called direct $\ell$-type transitions with $\Delta J = 0$. Those latter transitions have been investigated by several authors [56, 57, 58, 59, 60, 61, 62] for all deuterated isotopic species to a varying extent. The $^{14}$N-containing species show a significant hyperfine splitting for low $J$ rotational lines, mainly due to the electric nuclear quadrupole moment of the nitrogen nucleus, and to a smaller extent to its magnetic spin-rotation interaction. The most recent publications related to this subject are by Nguyen-van-Thanh and Rossi [63] for DCN and Preusser and Maki [64] for all deuterated isotopes up to 500 GHz. However, the experimental data as presented by Preusser and Maki lacks high accuracy as it was taken with Doppler limited resolution, whereas high precision measurements are only available for DCN for the $J = 2 \leftarrow 1$ and $J = 1 \leftarrow 0$ transition [65] and for few direct $\ell$-type transitions [61].

Therefore, we started a project to investigate the rotational spectra of eight isotopic species of hydrogen cyanide with sub-Doppler resolution in the vibrational ground and first excited bending state up to 1 THz with the Cologne Terahertz Spectrometer. Furthermore, to constrain the rotational constants and to extend the frequency region where reliable transition frequency predictions are possible, additional Doppler limited measurements were undertaken in the frequency region from 1.75 to 2.01 THz with the Cologne Sideband Spectrometer for Terahertz Applications (COSSTA). The precise prediction of rest frequencies of rotational transitions at high frequencies is necessary especially with regard to the future satellite mission Herschel and the stratospheric observatory SOFIA, both equipped with high resolution receivers up to 2 THz.

I am going to report in the following on the results for the deuterated species DCN, D$^{13}$CN, DC$^{15}$N and the triply substituted species D$^{13}$C$^{15}$N. Their rotational spectra were recorded in the vibrational ground and first excited bending state ($v_2 = 0, 1$) up to 2 THz. The $R$-branch transitions from $J = 3 \leftarrow 2$ to $J = 13 \leftarrow 12$ were measured with sub-Doppler resolution. This very high resolution (FWHM $\simeq$ 70 kHz) and precise

($\pm$ 3-10 kHz) saturation dip measurements allowed for resolving the underlying hyperfine structure due to the $^{14}$N nucleus in DCN and D$^{13}$CN for transitions as high as $J = 10 \leftarrow 9$. Additionally high $J$ $R$-branch ($J = 25 \leftarrow 24$ to $J = 28 \leftarrow 27$) transitions around 2 THz and direct $\ell$-type ($\Delta J = 0$, $J = 19$ to $J = 25$) transitions from 66 to 118 GHz were recorded in Doppler-limited resolution. For the ground state of D$^{13}$C$^{15}$N the $J = 1 \leftarrow 0$ transition was measured for the first time. The transition frequency accuracies of this transition for the other deuterated species were significantly improved. These new experimental data, together with available infrared rovibrational data and previously measured direct $\ell$-type transitions, were subjected to a global least squares analysis for each isotopomer. This yielded precise sets of molecular constants for the ground and first excited vibrational states, including the nuclear quadrupole and magnetic dipole constants of the $^{14}$N nucleus for DCN and D$^{13}$CN. The hyperfine structure due to the D, $^{13}$C and $^{15}$N nuclei have not be resolved, but led to a broadening of the observed saturation dips.

The investigation of the H-containing species is partly published elsewhere [66, 67, 68, 69].

## 4.2 Experimental Setup

Three different spectrometers were used to cover the various frequency regions: the Cologne Terahertz Spectrometer, the Cologne Sideband Spectrometer for Terahertz Applications and the AMC spectrometer. A detailed description of these systems has been given in Chapter 2. In this context, Section 2.1.1 is of special interest, summarising the requirements for performing sub-Doppler measurements with the Cologne Terahertz Spectrometer.

All measurements on the deuterated species were performed with isotopic enriched samples ($> 50\%$). The synthesis was done by the standard method introduced by King and Nixon [70] with isotopical enriched KCN samples and $D_2O$. The sample pressure was between $8 \times 10^{-3}$ and $0.15$ Pa for the sub-Doppler measurements, from $0.1$ to $1$ Pa for the high frequency $R$-branch and around $1$ Pa for the direct $\ell$-type transitions. For these latter measurements the absorption cell was heated to $\sim 500$ K with a resistive heating band.

## 4.3 Measurements

About 40 rotational transitions have been measured for each of the four deuterium cyanide isotopes DCN, D$^{13}$CN, DC$^{15}$N, D$^{13}$C$^{15}$N in the vibrational ground and first excited bending state making use of the three spectrometers described in Chapter 2. The recorded spectra vary according to molecular and spectrometer characteristics. Figures 4.3 to 4.12 display exemplary spectra for each frequency region. As has been elucidated in more detail in Section 3.2.2, for the isotopic species containing the $^{14}$N ($I_N = 1$) nucleus, each

rotational energy level (with the exception of the $J = 0$ state) is split into a triplet. This splitting causes a noticeable hyperfine structure in the low frequency rotational spectra. The lowest $J = 1 \leftarrow 0$ ground state transition, a hyperfine triplet, can be fully resolved with Doppler-limited techniques as shown in Fig. 4.3. According to the electric dipole selection rules ($\Delta J = 1$, $\Delta F = 0, \pm 1$) the hyperfine pattern of all higher $J$ transitions consists of a hyperfine sextett.

Figure 4.1 displays the calculated energy level scheme of the $J = 4$ and $J = 3$ rotational levels of ground state DCN. In addition to the considerable large hyperfine splitting due to the $^{14}$N nucleus, calculated splittings into additional triplets due to the deuterium nucleus are shown also, even though these lie in the kHz range and where not resolved in this study. The appropriate parameters for DCN were taken from different sources: the electric nuclear quadrupole interaction constant $eqQ_D = 194.4 \pm 2.2$ kHz and the magnetic spin-rotation interaction constant $C_D = -0.6 \pm 0.3$ kHz are from [65], whereas the spin-spin interaction constant $S_{DN}$, describing the interaction between the D and the N nuclei, was calculated from geometry *via*

$$S_{DN}[\text{kHz}] = -3.85 \cdot \frac{g_D\, g_N}{(r_{DN}[\text{Å}])^3} = -0.122\,\text{kHz} \tag{4.1}$$

with the gyromagnetic ratios $g_D = 0.857$, $g_{^{14}N} = 0.4036$ [38] and the nuclear distance $r_{DN} = 2.2187$Å from experimental equilibrium $r_e$ values [71]. The calculated splittings are of the order of the expected linewidth of the saturation dips and do therefore cause a broadening of the measured lines.

Since the $\Delta F = -1$ transitions were too weak to be detected in this experiment, Figs. 4.4 - 4.5 show only five saturation dips. The three $\Delta F = +1$ hyperfine components form a closely confined inner triplet, whereas the two $\Delta F = 0$ transitions are clearly separated and more widely spaced. In Fig. 4.5 a recorded Doppler-limited spectrum is superimposed on the saturation dip records, revealing no trace of the underlying hyperfine structure.

In the sequence of Figs 4.5 - 4.8 three characteristics of the performed saturation dip measurements are exemplified:
(i) With increasing $J$-value the separation of the inner $\Delta F = 1$ components decreases[2]. As an example, the $J$ dependency of the hyperfine splitting of the vibrational ground state of DCN is shown in Figure 4.2. In the case of the displayed D$^{13}$CN $J = 7 \leftarrow 6$ transition (Fig. 4.6) the separation of the hyperfine components is only ∼20 kHz and thereby below the achieved sub-Doppler resolution of ∼50 kHz.
(ii) The intensity of the observed $\Delta F = 0$ hyperfine transitions decrease faster with $J$ as the corresponding $\Delta F = 1$ transitions (relative intensity $\sim 1/J^2$) and could therefore be detected up to $J = 9 \leftarrow 8$.
(iii) For intermediate values of $J$ (Figs. 4.5- 4.7) additional saturation dips appear in the

[2]This behaviour is determined by the nuclear hyperfine constants (see chapter 4.4), therefore it differs in the ground and first excited bending state. The order of the hyperfine components is different in both states and for the $v_2 = 1^{e,f}$ the aforementioned assertion is not strictly true in the case of small $J$.

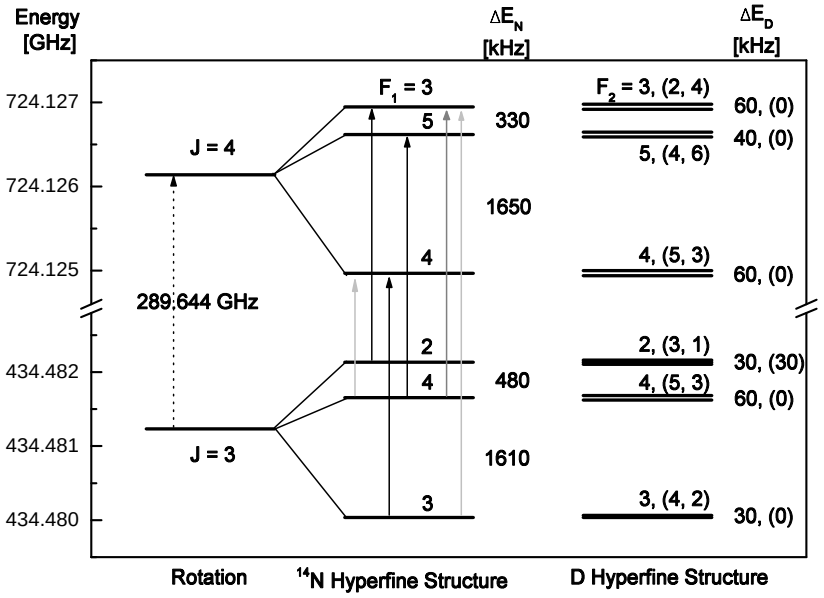


Figure 4.1: The calculated energy level scheme of the $J = 4 \leftarrow 3$ rotational transition of DCN ($v_2$=0). The hyperfine splitting due to the $^{14}$N nucleus lies in the MHz range, whereas the shown splitting caused by the deuterium nucleus is considerably smaller. Numbers in parentheses give the splitting for the much closer levels with $F_2 = (J - 1,\ J + 1)$. For further explanation refer to the text.

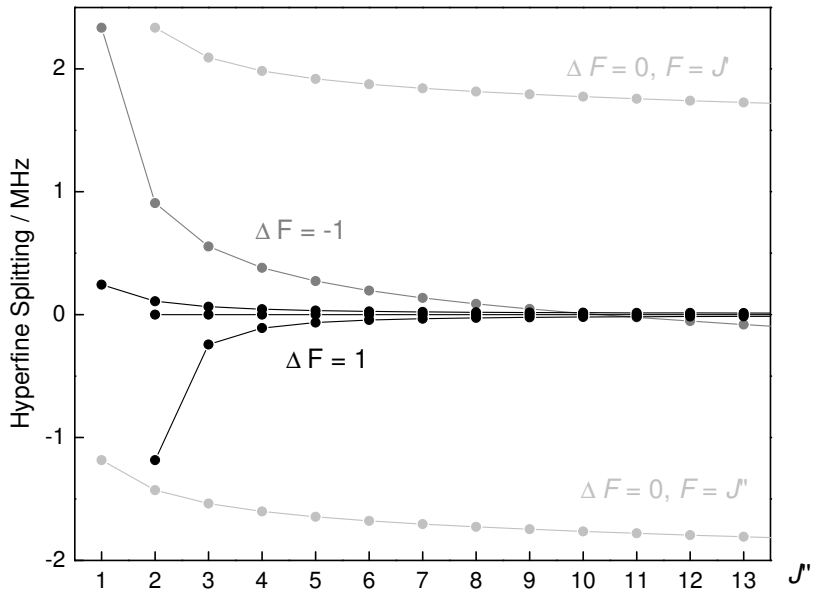


Figure 4.2: Calculated frequency shift of each DCN hyperfine transition in the vibrational ground state with respect to the unsplit line center over $J$". The colour coding is equivalent to that in Figure 4.1

spectra, as has been outlined already in Section 2.1.1. These so called crossover dips are generated if the incoming and the reflected wave interact with the same velocity class of molecules but via different transitions sharing one common level. Since this can only happen if the frequency separation of the two participating transitions is smaller than the Doppler linewidth (and the Doppler linewidth increases with frequency), no crossover dips appear in Fig. 4.4, because in this case the separation of the corresponding hyperfine components is too large. The labelling of the dips is done according to the participating hyperfine transitions, e.g. the $C_{87} - C_{77}$ saturation dip is generated by the $J_F : 7_8 \leftarrow 6_7$ and $7_7 \leftarrow 6_7$ transitions, thereby sharing a common lower level. The crossover dips occur at the arithmetic average frequency of the involved hyperfine components and might therefore be helpful to obtain additional frequency information, since only one of the unresolved $\Delta F = 1$ triplet components forms a crossover dip with a $\Delta F = 0$ transition. There is, however, in general an overlap of two crossover dips (one connecting states of common lower, one of common upper level)[3]. A more detailed analysis of the theory of crossover dips can be found in [26].

Although the two isotopic species DC$^{15}$N and D$^{13}$C$^{15}$N do not exhibit a measurable hyperfine structure, they were nevertheless measured in sub-Doppler resolution in the frequency range from 400 to 900 GHz with the objective of improved frequency accuracy (a factor of 5-10 for most lines). Exemplary spectra are shown in Figs. 4.9 and 4.10.
Both the transitions in the high frequency region (1.75 to 2.01 THz, Fig. 4.11) and the direct $\ell$-type transitions (Fig. 4.12) were recorded in Doppler resolution.

The splittings according to the D, $^{13}$C and $^{15}$N nuclear spin-rotation, electric quadrupole coupling and spin-spin interactions were not resolved in this experiment. I performed, however, calculations including the interaction of all participating nuclei. Corresponding spin rotation and electric nuclear quadrupole interaction constants have been taken from de Lucia and Gordy [65] (DCN), Garvey and de Lucia (D$^{13}$CN) [72] and Cazzoli and Dore (DC$^{15}$N) [73]. In those cases where no spin-rotation parameters were available from literature, they were estimated on condition that:

$$\frac{C_I}{g_I B} = const. \tag{4.2}$$

for all isotopic species and for all nuclei. Spin-spin interaction parameters were calculated from equation 4.1.

Whereas the calculated splitting of the strong $\Delta F = 1$ hyperfine components lies with a few kHz well below the achieved sub-Doppler resolution, it might cause a substantial broadening of the lines, as has been discussed already for the case of DCN.

A short summary of the dataset obtained in this study is given in Table 4.1, indicating especially which measurements were performed with sub-Doppler resolution. Tables containing all experimental transition frequencies used in the analysis can be found in the Appendices A.1-A.10.

[3]It is to be noted that the frequency difference of the two generated crossover dips is half that of the

Table 4.1: Summary of the measurements performed with the different Cologne spectrometers on DCN isotopomers in the vibrational ground (000) and first excited bending state (010). $J''$ denotes the lower level of the transition.

| | Low frequency [a] 66-117 GHz (AMC) | Sub-Doppler 207-960 GHz (THz-spectrometer) | High frequency 1.75-2.01 THz (COSSTA) |
|---|---|---|---|
| DCN | $J$ = 19, 20, 22-24 | (000) $J''$ = 2-12 | (000), (010) $J''$ = 25, 26 |
| | $J''$ = 0 | (010) $J''$ = 2-3, 5-9, 11-12 | |
| $D^{13}CN$ | $J$ = 19-25 | (000) $J''$ = 2-12 | (000), (010) $J''$ = 26, 27 |
| | $J''$ = 0 | (010) $J''$ = 2-12 | |
| $DC^{15}N$ | $J$ = 19-25 | (000) $J''$ = 2-6, 8-12 | (000), (010) $J''$ = 24-27 |
| | $J''$ = 0 | (010) $J''$ = 2-9, 11-12 | |
| $D^{13}C^{15}N$ | $J$ = 19-25 | (000) $J''$ = 2-6, 8-12 | (000), (010) $J''$ = 25-28 |
| | $J''$ = 0 | (010) $J''$ = 2-6, 8-12 | |

[a] In the first row, direct $\ell$-type transitions are summarised ($\Delta J = 0$).

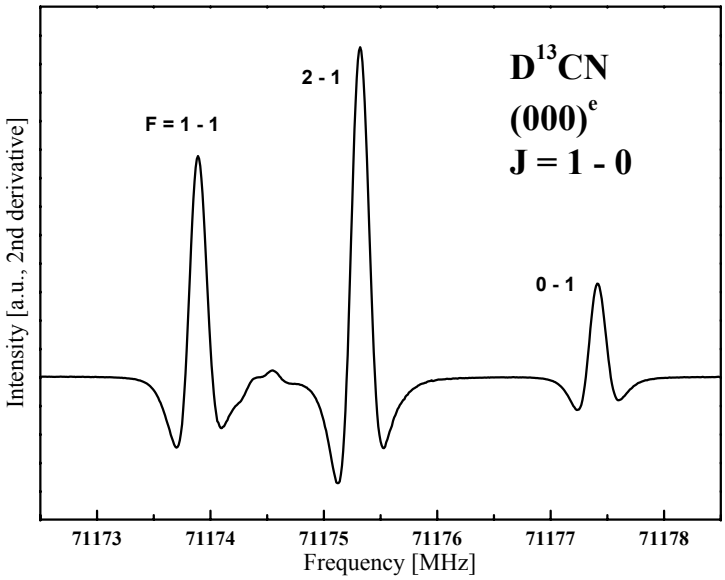


Figure 4.3: The $J = 1 \leftarrow 0$ rotational transition of $D^{13}CN$ in the ground vibrational state recorded in Doppler resolution with the AMC-spectrometer. The three allowed hyperfine components are labelled.

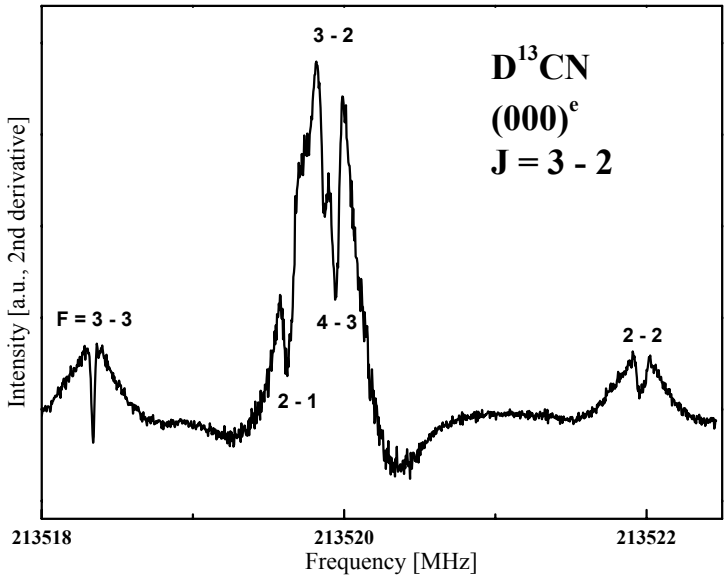


Figure 4.4: The $J = 3 \leftarrow 2$ rotational transition of $D^{13}CN$ in the vibrational ground state recorded in sub-Doppler resolution with the Cologne Terahertz Spectrometer. The five strongest saturation dips are resolved and identified.

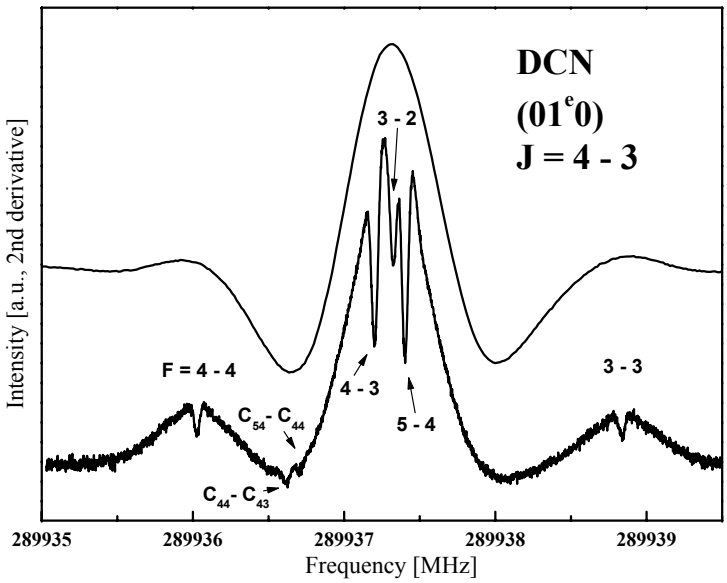


Figure 4.5: The $J = 4 \leftarrow 3$ rotational transition of DCN in the first excited bending state (010) recorded in sub-Doppler. For comparison, a Doppler-limited recording of the same transition is presented.

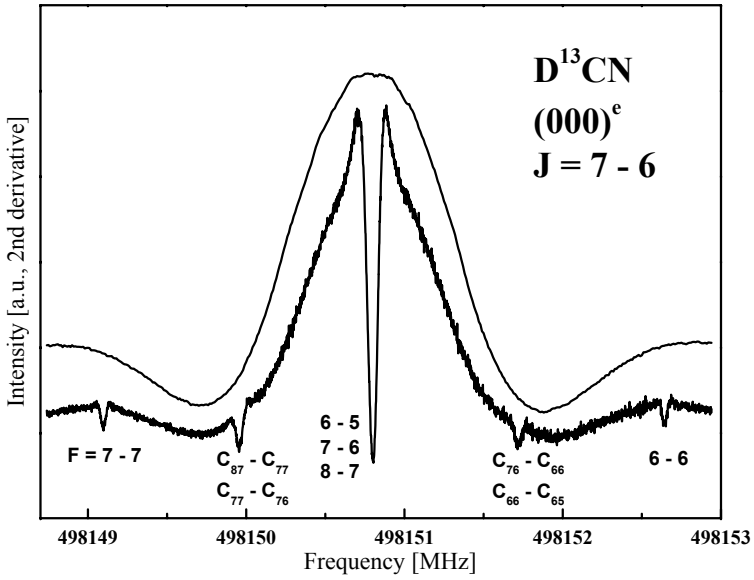


Figure 4.6: The $J = 7 \leftarrow 6$ rotational transition of $D^{13}CN$ in the vibrational ground state recorded in sub-Doppler resolution. The inner hyperfine components are not resolved. Two visible crossover transitions (explanation see text) are labelled.

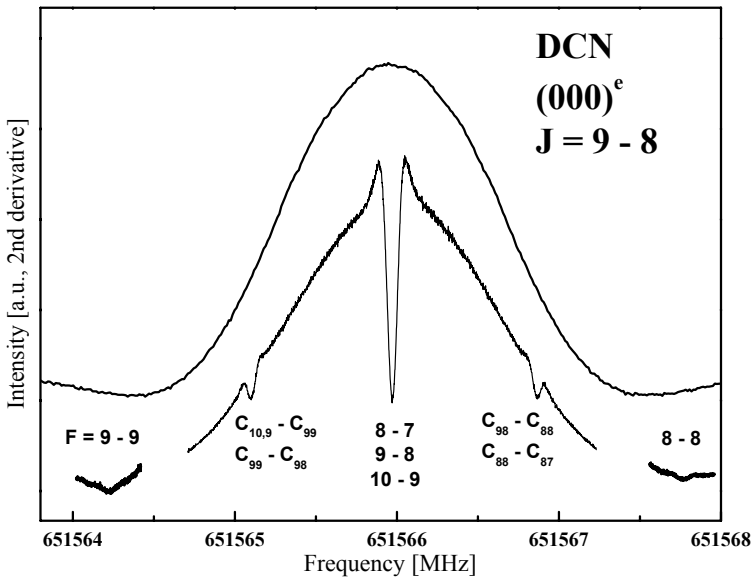


Figure 4.7: The $J = 9 \leftarrow 8$ rotational transition of DCN in the vibrational ground state recorded in sub-Doppler resolution. The intensity of the $\Delta F = 0$ components decreases faster than those of the $\Delta F = 1$ transitions.

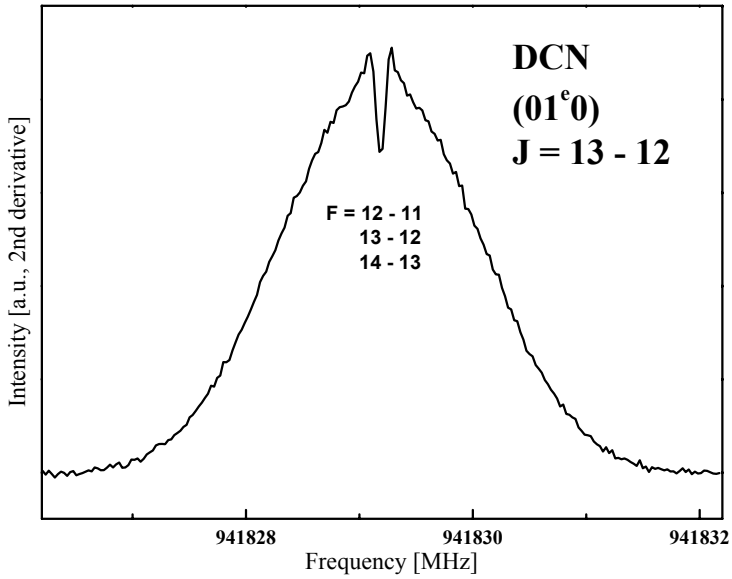


Figure 4.8: The $J = 13 \leftarrow 12$ rotational transition of DCN in the $v_2 = 1^e$ state is one of the highest transitions measured in sub-Doppler resolution. Only the unresolved inner hyperfine triplet can be seen superimposed on the Doppler broadened lineshape.

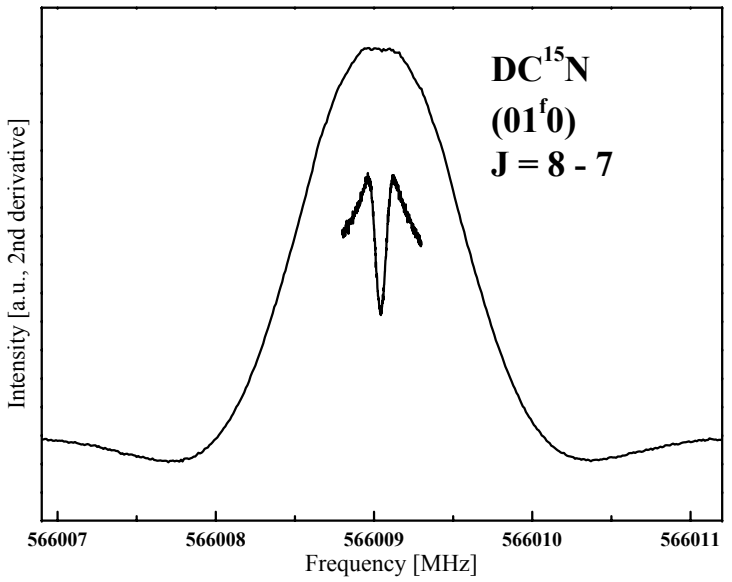


Figure 4.9: The $J = 8 \leftarrow 7$ rotational transition of $DC^{15}N$ in the $v_2 = 1^f$ state recorded in Doppler and sub-Doppler resolution is shown for comparison.

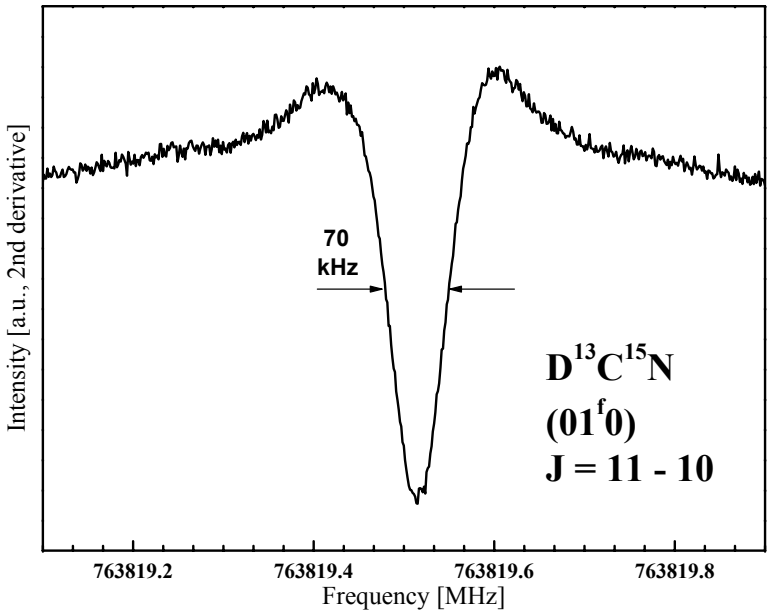


Figure 4.10: The $J = 11 \leftarrow 10$ rotational transition of the rare isotopomer D$^{13}$C$^{15}$N in the $v_2 = 1^f$ state recorded in sub-Doppler resolution. The linewidth (FWHM) of the saturation dip is $\sim$70 kHz.

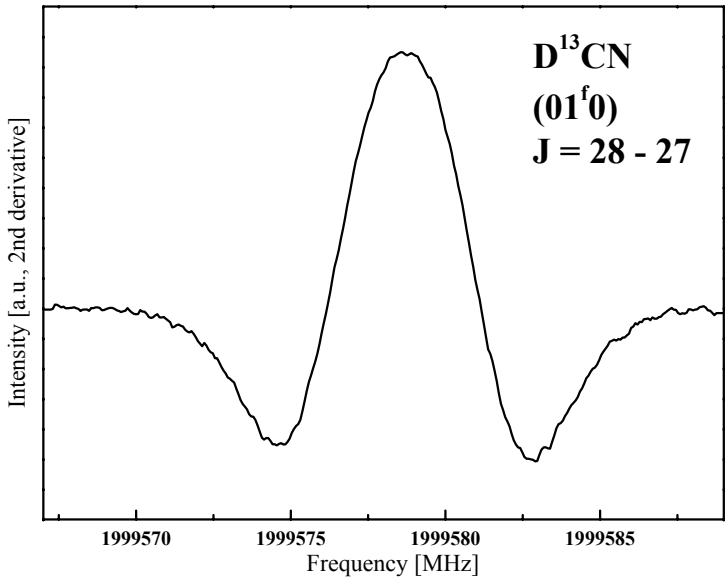


Figure 4.11: Exemplary spectrum recorded with COSSTA around 2 THz of the $J = 28 \leftarrow 27$ rotational transition of D$^{13}$CN in the $v_2 = 1^f$ vibrational state.

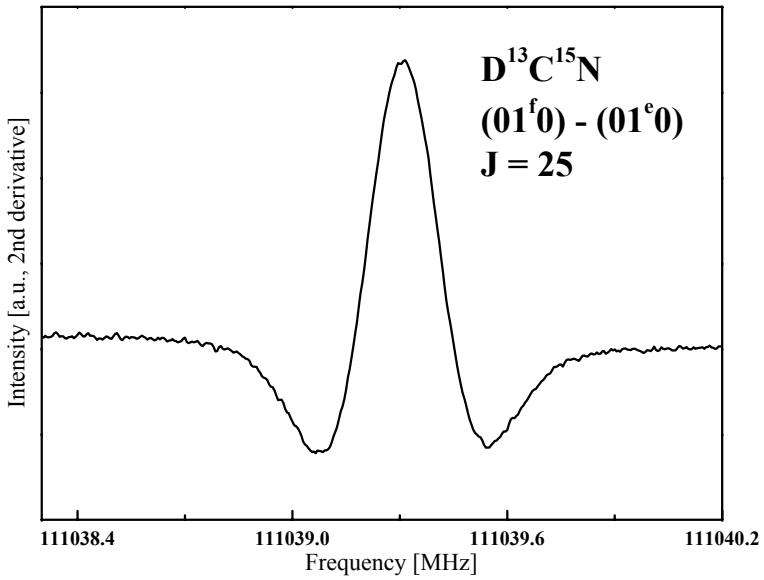


Figure 4.12: Exemplary spectrum of a direct $\ell$-type transition ($\Delta J = 0$, $J = 25$) of $D^{13}C^{15}N$ with the upper energy level $E_{up} = 1312.35$ cm$^{-1}$ above ground state. According to the selection rules, this transition connects the ($01^f0$) and ($01^e0$) vibrational states.

## 4.4 Analysis

The experimentally obtained transition frequencies were subjected to a least squares analysis using the program code developed by Pickett *et al.* [30]. The utilised expansion terms of the energy expression have been described in detail in Section 3.2.

The derived spectroscopic constants are collected in tables 4.2 - 4.5 and compared to previously published values by Preusser and Maki [64], Quapp *et al.* [74], and Möllmann *et al.* [75], respectively. As a supplement to the newly measured transition frequencies, most of the data published to date on rotational transitions of the deuterium cyanide isotopomers have been included in the fit. These additional data consist in detail of the $J = 2 \leftarrow 1$ rotational transition frequencies measured by De Lucia and Gordy [65], Winnewisser *et al.* [76] (DCN), Pearson *et al.* [71] ($D^{13}CN$) and Preußer *et al.* [64] ($D^{13}CN$, $DC^{15}N$, $D^{13}C^{15}N$) and direct $\ell$-type transitions given in Fliege *et al.* [61], Maki and Lide [59] (DCN, $DC^{15}N$) and Törring [58] (DCN, $D^{13}CN$, $DC^{15}N$). Furthermore, the infrared ($01^{e,f}0$)←(000) data by Möllmann *et al.* [75] (DCN, $D^{13}CN$) and Quapp *et al.* [74] ($D^{13}C^{15}N$) have been included.

involved $\Delta F = 1$ components. Lines that are resolved in the saturation dips therefore might not be resolved in the crossover dips.

Table 4.2: High precision rotational and hyperfine constants of DCN in the vibrational ground and first excited bending state.

| Parameter | | This work | Möllmann *et al.* [75] | Preusser and Maki [64] |
|---|---|---|---|---|
| $v_2 = 0$ | | | | |
| $B_0$ | MHz | 36207.462159(126) | 36207.46259(24) | 36207.46226(20) |
| $D_0$ | kHz | 57.74140(73) | 57.7652(27) | 57.730(14) |
| $H_0$ | Hz | 0.07326(63) | 0.0831(11) | |
| $eQq_0$ | MHz | −4.6934(49) | | −4.698(7) |
| $eQq_{J,0}$ | kHz | 0.349(115) | | |
| $C_{N,0}$ | kHz | 8.63(31) | | [8.23(18)][b] |
| $v_2 = 1$ | | | | |
| $B_1$ | MHz | 36337.020129(111) | 36337.02330(60) | 36337.0231(13) |
| $D_1$ | kHz | 59.83231(65) | 59.8587(28) | 59.852(24) |
| $H_1$ | Hz | 0.09682(59) | 0.1071(11) | |
| $eQq_1$ | MHz | −4.8145(76) | | −4.796(8) |
| $eQq_{J,1}$[a] | kHz | 0.349(115) | | |
| $eQq\eta$ | kHz | 346.1(80) | | [339(2)][c] |
| $C_{N,1}$ | kHz | 8.82(35) | | [8.23][b] |
| $q_1$ | MHz | 186.190702(51) | 186.190822(12) | 186.1908901(115) |
| $q_{1J}$ | kHz | 2.201498(192) | 2.20177(12) | 2.20278(15) |
| $q_{1JJ}$ | Hz | 0.041978(156) | 0.04260(14) | 0.04378(17) |
| $E$ | MHz | 17095750.65(32) | 17095750.50(54) | |
| $wrms$ | 0.955 | | | |

[a]Parameter fixed to ground state value

[b,c]Values in square brackets were fixed according to references [77], [61] resp.

Table 4.3: High precision rotational and hyperfine constants of $D^{13}CN$ in the vibrational ground and first excited bending state.

| Parameter | | This work | Möllmann *et al.* [75] | Preusser and Maki [64] |
|---|---|---|---|---|
| $v_2 = 0$ | | | | |
| $B_0$ | MHz | 35587.645800(182) | 35587.6508(18) | 35587.6479(19) |
| $D_0$ | kHz | 55.57890(96) | 55.617(14) | 55.576(35) |
| $H_0$ | Hz | 0.06300(80) | 0.0770(72) | |
| $eQq_0$ | MHz | −4.6972(49) | | −4.703(16) |
| $eQq_{J,0}$ | kHz | 0.224(102) | | |
| $C_{N,0}$ | kHz | 7.01(34) | | [8.23][b] |
| $v_2 = 1$ | | | | |
| $B_1$ | MHz | 35707.049846(161) | 35707.0554(14) | 35707.0571(13) |
| $D_1$ | kHz | 57.46879(83) | 57.507(13) | 57.529(25) |
| $H_1$ | Hz | 0.08348(76) | 0.0968(69) | |
| $eQq_1$ | MHz | −4.7848(47) | | −4.795(20) |
| $eQq_{J,1}$[a] | kHz | 0.224(102) | | |
| $eQq\eta$ | kHz | 334.4(50) | | [339][c] |
| $C_{N,1}$ | kHz | 6.77(30) | | [8.23][b] |
| $q_1$ | MHz | 182.294230(124) | 182.29421(27) | 182.29427(32) |
| $q_{1J}$ | kHz | 2.07675(31) | 2.07696(81) | 2.0775(20) |
| $q_{1JJ}$ | Hz | 0.037304(202) | 0.03783(69) | 0.0386(25) |
| $E$ | MHz | 16864069.24(34) | 16864069.34(63) | |
| $wrms$ | 1.09 | | | |

[a]Parameter fixed to ground state value

[b,c]Values in square brackets were fixed to DCN values according to references [77], [61] resp.

Table 4.4: High precision rotational and hyperfine constants of DC$^{15}$N in the vibrational ground and first excited bending state.

| Parameter | | This work | Preusser and Maki [64] |
|---|---|---|---|
| $v_2 = 0$ | | | |
| $B$ | MHz | 35169.797904(261) | 35169.79976(6) |
| $D$ | kHz | 54.39237(151) | 54.392(17) |
| $H$ | Hz | 0.06330(123) | |
| $rms$ | 0.45192 | | |
| $v_2 = 1$ | | | |
| $B_1$ | MHz | 35294.750863(193) | 35294.7545(16) |
| $D_1$ | kHz | 56.33892(115) | 56.354(30) |
| $H_1$ | Hz | 0.08815(100) | |
| $q_1$ | MHz | 176.080934(88) | 176.081035(62) |
| $q_{1J}$ | kHz | 2.01282(35) | 2.01329(115) |
| $q_{1JJ}$ | Hz | 0.03867(36) | 0.0366(45) |
| $wrms$ | 0.744 | | |

Table 4.5: High precision rotational and hyperfine constants of D$^{13}$C$^{15}$N in the vibrational ground and first excited bending state.

| Parameter | | This work | Quapp *et al.* [74] | Preusser *et al.* [64] |
|---|---|---|---|---|
| $v_2 = 0$ | | | | |
| $B_0$ | MHz | 34531.299725(184) | 34531.3005(19) | 34531.3019(9) |
| $D_0$ | kHz | 52.26535(96) | 52.245(11) | 52.279(14) |
| $H_0$ | Hz | 0.06074(73) | 0.0564(45) | |
| $v_2 = 1$ | | | | |
| $B_1$ | MHz | 34646.234158(177) | 34646.2356(15) | 34646.2382(7) |
| $D_1$ | kHz | 54.01254(95) | 53.991(11) | 54.033(13) |
| $H_1$ | Hz | 0.07816(75) | 0.0734(42) | |
| $q_1$ | MHz | 172.044884(124) | 172.04503(25) | 172.045118(135) |
| $q_{1J}$ | kHz | 1.89128(45) | 1.89124(66) | 1.89173(79) |
| $q_{1JJ}$ | Hz | 0.03349(42) | 0.03313(48) | 0.0336(9) |
| $E$ | MHz | 16825097.29(74) | 16825101.2(14) | |
| $wrms$ | 0.992 | | | |

## 4.5 Conclusions

The combination of the newly measured transitions with existing data yields the most comprehensive dataset on the deuterium cyanide isotopes DCN, D$^{13}$CN, DC$^{15}$N, D$^{13}$C$^{15}$N to date. The accuracy of the pure rotational spectroscopic constants $B, D$ and $H$ could be improved compared to previously published values [74, 75, 64] by a factor of ten for all isotopomers for both the vibrational ground and first excited bending state. The improvement in the accuracy of the $\ell$-type doubling constants is only a factor of two compared to that stated by Quapp *et al.* [74] and Möllmann *et al.* [75] deduced from infrared emission data alone. This is not surprising, since their data includes transitions involving rotational quantum numbers up to $J = 62$.

For the two $^{14}$N-containing species the first centrifugal correction to the electric quadrupole coupling constants $eQq_{J,0}$ ($eQq_{J,1}$ was fixed to a constant value during the fit), the asymmetry parameter of the electric field gradient $\eta$ (i.e. $eQq\eta = eQq \times \eta$) and the magnetic coupling constants $C_{N,0}$ and $C_{N,1}$ have been determined for the first time. The accuracy of the electric quadrupole coupling constants $eQq_{0,1}$ could be improved by a factor of $4 - 10$. It is to be noted that the influence of the vibrational angular momentum on the magnetic coupling constant $C_I$ has been omitted in the fit, the difference being too small to be deducible. Furthermore, from the infrared data [74, 75], the band center of the $\nu_2$-band $E = G(1,1) - G(0,0)$[4] could be derived.

The newly calculated, highly accurate parameter set was employed to predict rotational transitions in the ground and first excited bending state of all four isotopomers. The predicted frequency uncertainty for fairly strong transitions is less than $100$ kHz for frequencies up to $2.5$ THz and generally less than $30$ kHz in the intermediate frequency region not covered by the present high-resolution measurements. The full calculated transition frequencies, including hyperfine splitting, are published via the internet in the Cologne Database for Molecular Spectroscopy (CDMS) at *www.cdms.de*. These line predictions may prove helpful in the analysis of future far infrared high resolution astronomical observations, e.g. with SOFIA and Herschel.

[4] $G(v, l)$ denotes the vibrational term value.

# 5

# The Methylene Radical - $CH_2$

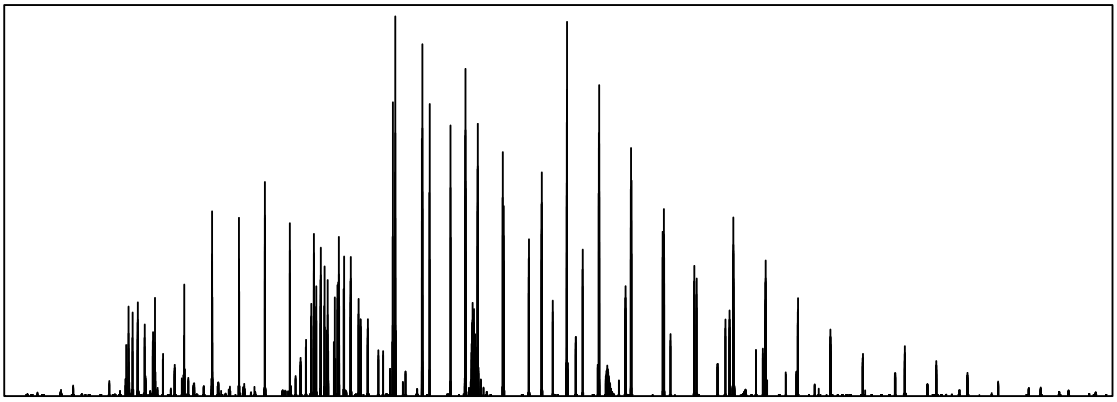

Methylene is a molecule of great astrophysical importance. It is thought to be very abundant in both the dense and diffuse interstellar medium and it is presumed to be produced quite early in the sequence of ion-molecule reactions. This qualifies $CH_2$ for acting as a test molecule for chemical models describing reaction pathways in the interstellar medium.

Its abundances have been predicted to be of the same order of magnitude as those of CH both in dense and diffuse interstellar clouds. Lee *et al.* [78] calculated relative abundances $X(\mathrm{CH_2}) = n_{CH_2}/(n_H + 2 \cdot n_{H_2})$ of $5 \cdot 10^{-7}$ to $10^{-11}$ depending on the total density, temperature, time of evolution and model characteristics. Similar high values between $2 \cdot 10^{-10}$ and $2.5 \cdot 10^{-8}$ were obtained by Ruffle and Herbst [13] with a model containing reactions on dust grain surfaces. For diffuse interstellar clouds van Dishoeck and Black [79] have developed a model, yielding e.g. for the diffuse material in the line of sight towards $\zeta$ Per a relative abundance $X(CH_2)$ of around $2.5 \cdot 10^{-8}$ at a temperature of $25$ K and a hydrogen density of $N_H = 500$ cm$^{-3}$. The high variability of calculated methylene abundances with the chemical model itself, i.e. the considered chemical network and reaction schemes, and the inherent model parameters, i.e. temperature, density and time of evolution, make $CH_2$ a perfect tool to test the model reliability.

The dominant formation process for methylene is via the dissociative recombination reaction of $CH_3^+$, and from the experimental branching ratios by Vejbi-Christensen *et al.* [80] it is clear that $CH_2$ is the main product of this reaction. A formation route for $CH_3^+$ via ion-molecule reactions has been proposed by Herbst [81], the complete reaction pathway looks as follows:

$$
\begin{array}{llll}
C + H_3^+ & \rightarrow CH^+ + H_2 & \rightarrow & CH_2^+ + H \\
C^+ + H_2 & & \rightarrow & CH_2^+ + h\nu \\
\hline
CH_2^+ + H_2 & \rightarrow CH_3^+ + H & & \\
 & CH_3^+ + e^- & \rightarrow & CH_2 + H \quad (40\,\%) \\
 & & \rightarrow & CH + H_2 \quad (14\,\%) \\
 & & \rightarrow & CH + H + H \quad (16\,\%) \\
 & & \rightarrow & C + H_2 + H \quad (30\,\%)
\end{array}
$$

The methylene radical has already been detected in the dense interstellar medium towards the two hot cores Orion KL and W51M [12]. The detected rotational transitions $N_{Ka,Kc} = 4_{04} - 3_{13}$ at $68 - 71$ GHz, however, connect two energetically relatively high-lying levels, with an excitation temperature higher than $200$ K. The chemical models predict, on the other hand, highly abundant $CH_2$ especially in the cold ($10 - 50$ K) interstellar medium. To probe these sources it is, therefore, favourable to employ molecular transitions between comparatively low lying energy levels.

This approach is complicated, however, by the molecular characteristics of the methylene radical. As a very light asymmetric rotor molecule following $b$-type selection rules, most of its pure rotational transitions happen to fall in the terahertz and sub-mm-wavelength region, as is demonstrated in Figure 5.1. This region is technically challenging both for astrophysical and spectroscopic investigations. Moreover, methylene is a short-living radical, which has to be produced *in-situ* in sufficient amounts for usage in a laboratory experiment. On the other hand, the standard models used to theoretically predict transition frequencies fail in the case of $CH_2$ due to its low barrier to linearity and on that account high centrifugal distortion terms.

In the following, I am going to present experimental data on two energetically low lying rotational transitions of $CH_2$ at terahertz frequencies (Section 5.2). Since the dataset on methylene is rather sparse, a summary of relevant previous work is given in Section 5.1, and a global analysis of all experimental data with the method of the Euler expansion of the rotational Hamiltonian is given in Section 5.3. These new results give reliable transition frequency predictions for a multitude of rotational $CH_2$ transitions in the terahertz region, and are of special importance for further terahertz observatories, like HIFI on board of Herschel, the SOFIA project and APEX/ALMA. The last part of this chapter, Section 5.4, presents the results of a search for $CH_2$ transitions in data of the ISO satellite, this search was triggered by the new analysis of the rotational spectrum.

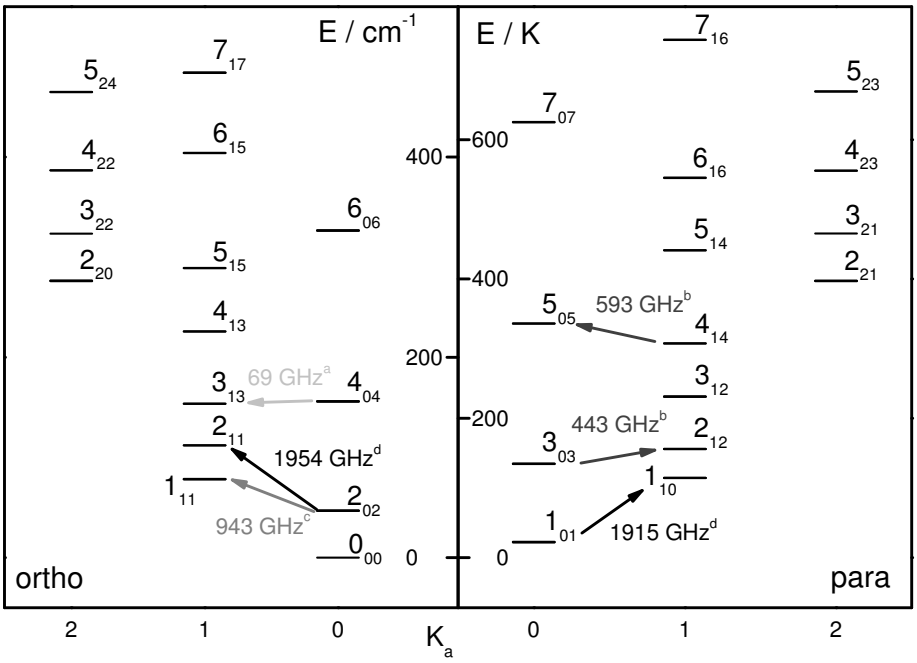


Figure 5.1: The calculated energy level scheme of $CH_2$, divided into ortho and para states. The energy is given in both $cm^{-1}$ and a temperature scale according to E[K]=$1.438 \cdot$E[$cm^{-1}$]. Rotational transitions measured to microwave accuracy are depicted by arrows: [a] Lovas *et al.* [82], [b] Ozeki *et al.* [83], [c] Michael *et al.* [84], [d] this work, Brünken *et al.* [85]

## 5.1 Previous Work

The first spectroscopic identification of the free methylene radical $CH_2$ was done by Herzberg and Shoosmith [86] in 1959 by its electronic $^3B_1$-$^1A_2$ transition in the UV. Although the geometrical structure of the molecule could not be determined at this point, a more detailed analysis of the data together with theoretical considerations led finally in 1971 to the assignment of the electronic ground state as one of $^3B_1$ symmetry and having a bent, symmetric structure [87]. The most recent structure analysis [88] yields a HCH equilibrium bond angle of $133.9308(21)°$.

The investigation of the rotation and rotation-vibration spectrum of methylene begun in 1981 by the observation of three transitions of the $\nu_2$ band with the LMR (laser magnetic resonance) technique by Sears *et al.* [89]. Soon thereafter, the same authors reported additionally ten rovibrational transitions in the infrared [90] and also thirteen pure rotational FIR transitions in the vibronic ground state [43] with the same method. Although these latter measurements were not field free and the obtained transition frequencies are thought to have an uncertainty of as high as $5$ MHz, the frequency predictions for other pure rotational transitions could be significantly refined. As a consequence, Lovas *et al.*

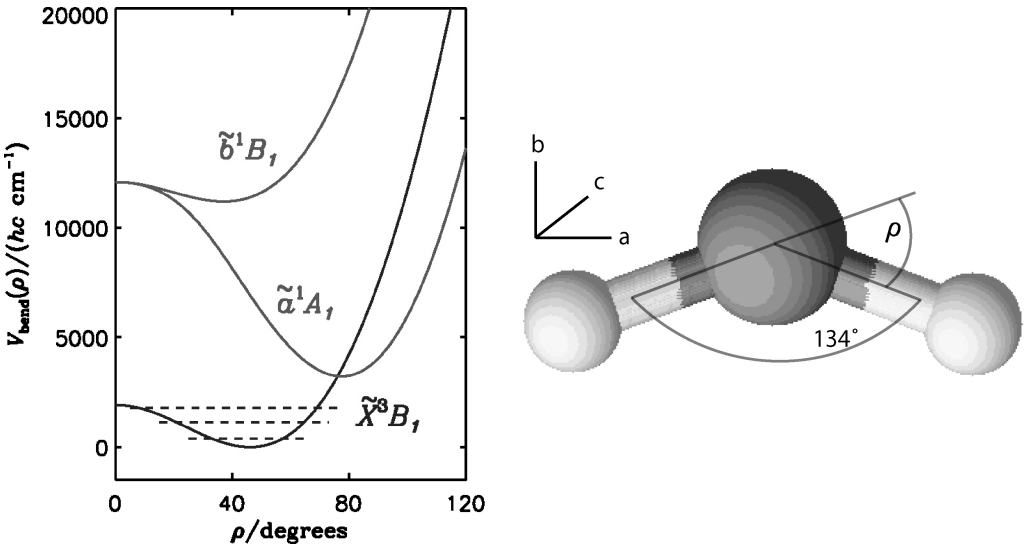


Figure 5.2: a) Potential energy curve of $CH_2$ for the three lowest electronic states versus $\rho = 180° - \angle HCH$ [88, 91]. The ground state exhibits a very low barrier to linearity. b) Sketch of the molecule and the designation of the molecular axis, $\rho$ and the bond angle are shown.

were able to measure the $4_{04} - 3_{13}$ rotational transition at around $70$ GHz with a Stark modulated microwave spectrometer to high precision [82]. Sears *et al.* fitted their data to a standard Watson-type $A$-reduced Hamiltonian including fine- and hyperfine interaction terms. From this analysis, they predicted both pure rotational transitions in the vibrational ground state and mid-infrared rovibrational transitions for $CH_2$ [92]. However, the convergence of the standard Hamiltonian is very poor in the case of the light and floppy $CH_2$, as will be outlined in more detail in Section 5.3, and predicted transition frequencies from this model have a high uncertainty especially for higher $N$ and $K$ values.

For this reason, Bunker and Jensen (and coworkers), employed both their non-rigid bender Hamiltonian [93, 94, 95] and the Morse oscillator-rigid bender internal dynamics Hamiltonian (MORBID) [88] to fit the $\tilde{X}\ ^3B_1$ methylene data. The advantage of this method is the possibility to fit all rovibrational and rotational lines of different isotopomers ($^{12}CH_2$, $^{13}CH_2$, $CD_2$) together, thereby reducing the number of needed fit-parameters. It was and is still, however, not possible to include hyperfine interaction terms to the analysis. Their analysis included field-free tunable diode laser absorption data of the $\nu_2$ bending fundamental band of $CH_2$ by Marshall and McKellar [96] and of five pure rotational transitions in the ground vibronic state at infrared frequencies involving $K_a = 4 \leftarrow 3$ by Sears [97]. During the same time, Bunker and Langhoff [98] computed an ab initio dipole moment for $\tilde{X}\ ^3B_1$ $CH_2$ depending on its geometry. With the most recent structural information, a dipole moment $\mu_b = 0.57$ D is obtained, and used in the analysis.

With the advent of high power, high resolution sub-mm-wavelength and terahertz radiation sources, the investigation of the widespread rotational spectrum of methylene

Table 5.1: The available dataset on the rotational spectrum of the methylene radical in its electronic and vibrational ground state prior to the new measurements. The LMR rovibrational data of the $\nu_2$ band [90] has been omitted. It was also not used in the global analysis of the data.

| Method | No. of lines | ortho | para | Reference |
|---|---|---|---|---|
| | | $4_{04} - 3_{13}$ | | [82] |
| rotational data | 4 | | $2_{12} - 3_{03}$ | [83] |
| · resolved fine structure | | | $5_{05} - 4_{14}$ | [83] |
| · resolved HFS | | $1_{11} - 2_{02}$ | | [84] |
| field free IR data | 5 | | | [97] |
| · resolved fine structure | | $N = 5..7$, $K_a : 4 \leftarrow 3$ | | |
| · partly resolved asymmetry | | | | |
| GSCD[a] | 23 | | | [96] |
| · resolved fine structure | | $N \leq 10$, $K_a \leq 3$ | | |
| · partly resolved asymmetry | | | | |
| FIR LMR[b] | 13 | | | [43] |
| · resolved fine structure | | $N \leq 6$, $K_a \leq 2$ | | |
| · resolved HFS | | | | |
| · not field free | | | | |

[a] Calculated Ground State Combination Differences

[b] These lines were not used in the global analysis

was now feasible. In 1995, Ozeki and Saito measured the $N_{KaKc} = 2_{12} \leftarrow 3_{03}$ and $5_{05} \leftarrow 4_{14}$ transitions of para $CH_2$ at around $442$ and $593$ GHz, resp., to $30$ kHz accuracy with a frequency multiplied Klystron as radiation source [83]. Very recently, Michael *et al.* were able to observe the energetically low-lying $N_{KaKc} = 1_{11} \leftarrow 2_{02}$ transition of the ortho species at around $943$ GHz with the Cologne Terahertz Spectrometer [99]. In this paper, they also presented a new fit of the available data to the standard Hamiltonian and achieved an extended set of rotational parameters. These parameter set served as a basis for the search of low-lying terahertz transitions as presented in the following chapter.

The known high accuracy data on rotational transitions of $\tilde{X}\ ^3B_1$ $CH_2$ in the vibrational ground state is visualised in Figure 5.1. A summary of all the available data can also be found in Table 5.1. It has to be emphasised that the dataset is very heterogeneous with respect to the achieved resolution and accuracy and, more importantly, that the high resolution data on methylene is very sparse.

## 5.2 Measurement of Low $N$ Pure Rotational Transitions of $CH_2$ in the Terahertz Regime

In contrast to other types of far infrared spectrometers, the laser sideband system in Cologne has a very good intrinsic frequency stability of $< 5$ kHz, or $2.5 \cdot 10^{-9}$, respectively. The frequency accuracy achieved for strong lines is 2-5$\cdot 10^{-8}$, and even weak or perturbed lines can be measured to $\sim 10^{-7}$. The high accuracy of measured transition frequencies can be transferred to the accuracy of rotational parameters deduced from an analysis of this data.

Two pure rotational transitions of methylene with sufficient intensity lie in the frequency range covered by COSSTA, the $N_{KaKc} = 2_{11} - 2_{02}$ multiplet of ortho-$CH_2$ and the $N_{KaKc} = 1_{10} - 1_{01}$ multiplet of para-$CH_2$ centered at $1.954$ and $1.915$ THz, respectively. As has been outlined in more detail in Section 3.3.3, each rotational energy level of $CH_2$ is split into a triplet due to the resulting electronic spin of $S = 1$. In the case of ortho-$CH_2$, where the nuclear spins of the two hydrogen atoms couple to give a resultant nuclear spin of $I = 1$, each of these fine structure levels is further split into a hyperfine triplet. The ortho-levels are those with $K_a + K_c$ even, as follows from the $^3B_1$ symmetry of the molecule. This leads to somewhat different energy level diagrams and spectra of the two species, ortho-spectra being much denser and more difficult to assign. The corresponding energy level schemes for both transitions are shown in Figures 5.3 and 5.4.

### 5.2.1 *In-situ* Production of Methylene

The methylene radical is a very unstable species and has to be produced in-situ in the absorption cell for spectroscopic investigations. The main destruction process of gas phase ground state $CH_2$ is via bimolecular association to form $C_2H_4$, which further decays to $C_2H_2$ + $H_2$ [100] and its lifetime is of the order of several hundred microseconds after production in a discharge [96], depending on the pressure and type of the used buffer gas. In this work I followed the attempt by Michael *et al.* [84]. A sketch of the experimental setup is given in Figure 5.5. In a first production step, commercially available diketene, $(CH_2CO)_2$, was processed through quartz wool with a flash vacuum pyrolysis at a temperature of $650$°C over a length of 15 cm. The ketene, $CH_2CO$ produced thereby is then continually discharged inside the absorption cell to form $CH_2$ and CO.

$$(CH_2CO)_2 \xrightarrow{\Delta} 2 \cdot CH_2CO \quad \xrightarrow{disch.} 2 \cdot (CH_2 + C0)$$

A voltage of up to $2.5$ kV can be applied between two cylindrical electrodes, an anode $\sim 10$ cm and a cathode $\sim 20$ cm in length, with a maximum allowed current of $200$ mA. The electrodes were open-ringed to avoid an induced current due to the magnetic field applied. The optimum production conditions were at a discharge current of $40$ mA and a pressure of $5 - 8$ Pa without buffer gas. The active region was $\sim 80$ cm with a cell diameter of $10$ cm. Due to the short lifetime of the methylene radical, all measurements were performed in full gas flow. A cryo trap was used to avoid contamination of the turbo

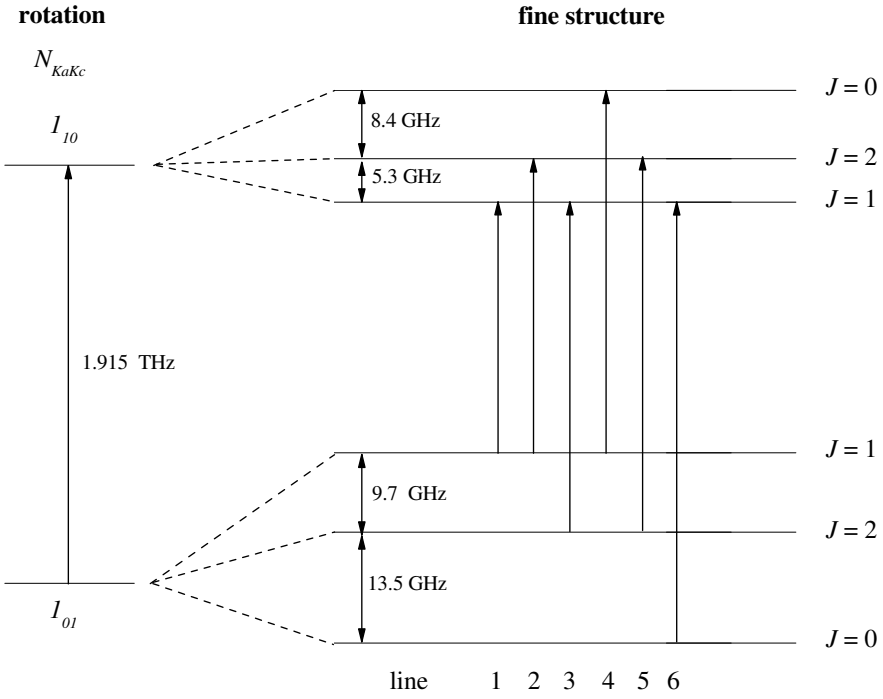


Figure 5.3: Energy level scheme of the para-$CH_2$ $N_{KaKc} = 1_{10} - 1_{01}$ multiplet measured with COSSTA. The splitting of the rotational levels by fine structure interaction is shown. Arrows depict the six allowed rotational - fine structure transitions, all of which have been measured; the transitions have been numbered sequentially with increasing frequency.

molecular pump (nominal exhaustion rate $55$ l/s at $10$ Pa) and the attached rotary pump. It was found that higher flow rates yielded higher line intensities.

It was necessary to cool the absorption cell in order to increase the population of the lower energy levels of the two transitions, which are at $15$ and $47$ cm$^{-1}$ (i.e. $20$ and $60$ K) for the $1_{01}$ and $2_{02}$ levels, respectively. The whole active region was covered with a copper cooling jacket, through which liquid nitrogen was pumped. The temperature was controlled by a diode thermometer and spanned the range of $-80$ to $-120$°C throughout the experiments. Care had to be taken to avoid a drop of temperature below $\sim -130$°C, since ketene freezes out at the cell walls at this temperature. A thermal insulation made of styrofoam and foam plastic surrounded the whole cell. The $\mu$ metal shielding for reduction of the earth magnetic field (see section 2.2) was affixed as the outmost layer.
As an alternative approach, acetic anhydride ($(CH_3CO)_2O$) instead of diketene was used as a precursor for ketene production.

$$(CH_3CO)_2O \xrightarrow{\Delta} CH_2CO + CH_3COOH$$

In this case, a pyrolysis temperature of $600$°C yielded optimal results. Since the achievable vapour pressure after pyrolysis did not exceed $3$ Pa, additionally $5$ Pa of He had to be used as a buffer gas to start the discharge. During the measurements the gas pressure increased to $\sim 7$ Pa due to heating by the discharge plasma and the He buffer gas supply was switched off. The discharge and temperature conditions were the same as in the

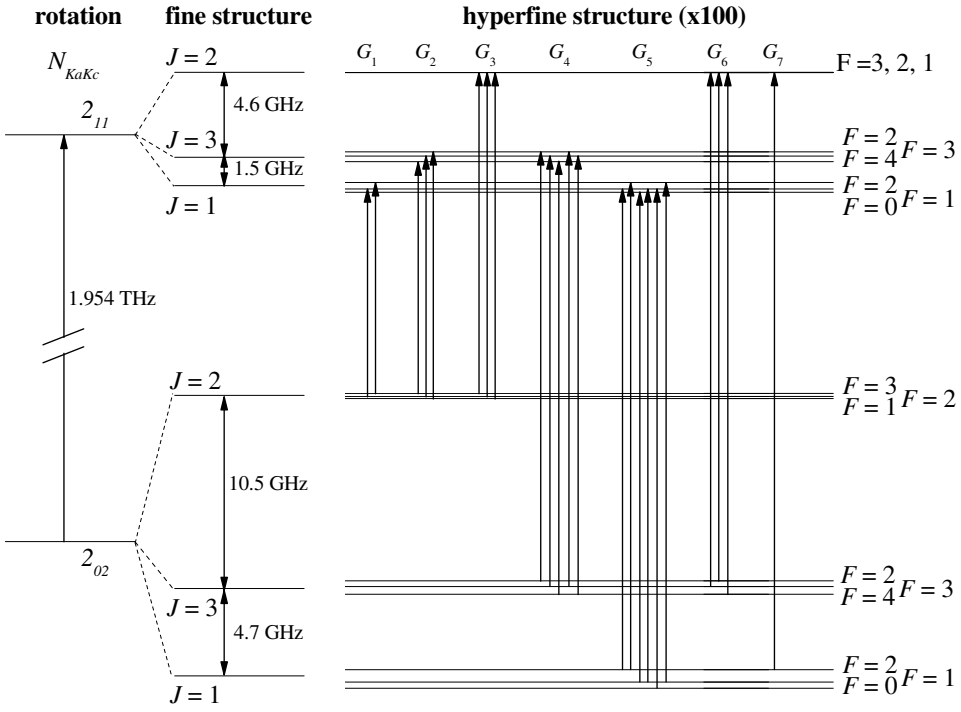


Figure 5.4: Energy level scheme of the ortho-$CH_2$ $N_{KaKc} = 2_{11} - 2_{02}$ multiplet measured with COSSTA. The splitting of the rotational levels by fine and hyperfine interaction is shown. In total, the number of allowed transitions is 60. Arrows depict the 23 transitions which actually have been measured, divided into seven frequency groups designated by $G_i$ ($i = 1 - 7$).

case of using diketene, since in both syntheses ketene is the intermediate pyrolysis product. The observed line intensities and signal-to-noise ratios were equivalent, indicating that the same very high molecular yield is achieved with both approaches. The latter approach has the advantage that it can be used for the production of deuterated methylene species, since (partially) deuterated acetic anhydride can be synthesised easier than (partially) deuterated diketene.

### 5.2.2 Zeeman Modulated $CH_2$ - Exemplary Spectra

The Zeeman-modulation, described in Section 2.2.1, was employed for the measurements of $CH_2$. Preceding tests with a pure frequency-modulated signal showed a considerably worse signal-to-noise ratio due to stronger baseline effects in this mode. The typical magnetic field strength applied was $2.5 - 3$ G at a modulation rate of $4$ kHz. A comparison of recorded spectra for different magnetic fields ranging from $2.4 - 6$ G, but otherwise identical conditions, is shown in Figure 5.6; a fading of the spectral features is clearly visible for higher magnetic fields. The search and initial assignment of the lines were performed with frequency predictions calculated by the Pickett code using rotational parameters published by Michael *et al.* [84]. The absolute frequency deviation was less than $5$ MHz for most of the lines but for the relative line positions, e.g. for the hyperfine

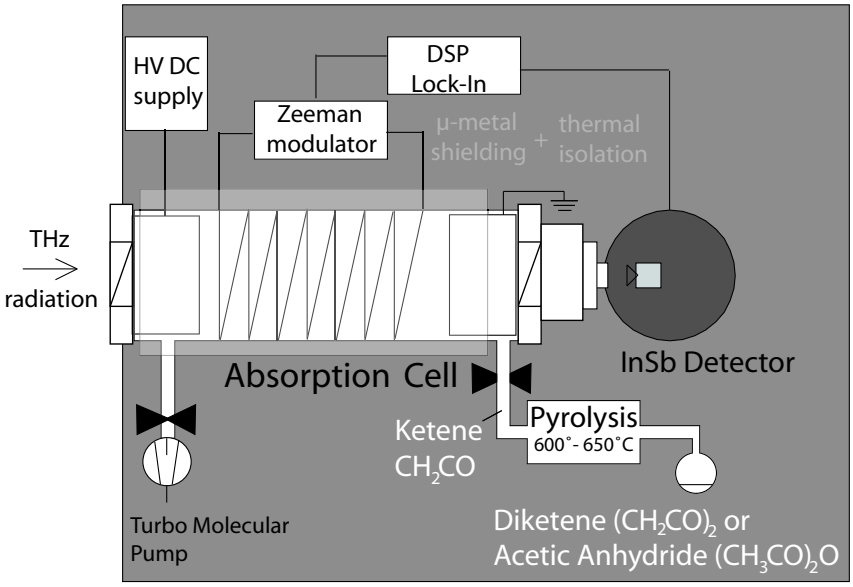


Figure 5.5: Experimental setup for the in-situ production of $CH_2$ at COSSTA. For further details please refer to the text.

splitting of ortho-$CH_2$, the predictions were considerably better and usually in the order of $1$ MHz or less.

During measurements, typical integration times were $200$ ms per datapoint with a frequency step size of $\sim 100$ kHz and often $2-6$ scans were averaged to obtain the final spectrum. The frequency stability of the FIR laser was better than $5$ kHz for all scans. Typical spectra are shown in Figures 5.7 and 5.8 for both the para- and ortho-$CH_2$ rotational transition together with calculated stick spectra of both multiplets. The labelling is according to the energy-level schemes shown in Figures 5.3 and 5.4. The line shape resembles a Gaussian profile in second derivative, as has been discussed in Section 2.2.1. For the para transition, all dipole-allowed lines have been measured, in the case of ortho-$CH_2$ all transitions with sufficient intensity, i.e. $23$ out of $60$ possible ones, have been measured and assigned. A complete list of the newly identified lines can be found in Table 5.2 together with estimated experimental uncertainties.

On closer inspection the recorded and calculated line intensities in Figure 5.8 do not seem to correspond too well. The calculated line intensities, shown in the form of a stick diagram in Figure 5.8 are deduced from transition dipole matrix elements, whereas the measured line intensities are affected by the detection method. As has been outlined in Section 2.2.1, the measured intensity of a transition measured with the Zeeman modulation technique depends on the $g$-factor of the participating upper energy level. The triplet shown in Figure 5.8 are the $\Delta N = \Delta J = \Delta F = 0$, $N_{KaKc} = 2_{11} - 2_{02}$, $J = 3$, $F = 2, 3, 4$ transitions, and they are only distinct in their $F$ quantum number. For the three hyperfine transitions under consideration, following Equation 2.19, the $g$ factors are $8/9$, $11/18$ and $1/2$, respectively, and their splitting of the two Zeeman-components, and,

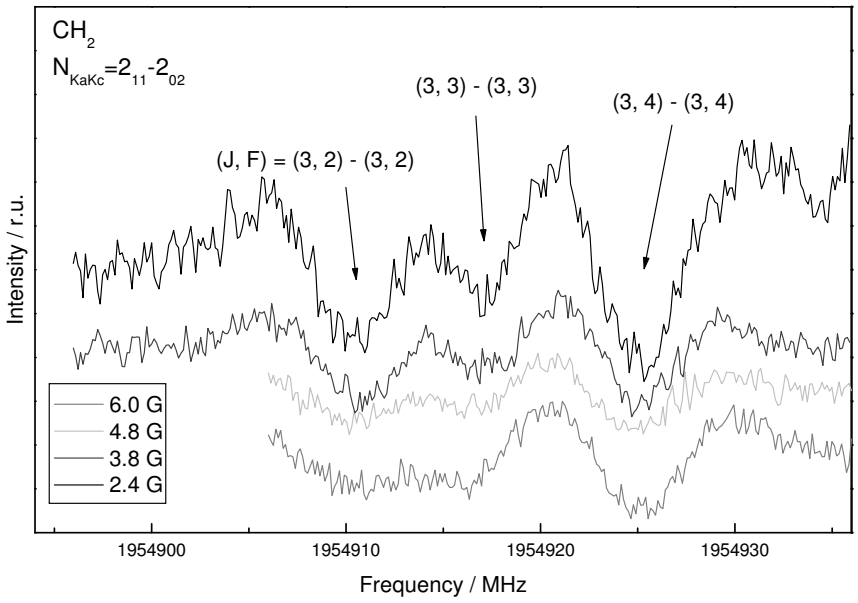


Figure 5.6: Four different traces of a hyperfine-triplet of $CH_2$ in Zeeman-modulation mode with different magnetic field strength. It is evident that a too high modulation range is obliterating the spectral features.

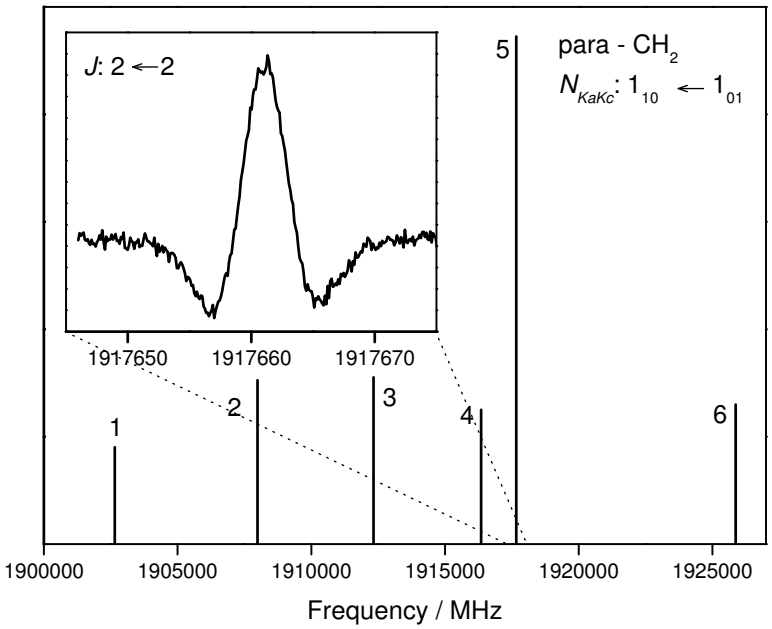


Figure 5.7: Calculated stick spectrum of the measured para-$CH_2$ transitions. The labelling of the lines is the same as in Figure 5.3. An exemplary spectrum recorded with COSSTA in Zeeman-modulation mode is shown, all six possible fine structure transitions have been measured.

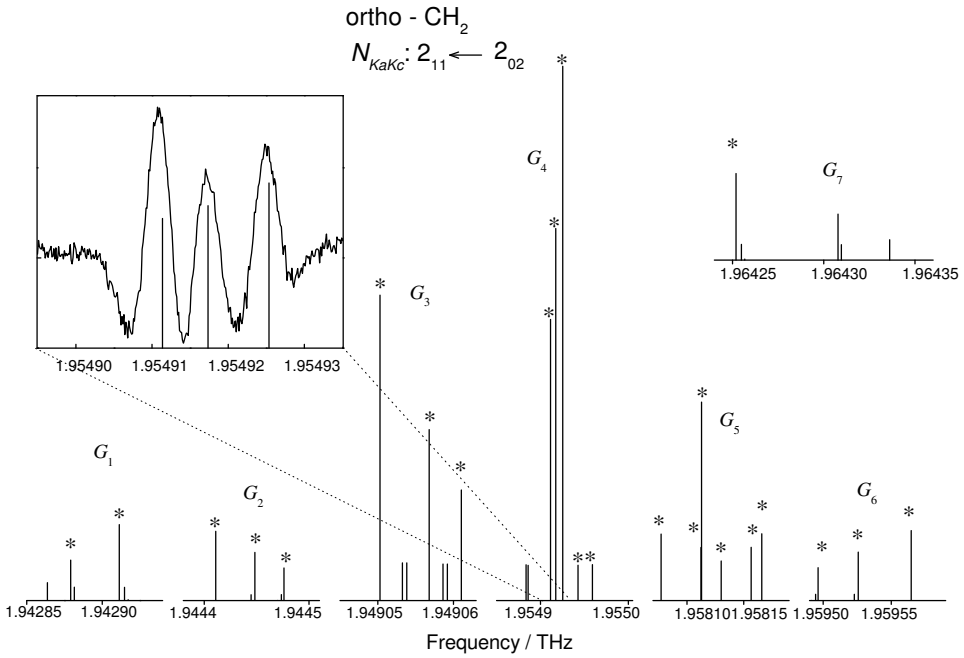


Figure 5.8: Calculated stick spectrum of the measured ortho-$CH_2$ transitions. The labelling of the groups of lines is the same as in Figure 5.4. An exemplary experimental spectrum of a closely spaced hyperfine triplet is shown, in total all lines marked with an asterisk were measured. Details on the observed intensities can be found in the text.

therefore, the recorded intensities, varies accordingly.

## 5.3 Global Analysis of the Data

A summary of the newly measured transitions of $CH_2$ near 2 THz is given in Table 5.2. The rather large experimental uncertainties stated in some cases are due to very weak and/or blended lines. Especially an analysis of blended lines is difficult, since the observed intensities depend critically on the particular Zeeman splitting of each line. Most of the lines were nevertheless included in the analysis to increase the sparse dataset, although with higher uncertainties and conclusively smaller weights. The initial assignment based on predictions from rotational parameters by Michael *et al.* [84] had to be changed in only a few cases of closely spaced triplets in the course of the analysis.

### 5.3.1 Standard $A$-reduced Hamiltonian

The standard $A$-reduced Hamiltonian from [84] was used in a first attempt to analyse the data. A detailed account of the form of the Hamiltonian is given in Section 3.3.3. Eleven rotational parameters, of which six centrifugal terms were fixed to previous values either

from [43] or [96], were used to fit the six high resolution microwave and terahertz rotational transitions. However, it was not possible to reproduce the measured transition frequencies to better than five times their experimental uncertainties. To constrain the centrifugal distortion parameters, in a next step the GSCD data from [96] and field-free IR data from [97] were added to the dataset and the number of rotational parameters was increased to 16, with one value fixed ($L_K$).

Table 5.2: Compilation of new experimental data used in the analysis of $CH_2$. All frequency information is in MHz.

| $N'_{Ka'Kc'}$ | $J'$ | $F'$ | $N''_{Ka''Kc''}$ | $J''$ | $F''$ | Frequency | $\Delta\nu$ | o-c. |
|---|---|---|---|---|---|---|---|---|
| para-transitions | | | | | | | | |
| $1_{10}$ | 1 | | $1_{01}$ | 1 | | 1902654.362 | 0.200 | 0.177 |
| $1_{10}$ | 2 | | $1_{01}$ | 1 | | 1907986.637 | 0.300 | 0.021 |
| $1_{10}$ | 1 | | $1_{01}$ | 2 | | 1912328.935 | 0.200 | 0.058 |
| $1_{10}$ | 0 | | $1_{01}$ | 1 | | 1916348.190 | 0.200 | 0.274 |
| $1_{10}$ | 2 | | $1_{01}$ | 2 | | 1917661.094 | 0.100 | −0.213 |
| $1_{10}$ | 1 | | $1_{01}$ | 0 | | 1925866.221 | 0.200 | 0.339 |
| ortho-transitions | | | | | | | | |
| $2_{11}$ | 1 | 1 | $2_{02}$ | 2 | 2 | 1942878.947 | 0.200 | −0.115 |
| $2_{11}$ | 1 | 2 | $2_{02}$ | 2 | 3 | 1942910.487 | 0.200 | −0.766 |
| $2_{11}$ | 3 | 4 | $2_{02}$ | 2 | 3 | 1944411.017 | 0.200 | 0.019 |
| $2_{11}$ | 3 | 3 | $2_{02}$ | 2 | 2 | 1944448.270 | 0.300 | −0.018 |
| $2_{11}$ | 3 | 2 | $2_{02}$ | 2 | 1 | 1944476.330 | 0.300 | 0.260 |
| $2_{11}$ | 2 | 3 | $2_{02}$ | 2 | 3 | 1949051.376 | [a] | |
| $2_{11}$ | 2 | 2 | $2_{02}$ | 2 | 2 | 1949058.720 | [a] | |
| $2_{11}$ | 2 | 1 | $2_{02}$ | 2 | 1 | 1949063.340 | [a] | |
| $2_{11}$ | 3 | 2 | $2_{02}$ | 3 | 2 | 1954910.784 | 0.500 | −0.582 |
| $2_{11}$ | 3 | 3 | $2_{02}$ | 3 | 3 | 1954917.270 | 0.500 | −0.069 |
| $2_{11}$ | 3 | 4 | $2_{02}$ | 3 | 4 | 1954925.038 | 0.500 | −0.315 |
| $2_{11}$ | 3 | 2 | $2_{02}$ | 3 | 3 | 1954943.129 | 0.500 | 0.418 |
| $2_{11}$ | 3 | 3 | $2_{02}$ | 3 | 4 | 1954959.111 | 0.500 | −0.004 |
| $2_{11}$ | 1 | 1 | $2_{02}$ | 1 | 2 | 1958077.452 | 0.500 | 0.304 |
| $2_{11}$ | 1 | 0 | $2_{02}$ | 1 | 1 | 1958112.867 | 0.300 | 0.581 |
| $2_{11}$ | 1 | 2 | $2_{02}$ | 1 | 2 | 1958112.867 | 0.300 | 0.000 |
| $2_{11}$ | 1 | 1 | $2_{02}$ | 1 | 1 | 1958130.100 | 0.500 | −0.015 |
| $2_{11}$ | 1 | 1 | $2_{02}$ | 1 | 0 | 1958156.446 | 0.500 | −0.136 |
| $2_{11}$ | 1 | 2 | $2_{02}$ | 1 | 1 | 1958165.435 | 0.500 | −0.398 |
| $2_{11}$ | 2 | 1 | $2_{02}$ | 3 | 2 | 1959496.844 | 0.300 | 0.498 |
| $2_{11}$ | 2 | 2 | $2_{02}$ | 3 | 3 | 1959526.242 | 0.300 | 0.395 |
| $2_{11}$ | 2 | 3 | $2_{02}$ | 3 | 4 | 1959564.919 | 0.200 | 0.260 |
| $2_{11}$ | 2 | 3 | $2_{02}$ | 1 | 2 | 1964253.432 | 0.500 | 1.513 |
| $2_{11}$ | 2 | 2 | $2_{02}$ | 1 | 2 | 1964253.432 | 0.500 | −1.452 |

[a] These lines were not included in the fit. The assignment is ambiguous due to their small frequency spacing and different Zeeman splitting.

A comparison of this analysis to that of Marshall and McKellar [96] and Michael *et al.* [84] can be found in Table 5.3. In contrast to the latter work, it was now possible to fit most of the rotational parameters, with the exception of $L_K$, which was not determined by the data, but had to be included to the analysis to fit the transitions involving higher $K_a$. For $L_K$ the value given by Marshall and McKellar was used. All rotational parameters used in the analysis are significantly determined, with uncertainties less than a tenth of the parameter value. Additional centrifugal distortion terms to the electronic and nuclear spin interaction parameters had to be included to account for the new data. Instead of the $N$-dependent distortion term to the dipole-dipole interaction tensor $T_{aaD}$, a $K$-dependent correction to the Fermi-contact interaction term was introduced ($a_{FK}$) and significantly improved the fit. The spin-rotation correction terms $\Delta^S$ included are well determined. The weighted rms (wrms) of the analysis is around 1.6, i.e. not all transitions are fitted to their experimental uncertainty. Including higher order centrifugal terms improves the quality of the fit to some extent, but these parameters are not well defined by the data. However, in comparison to Michael *et al.* the lower order $N$ and $K$ dependent parameters do not coincide in their error limits. This is due to the fact that more centrifugal distortion terms were used in the present analysis, but also indicates the high correlation of the rotational parameters.

The analysis of Marshall and McKellar [96] included rotational and rovibrational LMR data, but considerably less high accuracy MW data. Therefore, they were able to determine a larger number of rotational centrifugal distortion parameters, but generally all parameters were determined to less accuracy. It was possible to reproduce satisfactorily the available dataset, but the extrapolation to higher energy levels is doubtful with such a large and badly determined parameter set. The deviations to the present fit are acceptable, taking into account the different number of centrifugal distortion parameters included.

Although this new analysis is a great improvement over previous studies, the number of parameters needed (16 for the rotational part, up to decic order) is still too large to allow for accurate transition frequency predictions involving states with higher $N$ and $K$ values. A good extrapolation to higher quantum numbers cannot be expected, since experimental data on higher $N$ and especially $K_a$ is missing.

Table 5.3: Analysis of $CH_2$ data with the standard $A$-reduced Hamiltonian as described in Section 3.3.3. Comparison of the new results with previously published ones. All values are in MHz.

| Parameter | this work | Marshall and McKellar, [96] | Michael *et al.*, [84] |
|---|---|---|---|
| $A$ | 2212816.5(38) | 2212785.4(25) | 2190150.7(60) |
| $B$ | 253284.9(176) | 253337.(22) | 252321.55(181) |
| $C$ | 215436.6(174) | 215380.(22) | 216359.1(40) |
| $\Delta_K$ | 88741.2(38) | 88693.9(12) | [59690.147] |
| $\Delta_{NK}$ | −630.85(46) | −627.50(39) | −607.57(82) |
| $\Delta_N$ | 11.410(43) | 11.068(69) | [9.033] |
| $\delta_N$ | 2.7792(50) | 1.51(31) | [3.034] |
| $\delta_K$ | 502.1(87) | 544.(11) | |

Table 5.3: $CH_2$ standard analysis - continued.

| Parameter | this work | Marshall and McKellar, [96] | Michael *et al.*, [84] |
|---|---|---|---|
| $\Phi_K$ | 6606.684(200) | 6602.06(12) | |
| $\Phi_{KN}$ | −81.92(35) | −85.28(15) | [-58.211] |
| $\Phi_{NK}$ | −0.6845(56) | −0.344(25) | [0.384] |
| $\Phi_N$ | 0.002485(96) | −0.0015(117) | [0.00585] |
| $\phi_K$ | | 17.2(12) | |
| $\phi_{NK}$ | | −1.41(31) | |
| $\phi_N$ | | 0.00173(22) | |
| $L_K$ | [-195] | [-195] | |
| $L_{KKN}$ | 7.289(55) | 7.708(23) | |
| $L_{KN}$ | 0.03495(61) | 0.0142(20) | |
| $L_{NNK}$ | | 0.00069(29) | |
| $L_N$ | | −0.0000399(69) | |
| $P_{KKKN}$ | −0.22789(220) | −0.2413(11) | |
| $\alpha$ | 7783.28(10) | 7782.9(34) | 7839.4(65) |
| $\beta$ | 1223.494(110) | 1216.9(32) | 1314.1(111) |
| $\alpha_{SK}$ | −14.70(10) | [-24.9] | −57.5(49) |
| $\alpha_{SN}$ | 0.201(15) | | |
| $\beta_{SN}$ | −0.1000(146) | | |
| $\epsilon_{aa}$ | 20.657(119) | 14.2(22) | −44.5(73) |
| $\epsilon_{bb}$ | −153.850(35) | −153.50(59) | −164.35(119) |
| $\epsilon_{cc}$ | −124.731(90) | −123.61(81) | −161.3(59) |
| $\Delta^S_{KN}$ | −0.4315(270) | | |
| $\Delta^S_N$ | | | −0.080(31) |
| $\delta^S_N$ | 0.01163(126) | | |
| $a_F$ | −22.762(116) | | −16.81(28) |
| $a_{FK}$ | 1.7044(268) | | |
| $T_{aa}$ | 29.905(93) | | 32.32(21) |
| $T_{bb}$ | −14.713(60) | | −20.70(36) |
| $T_{aaD}$ | | 0.3121(119) | |
| wrms | 1.59 | | |

### 5.3.2 The Euler Approach

In the standard model used for the calculation and analysis of rotational energy levels, deviations from the rigid rotor model are handled as small perturbation terms in the Hamiltonian. The effective Hamiltonian is expressed as a power series in the angular momentum operators. In the case of methylene, however, centrifugal distortion terms are very large due to its floppiness. The standard $A$-reduced Hamiltonian is, therefore, beyond its limits, or, mathematically expressed, the power series does not converge for high values of the angular momentum quantum numbers, as will be quantified in the following paragraphs.

One approach, better suited to address this special problem, is certainly the MORBID analysis [88] mentioned already. In this model, experimental data can be used to improve

the potential energy surface, which is the basis for calculating transition frequencies, to some degree. However, this approach could not be utilised in this work, since the MORBID program is at the moment not able to account for the hyperfine interaction present in $CH_2$. Instead, I decided to work with the Euler approach described in Section 3.3.2. This method was developed to improve the convergence of the effective Hamiltonian, as was demonstrated successfully for the similarly light and floppy water molecule [1].

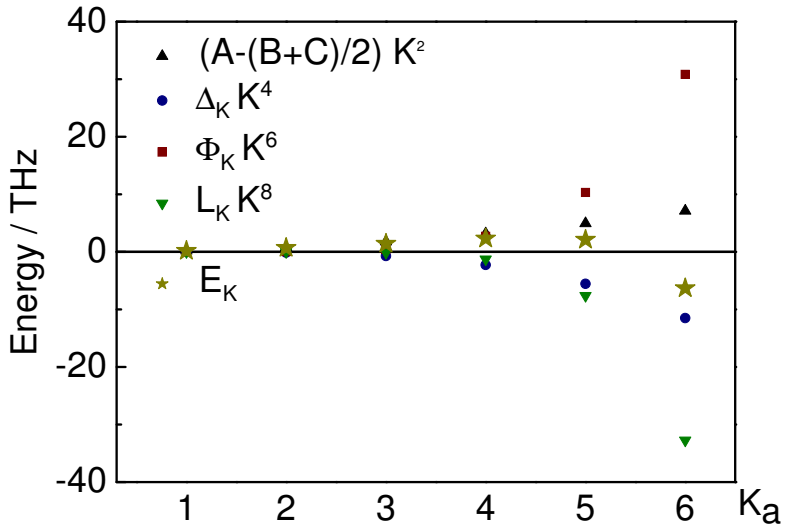


Figure 5.9: Plotted are the $K_a$ dependent terms in the $A$-reduced Hamiltonian and the sum E of the four lowest order terms against $K_a$. Used were rotational parameters of the present investigation.

The convergence behaviour of the standard, in this case Watson *A*-reduced, Hamiltonian can be expressed by using d'Alembert's criterion, as has been outlined in more detail in Section 3.3.2, Equation 3.30. The convergence radius in $K_a$ for $CH_2$ is $5$ or even only $4$ from the two lowest order root criteria. This means, strictly speaking, that this Hamiltonian is not able to describe energy levels with a value of $K_a > 3$ in the case of $CH_2$.

The (non)-convergence of the Hamiltonian can be visualised if one plots the pure $K_a$-dependent terms of the power series versus $K_a$, as has been done in Figure 5.9 using the parameter set obtained in this work from the standard Watson-type Hamiltonian.

The higher order contributions to the Hamiltonian increase dramatically in size with increasing $K_a$. Furthermore, the parameters have an alternating sign, and the higher order terms have the same absolute value as the first order term already for $K_a = 4$. The total energy E, defined here as the sum of all purely $K_a$-dependent terms up to octic order, actually turns to negative values for $K_a = 6$, clearly demonstrating the breakdown of the used model.

Since one of the main purposes of this work was to provide the astrophysical community with highly precise transition rest frequencies for future interstellar searches, and since further spectroscopic data is at the moment unlikely to be obtained easily, some effort was made to improve the theoretical analysis of $CH_2$ further by employing the Euler expansion of the Hamiltonian.

The Euler analysis generally affects only the rotational part of the Hamiltonian. The scalar spin parameters may be expanded in an Euler series, too, however, this was not necessary in the present analysis of $CH_2$. The Euler expansion is very sensitive to the values of the scaling parameters $a$ and $b$, and, especially in the case of a restricted experimental dataset, to the choice of the set of initial rotational parameters. These should be close enough to the real parameters to avoid convergence of the fit towards a local instead of a global minimum. To find such a reasonable initial parameter set, the calculated pure rotational energy levels up to $N = K_a = 6$ from Bunker *et al.* [95] were analysed in a first step by adding successively energy levels with higher quantum numbers to the fit. Fine and hyperfine interactions were neglected at this stage. Care was taken to achieve both a low wrms value and to keep most of the Euler parameters positive. Next, the initial parameter set was used to analyse the GSCD [96] and field-free IR data [97]. Fine and hyperfine structure terms were fixed to values of Marshall and McKellar [96]. Then, the microwave para-transitions were successively included and the fine structure parameters could be determined by the fit. As a last step, the ortho-transitions were added and all presently determined rotational, fine and hyperfine structure parameters could be obtained.

The final result of the analysis is shown in Table 5.4, in the column labeled A. One main improvement is the reduction of the number of needed rotational parameters to 14, compared to 16 with the standard analysis, with a still better wrms value. It has to be noted that the fixed $X_{4,0}$ coefficient can also be omitted without deterioration of the analysis [1], further reducing the number of parameters.

Table 5.4: Coefficients of the Euler expansion of the Hamiltonian for $CH_2$. The difference between the fits A and B is that in the latter case the weak, newly measured fine structure line at 581 GHz has been included. For comparison, the fine and hyperfine structure parameters are given for both the Euler and the Watson fits.

| Parameter | This work, Euler [a,b] | | This work, Watson [a] |
|---|---|---|---|
| | A | B | |
| $b$ | [0.00014] | | |
| $a$ | [0.03020] | | |
| $b_{off}$ | [0.0006] | | |
| $a_{off}$ | [0.0750] | | |
| $X_{0,1}$ | 234360.214(55) | 234360.217(55) | |
| $X_{1,0}$ | 2211494.1(34) | 2211494.2(34) | |
| $X_{2,0}$ | −20216.7(38) | −20216.7(38) | |
| $X_{1,1}$ | 8016.043(215) | 8016.081(214) | |

[1] This will, of course, change the remaining $K_a$-dependent parameters considerably

Table 5.4: $CH_2$ Euler analysis - continued

| Parameter | This work, Euler [a,b] | | This work, Watson [a] |
|---|---|---|---|
| | A | B | |
| $X_{0,2}$ | 21.7176(87) | 21.7195(87) | |
| $X_{3,0}$ | 3688.437(282) | 3688.440(282) | |
| $X_{2,1}$ | 130.015(170) | 130.005(170) | |
| $X_{1,2}$ | 0.9979(72) | 0.9975(72) | |
| $X_{0,3} \cdot 10^3$ | 5.065(93) | 5.041(93) | |
| $X_{4,0}$ | [50] | [50] | |
| $X_{3,1}$ | 17.4395(124) | 17.4401(124) | |
| $X_{2,2}$ | 0.13868(288) | 0.13872(288) | |
| $Y_{0,0}$ | 9628.837(99) | 9628.813(99) | |
| $Y_{0,1}$ | 2.5718(53) | 2.5723(53) | |
| | | | |
| $\alpha$ | 7783.39(10) | 7783.177(80) | 7783.28(10) |
| $\beta$ | 1223.640(110) | 1223.730(106) | 1223.494(110) |
| $\alpha_{SK}$ | −14.67(10) | −14.440(83) | −14.70(10) |
| $\alpha_{SN}$ | 0.161(15) | 0.2037(72) | 0.201(15) |
| $\beta_{SN}$ | −0.1726(145) | −0.1294(88) | −0.1000(146) |
| $\epsilon_{aa}$ | 20.674(119) | 20.444(134) | 20.657(119) |
| $\epsilon_{bb}$ | −153.884(35) | −154.034(41) | −153.850(35) |
| $\epsilon_{cc}$ | −124.672(90) | −124.667(88) | −124.731(90) |
| ${}^S\Delta_{KN}$ | −0.4329(270) | −0.310(35) | −0.4315(270) |
| ${}^S\delta_N$ | 0.01216(126) | | 0.01163(126) |
| ${}^S\Delta_N$ | | 0.02164(198) | |
| $a_F(H)$ | −22.777(116) | −22.813(115) | −22.762(116) |
| $a_{FK}(H)$ | 1.7014(268) | 1.7040(268) | 1.7044(268) |
| $T_{aa}(H)$ | 29.899(93) | 29.885(93) | 29.905(93) |
| $T_{bb}(H)$ | −14.709(60) | −14.701(60) | −14.713(60) |
| wrms | 1.09 | 1.17 | 1.59 |

[a] Numbers in parentheses denote one standard deviation in units of the last digits.

[b] Values in square brackets were held fixed during the fit.

It has been included with the objective to improve the predictive capability of the parameter set. Moreover, all except one coefficients in the Euler series are positive, a further improvement compared to the alternating signs of the parameters of the standard Hamiltonion[2].

Furthermore, the wrms value has been significantly improved to nearly unity, meaning that most transitions are reproduced to their experimental uncertainty. This indicates that with the Euler expansion the information of the experimental lines is sufficient to determine all relevant rotational parameters. In contrast, the comparatively high wrms value in the Watson analysis suggests that more rotational parameters are needed than can be determined from the data, due to the bad convergence of the model.

[2]Note: the quartic centrifugal distortion parameters in the standard form of the Watson Hamiltonian are defined to be positive, but contribute with a negative sign to the series expansion

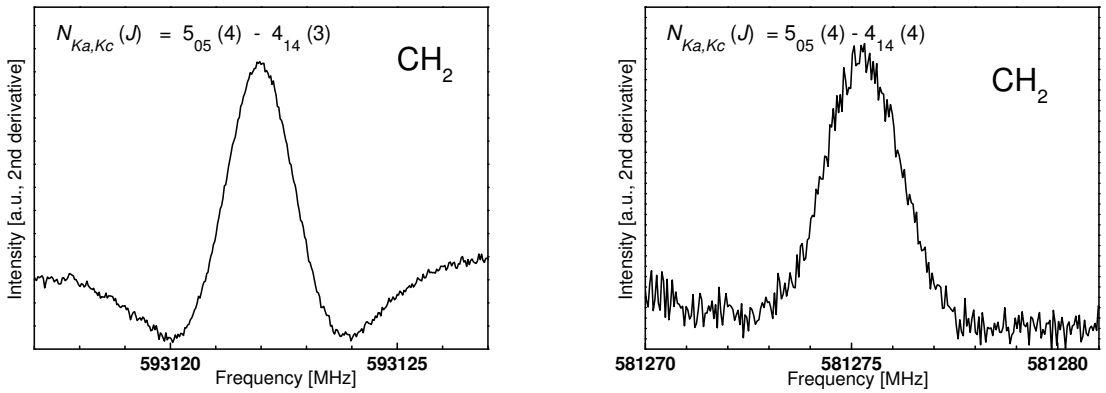


Figure 5.10: Fine structure components of the $N_{Ka,Kc} = 5_{0,5} - 4_{1,4}$ transition of $CH_2$ measured with the Cologne Terahertz Spectrometer. The weak $\Delta J = 0$ line in the right panel was measured for the first time. The different line shapes are due to differing $g$-factors of the participating levels.

For comparison, both the fine and hyperfine interaction parameters of the Watson and the Euler analysis are stated in Table 5.4. It is very encouraging that they agree in their error limits, indicating a very small correlation between rotational and (hyper)fine parameters.

The second parameter set (B) in Table 5.4 has been obtained after the inclusion of the weak $\Delta J = 0$, $N_{KaKc}(J) = 5_{05}\,(4) \leftarrow 4_{14}\,(4)$ fine structure line at $\sim 581$ GHz. This line has not been reported previously, in contrast to the around 20 times stronger $\Delta J = 1$ components of this rotational transitions [83]. It was measured in the course of this work in order to test the quality of the analysis. For this purpose, the Zeeman modulation cell was set up at the Terahertz Spectrometer. The experimental conditions were optimised by re-measuring the already published transitions. Both, a strong $\Delta J = 1$ and the newly measured weak $\Delta J = 0$ transition are shown in Figure 5.10. The measured transition frequency deviated by around $8\,\sigma$, i.e. $5$ MHz, from the predicted one. By exchanging the spin-rotation centrifugal distortion term ${}^S\delta_N$ with ${}^S\Delta_N$ in the original fit A, the line deviates by only $4\,\sigma$. With this change retained in the parameter set, the new line was fitted to a few kHz with the parameter set B. The changes in the parameters are generally within $3\,\sigma$, except for $\epsilon_{bb}$ and ${}^S\Delta_{KN}$. It was also searched for the second $\Delta J = 0$ component of this rotational transition. It has a comparable transition strength, but a much smaller $g_{J'}$-value of only $0.07$. Even with considerably higher magnetic fields, this line could not unambiguously be detected. A weak feature was observed at the position predicted from parameter set B.

A comparison of the Watson and the Euler parameter set is directly possible by utilising the conversion formulas derived in Section 3.3.2, summarised in Table 3.3; the results are stated in Table 5.5. The conversion formulas were derived assuming the description of the Hamiltonian as an infinite sum of operands, i.e. in general all expansion coefficients must be known to fully convert from one model to the other. Since this is obviously

Table 5.5: Comparison between Watson parameters converted from Euler series coefficients and from the direct fit. All parameters are in MHz.

| Parameter | Converted | Direct |
|---|---|---|
| $A$ | 2211494.1 | 2212816.5(38) |
| $B$ | 253617.9 | 253284.9(176) |
| $C$ | 215102.5 | 215436.6(174) |
| $\Delta_N$ | 11.0943 | 11.410(43) |
| $\Delta_{NK}$ | −650.91 | −630.85(46) |
| $\Delta_K$ | 87643.6 | 88741.2(38) |
| $\delta_N$ | 3.2058 | 2.7792(50) |
| $\delta_K$ | 718.9 | 502.1(87) |
| $\Phi_N$ | 0.0035960 | 0.002489(96) |
| $\Phi_{NK}$ | −0.5437 | −0.6845(56) |
| $\Phi_{KN}$ | −114.96 | −81.92(35) |
| $\Phi_K$ | 7041.994 | 6606.684(200) |
| $\phi_N$ | 0.00380588 | |
| $\phi_{NK}$ | 0.480111 | |
| $\phi_K$ | 53.681824 | |
| $L_N \cdot 10^6$ | −1.501037742 | |
| $L_{NNK} \cdot 10^3$ | −0.2737180074 | |
| $L_{NK}$ | 0.16230 | 0.03495(61) |
| $L_{KKN}$ | 17.903 | 7.289(55) |
| $L_K$ | −418.5 | [-195] |

not the case for the analysis of $CH_2$, the observed deviations between the parameters in Table 5.5 can easily be understood, especially for the higher order terms, were not all parameters of one order $k = m + n(+1)$ (see Section 3.3.2) have been determined in the analysis. Still, the parameters are of the same order, and discrepancies are also likely to appear from the special choice of $a$ and $b$.

A comparison between calculated transition frequencies to the LMR data of Sears *et al.* [92] can be done to get some information on the predictive capability of the obtained parameter set. The latter data had not been included in the analysis due to distrust in the derived field-free transition frequencies, but is ideally suited to estimate the fit quality of the present analysis. In Table 5.6, two exemplary rotational transitions are collected, the first of those has been measured both in this work and with LMR, the second only with LMR. The comparison for the $1_{10} - 1_{01}$ multiplet reveals differences up to more than 20 MHz between our high-accuracy experimental data and the LMR data. This discrepancy is bigger than the stated uncertainty for the LMR measurements of around 5 MHz. Having this in mind, the coincidence between the purely predicted $3_{12} - 3_{03}$ lines and the experimental LMR data is excellent. On both levels, only less accurate information from the GSCD data is in the fit.
Therefore, the present analysis is believed to have good predictive capability for the astro-

Table 5.6: Comparison between transition frequencies either measured in Cologne or predicted with the Euler parameter set and LMR data by Sears. $\Delta\nu$ denotes the difference in frequency between the Cologne and LMR data. All frequency values are in MHz.

| Transition | | | | This work [a] | o.-c.[b] | Sears [92][a] | $\Delta\nu$ |
|---|---|---|---|---|---|---|---|
| $N'_{Ka'Kc'}$ | $J'$ | $N''_{Ka''Kc''}$ | $J''$ | | | | |
| $1_{10}$ | 1 | $1_{01}$ | 1 | 1902654.362(200) | 0.177 | 1902677.(5) | −22.638 |
| $1_{10}$ | 2 | $1_{01}$ | 1 | 1907986.637(300) | 0.021 | 1907992.(5) | −5.327 |
| $1_{10}$ | 1 | $1_{01}$ | 2 | 1912328.935(200) | 0.058 | 1912343.(5) | −14.065 |
| $1_{10}$ | 0 | $1_{01}$ | 1 | 1916348.190(200) | 0.274 | 1916348.(5) | 0.190 |
| $1_{10}$ | 2 | $1_{01}$ | 2 | 1917661.094(100) | −0.213 | 1917659.(5) | 2.094 |
| $1_{10}$ | 1 | $1_{01}$ | 0 | 1925866.221(200) | 0.339 | 1925873.(5) | −7.779 |
| $3_{12}$ | 2 | $3_{03}$ | 3 | 2000540.485(375) | | 2000535.(5) | 5.485 |
| $3_{12}$ | 4 | $3_{03}$ | 3 | 2001934.335(390) | | 2001936.(5) | −1.665 |
| $3_{12}$ | 3 | $3_{03}$ | 3 | 2009466.204(363) | | 2009495.(5) | −28.796 |
| $3_{12}$ | 4 | $3_{03}$ | 4 | 2012938.582(405) | | 2012929.(5) | 9.582 |
| $3_{12}$ | 2 | $3_{03}$ | 2 | 2014130.399(363) | | 2014116.(5) | 14.399 |
| $3_{12}$ | 3 | $3_{03}$ | 4 | 2020470.451(371) | | 2020488.(5) | −17.549 |
| $3_{12}$ | 3 | $3_{03}$ | 2 | 2023056.118(390) | | 2023076.(5) | −19.882 |

[a] Numbers in parentheses denote one standard deviation in units of the last digits.

[b] Only given for the transitions measured in this work.

Otherwise, the calculated transition frequencies are given directly.

physically interesting transitions between comparably low lying rotational energy levels.

However, prediction of transition frequencies involving energy levels with $K_a > 1$ might be less accurate. No high precision data on these levels is contained in the fit, although the $K_a = 4 \leftarrow 3$ IR transitions from Sears [97] will give some constraint of the higher order $K_a$ dependent parameters. Moreover, since they are not contained in the GSCD data, there is no information at all for $K_a = 3 - 2$ and $2 - 1$ transitions in the dataset, leaving the relative energies of the $K_a$ stacks rather undefined.

It is again possible to use LMR data to get an estimate of the uncertainty for the higher energy levels. Sears *et al.* [43] also measured three $K_a = 2 \leftarrow 1$ transitions. A comparison between his deduced $K_a = 2$ energy levels (Sears, private communication) and those of the present analysis gives comparatively small differences of less than $150$ MHz. This is only a few times the stated uncertainty of the fit (around $25$ MHz) for these levels and constrains the experimental laboratory search for rotational transitions involving $K_a = 2$ - levels to an easily manageable frequency range. An inclusion of these six energy levels in the analysis with an estimated uncertainty of $20$ MHz gives an wrms of $1.8$ with only slightly changed rotational parameters and not much improved prediction of the $K_a = 2$ energy levels, suggesting that the present predictions actually may be better than the extrapolated zero-field frequencies from the LMR measurements.

For even higher energy levels, we can only compare the different theoretical models. A comparison to energy levels derived by Bunker *et al.* [95], employing the non-rigid bender approach, gives a difference of around $200$ GHz for the $K_a = 3$ and $4$ levels, of $450$ GHz for the $K_a = 5$, and $1500$ GHz for the $K_a = 6$ energy levels. Obviously, the agreement is far from perfect, but one has to keep in mind that i) this is a comparison to *ab initio* values and ii) no information on $K_a$ values higher than four is contained in the fit. Therefore, this result is acceptable.

Furthermore, the increase of energy differences with increasing $K_a$ is a rather smooth one. The Watson model, in comparison, behaves erratic for values of $K_a > 4$: whereas for $K_a \leq 4$ the deviations to the MORBID predictions are similar or better than those of the Euler model, for $K_a = 5$ the deviation is already $13200$ GHz and for $K_a = 6$ the total energy turns to negative values, as has been mentioned already at the beginning of this section.

Therefore, it is clearly demonstrated that the standard Watson-type Hamiltonian is the wrong model to describe the very light and floppy $CH_2$ molecule. The Euler model, on the other hand, is capable of reproducing the experimental data known to date and, moreover, in principle able to be applied to higher $N$ and $K_a$ data.

In any case, there is still need for additional high accuracy laboratory data on this molecule, especially between levels with higher $N$ and $K$ values. The present analysis yields frequency predictions for transitions involving $K_a = 2$ levels which are accurate enough to be searched for in the laboratory.
For transitions involving the lower $N$ and $K_a$ levels, highly precise frequency predictions are obtained. These lower energy levels are thought to be primarily populated in the interstellar medium.

A linelist of predicted transition frequencies up to $N = 6$ and $K_a = 1$ is given in the appendix in Table B.2 for frequencies below 5 THz.

## 5.4 Interstellar Detection of Cold $CH_2$

As has been outlined in the introduction to this chapter, the only unambiguous interstellar detection of methylene had been made by Hollis *et al.* [12]. They clearly identified the $4_{04} - 3_{13}$ multiplet between $68$ and $71$ GHz in emission towards the two dense hot core sources Orion KL and W 51 M, which provide excitation to the energetically high-lying $4_{04}$ energy level at $\sim$215 K.

The present laboratory measurements and subsequent data analysis improved the predictions of transition frequencies of $CH_2$ involving low energy rotational levels. Consequently, we decided to perform a search for $CH_2$ in cold interstellar sources. In a collaboration with E. Polehampton from the Max-Planck-Institut für Radioastronomie (Bonn) it

was searched for these transitions in observational data of the Infrared Space Observatory (ISO) Long Wavelength Spectrometer (LWS, Clegg *et al.* [101]). The frequency coverage of this spectrometer is $43 - 198$ $\mu$m, i.e. $1.53 - 6.38$ THz, with a spectral resolution of around $30$ kms$^{-1}$, i.e. $20 - 30$ MHz.
A list of the predicted transition frequencies in the frequency range covered by ISO LWS, involving the four lowest rotational energy levels, together with the lower level energy $E_{lower}$ and the calculated line strength $S_{ij}$ [3] is collected in Table 5.7. Since no resolution of the hyperfine structure is expected, intensity weighted transition frequencies are given for the ortho-states.

It was searched for all these transitions in the ISO data towards the galactic center source Sgr B2, and fine structure absorption lines belonging to two rotational transitions, the $N_{KaKc} = 1_{11} - 0_{00}$ starting from the lowest ortho-, and the $N_{KaKc} = 2_{12} - 1_{01}$ starting from the lowest para-level of $CH_2$, have been unambiguously detected.

The observed lines are shown in the two lower panels of Figure 5.4. The shape of the line profiles are not due to the unresolved hyperfine structure, but arises from absorbing gas in the galactic spiral arms with different velocity components in the line of sight towards the FIR continuum source Sgr B2. The peak absorption arises from molecular gas in the region of Sgr B2, at a velocity of $\sim 65$ kms$^{-1}$. Since the absorption profiles observed in $CH_2$ are too weak to allow for an analysis of the structure of these line-of-sight velocity components, strong absorption lines of the CH $^2\Pi_{1/2}$, $J = 3/2 - 1/2$ $\Lambda$-doublet, shown in the upper panel of Figure 5.4 have been used to fit the line shape. This data has also been observed with the ISO LWS. The calculated line profile shown for $CH_2$ has then been obtained by assuming the same velocity structure and a fixed ratio of $CH_2$ to CH in all absorbing molecular clouds in the line of sight.

For ortho-$CH_2$, we clearly detect absorption from the $1_{11} - 0_{00}$, $J = 2 - 1$ and $J = 1 - 1$ fine structure components at $\sim 2.35$ THz. The weaker $J = 1 - 0$ component is not detected above the noise in the spectrum. The strongest fine structure component of the $2_{11} - 2_{02}$ transition ($J = 3 - 3$) from the next highest ortho energy level is blended with strong NH absorption at this frequency (around $1.91$ THz), whereas its weaker components are not detected above the noise level. For the strongest component of the other transition starting from the same level, the $3_{13} - 2_{02}$, a tentative detection at a level $\sim 3\sigma$ can be made. No higher level ortho-transitions were detected above the noise in the data. In the case of para-$CH_2$, the strongest fine structure component of the $2_{12} - 1_{10}$ transition ($J = 3 - 2$) at $\sim 2.8$ THz has been detected. This transition starts from the lowest energy level of the para species. The other transition possible from this level is the $1_{10} - 1_{01}$ at $\sim 1.95$ THz. The predicted intensity of this transition gives a value consistent with the noise level in the spectrum at this frequency. No further para transitions from energetically higher energy levels were detected above the noise in the data.

[3] The dimensionless linestrength $S_{ij} = \frac{\boldsymbol{\mu_{ij}}}{\mu^2}$, where $\boldsymbol{\mu_{ij}}$ is the transition matrix element and $\mu$ the permanent dipole moment, can be calculated from the intensities $I(T)$ of the Pickett predictions by $S_{ij}\mu = 2.40251 \cdot 10^4 I(T) Q_{rs}(T) \nu^{-1} (e^{-E"/kT} - e^{-E'/kT})^{-1}$ with $I$ in nm$^2$MHz, $\nu$ in MHz, and $\mu$ in Debye.

Table 5.7: Calculated frequencies, uncertainties, lower energy levels $E_{lower}$ and line strengths $S_{ij}$ for the low-lying transitions of $CH_2$ in the frequency region covered by the ISO LWS, ignoring hyperfine-structure in the ortho transitions. The detected lines towards Sgr B2 are marked with an asterisk.

| $N'_{Ka'Kc'}$ | $J'$ | $N''_{Ka''Kc''}$ | $J''$ | Frequency [MHz] | $E_{lower}$ [cm$^{-1}$] | $S_{ij}$ |
|---|---|---|---|---|---|---|
| $1_{10}$ | 1 | $1_{01}$ | 1 | 1902654.172(148) | 15.8976 | 0.366 |
| $1_{10}$ | 2 | $1_{01}$ | 1 | 1907986.465(142) | 15.8976 | 0.615 |
| $1_{10}$ | 1 | $1_{01}$ | 2 | 1912329.005(116) | 15.5749 | 0.622 |
| $1_{10}$ | 0 | $1_{01}$ | 1 | 1916347.953(170) | 15.8976 | 0.500 |
| $1_{10}$ | 2 | $1_{01}$ | 2 | 1917661.297(83) | 15.5749 | 1.884 |
| $1_{10}$ | 1 | $1_{01}$ | 0 | 1925865.835(172) | 15.1234 | 0.513 |
| $2_{11}$ | 1 | $2_{02}$ | 2 | 1942895.858(104) | 47.1390 | 1.141 |
| $2_{11}$ | 3 | $2_{02}$ | 2 | 1944438.793(129) | 47.1390 | 1.139 |
| $2_{11}$ | 2 | $2_{02}$ | 2 | 1949054.582(146) | 47.1390 | 5.153 |
| $2_{11}$ | 3 | $2_{02}$ | 3 | 1954919.352(144) | 46.7894 | 9.254 |
| $2_{11}$ | 1 | $2_{02}$ | 1 | 1958121.546(144) | 46.6311 | 3.313 |
| $2_{11}$ | 2 | $2_{02}$ | 3 | 1959535.142(120) | 46.7894 | 1.136 |
| $2_{11}$ | 2 | $2_{02}$ | 1 | 1964280.270(136) | 46.6311 | 1.136 |
| $3_{12}$ | 2 | $3_{03}$ | 3 | 2000540.485(375) | 93.9373 | 0.275 |
| $3_{12}$ | 4 | $3_{03}$ | 3 | 2001934.335(389) | 93.9373 | 0.271 |
| $3_{12}$ | 3 | $3_{03}$ | 3 | 2009466.204(363) | 93.9373 | 2.868 |
| $3_{12}$ | 4 | $3_{03}$ | 4 | 2012938.582(405) | 93.5703 | 4.116 |
| $3_{12}$ | 2 | $3_{03}$ | 2 | 2014130.399(363) | 93.4840 | 2.162 |
| $3_{12}$ | 3 | $3_{03}$ | 4 | 2020470.451(371) | 93.5703 | 0.271 |
| $3_{12}$ | 3 | $3_{03}$ | 2 | 2023056.118(390) | 93.4840 | 0.275 |
| $1_{11}$ | 1 | $0_{00}$ | 1* | 2344722.585(520) | −0.0029 | 3.016 |
| $1_{11}$ | 2 | $0_{00}$ | 1* | 2348624.479(514) | −0.0029 | 4.993 |
| $1_{11}$ | 0 | $0_{00}$ | 1 | 2354740.673(544) | −0.0029 | 0.989 |
| $2_{12}$ | 1 | $1_{01}$ | 1 | 2770895.82(156) | 15.8976 | 0.384 |
| $2_{12}$ | 2 | $1_{01}$ | 1 | 2779532.77(155) | 15.8976 | 1.134 |
| $2_{12}$ | 1 | $1_{01}$ | 2 | 2780570.65(157) | 15.5749 | 0.027 |
| $2_{12}$ | 3 | $1_{01}$ | 2* | 2783068.09(154) | 15.5749 | 2.099 |
| $2_{12}$ | 2 | $1_{01}$ | 2 | 2789207.61(155) | 15.5749 | 0.367 |
| $2_{12}$ | 1 | $1_{01}$ | 0 | 2794107.48(156) | 15.1234 | 0.487 |
| $3_{13}$ | 2 | $2_{02}$ | 2 | 3188247.21(375) | 47.139 | 0.685 |
| $3_{13}$ | 2 | $2_{02}$ | 3 | 3198727.77(375) | 46.7894 | 0.021 |
| $3_{13}$ | 3 | $2_{02}$ | 2 | 3199416.36(374) | 47.139 | 5.373 |
| $3_{13}$ | 4 | $2_{02}$ | 3 | 3200796.52(373) | 46.7894 | 7.750 |
| $3_{13}$ | 2 | $2_{02}$ | 1 | 3203472.90(374) | 46.6311 | 3.599 |
| $3_{13}$ | 3 | $2_{02}$ | 3 | 3209896.92(374) | 46.7894 | 0.657 |
| $4_{14}$ | 3 | $3_{03}$ | 3 | 3589954.37(788) | 93.9373 | 0.161 |
| $4_{14}$ | 3 | $3_{03}$ | 4 | 3600958.62(788) | 93.5703 | 0.003 |
| $4_{14}$ | 4 | $3_{03}$ | 3 | 3601796.02(787) | 93.9373 | 2.381 |
| $4_{14}$ | 5 | $3_{03}$ | 4 | 3602298.22(786) | 93.5703 | 3.100 |
| $4_{14}$ | 3 | $3_{03}$ | 2 | 3603544.29(787) | 93.4840 | 1.809 |
| $4_{14}$ | 4 | $3_{03}$ | 4 | 3612800.27(788) | 93.5703 | 0.156 |

[a] Numbers in parentheses show one times the standard deviation in units of the last significant digits

The analysis of this data allowed not only for the determination of the total $CH_2$ column density along the line of sight ($N = (7.5 \pm 1.1) \cdot 10^{14}$ cm$^{-2}$), summed over all velocities in both the ortho and para states, an estimation of the rotational temperature of the Sgr B2 source of $T_{rot} < 40^{+14}_{-11}$ K from the two observed ortho transitions and, assuming only the lowest three energy levels in Sgr B2 to be populated, the determination of an ortho-to-para ratio for $CH_2$ of $1.6^{+0.9}_{-0.6}$. Furthermore, a ratio of [CH/$CH_2$]=2.7$\pm$0.5 for all velocity components could be derived. Since the data on $CH_2$ and CH are recorded with the same observational parameters (beamsize, calibration, etc.) and involving levels of similar energy, they provide the best comparison of the two species to date.

Furthermore, the strongest ortho-$CH_2$ fine structure component ($J = 2 - 1$) of the $1_{11} - 0_{00}$ rotational transition is clearly detected in absorption towards the active star forming region W 49 N, yielding column densities for the $0_{00}$ level of $(0.8 \pm 0.4) \cdot 10^{14}$ cm$^{-1}$ and $(1.2 \pm 0.4) \cdot 10^{14}$ cm$^{-1}$ for the two velocity components considered in the line analysis at $37$ kms$^{-1}$ and $61$ kms$^{-1}$ respectively (see Figure 5.4).

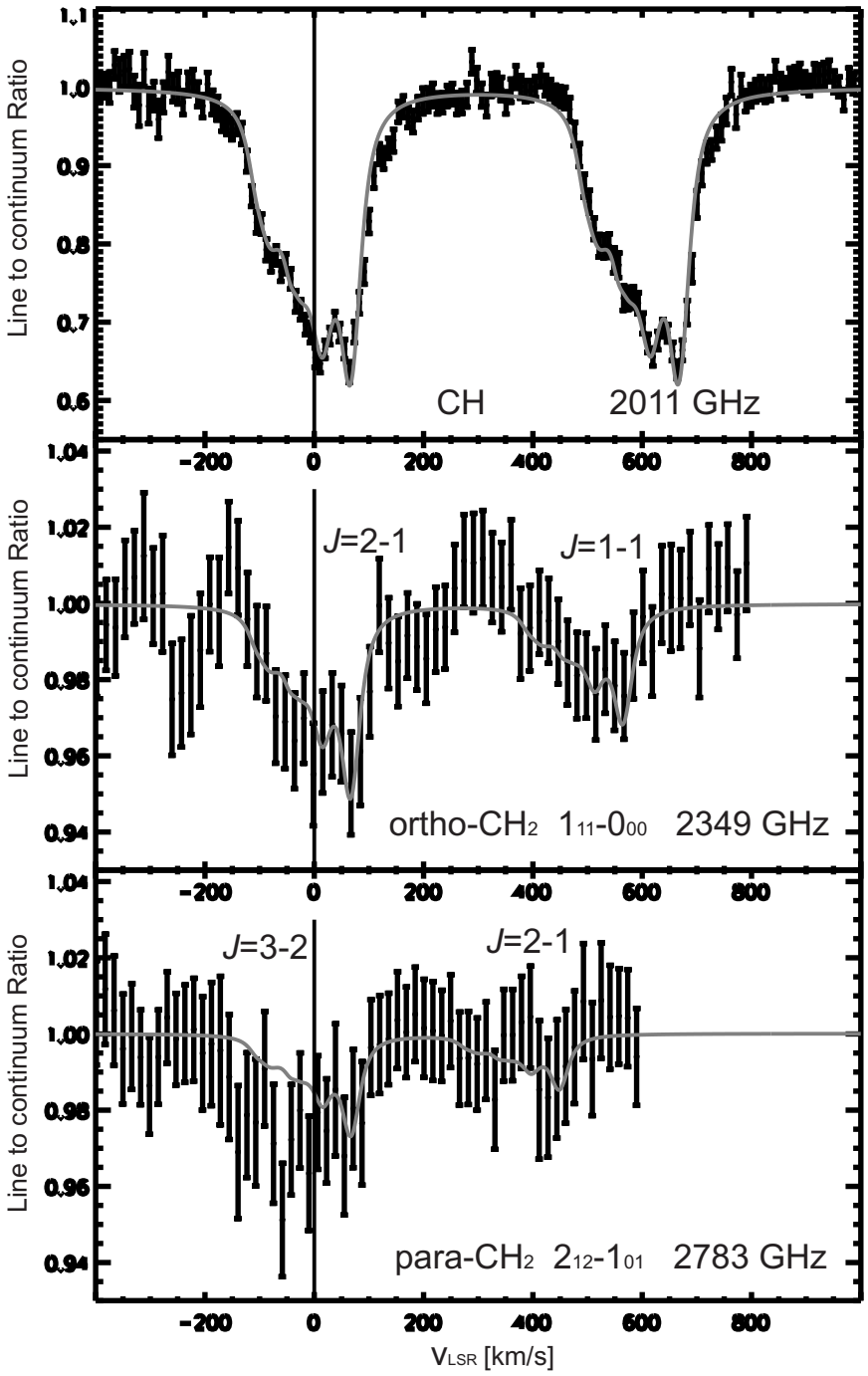


Figure 5.11: **Upper panel**: Data and fit of the CH $^2\Pi_{1/2}$, $J = 3/2 - 1/2$ doublet line towards Sgr B2, measured with ISO. This line was used to determine the contributions of the different velocity components in the line of sight. **Lower two panels**: a model line based on the CH line shape has been fitted to the data around the two lowest energy transitions of $CH_2$. The fit was carried out to the strongest fine structure component in each case.

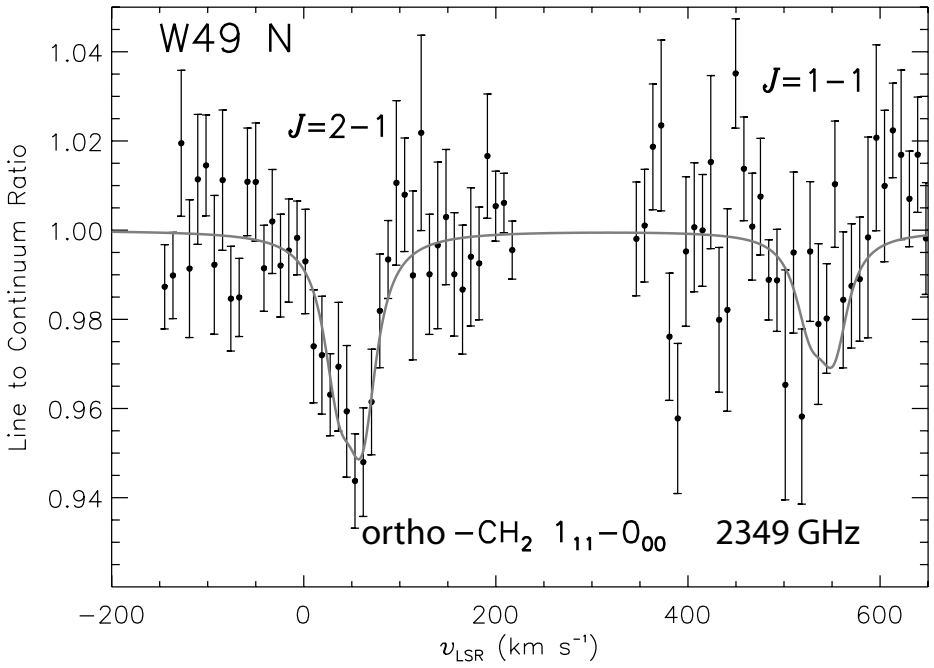


Figure 5.12: Data around the $J = 2 - 1$ ($2349$ GHz) and $J = 1 - 1$ ($2345$ GHz) fine structure components of the $N_{KaKc} = 1_{11} - 0_{00}$ $CH_2$ transition towards W 49 N. The solid line shows a model derived from a fit to the $J = 2 - 1$ component and the expected relative line strength of the $J = 1 - 1$ component.

## 5.5 Conclusions

The high-resolution measurements of two energetically low-lying rotational transitions of the methylene radical at terahertz (FIR) frequencies considerably improve the sparse dataset on this molecule. For the ortho-$CH_2$ $N_{KaKc} = 2_{11} - 2_{02}$ rotational transition, centered at $1.95$ THz, $23$ hyperfine components have been resolved in total, yielding valuable information on the underlying hyperfine interaction. The six measured fine structure lines around $1.92$ THz belong to the $1_{10} - 1_{01}$ transition, the lower level being the rotational ground state of para-$CH_2$. The energetically lowest rotational levels are those predominantly populated in the cold interstellar medium.

It was found that, although capable of reproducing the experimental data to some extent, the standard analysis fails even for moderate values of the angular momentum quantum numbers. Therefore, the subsequent global analysis of all field-free rotational data on the electronic and vibrational ground state was done using an Euler series describing the rotational energies. With this approach the number of parameters needed to fit the dataset was significantly decreased. With the standard power series expansion, almost as many rotational parameters as measured transitions was needed. The new analysis has, therefore, an improved predictive capability, as was demonstrated by comparing predicted transition frequencies to previous experimental and theoretical work. Moreover, and even more important, the Euler model is in principle capable of describing also higher $N$ and $K_a$ energy levels, for which the standard analysis fails.

Transition frequency predictions based on the new analysis assist the laboratory search for transitions involving higher $N$ and $K_a$ energy levels, which, in turn, can be used to further improve the analysis. Although the quality of predictions to $K_a$ values higher than two is at the present stage still very poor, a successive laboratory investigation towards ever higher rotational levels is now feasible.

Since many rotational transitions are still not accessible easily in the laboratory, the newly predicted transition frequencies can be used as a basis for subsequent astronomical searches for cold $CH_2$, as has been demonstrated by the detection of $CH_2$ towards the galactic center source Sgr B2.

These results encourage further searches for cold $CH_2$ via its terahertz transitions towards other molecular cloud complexes. The advent of future submm-wavelength and FIR telescopes like APEX/ALMA, Herschel and SOFIA will allow for the observation of several energetically low lying $CH_2$ transitions, e.g. the $1_{11} - 2_{02}$ transition at $950$ GHz with APEX/ALMA or the $1_{10} - 1_{01}$ multiplet at $1.9$ THz with the HIFI[4] instrument of the Herschel satellite or the GREAT[5] receiver on board SOFIA, although the lines are at the specified limit of the covered frequency range.

[4]Heterodyne Instrument for the Far Infrared

[5]German Receiver for Astronomy at Terahertz Frequencies

6

# The Water Molecule: Measurements and Analysis of Terahertz Data

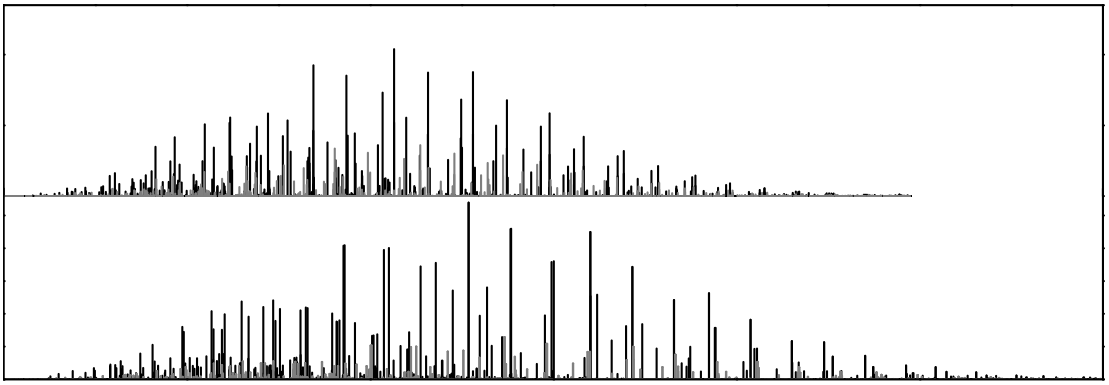

Water ($H_2O$) is probably the most important and most investigated molecular species. It is of great importance both for atmospheric and astrophysical science, and also for fundamental science.

Although only a trace gas in the Earth's atmosphere, water can be regarded as the main greenhouse gas, being responsible for about $70\%$ of absorption in the atmosphere. This is mainly due to its large dipole moment ($\sim 1.8$ D) and very dense rotational and rovibrational spectrum in the infrared and far infrared, respectively. Quantitative atmospheric models need highly accurate spectroscopic values of transition frequencies and intensities. It was found to be necessary to include the influence of the singly deuterated water molecule, HDO, into these calculations, even though its mean terrestrial abundance is smaller by a factor of $1.5 \cdot 10^{-4}$ compared to $H_2O$.

Quite certainly because water is one of the major constituents responsible for the origin of life on earth, it was also sought for in a multitude of extraterrestrial environments. Water vapour has been detected in the planetary atmospheres of Jupiter, Saturn

[102], Mars (e.g. [103]), and Venus (e.g. [104]). It is also abundant in the comae of comets [105]. Rotational water transitions have been detected in the line-of-sight molecular clouds towards the galactic center [106], towards molecular cloud cores [107], towards red supergiant stars [108, 109], and its infrared spectrum has been observed even in sunspots [110]. Very surprising was the detection of a water rotational line in the circumstellar envelope of the ageing carbon-rich star IRC+10216 [111]. All oxygen is usually bound in CO in these stars, and the detection of $H_2O$ has been attributed to the evaporation of small icy bodies orbiting the star due to its extending enevelope. Moreover, water has been detected in extragalactic sources by means of its strong maser emission line at 22 GHz [112]. Water is everywhere!

However, the observation of rotational water lines is generally very difficult with ground based telescopes because of the strong absorption of atmospheric water vapour. Therefore, water has been, is and will be one of the main research topics of satellite missions such as the NASA Submillimeter Wave Astronomy Satellite (SWAS), the Infrared Space Telescope (ISO), the Swedish ODIN submillimeter wavelength satellite, the future Heterodyne Instrument for the Far Infrared (HIFI) on board the Herschel satellite, and also of the airborne Stratospheric Observatory for Infrared Astronomy (SOFIA).

Another approach to bypass the limitations of ground-based telescopes is the observation of isotopically substituted water species. Meyer *et al.* [113], for example, have directly observed the ground state rotational transition of HDO in the comet Hale-Bopp at 465 GHz with the James Clark Maxwell Telescope (JCMT). Encrenaz *et al.* measured HDO with the IRAM 30 m radio telescope at 226 GHz towards Mars [114] and also towards Venus [115]. From these measurements, temperature and pressure profiles of water vapour could be determined assuming a fixed HDO/$H_2O$ ratio.

It is important to note that deuterium-containing molecules are considerably enhanced in certain regions of the interstellar medium when compared to terrestrial values. The HDO/$H_2O$ ratio in the Martian and Venusian atmospheres was found to be $6 \pm 3$ and even $120 \pm 40$ times higher than in the Earth's atmosphere. This is thought to be due to a predominant escape of hydrogen compared to deuterium atoms into free space.

An even higher deuterium enhancement can be observed in cold interstellar clouds ($\sim$10-30) K. Whereas the cosmic D/H ratio is $\sim 10^{-5}$, some deuterated species, for example $D_2CO$ and $H_2D^+$, have been observed to reach abundances of more than 1% of their un-deuterated analogous [116, 117]. Very recently, even the triply deuterated species ammonia $ND_3$ [51, 118] and methanol $CD_3OH$ [119] have been observed in a variety of dense, prestellar cores with molecular deuterium to hydrogen ratios as high as $10^{-3}$ and $10^{-2}$, respectively. This can be explained by the fact that chemical reactions leading to a higher degree of deuteration are energetically favoured due to a lower zero point vibrational energy of the heavier deuterated molecules. Additionally, the freeze out of the main molecular reaction partner CO onto dust grains at temperatures below 16 K is thought to be responsible for further enhancement of D-containing species in the gas phase of cold prestellar cores [10].

Consequently, it was possible to observe energetically low lying rotational transitions of the singly deuterated water isotopomer HDO in a variety of interstellar sources [120, 121, 122] up to a frequency of 894 GHz [123]. Actually, most of its energetically low lying transitions fall into the submillimeter-wavelength region. Furthermore, HDO has also been observed in high abundance towards several hot core star-forming regions [124] at considerably higher temperatures and very recently towards the inner envelope of a solar-type protostar, where a HDO/$H_2O$ ratio of $\sim$3 % has been determined [125]. Here, the enhancement is believed to reflect that of dust grains formed during colder periods from which HDO is evaporated. Astronomical observations of HDO rotational transitions and determination of HDO/$H_2O$ fractionation rates are, therefore, important to gain insights into formation processes of interstellar molecules.

Doubly deuterated water has not been detected in the interstellar medium to date, although a sufficient enhancement is possible in cold prestellar cores, as has been discussed in the last paragraphs. No energetically low rotational transition of $D_2O$ lies at a frequency below 300 GHz; the strongest absorption lines appear at 607 and 898 GHz in environments around 10 K. A future interstellar detection of $D_2O$ is certainly favoured by the advent of highly sensitive submillimeter wavelength telescopes like the Atacama Large Millimeter Array (ALMA) or the satellite mission Herschel, which will be operable up to terahertz frequencies.

Water and its isotopomers are also of interest for purely fundamental science. It is the prototypically bent, triatomic asymmetric rotor molecule. The calculation of its rotational and vibrational energy levels is a challenging problem because its lightness and non-rigidity cause large centrifugal distortion effects.

Water has, therefore, been the subject of many theoretical investigations. It has long been known that the standard power series expansion of the Hamiltonian in terms of rotational angular momentum operators, which is based on perturbation theory, does show poor convergence in the case of water. Several attempts have been made to improve the convergence behaviour of the series expansion. These approaches consist of Padé series [126], Borel approximations [127], and the generating function approach [128]. They all use effective Hamilton operators to fit the spectroscopic parameters to experimental data. A more elaborate method is the calculation of rotational and rovibrational energy levels from a potential energy surface (PES) by means of the variational method. Purely *ab initio* potential energy surfaces are generally not accurate enough to account for spectroscopically derived transition frequencies. Two distinct approaches were carried out in the past to improve the accuracy. Whereas Polyansky *et al.* [129, 130], as well as Coudert [131, 132, 133, 19] fitted a parametrised potential energy function directly to experimental data, Partridge and Schwenke started from a purely *ab initio* PES which was subsequently refined by comparison to experimental line positions [134]. However, these calculations are very extensive, and only very elaborate calculations can reproduce the observed transition frequencies to experimental uncertainty. Furthermore, their predictive capability is limited [18].

Experimental water data has also been used to investigate effects of Born-Oppenheimer breakdown in theoretical models [135].

In the following sections, new highly accurate measurements of purely rotational transitions of HDO and $D_2O$ in the vibrational ground and first excited bending state are presented. They extend into the terahertz frequency range and significantly improve the knowledge on higher $J$ and $K$ rotational energy levels. A global analysis of the newly obtained data together with published data in the framework of an Euler expansion of the Hamiltonian is presented for both species. The results of this analysis are discussed and compared to previous studies.

## 6.1 $D_2O$

A sketch of the geometrical structure of the fully deuterated water isotopomer, $D_2O$, is shown in Figure 6.2. $D_2O$ possesses a $C_{2v}$ symmetry with the $x = b$ - axis as symmetry axis. The labelling of the axes is according to the $I^r$ representation where $x = b$, $y = c$,

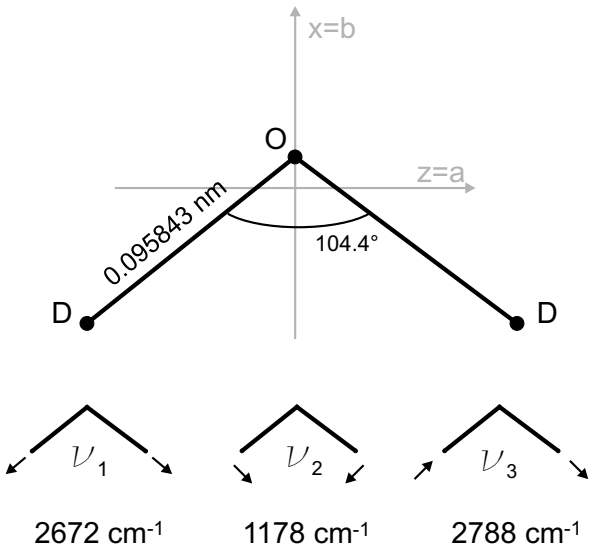


Figure 6.1: Top: Geometrical structure and principal axes system of the moment of inertia of $D_2O$ [136]. The $y = c$ axis is perpendicular to the molecule plane. Bottom: Vibrational modes of the $D_2O$ molecule, $\nu_1$ symmetric stretch, $\nu_2$ bending, $\nu_3$ antisymmetric stretch with corresponding energies [137].

and $z = a$, since $D_2O$, with an asymmetry factor $\kappa = \frac{2B-A-C}{A-C} = -0.541$ and $-0.570$ for the $v_2 = 0$, and 1 vibrational states, respectively, is closer to the prolate than oblate limit.

The two D atoms are bosons, consequently the wavefunction of $D_2O$ has to be symmetric with respect to the exchange of these indistinguishable particles. For fully symmetric electronic and vibrational states, this gives a nuclear spin-statistical weight of 6 for rotational levels with $K_a + K_c$ even and 3 for levels with $K_a + K_c$ odd.
The dipole moment of $D_2O$ lies fully along the $b$-axis, and is around $1.85$ D for the vibrational ground state and slightly smaller for the first excited bending state [138]. This gives rise to transitions following the selection rules $\Delta J = 0, 1$, $\Delta K_a = 1, 3, 5, ...$, and $\Delta K_c = 1, 3, 5, ...$ for rotational transitions in the $v_2 = 0$, and 1, and for rovibrational transitions in the $\nu_2$ band. The vibrational dipole moment of the fundamental bending is considerably smaller, around $0.110$ D [139].

The available spectroscopic dataset was not as extended and complete for $D_2O$ as in the case of the main isotopomer $H_2O$. In particular, high accuracy rotational data on high

$J$ and $K_a$ quantum numbers was lacking, even more so for vibrationally excited states.

In the course of the present spectroscopic project on water isotopomers, around 130 new pure rotational transition frequencies of $D_2O$ were obtained in the vibrational ground and first excited bending state. These transition fell in several frequency bands between $10$ and $2400$ GHz and were obtained with different spectrometers at Cologne, the JPL and the University of Kiel.

Subsequent to these measurements, a global analysis of rovibrational and purely rotational data on $D_2O$ ($v_2 = 0,\ 1$) was performed with an Euler expansion of the Hamiltonian.

### 6.1.1 Previous Work

The summary of previous work on $D_2O$ given in this section is limited to data on the ground and first excited bending state. To my knowledge no experimental data on pure rotational transitions in any higher vibrational state of $D_2O$ exists. Several works, however, study its IR rovibrational spectra up to the $n = 4$th polyad ($n = v_1 + v_2/2 + v_3$) [137, 140, 141, 142, 143, 144, 145, 146, 147, 148].

Prior to this study, $208$ rotational transitions in the vibrational ground and only $21$ in the first excited bending state were reported with microwave accuracy, involving energy levels up to $J,\ K_a = 12,\ 9$ and $= 8,\ 5$, respectively. The majority of these ($144$) were comparatively strong transitions measured with a frequency tunable far-infrared spectrometer (TuFIR) between $500$ and $5000$ GHz by Matsushima *et al.* [149]. The other lines originate from several earlier investigations, all references are compiled in a work by Messer *et al.* [150], who extended the dataset with a frequency-multiplied Klystron spectrometer to $1100$ GHz. Additionally, two rotational transitions were reported by Baskakov *et al.* [151] around $460$ GHz.

An overview of all rovibrational and rotational data is given in Table 6.1.1. In IR experiments, additional 3869 lines were recorded with varying accuracy. The datasets do overlap in some cases, for example those of Camy-Peyret *et al.* [152] and Toth [139] in the frequency range between $\sim 1040 - 1660$ cm$^{-1}$, yielding redundant information on some lines. The deviations between transition frequencies reported in different works are in general of the size of the stated experimental uncertainty. For completeness purpose, a recent work by Bernath *et al.* [143] is also included. However, this data has not been used in the subsequent analysis, for reasons given in Section 6.1.3.

The recent study of far-infrared emission spectra of $D_2O$ by Mellau *et al.* [153] is of special interest for the present work. They recorded pure rotational ($v_2 = 0,\ 1$) and rovibrational ($v_2 = 1 - 0$) transitions of hot $D_2O$ up to very high $J$ and $K_a$ values with a Fourier transform spectrometer. Moreover, after analysing their data, they were able

to complete the assignment of the very accurate absorption data of Toth [139] with more than $180$ additional transitions of the $\nu_2$ band. Including their data to the global analysis constrains the higher order fit parameter of the Euler expansion, as will be discussed in more detail in Section 6.1.3.

Methods to analyse $D_2O$ data in previous works were many. Mellau and coworkers used the generating function approach to fit their $v_2 = 0$ and $1$ and previous data to an rms value of $0.001 - 0.0012$ cm$^{-1}$. They found that the standard $A$-reduced Hamiltonian, used by other authors [154, 152], does not provide satisfactory results for their high $J$ and $K_a$ data, due to the bad convergence or even divergence of the power series.
On the other hand, Bernath and coworkers [143] analysed their data with a variational approach starting from an *ab initio* potential energy surface (PES) by Polyansky *et al.* [156]. The same method was used earlier by Partidge and Schwenke [134], they optimized a high quality PES by fitting it to experimental energy levels for different isotopomers of water. The advantage of this method is its capacity to fit many vibrational states simultaneously. Mellau *et al.* demonstrated, however, that the rotational energy levels predicted with this method are only reliable for values of $J < 12 - 15$.

### 6.1.2 New Dataset

Around $130$ pure rotational transitions of $D_2O$ in its vibrational ground and first excited bending state have been newly measured in total, covering a frequency range between $\sim 100$ and $2400$ GHz (see also Table 6.1.1). The newly measured lines have been collected in Table C.1 in the appendix to this work together with all previously reported high resolution data. Either pure $D_2O$ samples, or a 1:1 mixture of $H_2O$ and $D_2O$ was used for the measurements. The latter case allowed for simultaneous investigation of all three isotopic species without too much time overlay due to sample exchange and was used for stronger lines mainly.

Around $40$ of the newly measured line positions were provided by the spectroscopy group at the JPL. Different frequency multiplier chains were used as radiation sources, up to a frequency of $1.79$ THz. Transitions involving $J < 15$ and $K_a < 11$ with a calculated intensity of only $\sim 4 \cdot 10^{-7}$ nm$^2$ MHz or $\sim 1.3 \cdot 10^{-25}$ cm$^{-1}$/(molecule/cm$^2$), have been measured at room temperature in the range between $540 - 680$ GHz.

Two low frequency transitions at $10.9$ GHz were recorded with high accuracy with the X-band Fourier Transform Microwave Spectrometer in Kiel, partly resolving the underlying hyperfine structure due to the two deuterium nuclei. Since the available information on $D_2O$ hyperfine structure consists of these two rotational transitions only (see also beam maser experiments by Bluyssen *et al.* [157, 158] and Zeeman experiments by Kukolich [159]) and Stark measurements of hyperfine transitions in the $J_{KaKc} = 1_{11}$ and $1_{01}$ rotational states [160], no attempt was made to analyse the hyperfine structure in this work. However, the data obtained in Kiel was analysed with the aid of previ-

Table 6.1: Available rovibrational and rotational data on the ground and first excited bending state ($v_2 = 1$) of $D_2O$. For each dataset, the corresponding highest $J$ and $K_a$ quantum numbers, on which information is contained, is given. The numbers in parentheses in the # lines column give the number of lines omitted from the fit.

| Ref. | Frequency range | Accuracy | $v_2 = 0$ | | | $v_2 = 1$ | | | $v_2 = 1 - 0$ | total |
|---|---|---|---|---|---|---|---|---|---|---|
| | | | $J_{max}$ | $K_{max}$ | # lines | $J_{max}$ | $K_{max}$ | # lines | # lines | # lines |
| | $cm^{-1}$ | $10^{-3}$ $cm^{-1}$ | | | | | | | | |
| Johns *et al.* [154] | 22-220 | 0.2 | 12 | 7 | 199 | | | | | 199 |
| Paso *et al.* [155] | 110-414 | 0.2 | 19 | 11 | 241(5) | | | | | 241(5) |
| Mellau *et al.* [153] | 321-860 | 0.5-1 | 26 | 26 | 506(7) | 25 | 25 | 389(23) | 77(3) | 972(33) |
| Mellau *et al.* [153] | 894-1658 | 1-3 | 21 | 13 | | 22 | 13 | | 181 | 181 |
| Toth [139] | 727-1643 | 0.1-1 | 23 | 11 | | 24 | 11 | 1437(4) | 1437(4) | |
| Camy-Peyret *et al.* [152] | 1039-1586 | 0.4 | 17 | 10 | | 18 | 11 | | 839(2) | 839(2) |
| Bernath *et al.* [143] [a] | 380-1880 | 1 | 30 | 30 | 667 | 30 | 27 | 516 | 927 | 2110 |
| | GHz | MHz | | | | | | | | |
| Messer *et al.* [150] | 10-1065 | 0.05 | 12 | 9 | 64 | 8 | 5 | 21 | | 85 |
| Baskakov *et al.* [151] | 460-470 | 0.05 | | | | 6 | 4 | 2 | | 2 |
| Matsushima *et al.* [149] | 555-5145 | 0.04-0.40 | 8 | 7 | 156 | | | | | 156 |
| This work, JPL | 105-1787 | 0.05-0.15 | 14 | 10 | 23 | 10 | 6 | 17 | | 40 |
| This work, Cologne | 698-2377 | 0.05-0.30 | 16 | 10 | 55(2) | 15 | 7 | 34 | | 88(2) |
| This work, Kiel | 10 | 0.008 | 5 | 4 | 2 | | | | | 2 |

[a] This data has not been used in the analysis

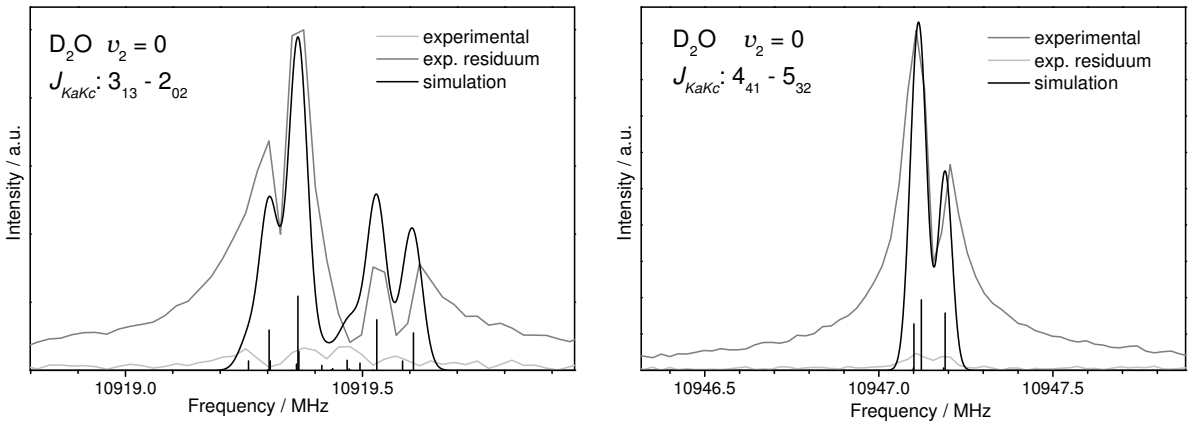


Figure 6.2: Two low frequency transitions measured with the Kiel FTMW spectrometer. The lines were analysed taking into account the underlying hyperfine structure. A simulated spectrum, as well as a stick spectrum, is shown also.

ously known hyperfine-structure parameters to improve their transition frequency accuracy. Both measured lines are shown in Figure 6.2 and compared to a simulated spectrum with a line width of 40 kHz. Nuclear quadrupole coupling and spin-rotation constants by Bhattacharjee *et al.* [160] were used for the simulation. To obtain the third diagonal element of the spin-rotation tensor, which has not experimentally been derived, the out of plane component $M_{cc}$ was obtained by scaling according to $M_{cc}(\mathrm{D_2O}) = M_{cc}(\mathrm{HDO}) \cdot C(\mathrm{D_2O})/C(\mathrm{HDO})$. The spin-spin interaction terms were calculated from molecular geometry. As can be seen in Figure 6.2, the agreement between experimental and simulated spectrum is very good. Therefore, the line positions experimentally obtained were intensity averaged according to the calculated values and included in the analysis. The accuracy could be significantly improved compared to previously reported values by Messer *et al.* [150].

Measurements between $698 - 941$ GHz were performed with the Cologne Terahertz Spectrometer, utilizing two very high frequency BWOs. The cell was heated with a resistive heating tape to $\sim 150$°C to populate the higher energy levels accordingly. With this method it was possible to measure some very high $J$ and $K_a$ lines, up to $J = 16$ and $K_a = 10$, the highest quantum numbers for microwave measurements so far.

Moreover, $37$ rotational transitions of $D_2O$ have been recorded with COSSTA between $1.75$ and $1.99$ THz. Here, a DC glow discharge was used in selected cases to gain intensity for energetically high lying transitions.
In the same frequency range, between $1.75$ and $1.86$ THz, around 20 rotational lines have been measured with a MoMeD frequency tripler fabricated by the JPL, which we were able to use for a few days during test measurements at Cologne (see Section 2.1.2).

Only four of these lines were not measured with COSSTA and included in the dataset. The agreement in the obtained transition frequencies for lines measured with the sideband and the multiplier system was well within the experimental uncertainty in all cases.
Furthermore, the signal-to-noise ratio of both systems is comparable, as is demonstrated

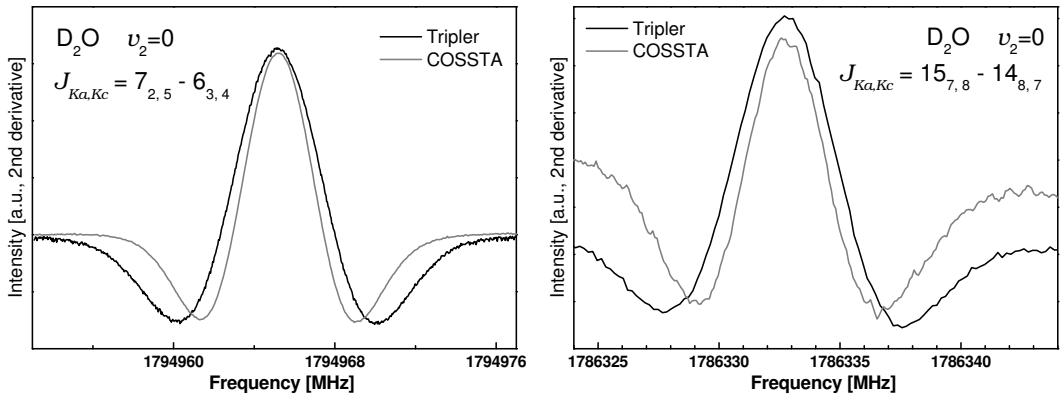


Figure 6.3: Exemplary spectra of a strong (left) and a weak (right) $D_2O$ transition measured both with COSSTA and the JPL tripler. Differences in the line width are due to a different amplitude of the frequency modulation.

in Figure 6.3 for a very weak and a comparatively strong $D_2O$ line. Integration times were similar ($\sim$ 1 s per data point). The gas pressure was higher by a factor of ten for the measurements with COSSTA, compensating for the absorption cell being shorter by a factor of three. The larger linewidth of the tripler spectrum is due to a higher amplitude of the frequency modulation, which was set to around 2 MHz for the Tripler and 1 MHz for the COSSTA measurements. This value should be reduced accordingly for further measurements. In the case of the weak line, the line shape is affected by baseline effects.

In the course of his diploma thesis at the Cologne laboratory, Christian Endres recorded three additional $D_2O$ lines, one at around $1.4$ THz with a newly developed Superlattice Multiplier Spectrometer, based on the AMC spectrometer described earlier, and two at $\sim 2.4$ THz with a JPL MoMeD frequency tripler designed for an output frequency of $2.7$ THz.

All experimental data on pure rotational transitions of $D_2O$ measured to microwave accuracy is given in Table C.1 of the Appendix.

### 6.1.3 Analysis and Results

A common problem of analyses of spectroscopic data with the aid of series expansions is the predictive capability for transition frequencies and energy levels of higher quantum numbers. A large number of centrifugal distortion terms has to be contained in the Hamiltonian for fitting highly accurate microwave and submillimeter-wavelength data to its experimental uncertainty. On the other hand, strong correlations of these parameters and the propagation of their uncertainties usually introduce large errors for extrapolations to higher energy levels.

In the present analysis, very accurate microwave and FIR data up to comparatively high $J$ and $K_a$ quantum numbers is combined with a very complete IR dataset on extremely high-lying rotational energy levels ($E_{upper} < 9600$ cm$^{-1}$). This latter dataset has a restricting influence on the higher order centrifugal distortion parameters. As in the case of $H_2O$ and HDO, the Euler expansion of the Hamiltonian as described in Section 3.3.2 has been employed to perform a least squares fit to the data.

A linelist has been created containing all experimental data on $D_2O$ ($v_2 = 0, 1$) known to date, except that of Bernath *et al* [143], to perform the analysis. Some of the datasets partly overlap, however, all data was used in the analysis and a comparison can be done by the weighted root mean square (wrms) value of each distinct dataset (see Table 6.3).

Step-by-step higher $J$ and $K_a$ levels have been included, and higher expansion terms were added to the fit when necessary. The $a$ and $b$ constants, defining the transformation of the angular momentum operators in the Euler approach, have been varied at each step to both yield a good wrms and reasonable parameter values. Care was taken to make as much of the $K_a$ dependent expansion terms positive in order to avoid an alternating series. The data of Mellau *et al.* [153] was included as a last step in the analysis, since it contains information on the highest $J$ and $K_a$ values.

Some restrictions have to be made to the data sets. Since no vibrational interaction terms were included in the analysis, rotational transitions belonging to energy levels perturbed by these interactions have to be omitted. The perturbation is either due to Fermi or Coriolis interaction, for vibrational states with the same or different symmetry, respectively. Energetically high lying rotational levels in the $v_2 = 1$ or (010) vibrational state can interact via Coriolis coupling with, for example, the (001) and via Fermi interaction with, for example, the (020) or (100) states, respectively. Due to the high rotational constants of $D_2O$, the energy levels begin to overlap already for moderate values of $J$, as is demonstrated in Figure 6.4, where calculated energy levels of the (010) state are compared to an incomplete, since experimental, set of energy levels of the (020) state [143].
Sixteen transitions of the dataset by Mellau *et al.* [153] are accidentally perturbed by resonances of the $v_2 = 1$ rotational states with higher rovibrational states, and have thus been excluded from the fit. Two new resonating states have been verified in the present analysis. In detail, the perturbed states are the $J_{Ka,Kc} = 24_{13,11}$, $25_{10,15}$, $25_{11,14}$, $25_{13,12}$, $24_{10,14}$, $24_{6,18}$ and the $K_a = 16$ levels of $J = 23$, 24, and 25.
Additionally, 17 rotational transitions of this dataset have been omitted as proposed by the authors, presumably belonging to very weak or blended lines. The numbers of lines omitted from the other datasets based on fit criteria, only 13 in total, are given in parentheses in Table 6.1.1.

The results of the analysis are shown in Table 6.2 for both the vibrational ground and the first excited bending state. Only parameters sufficiently determined ($X/\Delta X \geq 10$) were kept in the fit. A number of 52 rotational parameters in the ground state, and 53 for the first excited bending state were needed to obtain an overall wrms value of 1.4.

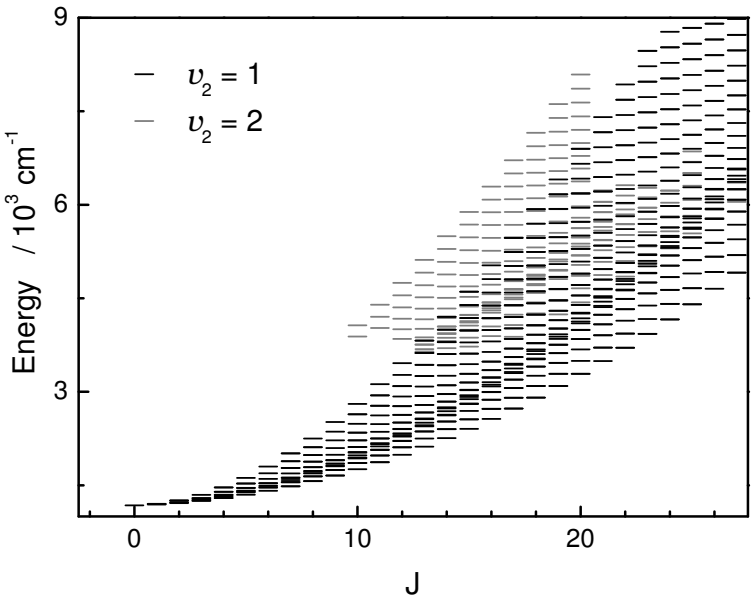


Figure 6.4: Calculated energy levels of the $v_2 = 1$ state (black) together with experimental levels of the $v_2 = 2$ state (grey) [143]. Closely spaced energy levels of both states can be perturbed by Fermi interaction.

For comparison, Johns *et al.* already needed $30$ parameters to fit data up to $J_{max} = 12$, $K_{a,max} = 8$ of the vibrational ground state of $D_2O$ with a standard $A$-reduced Hamiltonian. Moreover, the root criteria gives convergence radii for the standard power series of $K_{a,max} = 19$ and $K_{a,max} = 17$ for the $v_2 = 0$ and $v_2 = 1$ vibrational states, respectively (with rotational parameters from Messer *et al.* [150]). With this in mind it is understandable that in a first attempt to fit the complete dataset with a standard $A$-reduced Hamiltonian in the course of this work, even a parameter set with more than $120$ rotational parameters up to order $n = 10$ yielded wrms values of not better than $10$. The Euler expansion of the Hamiltonian is clearly better suited to account for the experimental data.

A closer look at Table 6.2 reveals some differences in the fitting behaviour of the vibrational ground and first excited bending state of $D_2O$. The ratio of each parameter in the $v_2 = 1$ state to that in the $v_2 = 0$ state is given in the last column. With increasing order of the parameter the ratio increases significantly, in particular for the $K_a$-dependent terms. This can be explained by higher rotational-vibrational interactions for the first excited bending state, resulting in higher contributions of the bending vibration to the effective centrifugal distortion terms. This behaviour is also reflected by the higher $a$ constant in the $v_2 = 1$ state, defining the Euler transformation of the angular momentum operator in $a$-direction.

Table 6.2: Coefficients of the Euler expansion for $D_2O$ for both the vibrational ground and first excited bending state $v_2 = 1$ in MHz. Numbers in parentheses give one times the standard deviation. The ratio of the parameters of the vibrational excited to the vibrational ground state is given in the last column.

| Parameter | $v_2 = 0$ | $v_2 = 1$ | ratio $\frac{v_2=1}{v_2=0}$ |
|---|---|---|---|
| $b$ | 0.00022 | 0.000185 | 0.84 |
| $a$ | 0.00125 | 0.00185 | 1.48 |
| $b_{off}$ | 0.00022 | 0.000185 | 0.84 |
| $a_{off}$ | 0.00125 | 0.00185 | 1.48 |
| $X_{0,1}$ | 181648.1286(193) | 181799.8960(53) | 1.00 |
| $X_{1,0}$ | 462278.8140(50) | 498675.7755(176) | 1.08 |
| $X_{0,2}$ | 30.670383(68) | 23.557937(130) | 0.77 |
| $X_{1,1}$ | 355.899304(291) | 465.62214(141) | 1.31 |
| $X_{2,0}$ | 336.84729(50) | 548.60011(217) | 1.63 |
| $X_{0,3} \cdot 10^3$ | 6.68843(111) | 4.87850(109) | 0.73 |
| $X_{1,2}$ | 0.1096512(65) | 0.1284004(268) | 1.17 |
| $X_{2,1}$ | 0.4150565(199) | 0.795541(104) | 1.92 |
| $X_{3,0}$ | 0.5939367(243) | 1.450706(108) | 2.44 |
| $X_{0,4} \cdot 10^6$ | 1.0693(88) | 0.5102(34) | 0.48 |
| $X_{1,3} \cdot 10^3$ | 0.035494(48) | 0.042414(212) | 1.19 |
| $X_{2,2} \cdot 10^3$ | 0.04904(49) | −0.13042(217) | −2.66 |
| $X_{3,1} \cdot 10^3$ | 0.89440(74) | 2.4596(34) | 2.75 |
| $X_{4,0} \cdot 10^3$ | 0.07588(62) | 0.18892(290) | 2.49 |
| $X_{0,5} \cdot 10^9$ | 0.780(35) | 0.2045(35) | 0.26 |
| $X_{1,4} \cdot 10^6$ | 0.010077(79) | 0.01847(55) | 1.83 |
| $X_{2,3} \cdot 10^6$ | −0.09992(274) | −0.2721(94) | 2.72 |
| $X_{3,2} \cdot 10^6$ | 1.6242(216) | 6.371(58) | 3.92 |
| $X_{4,1} \cdot 10^6$ | −0.2188(152) | −1.250(56) | 5.71 |
| $X_{5,0} \cdot 10^6$ | 2.0429(84) | 12.066(46) | 5.91 |
| $X_{0,6} \cdot 10^{12}$ | −0.841(64) | −6.31(45) | 7.50 |
| $X_{2,4} \cdot 10^9$ | 0.0687(32) | −0.1747(108) | −2.54 |
| $X_{3,3} \cdot 10^9$ | 0.674(34) | 3.409(110) | 5.06 |
| $X_{4,2} \cdot 10^9$ | −3.311(45) | −29.62(40) | 8.95 |
| $X_{5,1} \cdot 10^9$ | 4.372(82) | 29.03(36) | 6.64 |
| $X_{6,0} \cdot 10^9$ | −4.035(65) | −41.88(40) | 10.38 |
| $X_{0,7} \cdot 10^{15}$ | 0.617(43) | | |
| $X_{5,2} \cdot 10^{12}$ | 5.271(250) | 9.83(168) | 1.86 |
| $X_{6,1} \cdot 10^{12}$ | −6.475(238) | −27.29(164) | 4.21 |
| $X_{7,0} \cdot 10^9$ | 0.012958(274) | 0.20352(194) | 15.71 |
| $X_{6,2} \cdot 10^{12}$ | | 0.1941(32) | |
| $X_{7,1} \cdot 10^{12}$ | 0.01380(47) | 0.0679(34) | 4.92 |
| $X_{8,0} \cdot 10^{12}$ | −0.01954(58) | −0.4719(47) | 24.15 |
| $X_{9,0} \cdot 10^{15}$ | 0.01815(49) | 0.6058(46) | 33.38 |
| $Y_{0,0}$ | 18195.07294(45) | 19104.28317(135) | 1.05 |
| $Y_{0,1}$ | 0.3128618(112) | −0.553911(36) | −1.77 |

Table 6.2: $D_2O$ Euler expansion - continued

| Parameter | $v_2 = 0$ | $v_2 = 1$ | ratio $\frac{v_2=1}{v_2=0}$ |
|---|---|---|---|
| $Y_{1,0}$ | 8.62343(34) | 8.66816(121) | 1.01 |
| $Y_{0,2} \cdot 10^3$ | 0.237330(85) | 0.337473(232) | 1.42 |
| $Y_{1,1} \cdot 10^3$ | −5.5308(38) | −12.9521(168) | 2.34 |
| $Y_{2,0}$ | 0.112359(59) | 0.283685(219) | 2.52 |
| $Y_{0,3} \cdot 10^6$ | −0.036612(177) | −0.07887(39) | 2.15 |
| $Y_{1,2} \cdot 10^6$ | −3.4277(132) | −9.758(78) | 2.85 |
| $Y_{2,1} \cdot 10^3$ | 0.08501(33) | 0.21409(129) | 2.52 |
| $Y_{3,0} \cdot 10^3$ | −0.47551(308) | −2.3083(123) | 4.85 |
| $Y_{1,3} \cdot 10^9$ | | −2.870(115) | |
| $Y_{2,2} \cdot 10^6$ | 0.10443(96) | 0.42649(248) | 4.08 |
| $Y_{3,1} \cdot 10^6$ | −0.8529(116) | −2.791(41) | 3.27 |
| $Y_{4,0} \cdot 10^6$ | 3.409(63) | 26.113(232) | 7.66 |
| $Y_{2,3} \cdot 10^9$ | −0.01815(148) | | |
| $Y_{3,2} \cdot 10^9$ | −0.1173(116) | −3.368(48) | 28.71 |
| $Y_{4,1} \cdot 10^9$ | 2.998(120) | 18.15(40) | 6.05 |
| $Y_{5,0} \cdot 10^9$ | −7.818(170) | −127.35(118) | 16.29 |
| $Y_{4,2} \cdot 10^{12}$ | | 4.441(182) | |
| $Y_{5,1} \cdot 10^{12}$ | −3.367(132) | −32.04(63) | 9.52 |
| $Y_{6,0} \cdot 10^{12}$ | 6.383(195) | 216.10(251) | 33.86 |
| $E$ | 35326908.593(177) | | |
| wrms | 1.43 | | |

The quartic and sextic planarity conditions as defined in Equations 3.42, 3.43 in Section 3.3.2 are not fulfilled in the case of $D_2O$. This is not unexpected, since these conditions are derived for equilibrium rotational constants and for $D_2O$ there exist large contributions to the ground and first vibrationally excited state rotational parameters from the vibrational motion. The quartic and sextic defects have been evaluated for both vibrational states to be:

| | $v_2 = 0$ | $v_2 = 1$ |
|---|---|---|
| $\Delta_Q$ | 740847.911 $MHz^2$ | 2481641.998 $MHz^2$ |
| $\Delta_S$ | -227.152 $MHz^2$ | -1104.947 $MHz^2$ |

A comparison of the obtained rotational parameters to previously published work is difficult, since the methods used are different and a complete transformation of the parameter sets is in general not possible. The most recent work on $D_2O$, by Mellau *et al.* [153], employed the generating function approach for the analysis and they needed $42$ and $45$ parameters to obtain IR rms values of $0.0010$ and $0.0012$ $cm^{-1}$ for the ground and first excited bending state, respectively. Although in the Euler expansion presented here, a slightly higher number of parameters is needed, the overall IR rms value of $0.00087$ $cm^{-1}$ obtained for both states is a significant improvement. For the microwave

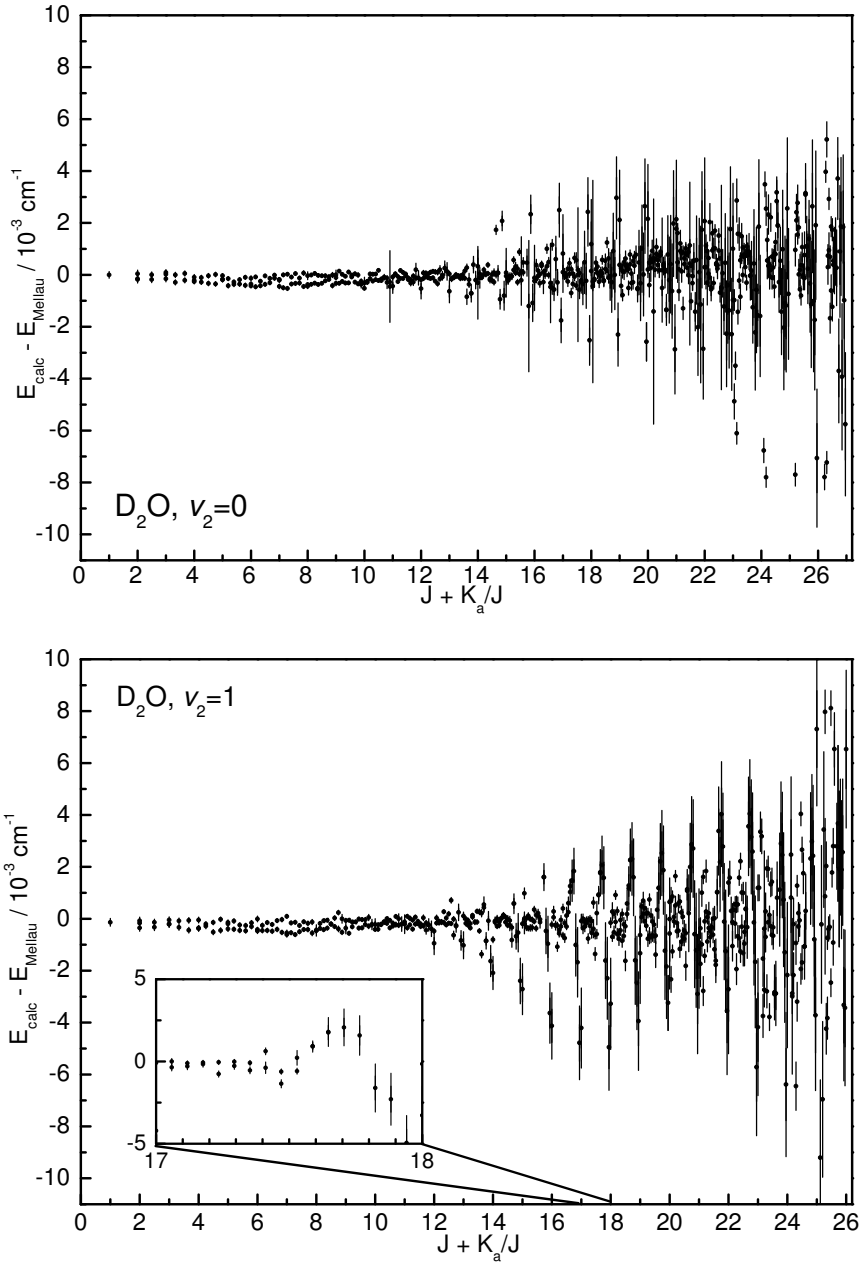


Figure 6.5: Comparison of calculated energy levels of the $v_2 = 0$ (top) and $v_2 = 1$ (bottom) states of $D_2O$ with experimental levels given by Mellau *et al.* [153].

and submillimeter-wavelength data a rms of only $0.122$ MHz is achieved, together with the weighted rms of $1.43$ this is an excellent result for this extensive dataset.

The following statistical results are obtained after defining $\sigma_{rel} = \frac{|\nu_{obs}-\nu_{calc}|}{\sigma}$, taking into account $4201$ lines, of which $13$, with $\sigma_{rel} > 10$, have been omitted from the final analysis:

| | | | | | number of lines | wrms |
|---|---|---|---|---|---|---|
| 0 | $\leq$ | $\sigma_{rel}$ | $<$ | 3 | 95 % | 0.98 |
| 3 | $\leq$ | $\sigma_{rel}$ | $<$ | 5 | 3.2 % | 1.18 |
| 5 | $\leq$ | $\sigma_{rel}$ | $<$ | 10 | 1.5 % | 1.43 |
| 10 | $\leq$ | $\sigma_{rel}$ | | | 0.3 % | |

The last column gives the wrms that would be achieved by omitting all lines with $\sigma_{rel}$ larger than the upper limit stated. However, in the limit $\sigma_{rel} < 5$ mostly lines with high $J$ or $K_a$ values ($> 20$) are rejected , and the fit does not converge correctly in these cases, since information on the higher centrifugal distortion terms is lacking. The $10\,\sigma_{rel}$ limit was kept, therefore, for the final analysis.

The excellent agreement between energy levels calculated from the presented Euler expansion of the Hamiltonian with the experimental values of Mellau *et al.* [153] is demonstrated in Figure 6.5. The energy differences are plotted against $J + \frac{Ka}{J}$ for both vibrational states. The error bars shown are those of the experimental values.
The overall deviation does not exceed $0.01$ cm$^{-1}$. For comparison, energy levels predicted from the more exact potential energy surface model by Partridge and Schwenke [134] deviate as much as $0.8$ cm$^{-1}$ from the observed levels.
The periodic behaviour of the deviations for a certain $J$ value with increasing $K_a$, displayed in more detail for $J = 17$ in the inlay of the bottom graph, is an artefact of the Euler series expansion and the fact that the highest $K_a$ participating in the highly accurate submillimeter-wavelength data is $K_a = 10$.

Moreover, differences of the calculated energy-levels to the experimental ones by Bernath *et al.* [143] are less than $0.3$ cm$^{-1}$ for levels up to $J = K_a = 30$ for the vibrational ground and less than $0.5$ cm$^{-1}$ for levels up to $J = 30$, $K_a = 27$ for the first excited bending state. This data is not included in the fit and allows, therefore, for an independent test of the predictive capability of the present analysis.

A summary of the weighted root mean square of each dataset used in the analysis is given in Table 6.3. In general, two reasons are responsible for a wrms$\neq 1$, either the stated experimental uncertainty is too optimistic (wrms$> 1$) or pessimistic (wrms$< 1$), or the utilized Hamiltonian contains too many (wrms$< 1$) or not enough (wrms$> 1$) terms. A third option, the use of an incorrect model, can be excluded in the case of the Euler expansion.
In the case of the Mellau emission data, certainly the second argument holds. It is, however, not possible to include more expansion terms to the Hamiltonian, since this would

Table 6.3: The weighted root mean square (wrms) of each separate dataset of $D_2O$.

| Ref. | # lines | wrms |
|---|---|---|
| Johns *et al.* [154] | 199 | 0.81 |
| Paso *et al.* [155] | 241(5) | 0.58 |
| Mellau *et al.* (emission) [153] | 972(33) | 2.08 |
| Mellau *et al.* (absorption) [153] | 181 | 0.83 |
| Toth [139] | 1437(4) | 1.34 |
| Camy-Peyret *et al.* [152] | 839(2) | 1.04 |
| Bernath *et al.* [143] $J,\ K_a < 26$ [a] | 1577 | 4.3 |
| Bernath *et al.* [143] $J < 31,\ K_a < 28$ [a] | 2110(302) | 2.5 |
| Messer *et al.* [150] | 85 | 1.84 |
| Matsushima *et al.* [149] | 156 | 1.21 |
| Baskakov *et al.* [151] | 2 | 0.51 |
| This work, JPL | 40 | 0.99 |
| This work, Cologne Terahertz Spectrometer | 34(1) | 1.21 |
| This work, COSSTA | 37(1) | 1.18 |
| This work, Superlattice | 1 | 1.80 |
| This work, 2.7 THz tripler | 2 | 1.57 |
| This work, Tripler | 4 | 1.37 |
| This work, Kiel | 2 | ´1.50 |
| | | 1.4 |

[a] This data has not been used in the analysis

require higher $K_a$ data with microwave accuracy, which is at the present stage not available. Here, further measurements with for example hot water samples would be of help. On the other hand, the aforementioned interactions of rotational levels in the $v_2 = 1$ vibrational state with levels in higher excited vibrational states has not been taken into account by the present model. To do so would require the inclusion of all possibly interacting vibrational states into the analysis, which is clearly beyond the scope of the present investigation. In the case of the data by Messer *et al.*, however, where there are no rotational transitions involving energy levels with extremely high $J$ or $K_a$ present in the dataset, the comparatively high wrms value indicates that the author underestimated the experimental uncertainties.

It was found that lines measured both by Bernath *et al.* [143] and Mellau deviated in frequency more than their standard uncertainty in many cases. Since the latter dataset fitted much better, and also many wrong assignments were found in the former dataset, the Bernath data was omitted from the analysis. The problems encountered are also reflected in the high wrms value of this dataset in Table 6.3, and the high amount of lines being rejected in the fit for energetically high-lying rotational levels.

## 6.2 HDO

In contrast to $H_2O$ and $D_2O$, the singly deuterated water molecule (HDO) is an asymmetric rotor molecule possessing no element of symmetry except the reflection at the molecular plane. The isotopic substitution with deuterium does not affect its geometrical structure, but rotates the principal axes system of the moment of inertia by $21.09$ ° over the out of plane $y$-axis compared to that of the symmetric water species. The situation is visualised in Figure 6.2. Judged by Ray's asymmetry parameter $\kappa = -0.683$ and $-0.696$ for the vibrational ground [150] and the first excited bending state [161], respectively, the $I^r$ representation ($x = b$, $y = c$, $z = a$), well suited to describe molecules approaching the prolate limit, is used to transform the molecular axes system ($x,\ y,\ z$) to the principal system of the moment of inertia ($a,\ b,\ c$).

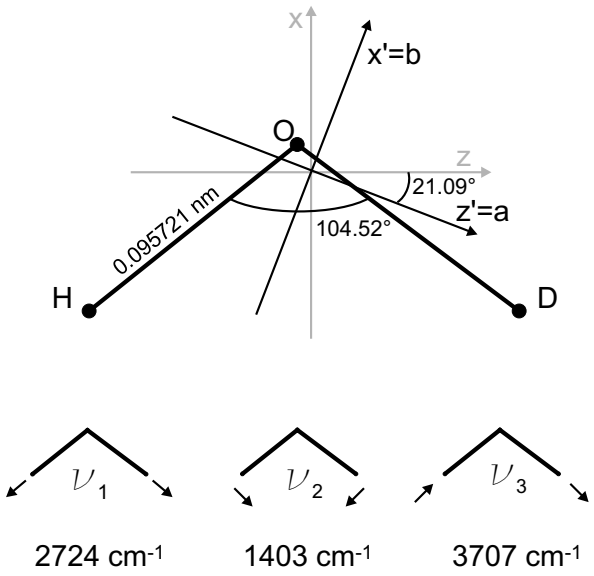


Figure 6.6: Top: Geometrical structure and principal axes system of the moment of inertia of HDO [162]. The $y = c$ axis is perpendicular to the molecule plane. Bottom: Vibrational modes of the HDO molecule, $\nu_1$ symmetric stretch, $\nu_2$ bending, $\nu_3$ antisymmetric stretch with corresponding energies.

Consequently, the dipole moment of HDO has non-zero projections both along the $a$ and $b$-axis of around $0.66$ and $1.73$ D, respectively in the vibrational ground state [163], and in addition to the $\Delta K_a = 1,\ 3,\ 5,\ ...$, $\Delta K_c = 1,\ 3,\ 5,\ ...$ $b$-type transitions, also $a$-type transitions with $\Delta K_a = 0,\ 2,\ 4,\ ...$, $\Delta K_c = 1,\ 3,\ 5,\ ...$ are allowed by the dipole selection rules. This gives rise to a larger number of observable transitions per frequency interval. In particular in the low frequency regime well below $100$ GHz, a plethora of $\Delta J = 0$, $\Delta K_a = 0$, $\Delta K_c = 1$ transitions are accessible, connecting prolately paired, asymmetry-splitted levels belonging to the same $J_{Ka}$.

Despite this advantage over the species $H_2O$ and $D_2O$, the available dataset on HDO spans a much smaller $J$ and $K_a$ range. As in the case of $D_2O$, high resolution purely rotational data is lacking for higher $J$ and $K_a$ values, especially in the vibrationally excited states.

For this reason, around $150$ rotational transitions have been newly measured to highest accuracy in the vibrational ground and first excited bending state of HDO in the frequency range between $8 - 2540$ GHz, employing different spectrometers. This data has been combined with all relevant previously published work on this molecule and analysed in a global fit of the $v_2 = 0$ and $1$ vibrational states with an Euler expansion of the Hamiltonian.

### 6.2.1 Previous Work

Due to its importance for atmospheric and astrophysical science, and also out of pure spectroscopic interest, there have been many spectroscopic investigations of the singly deuterated water molecule (HDO) during the last years. Ro-vibrational spectra of HDO have been recorded from the infrared to the near ultraviolet frequency region with Fourier Transform as well as with intracavity laser absorption spectroscopy (ICLAS) up to the $n = 5.5$th polyad ($n = v_1 + v_2/2 + v_3$) by several groups, e.g. [164, 165, 166, 167, 168, 169, 170, 171, 172, 148, 173, 174].

However, high accuracy data on pure rotational transitions in the submillimeter wavelength and terahertz region, especially important for astrophysical investigations, is rare. Messer *et al.* have compiled all submillimeter data up to the year 1984 [150] and extended the measurements on HDO to $1010$ GHz. Three additional lines in the $v_2 = 1$ state were reported by Baskakov *et al* [151] a few years later. However, two of these seem to be misassigned because they show a deviation of more than $1$ GHz from the predicted transition frequencies. This means that in total only $92$ rotational transitions frequencies were known experimentally, and only $10$ of these belong to transitions in the first vibrationally excited bending state $v_2 = 1$. Moreover, important information on levels high in rotational energy, i.e. belonging to high $J$ and $K_a$ levels, is lacking.

A summary of previous work relevant to the present investigation is given in Table 6.4. The first entries consist of rovibrational ($v_2 = 1 \leftarrow 0$) and rotational data in the vibrational ground state measured with Fourier transform spectrometers from the far-infrared to the infrared region. For each dataset the number of measured transitions, the experimental uncertainty, and the highest $J$ and $K_a$ values in each vibrational state are given. Disregarding the emission data by Bernath, the highest $K_a$ values, on which experimental information is gained, is $K_a = 10$ in both the vibrational ground and first excited bending state. This value is considerably smaller than those for the main isotopomer $H_2O$ and even the doubly deuterated $D_2O$. This might in part be due to the fact that no pure HDO samples are available. Fast proton exchange will always yield a stochiometric mixture

Table 6.4: Available rovibrational and rotational data on the ground and first excited bending state ($v_2 = 1$) of HDO. For each dataset, the corresponding highest $J$ and $K_a$ quantum numbers, on which information is contained, is given. The numbers in parentheses in the # lines column give the number of lines omitted from the fit.

| Ref. | Frequency range | Accuracy | $v_2 = 0$ | | | $v_2 = 1$ | | | $v_2 = 1 - 0$ | total |
|---|---|---|---|---|---|---|---|---|---|---|
| | | | $J_{max}$ | $K_{max}$ | # lines | $J_{max}$ | $K_{max}$ | # lines | # lines | # lines |
| | $cm^{-1}$ | $10^{-3}$ $cm^{-1}$ | | | | | | | | |
| Johns *et al.* [154] | 22-339 | 0.2 | 10 | 8 | 224(1) | | | | | 224(1) |
| Paso *et al.* [155] | 170-518 | 0.2 | 17 | 9 | 358(5) | | | | | 358(5) |
| Toth [175] | 617-2065 | 0.1-0.5 | 20 | 10 | 118(5) | 19 | 10 | | 1863(6) | 1981(11) |
| Flaud *et al.* [161] | 1040-1887 | 0.4 | 17 | 8 | | 16 | 8 | | 1287(1) | 1287(1) |
| Bernath *et al.* [176], [172] [a] | 381-1087 | 1 | 30 | 20 | 466 | 30 | 19 | 319 | 1360 | 2145 |
| Guelachvili [177] [a] | 1066-2060 | | | | | | | | | |
| | GHz | MHz | | | | | | | | |
| Messer *et al.* [150] [b] | 486-1099 | 0.05-0.3 | 13 | 7 | 82(10) | 6 | 3 | 9(2) | | 91(12) |
| Baskakov *et al.* [151] | 230-346 | 0.05 | | | | 7 | 3 | 3(2) | | 3(2) |
| Matsushima *et al.* [178] | 2477 | 0.15 | 6 | 3 | 1 | | | | | 1 |
| Siemsen *et al.* [179] | 44372 | 0.002 | 5 | 1 | | 5 | 2 | | 1 | 1 |
| This work, JPL | 71-2538 | 0.05-0.20 | 16 | 8 | 40 | 13 | 4 | 27 | | 67 |
| This work, Cologne | 698-2352 | 0.05-0.50 | 14 | 8 | 48 | 11 | 5 | 23 | | 71 |
| This work, Kiel [b] | 8-25 | 0.0002-0.013 | 14 | 6 | 7 | 11 | 5 | 5 | | 12 |
| Treacy *et al.* [180] | 486 & 248 | 0.002 | 5 | 4 | 2 | | | | | 2 |
| Kukolich [181] | 10 | 0.0005 | 2 | 2 | 1 | | | | | 1 |
| Fry *et al.* [182] | 5-22 | 0.004 | 5 | 3 | 3 | | | | | 3 |

[a] This data has not been used in the analysis

[b] Lines in parentheses have been omitted because more accurate hyperfine resolved data exists.

of $D_2O$, HDO, and $H_2O$. The datasets are mostly complementary, although there is an overlap of data by Toth [175] and Flaud *et al.* [161], and also by Guelachvili [177]. The latter data has not been used in the analysis, since the measurements by Toth and Flaud were more sensitive and had smaller experimental uncertainties.

The next entries summarize the previous and also the present high accuracy submillimeter wavelength and terahertz measurements. One line has been reassigned from a work on $H_2O$ employing tunable far-infrared spectroscopy [178].
Of special interest is the one line reported by Siemsen *et al.* [179]. They measured a $\nu_2$-band transition near $1480$ cm$^{-1}$ or $44$ THz with an accuracy of $2$ kHz, better than those reported for most of the submillimeter or millimeter wavelength measurements. The transition frequency was measured as a by-product in a heterodyne-experiment to define an optical frequency standard by means of cesium-clock-based frequency chains. This line gives valuable information on the band origin of the $\nu_2$ bending state ($v_2 = 1 - 0$), as will be outlined in more detail in Section 6.2.4.

The last section of Table 6.4 contains beam maser spectroscopy data of several *a*-type transitions at low frequencies. The underlying hyperfine structure due to the H and D atoms has been resolved partly for these transitions. Only the most recent publications corresponding to each line are given since they were found to report the most accurate transition frequencies. Studies of the hyperfine structure of HDO on the same transitions have also been performed at earlier dates by Thaddeus *et al.* [162] and Verhoeven *et al.* [158, 157, 45].

Whereas Flaud *et al.* [161] and Messer *et al.* [150] made an attempt to fit their data to a standard *A*-reduced Watson-type Hamiltonian, later work reported transition frequencies and experimental energy levels only. Bernath *et al.* used frequency predictions from the potential energy surface (PES) by Partridge and Schwenke [134] to assign their recorded spectrum, but no attempt was made to redefine the PES by these measurements, as in the case of $D_2O$ [143].

### 6.2.2 New Dataset

About $80$ rotational transitions of HDO in the vibrational ground and first excited bending state have been recorded with the Cologne spectrometers and the Fourier Transform Microwave (FTMW) Spectrometer in Kiel. Together with nearly $70$ additional transitions measured by the spectroscopy group at the Jet Propulsion Laboratories (JPL), the dataset on HDO could be significantly extended by more than $115$ newly measured and assigned lines in the frequency range between $8$ and $2538$ GHz. Of these, $48$ belong to the $v_2 = 1$ state, accounting for more than $80$% of the known high accuracy data in this state. Selected lines were recorded both at JPL and in Cologne, showing excellent agreement in the derived transition frequencies. Furthermore, the hyperfine structure of two lines was partly resolved by the FTMW measurements. A detailed description of the spectrometers utilized for these measurement can be found in the experimental section of this work

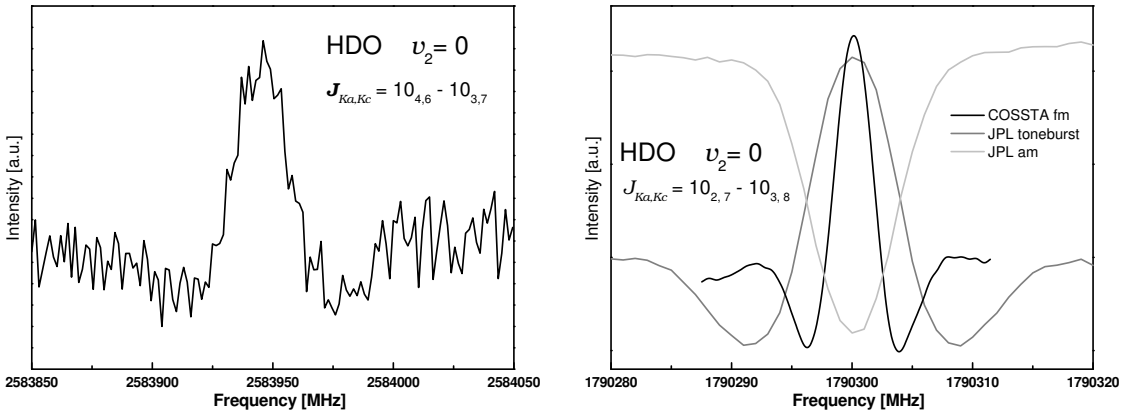


Figure 6.7: Two high frequency transitions of HDO as measured with the JPL frequency multiplier chain in Cologne (left) and by the JPL group (right). For comparison, in the right panel, the same transition, measured with COSSTA, is shown. The line intensities are scaled by an arbitrary factor.

(Chapter 2). A complete linelist of all newly measured transition frequencies, together with all high-accuracy microwave to submillimeter wavelength data reported to date, has been compiled in the appendix in Table C.2. A summary of the newly measured lines is given in Table 6.4.

Predictions based on a fit of previously published data were used for assignment purposes. All of the present lines were found within $10$ MHz of the initial predictions. For transitions involving low $J$ and $K_a$ values, deviations were smaller, typically less than $1$ MHz.

All measurements were performed with a sample consisting of a mixture of $H_2O$ and $D_2O$ with a volume ratio of $1:1$, resulting in a stochiometric mixture of $H_2O$ : HDO : $D_2O$ of $1:2:1$. The gas pressure was varied according to the expected linestrength and the spectrometer used. For measurements at the Cologne Terahertz Spectrometer and COSSTA, values ranged typically from $0.2-8$ Pa for room temperature and heated sample measurements, and from $1-60$ Pa for measurements employing a DC glow discharge. At Kiel, gas pressure was varied between $0.05$ and $0.4$ Pa, and no pressure dependency of the derived transition frequencies could be determined within the experimental uncertainties for pressures up to $1$ Pa.

The measurements at JPL were performed at room temperature with different frequency multiplier chains, pumped by a microwave synthesizer. The highest frequencies were achieved by pumping a planar monolithic membrane Schottky diode (MoMeD) with the output of a high-power frequency multiplier chain at $\sim 850$ GHz. Output radiation with both the doubled and tripled input frequency was generated with sufficient power to record spectra in the $\sim 1.7$ and $\sim 2.5$ THz region. One HDO transition at $2.54$ THz was measured in Cologne during test measurements with the same diode and a $\sim 850$ GHz BWO as pumping source. Two of these high frequency spectra are shown in Figure 6.7.

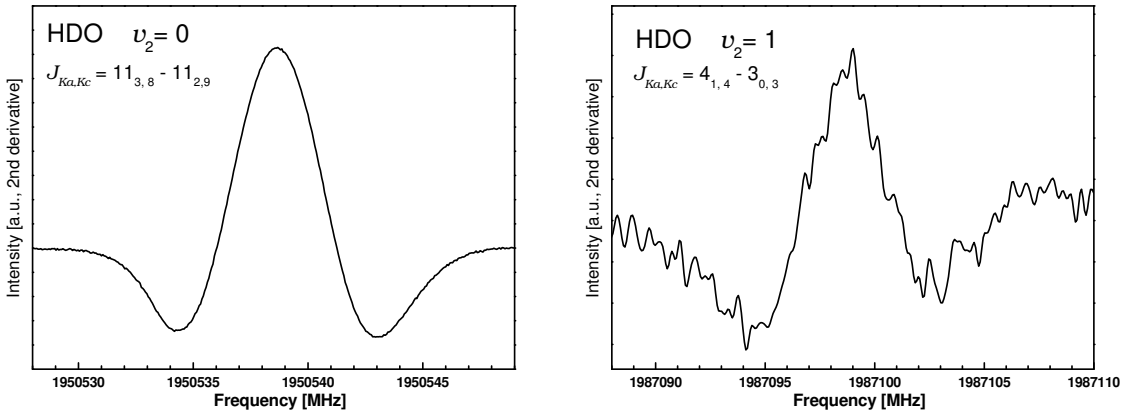


Figure 6.8: Two rotational transitions of HDO measured with COSSTA in the 2 THz region. The predicted intensity of the line in the right panel is smaller by a factor of 400 and the weakest HDO line detected with this spectrometer.

In the right panel, a transition measured both with the JPL multiplier chain and the laser sideband system COSSTA is shown for comparison.

The variation in the lineshapes and -widths stem from different detection methods, frequency, amplitude and toneburst modulation, respectively. To date no direct power measurements exist for this specific multiplier chain at this frequency, but the comparable signal to noise ratio suggests a similar output power as for the laser sideband system, which was measured to be around $0.5-1$ $\mu$W. However, since different detection methods and detectors with different sensitivities were used, this is not a strong argument.
The transition frequencies derived from both individual measurements deviate by $20$ kHz only, i.e. well within their experimental uncertainties, demonstrating once more the extremely high frequency accuracy of both systems.

In total, $38$ lines have been recorded with COSSTA in the frequency range from $1.76 - 1.99$ THz. The weakest line detected, the $J_{Ka,Kc} = 14_{5,10} \leftarrow 13_{6,7}$ transition of the $v_2 = 0$ state, with a lower state energy of $1958$ cm$^{-1}$, has an intensity of $4.0 \cdot 10^{-5}$ nm$^2$ MHz, or $1.4 \cdot 10^{-23}$ cm$^{-1}$(cm$^2$/molecule) at $300$ K. This corresponds to a peak absorption coefficient in the Doppler limit of $\alpha_{\max} = 1.3 \cdot 10^{-4}$ cm$^{-1}$ (see Section 2.2). The absorption cell had a length of $1.5$ m. A DC glow discharge was used to populate the higher energy levels accordingly and increase the intensity of this and other high energy transitions. Exemplary spectra of a comparatively strong and the aforementioned weak transition are depicted in Figure 6.8 in the left and right panel, respectively.

With the Cologne Terahertz Spectrometer, $22$ pure rotational lines were recorded in the $v_2 = 0$, and $10$ in the $v_2 = 1$ vibrational state. Two high frequency BWO tubes were employed for this purpose, covering the frequency region from $690$ to $970$ GHz. The $3$ m long absorption cell could be resistively heated to $\sim 150$ °C to enhance the population of higher energy levels. The higher radiation power of a few mW, combined with the longer absorption cell, yields an extremely high sensitivity of this spectrometer. Consequently, even very weak HDO absorption lines have been detected. One example, the

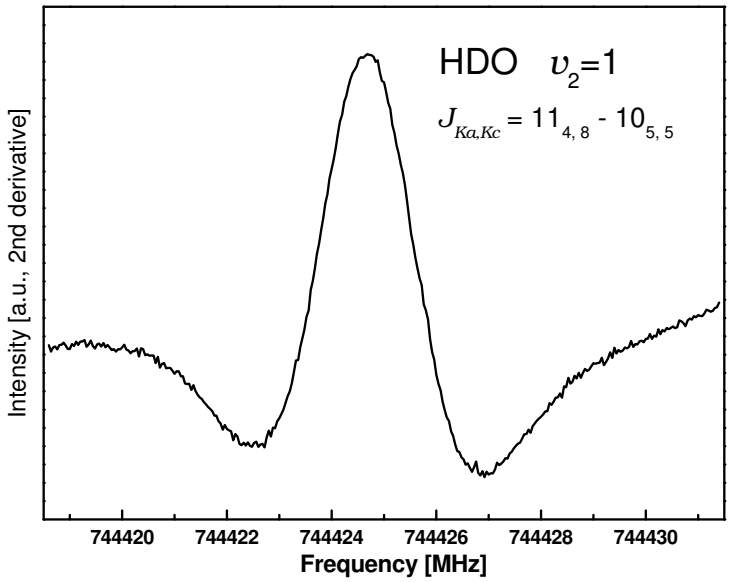


Figure 6.9: A weak rotational transition of HDO in the first excited vibrational bending state, measured with the Cologne Terahertz Spectrometer.

$11_{4,8} \leftarrow 10_{5,5}$ $b$-type $\Delta K_c = 3$ rotational transition in the $v_2 = 1$ vibrational state, with a lower state energy of $2691$ cm$^{-1}$, is shown in Figure 6.9. At $300$ K, the intensity of this line is only $1.7 \cdot 10^{-7}$ nm$^2$ MHz ($5.5 \cdot 10^{-26}$ cm$^{-1}$(cm$^2$/molecule)), or, making the same assumptions as above, $1.9 \cdot 10^{-6}$ cm$^{-1}$. This means, the absorbed intensity at line center accounts for only $0.05$% over the whole absorption length. This high sensitivity allowed for the measurement of several weak $a$-type, $\Delta K_a$=2 and $\Delta K_c$=3 transitions, yielding valuable information for the subsequent analysis, especially on the asymmetry splitting and higher order centrifugal distortion terms.

In the microwave region below $\sim 40$ GHz, the technique of Fourier transform microwave (FTMW) spectroscopy allows for the investigation of still weaker absorption lines. Several $a$-type transitions of HDO fall into this low frequency region. Therefore, the Kiel FTMW spectrometers (X- and K-band) were utilized to record $12$ rotational transitions between $5$ and $24$ GHz. Of these, seven had been summarized earlier in Messer *et al.* [150], but their accuracy could be significantly improved. Five transitions belong to the vibrational excited state, and only one transition does not follow $a$-type selection rules.

Given the high sensitivity and frequency resolution of the FTMW, it was also possible to resolve the hyperfine structure of two $a$-type ($\Delta K_a = 2$, $\Delta K_c = 3$) transitions partly. The measured power spectrum of these lines, together with the simulated total power line shape, based on the successive hyperfine structure analysis described later, is shown in Figure 6.10. The weakest line measured in Kiel is the $J_{Ka,Kc} = 11_{5,6} - 11_{5,7}$ rotational transition in the $v_2 = 1$ vibrational state. This line is almost a factor $1000$ less intense as the weakest transition detected with the Cologne Terahertz Spectrometer.

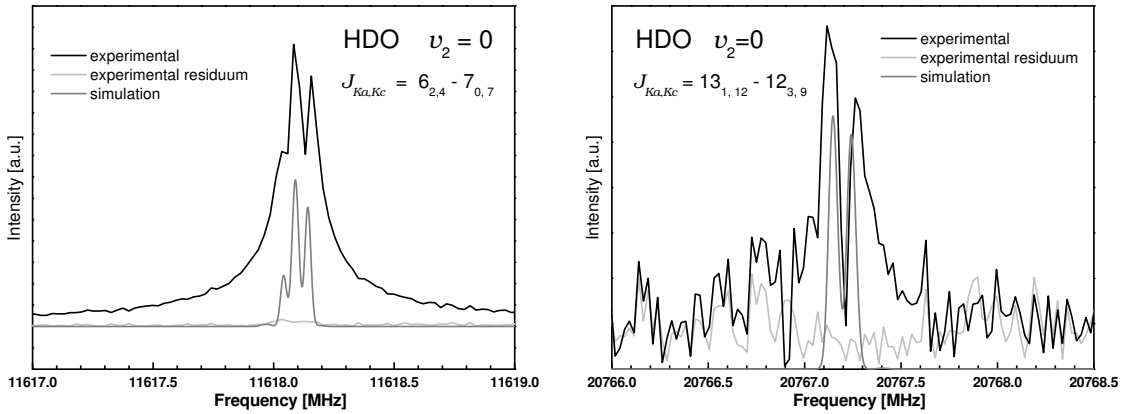


Figure 6.10: Two low frequency transitions of HDO measured with the Kiel FTMW spectrometer. The lines were analysed taking into account the underlying hyperfine structure. Simulated spectra, with an assumed linewidth of 25 and 40 kHz, respectively, are shown for comparison with the experimental power spectra and the residua of the fit.

### 6.2.3 Analysis and Results

An experimental linelist was compiled including the IR, microwave, millimeter and submillimeter wavelength and terahertz data summarised in Table 6.4. In total, 4102 rotational transitions in the $\upsilon_2 = 0$ and 1, and in the $\nu_2$ band were included with some overlap in certain frequency regions. This data was subjected to a global least squares analysis employing the Euler expansion of the Hamiltonian (see Section 3.3.2 for details). Subsequently, transitions with ever higher $J$ and $K_a$ values were added to the fit and the number of rotational expansion coefficients was increased accordingly. Moreover, the $a$ and $b$ constants defining the Euler transformation were adjusted after each inclusion of new parameters to similarly obtain a good wrms value and reasonable spectroscopic parameters.

In the course of the analysis, $18$ transitions of the $\nu_2$ band were omitted due to fit criteria. They presumably belong to weak or blended lines. Additionally, $12$ rotational transitions were excluded, since data with considerably higher accuracy was contained in the data set. Two more lines by Baskakov *et al.* [151] were excluded from the data because they are obviously misassignments. The dataset by Bernath *et al.* [176], [172] had to be omitted completely. They only stated an universal uncertainty for strong, isolated lines, a condition which was not fulfilled for most of the HDO lines, as comparisons to data by Toth [175] and Flaud *et al.* [161] revealed. Of the remaining $4070$ lines, $1552$ are $a$-type transitions with $\Delta K_a = 0$ ($1096$ lines), $= 2$ ($449$), $= 4$ ($4$), and $= 6$ ($1$).

The results of the Euler analysis are shown in Table 6.5. To increase the predictive capability of the analysis, only parameters well defined ($X/\Delta X \geq 10$) were kept in the fit.

The inclusion of more and higher order centrifugal distortion parameters, especially the diagonal terms, yielded an improved wrms value and better fitting of the high-accuracy rotational data, but on account of insufficient determination of lower order parameters.

It was found that better results were reached with different diagonal and off-diagonal $a$ and $b$ constants. The off-diagonal values are $15-30\%$ higher than the diagonal values. A similar increase is also needed for the $v_2 = 1$ state compared to the ground state. This is expected, since centrifugal distortion is larger in the excited bending states and also indicated by the convergence radii of the ground [150] and first excited bending state [161] of $K_a = 16$ and 13, respectively, calculated from a Watson Hamiltonian parameter set.

Table 6.5: Coefficients of the Euler expansion for HDO for both the vibrational ground and first excited bending state $v_2 = 1$ in MHz. Numbers in parentheses give one times the standard deviation. The ratio of the parameters of the vibrational excited to the vibrational ground state is given in the last column.

| Parameter | $v_2 = 0$ | $v_2 = 1$ | ratio $\frac{v_2=1}{v_2=0}$ |
|---|---|---|---|
| $b$ | 0.00022 | 0.00026 | 1.18 |
| $a$ | 0.003 | 0.004 | 1.33 |
| $b_{off}$ | 0.00025 | 0.00030 | 1.20 |
| $a_{off}$ | 0.004 | 0.0046 | 1.15 |
| $X_{0,1}$ | 232483.9292(49) | 233225.8439(59) | 1.00 |
| $X_{1,0}$ | 701931.6767(180) | 764886.6185(257) | 1.09 |
| $X_{0,2}$ | 40.305256(125) | 48.218249(204) | 1.20 |
| $X_{1,1}$ | 795.92696(113) | 1078.35220(306) | 1.35 |
| $X_{2,0}$ | 1683.59026(275) | 2310.2366(64) | 1.37 |
| $X_{0,3} \cdot 10^3$ | 7.74564(131) | 11.46182(234) | 1.48 |
| $X_{1,2}$ | 0.3316444(177) | 0.570287(66) | 1.72 |
| $X_{2,1}$ | 2.384241(119) | 4.27276(42) | 1.79 |
| $X_{3,0}$ | 5.060321(245) | 9.98487(87) | 1.97 |
| $X_{0,4} \cdot 10^6$ | 1.4553(62) | 2.3852(101) | 1.64 |
| $X_{1,3} \cdot 10^3$ | 0.062763(105) | 0.14035(54) | 2.24 |
| $X_{2,2} \cdot 10^3$ | 0.60268(150) | 0.0951(67) | 0.16 |
| $X_{3,1} \cdot 10^3$ | 7.7465(68) | 20.1390(273) | 2.60 |
| $X_{4,0}$ | 0.0129092(119) | 0.028161(54) | 2.18 |
| $X_{0,5} \cdot 10^9$ | 0.3267(110) | 0.7234(157) | 2.21 |
| $X_{1,4} \cdot 10^6$ | 0.042768(258) | 0.14141(131) | 3.31 |
| $X_{2,3} \cdot 10^6$ | 0.2192(46) | −0.897(37) | −4.09 |
| $X_{3,2} \cdot 10^3$ | 0.016669(81) | 0.07593(36) | 4.56 |
| $X_{4,1} \cdot 10^3$ | 0.022906(187) | 0.03707(109) | 1.62 |
| $X_{5,0} \cdot 10^3$ | 0.047209(300) | 0.21335(155) | 4.52 |
| $X_{2,4} \cdot 10^9$ | | 1.177(76) | |
| $X_{3,3} \cdot 10^9$ | | 9.40(40) | |
| $X_{4,2} \cdot 10^6$ | −0.04823(107) | −0.06999(173) | 1.45 |
| $X_{5,1} \cdot 10^6$ | 0.03402(231) | 0.3877(188) | 11.40 |
| $X_{6,0} \cdot 10^6$ | 0.0390(37) | −0.4241(205) | −10.87 |

Table 6.5: HDO Euler expansion - continued

| Parameter | $v_2 = 0$ | $v_2 = 1$ | ratio $\frac{v_2=1}{v_2=0}$ |
|---|---|---|---|
| $X_{4,3} \cdot 10^9$ | 0.04610(82) | | |
| $X_{5,2} \cdot 10^9$ | 0.2698(74) | | |
| $X_{6,1} \cdot 10^9$ | 0.5729(108) | 2.313(121) | 4.04 |
| $X_{7,0} \cdot 10^9$ | 0.8184(172) | 7.836(100) | 9.57 |
| $Y_{0,0}$ | 20214.62002(195) | 21848.8445(95) | 1.08 |
| $Y_{0,1}$ | 1.4037846(248) | 2.081501(60) | 1.48 |
| $Y_{1,0}$ | 13.79047(200) | −12.0930(114) | −0.88 |
| $Y_{0,2} \cdot 10^3$ | 0.097503(216) | 0.47833(62) | 4.91 |
| $Y_{1,1}$ | 0.0140434(141) | 0.011763(45) | 0.84 |
| $Y_{2,0}$ | 0.43106(34) | 1.48218(210) | 3.44 |
| $Y_{0,3} \cdot 10^6$ | −0.02878(69) | −0.06862(223) | 2.38 |
| $Y_{1,2} \cdot 10^3$ | −0.023189(58) | −0.085817(177) | 3.70 |
| $Y_{2,1} \cdot 10^3$ | 0.26533(133) | 0.8987(57) | 3.39 |
| $Y_{3,0} \cdot 10^3$ | −3.8287(193) | −28.386(128) | 7.41 |
| $Y_{2,2} \cdot 10^6$ | 0.5089(35) | 3.1444(179) | 6.18 |
| $Y_{3,1} \cdot 10^6$ | −1.510(35) | −14.471(135) | 9.58 |
| $Y_{4,0} \cdot 10^3$ | 0.03805(36) | 0.3595(256) | 9.45 |
| E | 42075381.817(152) | | |
| wrms | 1.20 | | |

Whereas the $A = X_{1,0}$ parameter is around 10% larger in the $v_2 = 1$ state than in the ground state, there is a significant increase for higher order terms, as can be seen by the parameter ratios in the last column of Table 6.5. Nearly all diagonal parameters are positive, this is especially important for the $K_a$ dependent ones, for which only the $X_{6,0}$ parameter in the $v_2 = 1$ state is negative. The alternating behaviour of the power series could be removed.

The overall wrms of $1.20$ is excellent, especially the infrared data is reproduced to or better than its experimental uncertainty. The individual wrms values of each separate dataset are compiled in Table 6.6. The absolute IR rms for the combined fit of the $v_2 = 0$ and $1$ states is $0.00018$ cm$^{-1}$, which is an apparent advancement over the value of $0.0007$ cm$^{-1}$ reported in [161] for a fit of experimental energy levels in the $v_2 = 1$ state only. If only their dataset is considered, an even slightly better IR rms of $0.00017$ cm$^{-1}$ is obtained. This improvement quite certainly reflects the inapplicability of the Watson model for the analysis of HDO data.

The separate wrms values are larger for the high accuracy rotational data, around $2$ for all cases. Again, the inclusion of higher order centrifugal distortion terms improves the fit, but leads to higher uncertainties of the parameters and consequently of transition frequency extrapolations of lines with higher $J$ and $K_a$ values. The highest $K_a$ values for which high accuracy information is contained in the fit are $8$ and $7$ for the vibrational

ground and first excited bending state, respectively, preventing the addition of higher order $K_a$ dependent terms to the Hamiltonian. On the other hand, the comparatively high value

Table 6.6: The weighted root mean square (wrms) of each separate dataset of HDO.

| Ref. | # lines | wrms |
|---|---|---|
| Johns *et al.* [154] | 224(1) | 1.11 |
| Paso *et al.* [155] | 358(5) | 0.74 |
| Toth [175] | 1981(10) | 1.47 |
| Flaud *et al.* [161] | 1287(1) | 0.42 |
| Messer *et al.* [150] | 91(12) | 1.96 |
| Siemsen *et al.* [179] | 1 | 0.12 |
| This work, JPL | 67 | 1.95 |
| This work, Cologne | 71 | 1.79 |
| This work, Kiel | 12 | 3.01 |
| HFS: [180] [181] [182] and this work | 8 | 1.62 |
| | | 1.20 |

of 3 for the Kiel FTMW data, including two transitions with partially resolved HFS structure, indicates that the experimental uncertainties, derived from a fit to the time-domain spectra, are too optimistic.

As has been outlined in the last section, earlier beam maser experiments resolved the hyperfine structure of several low frequency HDO transitions. Additionally, two high $J$ lines have been newly recorded in Kiel with partially resolved HFS. All these transitions belong to ground state HDO and are summarised in Table C.3. In the first step of the analysis, intensity averaged line positions have been calculated to include this high accuracy data. At a later stage, hyperfine interaction terms have been added to the Hamiltonian to account for these lines. The different types of interaction are described in some detail in Section 3.3.4. The results of the analysis are shown in Table 6.7 and compared to the most recent study by Fry and Kukolich [182].

The deuterium nuclear quadrupole coupling tensor $\chi_{ij}$ and the deuterium-hydrogen nuclear spin-spin coupling tensor $D_{ij}$ (DH) are traceless, and the $c$ component of both has been kept at a fixed ratio to the determinable $a$ and $b$ components. The spin-spin coupling terms have been calculated from the molecular geometry with Equation 3.54 and the structural information given above. They were not determinable by the fit. A $J$-dependent centrifugal distortion correction to the hydrogen spin-rotation constant, $C_{aa\,J}$, has been included, reducing the wrms of the HFS-split lines from $1.82$ to $1.62$. The constant is well defined and necessary presumably due to the inclusion of the high $J$ $13_{1,12} - 12_{3,9}$ transition.

The overall agreement between the previous parameter set and that by [182] is good, only $C_{bb}$ (H) deviates by more than $3\sigma$. This might be an effect of the additional centrifu-

Table 6.7: Hyperfine interaction constants of HDO in the vibrational ground state in kHz. Numbers in square brackets were kept fixed during the analysis.

| | This work | Fry and Kukolich [182] | Olsen *et al.* [183] |
|---|---|---|---|
| $\chi_{aa}$ (D) | $275.77(53)$ | $276.45(88)$ | $276.6$ |
| $\chi_{bb}$ (D) | $-105.50(291)$ | $-110.97(146)$ | $-102.6$ |
| $\chi_{cc}$ (D) | $[-170.27]$ | $-165.77(110)$ | $-173.9$ |
| $C_{aa}$ (D) | $-1.368(109)$ | $-1.33(20)$ | |
| $C_{bb}$ (D) | $-4.131(282)$ | $-4.38(36)$ | |
| $C_{cc}$ (D) | $-3.414(209)$ | $-2.99(24)$ | |
| $C_{aa}$ (H) | $-58.61(39)$ | $58.42(47)$ | |
| $C_{aa\,J}$ (H) | $0.198(33)$ | | |
| $C_{bb}$ (H) | $-8.97(59)$ | $-5.46(83)$ | |
| $C_{cc}$ (H) | $-23.22(57)$ | $-24.11(55)$ | |
| $D_{aa}$ (DH) | [-8.563][a] | [a] | |
| $D_{bb}$ (DH) | [3.250][a] | [a] | |
| $D_{cc}$ (DH) | [5.313][a] | [a] | |

[a] Values were calculated from geometry

gal distortion term. The uncertainty could be reduced for most parameters.

Very recently, Olsen *et al.* [183] reported *ab initio* calculations of the electric field gradient for the water molecule at the position of the hydrogen and oxygen atoms. They included ro-vibrational corrections and stated the quadrupole coupling constants for several isotopic water species including HDO at a temperature of $296$ K. Their published tensor elements were given in the principal system of the moment of inertia of $H_2O$ and $D_2O$ and a rotation about the $y = c$ axis about $20.09°$ has been performed to obtain the values in the principal axes system of HDO stated in Table 6.7.

The agreement of the *ab initio* values to the experimental ones is better than $3$ % or $2\sigma$. There are several reasons that might be responsible for this small discrepancy. Olsen *et al.* state an uncertainty of around $1$ % for their equilibrium quadrupole coupling constants, but the introduction of ro-vibrational corrections, depending upon experimental molecular force fields, will give rise to additional uncertainties. Furthermore, the rotation of the quadrupole coupling tensor into the principal axis system of the moment of inertia was based upon the equilibrium molecular geometry and not that of the $v_2 = 0$ state.

### 6.2.4 HDO as a Secondary Frequency Standard for IR Measurements

Water vapour lines are commonly used for the calibration of Fourier Transform far-infrared and infrared measurements. Water is especially well suited for this purpose because its ro-vibrational and purely rotational spectrum is widely stretched in frequency

and comparatively dense. However, column densities of the main isotopomer $H_2O$ are often too high inside the spectrometer, resulting in saturated lines, and water, as a pollutant, is found along the whole optical path, leading to asymmetric or broadened line shapes.

As a consequence, transitions of deuterated water species are commonly used for calibration. Line lists employed for this purpose stem again from Fourier Transform measurements, calibrated with $H_2O$ or OCS spectra. The most recent compilation of HDO transitions in the $\nu_2$ band is by Toth [175], reporting around $1860$ lines with a resolution of $0.0001 - 0.0005$ cm$^{-1}$, see Table 6.4 also.

In the global analysis of the $v_2 = 0$ and $1$ vibrational states presented in the preceding section, the information on the state dependent rotational and centrifugal distortion parameters of lower order will, in general, come from the included highly accurate microwave, millimeter and submillimeter wavelength transitions, whereas, on the other hand, the vibrational band center $E = G(v_2 = 1) - G(v_2 = 0)$ and higher order centrifugal distortion parameters are determined by the ro-vibrational lines. Conversely, provided that spectroscopic parameters belonging to each state are precisely determined, the accuracy of frequency predictions for ro-vibrational transitions in the $\nu_2$ band is on principle only limited by the uncertainty of the experimentally determined vibrational energy.

Siemsen *et al.* [179] reported one $\nu_2$-band transition of HDO to an accuracy of only 2 kHz, or $\sim 7 \cdot 10^{-8}$ cm$^{-1}$, as has been outlined in more detail in Section 6.2.2. To transfer this extremely high accuracy to the band center energy $E$ at least to some extent, a closed chain of rotational transitions was measured starting from the rotational ground states $J_{Ka,Kc} = 0_{0,0}$ to the participating levels $5_{1,5}$ and $5_{2,4}$ of the $v_2 = 0$ and $v_2 = 1$ states, respectively. An excerpt of the energy level scheme of HDO for both states is shown in Figure 6.11. Transitions measured to microwave accuracy are depicted as arrows. Grey arrows indicate transitions participating in the closed chains. Actually, two different chains can be formed in the $v_2 = 1$ state regarding the $5_{4,2}$ level.

In the $v_2 = 0$ state, the chain transitions have estimated experimental uncertainties of $14$ to $300$ kHz and are fitted to around $100$ kHz or better. For $v_2 = 1$, estimated uncertainties are between $50$ and $500$ kHz and the lines are fitted to around $300$ kHz, with one exception, the $J_{Ka,Kc} = 4_{1,4} - 3_{0,3}$ transition with a deviation of around $700$ kHz. However, this transition is in the branched part of the chain. Therefore, the uncertainty of the derived band center $E = 42075381.817(152)$ MHz, or $1403.4752396(51)$ cm$^{-1}$, reflects directly the experimental uncertainty of the high accuracy rotational data. Predictions of energy levels of the $v_2 = 1$ state from the parameter set obtained in this work are better than $0.0002$ cm$^{-1}$ up to $4000$ cm$^{-1}$ and better than $0.00001$ cm$^{-1}$ for levels with energy below $2500$ cm$^{-1}$. In the $v_2 = 0$ state, levels up to $2000$ cm$^{-1}$ are known to better than $0.00002$ cm$^{-1}$. For higher energies the propagated uncertainties of the rotational parameters are becoming larger.

For room temperature absorption spectra of the $\nu_2$ band of HDO, the typical method for its use as a calibration gas, it is reasonable to assume only rotational energy levels of

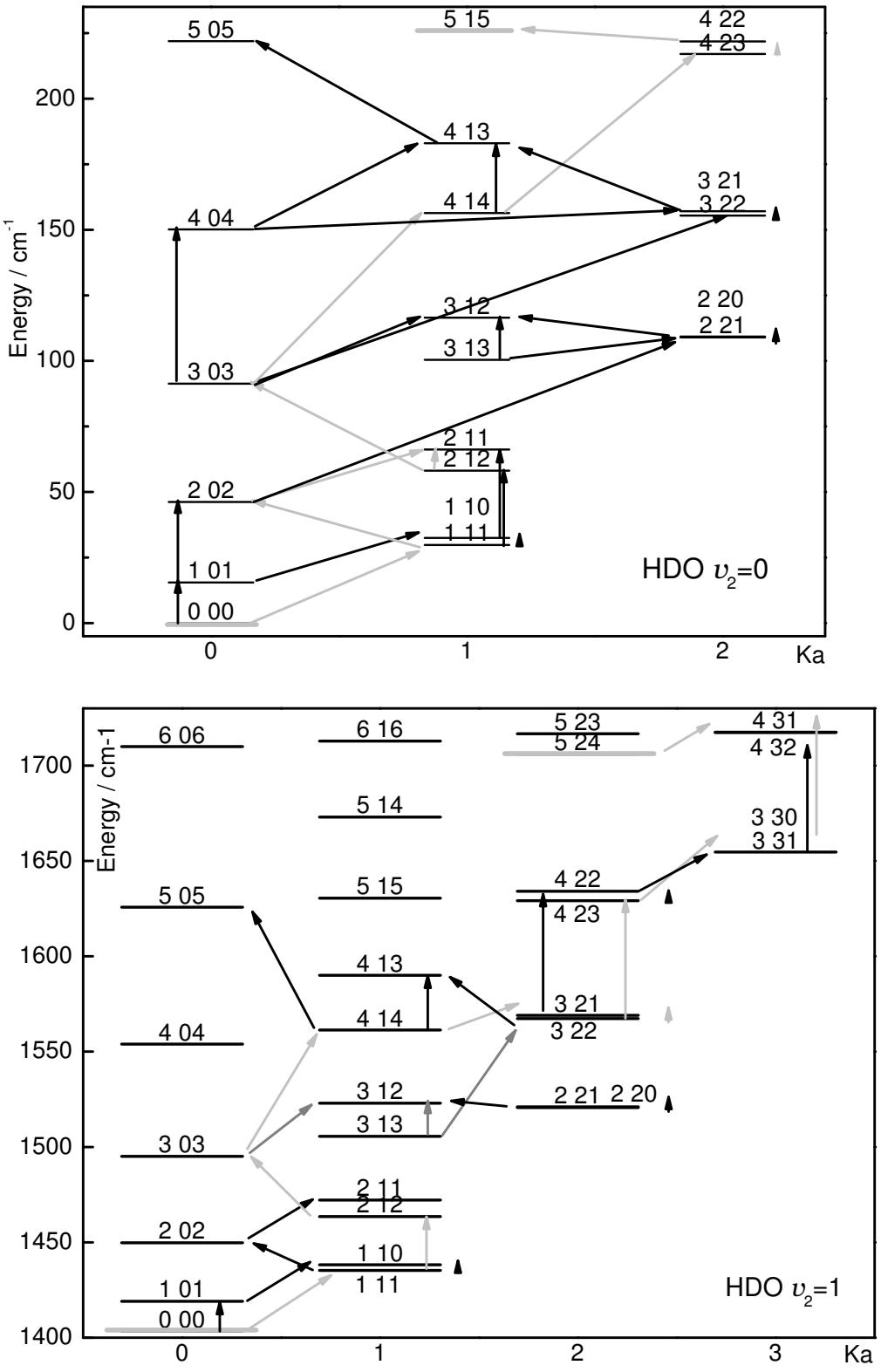


Figure 6.11: Excerpt from the energy level scheme of HDO with measured rotational transitions depicted as arrows. Grey arrows show the closed chain of transitions connecting the ground state rotational level with levels participating in the highly accurate heterodyne IR measurement.

the $v_2 = 0$ state below $2500$ cm$^{-1}$ to be sufficiently populated. For this case, transition frequency predictions for the $\nu_2$-band were performed with the derived parameter set up to $60$ THz, or $2000$ cm$^{-1}$. Predicted frequency uncertainties are below $5{\cdot}10^{-4}$cm$^{-1}$ in all cases and better than $3{\cdot}10^{-5}$ cm$^{-1}$ for strong lines ($I \geq 2{\cdot}10^{-22}$cm$^{-1}$/(molecule cm$^{-2}$)).

These predictions are, therefore, extremely well suited to serve as a calibration line list for Fourier Transform infrared spectrometer up to $2000$ cm$^{-1}$. The frequency accuracy has been improved by a factor of ten for strong lines compared to experimental values.

## 6.3 Conclusions

The addition of a total of more than $250$ HDO and $D_2O$ purely rotational transitions with extremely high frequency accuracy does considerably improve the dataset on the deuterated water species. The data has been extended both in frequency towards the terahertz regime and in energy, involving transitions with high $J$ and $K$ quantum numbers.

Whereas accurate transition frequencies measured in laboratory experiments can per se be used for the identification of interstellar molecules or for calibration purposes, a thorough analysis of the data yields valuable information on molecular parameters and is essential for the prediction of hitherto unmeasured transitions, either in frequency regimes not yet explored experimentally or of intensities not in the range of even the most sensitive spectroscopic techniques.

It has been demonstrated that in the case of water isotopomers the standard model for analysing its rotational and rovibrational spectra, the power series expansion known as Watson's $A$-reduction, is at its limits. The inclusion of transitions between energetically high lying energy levels with considerably high angular momentum quantum numbers requires the introduction of models better suited to cope with the large centrifugal distortion effects present in light dihydride molecules like water.

The Euler approach was successfully applied to analyse the rotational and rovibrational spectra of both HDO and $D_2O$ in the vibrational ground and first excited bending state. The extensive dataset on $D_2O$, up to $J = K_a = 25$, could be reproduced within this model to almost its experimental uncertainty, even though the disturbance of energetically high energy levels by accidental resonances complicates the situation. The predictive capability has been demonstrated to be excellent and comparable to much more elaborate theoretical approaches.

In the case of HDO, the considerable extension of the dataset, in particular for the vibrationally excited bending state, allowed for the most accurate analysis to date. The quality of the fit, especially for the $\nu_2$ band transitions, has been improved by a factor of $4$ over previous results. Moreover, since the rotational and centrifugal distortion parameters in the $v_2 = 0$ and $v_2 = 1$ vibrational states are known to high accuracy from the new high precision submillimeter-wavelength data, it was possible to derive the band center energy $E$ of the fundamental bending mode to the same accuracy by inclusion of only one very precise IR heterodyne $\nu_2$ transition. This allows to use transition frequency predictions from the present analysis as secondary standard for infrared spectroscopy in the frequency range between $1000 - 2000$ cm$^{-1}$.

# A

# Experimental Data - Deuterium Cyanide

In the following tables, the experimental data on all deuterium cyanide isotopomers investigated in this work are summarised. All lines were measured in Cologne, either in Doppler or sub-Doppler mode, if not indicated otherwise. Lines from earlier studies which were included in the fit, are marked by lower case letters:

- a - F. DeLucia and W. Gordy (1969)[65]
- b - M. Winnewisser *et al.* (1971) [76]
- c - E. Fliege *et al.* (1984) [61]
- d - T. Törring (1961) [58]
- e - A. G. Maki and D. R. Lide (1967) [59]
- f - E. F. Pearson *et al.* (1976) [71]
- g - J. Preusser and A. G. Maki (1993) [64]

In the case of blended lines, the o.-c. value states the difference of the measured average line position to the calculated transition frequency of each participating component independently. For the vibrationally excited states ($01^{e,f}0$), the relative intensities are calculated relative to the total intensity of both states. Consequently, for one state, the relative intensities sum up to 50% only. For each measured transition frequency the estimated experimental frequency uncertainty (1 $\sigma$), written in brackets, is in units of the least significant digits.

Not included in these tables is data from IR measurements.

# A.1 DCN

Table A.1: Rotational spectrum of DCN in the vibrational ground state. For each transition a calculated hyperfine-free rotational frequency is given followed by the measured hyperfine lines. Please refer to the text as to which lines where measured in sub-Doppler and which in Doppler resolution. Intensities were calculated for the linear and saturation experiment in absolute (given is the dimensionless intrinsic line strength) and relative units.

| $J'$ | $F'$ | $J''$ | $F''$ | Frequency [MHz][a] | o.-c. [MHz] | $I_{abs,lin}$ | $I_{rel,lin}$ | $I_{abs,sat}$ | $I_{rel,sat}$ |
|---|---|---|---|---|---|---|---|---|---|
| 1 | ← | 0 | | 72414.6909(0002) | | | | | |
| 1 | 1 | 0 | 1 | 72413.504(010) | −0.008 | 1.00E+00 | 33.33 | 1.00E+00 | 25.71 |
| 1 | 2 | 0 | 1 | 72414.933(010) | −0.004 | 1.67E+00 | 55.56 | 2.78E+00 | 71.43 |
| 1 | 0 | 0 | 1 | 72417.028(010) | 0.004 | 3.33E-01 | 11.11 | 1.11E-01 | 2.86 |
| 2 | ← | 1 | | 144827.9960(0003) | | | | | |
| 2 | 1 | 1 | 0 | 144826.822(005)$a$ | 0.002 | 6.67E-01 | 11.11 | 4.44E-01 | 4.03 |
| 3 | ← | 2 | | 217238.5297(0006) | | | | | |
| 3 | 3 | 2 | 3 | 217236.999(005) | −0.004 | 3.33E-01 | 3.70 | 1.11E-01 | 0.44 |
| 3 | 2 | 2 | 1 | 217238.300(010) | 0.004 | 1.80E+00 | 20.00 | 3.24E+00 | 12.73 |
| 3 | 3 | 2 | 2 | 217238.555(010) | 0.017 | 2.67E+00 | 29.63 | 7.11E+00 | 27.93 |
| 3 | 4 | 2 | 3 | 217238.612(010) | 0.009 | 3.86E+00 | 42.86 | 1.49E+01 | 58.43 |
| 3 | 2 | 2 | 3 | 217239.079(010) | −0.012 | 9.52E-03 | 0.11 | 9.07E-05 | 0.00 |
| 3 | 2 | 2 | 2 | 217240.622(010) | −0.004 | 3.33E-01 | 3.70 | 1.11E-01 | 0.44 |
| 4 | ← | 3 | | 289644.9062(0008) | | | | | |
| 4 | 4 | 3 | 4 | 289643.313(003) | −0.004 | 2.50E-01 | 2.08 | 6.25E-02 | 0.14 |
| 4 | 3 | 3 | 2 | 289644.803(005) | −0.006 | 2.86E+00 | 23.81 | 8.16E+00 | 17.64 |
| 4 | 4 | 3 | 3 | 289644.921(005) | 0.004 | 3.75E+00 | 31.25 | 1.41E+01 | 30.39 |
| 4 | 5 | 3 | 4 | 289644.957(005) | −0.005 | 4.89E+00 | 40.74 | 2.39E+01 | 51.65 |
| 4 | 3 | 3 | 3 | 289646.897(003) | 0.000 | 2.50E-01 | 2.08 | 6.25E-02 | 0.14 |
| 5 | ← | 4 | | 362045.7401(0011) | | | | | |
| 5 | 5 | 4 | 5 | 362044.106(010) | −0.003 | 2.00E-01 | 1.33 | 4.00E-02 | 0.05 |
| 5 | 4 | 4 | 3 | 362045.687(010) | −0.004 | 3.89E+00 | 25.93 | 1.51E+01 | 20.66 |
| 5 | 5 | 4 | 4 | 362045.773(002) | 0.019 | 4.80E+00 | 32.00 | 2.30E+01 | 31.48 |
| 5 | 6 | 4 | 5 | 362045.773(002) | −0.015 | 5.91E+00 | 39.39 | 3.49E+01 | 47.71 |
| 5 | 4 | 4 | 4 | 362047.669(010) | −0.002 | 2.00E-01 | 1.33 | 4.00E-02 | 0.05 |
| 6 | ← | 5 | | 434439.6461(0014) | | | | | |
| 6 | 6 | 5 | 6 | 434437.985(005) | 0.002 | 1.67E-01 | 0.93 | 2.78E-02 | 0.03 |
| 6 | 6/7 | 5 | 6/6 | 434438.830(003) | 0.006 | | | 2.16E-02 | 0.02 |
| 6 | 6/6 | 5 | 6/5 | 434438.830(003) | 0.006 | | | 2.07E-02 | 0.02 |
| 6 | 5 | 5 | 4 | 434439.671(003) | 0.051 | 4.91E+00 | 27.27 | 2.40E+01 | 22.62 |
| 6 | 6 | 5 | 5 | 434439.671(003) | 0.008 | 5.83E+00 | 32.41 | 3.40E+01 | 32.05 |
| 6 | 7 | 5 | 6 | 434439.671(003) | −0.020 | 6.92E+00 | 38.46 | 4.79E+01 | 45.14 |
| 6 | 6/5 | 5 | 5/5 | 434440.593(003) | 0.003 | | | 8.08E-03 | 0.01 |
| 6 | 5/5 | 5 | 5/4 | 434440.593(003) | 0.003 | | | 5.46E-03 | 0.01 |
| 6 | 5 | 5 | 5 | 434441.536(005) | −0.001 | 1.67E-01 | 0.93 | 2.78E-02 | 0.03 |
| 7 | ← | 6 | | 506825.2394(0019) | | | | | |
| 7 | 7 | 6 | 7 | 506823.555(005) | 0.004 | 1.43E-01 | 0.68 | 2.04E-02 | 0.01 |
| 7 | 7/8 | 6 | 7/7 | 506824.406(005) | 0.000 | | | 5.60E-02 | 0.04 |
| 7 | 7/7 | 6 | 7/6 | 506824.406(005) | 0.000 | | | 5.26E-02 | 0.04 |
| 7 | 6 | 6 | 5 | 506825.255(010) | 0.028 | 5.92E+00 | 28.21 | 3.51E+01 | 24.15 |
| 7 | 7 | 6 | 6 | 506825.255(010) | −0.004 | 6.86E+00 | 32.65 | 4.70E+01 | 32.37 |
| 7 | 8 | 6 | 7 | 506825.255(010) | −0.028 | 7.93E+00 | 37.78 | 6.29E+01 | 43.33 |
| 7 | 7/6 | 6 | 6/6 | 506826.176(005) | 0.003 | | | 3.26E-02 | 0.02 |
| 7 | 6/6 | 6 | 6/5 | 506826.176(005) | 0.003 | | | 2.51E-02 | 0.02 |
| 7 | 6 | 6 | 6 | 506827.095(005) | −0.006 | 1.43E-01 | 0.68 | 2.04E-02 | 0.01 |
| 8 | ← | 7 | | 579201.1351(0024) | | | | | |
| 8 | 8 | 7 | 8 | 579199.427(010) | 0.002 | 1.25E-01 | 0.52 | 1.56E-02 | 0.01 |
| 8 | 8/9 | 7 | 8/8 | 579200.292(010) | 0.000 | | | 1.05E-01 | 0.06 |
| 8 | 8/8 | 7 | 8/7 | 579200.292(010) | 0.000 | | | 9.84E-02 | 0.05 |

Table A.1: DCN $v_2 = 0$ transitions - continued

| $J'$ | $F'$ | $J''$ | $F''$ | Frequency [MHz][a] | o.-c. [MHz] | $I_{abs,lin}$ | $I_{rel,lin}$ | $I_{abs,sat}$ | $I_{rel,sat}$ |
|---|---|---|---|---|---|---|---|---|---|
| 8 | 7 | 7 | 6 | 579201.154(010) | 0.022 | 6.93E+00 | 28.89 | 4.81E+01 | 25.25 |
| 8 | 8 | 7 | 7 | 579201.154(010) | −0.003 | 7.88E+00 | 32.81 | 6.20E+01 | 32.57 |
| 8 | 9 | 7 | 8 | 579201.154(010) | −0.024 | 8.94E+00 | 37.25 | 7.99E+01 | 41.98 |
| 8 | 8/7 | 7 | 7/7 | 579202.062(005) | 0.002 | | | 7.79E-02 | 0.04 |
| 8 | 7/7 | 7 | 7/6 | 579202.062(005) | 0.002 | | | 6.40E-02 | 0.03 |
| 8 | 7 | 7 | 7 | 579202.969(010) | −0.006 | 1.25E-01 | 0.52 | 1.56E-02 | 0.01 |
| 9 | ← | 8 | | 651565.9490(0030) | | | | | |
| 9 | 9 | 8 | 9 | 651564.220(005) | −0.001 | 1.11E-01 | 0.41 | 1.23E-02 | 0.01 |
| 9 | 9/10 | 8 | 9/ 9 | 651565.095(005) | −0.003 | | | 1.64E-01 | 0.07 |
| 9 | 9/9 | 8 | 9/8 | 651565.095(005) | −0.003 | | | 1.53E-01 | 0.06 |
| 9 | 8 | 8 | 7 | 651565.972(005) | 0.019 | 7.94E+00 | 29.41 | 6.31E+01 | 26.10 |
| 9 | 9 | 8 | 8 | 651565.972(005) | −0.001 | 8.89E+00 | 32.92 | 7.90E+01 | 32.70 |
| 9 | 10 | 8 | 9 | 651565.972(005) | −0.021 | 9.95E+00 | 36.84 | 9.90E+01 | 40.95 |
| 9 | 9/8 | 8 | 8/8 | 651566.872(005) | 0.005 | | | 1.39E-01 | 0.06 |
| 9 | 8/8 | 8 | 8/7 | 651566.872(005) | 0.005 | | | 1.19E-01 | 0.05 |
| 9 | 8 | 8 | 8 | 651567.768(010) | −0.003 | 1.11E-01 | 0.41 | 1.23E-02 | 0.01 |
| 10 | ← | 9 | | 723918.2973(0038) | | | | | |
| 10 | 10/11 | 9 | 10/10 | 723917.439(010) | 0.000 | | | 2.26E-01 | 0.08 |
| 10 | 10/10 | 9 | 10/ 9 | 723917.439(010) | 0.000 | | | 2.11E-01 | 0.07 |
| 10 | 9 | 9 | 8 | 723918.320(010) | 0.013 | 8.95E+00 | 29.82 | 8.01E+01 | 26.79 |
| 10 | 10 | 9 | 9 | 723918.320(010) | −0.004 | 9.90E+00 | 33.00 | 9.80E+01 | 32.79 |
| 10 | 11 | 9 | 10 | 723918.320(010) | −0.022 | 1.10E+01 | 36.51 | 1.20E+02 | 40.14 |
| 10 | 10/9 | 9 | 9/9 | 723919.211(010) | 0.001 | | | 2.08E-01 | 0.07 |
| 10 | 9/9 | 9 | 9/8 | 723919.211(010) | 0.001 | | | 1.83E-01 | 0.06 |
| 11 | ← | 10 | | 796256.7964(0048) | | | | | |
| 11 | 11/12 | 10 | 11/11 | 796255.935(010) | 0.004 | | | 2.88E-01 | 0.08 |
| 11 | 11/11 | 10 | 11/10 | 796255.935(010) | 0.004 | | | 2.69E-01 | 0.07 |
| 11 | 10 | 10 | 9 | 796256.825(010) | 0.014 | 9.95E+00 | 30.16 | 9.90E+01 | 27.35 |
| 11 | 11 | 10 | 10 | 796256.825(010) | 0.000 | 1.09E+01 | 33.06 | 1.19E+02 | 32.86 |
| 11 | 12 | 10 | 11 | 796256.825(010) | −0.018 | 1.20E+01 | 36.23 | 1.43E+02 | 39.48 |
| 12 | ← | 11 | | 868580.0636(0059) | | | | | |
| 12 | 11 | 11 | 10 | 868580.091(010) | 0.009 | 1.10E+01 | 30.43 | 1.20E+02 | 27.83 |
| 12 | 12 | 11 | 11 | 868580.091(010) | −0.004 | 1.19E+01 | 33.10 | 1.42E+02 | 32.92 |
| 12 | 13 | 11 | 12 | 868580.091(010) | −0.020 | 1.30E+01 | 36.00 | 1.68E+02 | 38.94 |
| 13 | ← | 12 | | 940886.7165(0073) | | | | | |
| 13 | 12 | 12 | 11 | 940886.755(010) | 0.017 | 1.20E+01 | 30.67 | 1.43E+02 | 28.24 |
| 13 | 13 | 12 | 12 | 940886.755(010) | 0.005 | 1.29E+01 | 33.14 | 1.67E+02 | 32.97 |
| 13 | 14 | 12 | 13 | 940886.755(010) | −0.011 | 1.40E+01 | 35.80 | 1.95E+02 | 38.49 |
| 26 | ← | 25 | | 1878733.7425(0679) | | | | | |
| 26 | 26 | 25 | 26 | 1878733.728(050) | 1.955 | 3.85E-02 | 0.05 | 1.48E-03 | 0.00 |
| 26 | 25 | 25 | 24 | 1878733.728(050) | −0.065 | 2.50E+01 | 32.03 | 6.24E+02 | 30.75 |
| 26 | 26 | 25 | 25 | 1878733.728(050) | −0.069 | 2.60E+01 | 33.28 | 6.74E+02 | 33.22 |
| 26 | 27 | 25 | 26 | 1878733.728(050) | −0.084 | 2.70E+01 | 34.59 | 7.28E+02 | 35.88 |
| 26 | 25 | 25 | 25 | 1878733.728(050) | −1.723 | 3.85E-02 | 0.05 | 1.48E-03 | 0.00 |
| 27 | ← | 26 | | 1950663.1048(0782) | | | | | |
| 27 | 27 | 26 | 27 | 1950663.153(050) | 2.033 | 3.70E-02 | 0.05 | 1.37E-03 | 0.00 |
| 27 | 26 | 26 | 25 | 1950663.153(050) | −0.003 | 2.60E+01 | 32.08 | 6.75E+02 | 30.85 |
| 27 | 27 | 26 | 26 | 1950663.153(050) | −0.007 | 2.70E+01 | 33.29 | 7.27E+02 | 33.22 |
| 27 | 28 | 26 | 27 | 1950663.153(050) | −0.023 | 2.80E+01 | 34.55 | 7.83E+02 | 35.78 |
| 27 | 26 | 26 | 26 | 1950663.153(050) | −1.658 | 3.70E-02 | 0.05 | 1.37E-03 | 0.00 |

Table A.2: Rotational spectrum of DCN in the first excited vibrational state $v_2 = 1^{e,f}$. For each transition a calculated hyperfine-free rotational frequency is given followed by the measured hyperfine lines. Please refer to the text as to which lines where measured in sub-Doppler and which in Doppler resolution. Intensities were calculated for the linear and saturation experiment in absolute (given is the dimensionless intrinsic line strength) and relative units.

| $J'$ | $F'$ | $J''$ | $F''$ | Frequency [MHz][a] | o.-c. [MHz] | $I_{abs,lin}$ | $I_{rel,lin}$ | $I_{abs,sat}$ | $I_{rel,sat}$ |
|---|---|---|---|---|---|---|---|---|---|
| 2 | ← | 1 | (e) | 144974.2984(0004) | | | | | |
| 2 | 2 | 1 | 1 | 144973.180(150)$b$ | 0.081 | 1.70E+01 | 12.5 | 2.80E+02 | 10.12 |
| 2 | 1 | 1 | 1 | 144974.640(100)$b$ | 0.444 | 5.60E+00 | 4.17 | 3.20E+01 | 1.12 |
| 2 | 3 | 1 | 2 | 144974.640(100)$b$ | 0.046 | 3.20E+01 | 23.33 | 9.90E+02 | 35.27 |
| 2 | 1 | 1 | 0 | 144976.170(100)$b$ | 0.037 | 7.50E+00 | 5.56 | 5.60E+01 | 2 |
| | | | | | | | | | |
| 2 | ← | 1 | (f) | 145718.9907(0004) | | | | | |
| 2 | 2 | 1 | 1 | 145717.850(150)$b$ | 0.059 | 1.70E+01 | 12.5 | 2.80E+02 | 10.12 |
| 2 | 1 | 1 | 1 | 145719.280(100)$b$ | 0.219 | 5.60E+00 | 4.17 | 3.20E+01 | 1.12 |
| 2 | 3 | 1 | 2 | 145719.280(100)$b$ | −0.014 | 3.20E+01 | 23.33 | 9.90E+02 | 35.27 |
| 2 | 1 | 1 | 0 | 145720.760(100)$b$ | 0.021 | 7.50E+00 | 5.56 | 5.60E+01 | 2 |
| | | | | | | | | | |
| 3 | ← | 2 | (e) | 217457.9237(0006) | | | | | |
| 3 | 3 | 2 | 3 | 217456.888(010) | 0.004 | 1.00E+01 | 1.85 | 1.10E+02 | 0.22 |
| 3 | 3 | 2 | 2 | 217457.624(005) | 0 | 8.30E+01 | 14.81 | 6.90E+03 | 13.89 |
| 3 | 2 | 2 | 1 | 217458.053(010) | 0.008 | 5.60E+01 | 10 | 3.10E+03 | 6.33 |
| 3 | 4 | 2 | 3 | 217458.053(010) | −0.006 | 1.20E+02 | 21.43 | 1.40E+04 | 29.07 |
| 3 | 2 | 2 | 2 | 217459.138(010) | −0.004 | 1.00E+01 | 1.85 | 1.10E+02 | 0.22 |
| | | | | | | | | | |
| 3 | ← | 2 | (f) | 218574.8302(0006) | | | | | |
| 3 | 3 | 2 | 3 | 218573.685(010) | 0.006 | 1.00E+01 | 1.85 | 1.10E+02 | 0.22 |
| 3 | 3 | 2 | 2 | 218574.532(010) | 0.002 | 8.30E+01 | 14.81 | 6.90E+03 | 13.89 |
| 3 | 2 | 2 | 1 | 218574.965(010) | 0.031 | 5.60E+01 | 10 | 3.10E+03 | 6.33 |
| 3 | 4 | 2 | 3 | 218574.964(010) | −0.005 | 1.20E+02 | 21.43 | 1.40E+04 | 29.07 |
| 3 | 2 | 2 | 2 | 218576.214(010) | 0.01 | 1.00E+01 | 1.85 | 1.10E+02 | 0.22 |
| | | | | | | | | | |
| 4 | ← | 3 | (e) | 289937.3207(0008) | | | | | |
| 4 | 4 | 3 | 4 | 289936.026(010) | 0 | 1.50E+01 | 1.04 | 2.20E+02 | 0.07 |
| 4 | 4 | 3 | 3 | 289937.199(003) | −0.001 | 2.20E+02 | 15.62 | 4.90E+04 | 15.18 |
| 4 | 3 | 3 | 2 | 289937.326(003) | 0 | 1.70E+02 | 11.9 | 2.80E+04 | 8.81 |
| 4 | 5 | 3 | 4 | 289937.404(003) | 0.005 | 2.90E+02 | 20.37 | 8.30E+04 | 25.8 |
| 4 | 3 | 3 | 3 | 289938.837(005) | −0.007 | 1.50E+01 | 1.04 | 2.20E+02 | 0.07 |
| | | | | | | | | | |
| 4 | ← | 3 | (f) | 291426.2830(0008) | | | | | |
| 4 | 4 | 3 | 4 | 291424.874(010) | 0.001 | 1.50E+01 | 1.04 | 2.20E+02 | 0.07 |
| 4 | 4 | 3 | 3 | 291426.152(003) | −0.011 | 2.20E+02 | 15.62 | 4.90E+04 | 15.18 |
| 4 | 3 | 3 | 2 | 291426.269(003) | −0.012 | 1.70E+02 | 11.9 | 2.80E+04 | 8.81 |
| 4 | 5 | 3 | 4 | 291426.357(003) | −0.007 | 2.90E+02 | 20.37 | 8.30E+04 | 25.8 |
| 4 | 3 | 3 | 3 | 291427.945(010) | −0.01 | 1.50E+01 | 1.04 | 2.20E+02 | 0.07 |
| | | | | | | | | | |
| 6 | ← | 5 | (e) | 434877.7926(0015) | | | | | |
| 6 | 6 | 5 | 6 | 434876.278(010) | 0.006 | 2.30E+01 | 0.46 | 5.40E+02 | 0.01 |
| 6 | 6/ 7 | 5 | 6/ 6 | 434877.033(005) | −0.002 | | | 1.40E+02 | 0 |
| 6 | 6/ 6 | 5 | 6/ 5 | 434877.033(005) | −0.002 | | | 1.80E+02 | 0 |
| 6 | 6 | 5 | 5 | 434877.780(050) | 0.022 | 8.10E+02 | 16.2 | 6.60E+05 | 16.01 |
| 6 | 5 | 5 | 4 | 434877.780(050) | 0.004 | 6.80E+02 | 13.64 | 4.70E+05 | 11.34 |
| 6 | 7 | 5 | 6 | 434877.830(050) | −0.001 | 9.60E+02 | 19.23 | 9.30E+05 | 22.54 |
| 6 | 6/ 5 | 5 | 5/ 5 | 434878.615(005) | −0.001 | | | 4.10E+01 | 0 |
| 6 | 5/ 5 | 5 | 5/ 4 | 434878.615(005) | −0.001 | | | 3.60E+01 | 0 |
| 6 | 5 | 5 | 5 | 434879.460(010) | −0.006 | 2.30E+01 | 0.46 | 5.40E+02 | 0.01 |
| | | | | | | | | | |
| 6 | ← | 5 | (f) | 437110.1809(0015) | | | | | |
| 6 | 6 | 5 | 6 | 437108.550(010) | 0.009 | 2.30E+01 | 0.46 | 5.40E+02 | 0.01 |
| 6 | 6/ 7 | 5 | 6/ 6 | 437109.361(005) | −0.003 | | | 2.00E+03 | 0.05 |
| 6 | 6/ 6 | 5 | 6/ 5 | 437109.361(005) | −0.003 | | | 2.20E+03 | 0.05 |
| 6 | 6 | 5 | 5 | 437110.159(050) | 0.013 | 8.10E+02 | 16.2 | 6.60E+05 | 16.01 |
| 6 | 5 | 5 | 4 | 437110.159(050) | −0.003 | 6.80E+02 | 13.64 | 4.70E+05 | 11.34 |
| 6 | 7 | 5 | 6 | 437110.230(050) | 0.009 | 9.60E+02 | 19.23 | 9.30E+05 | 22.54 |
| 6 | 6/ 5 | 5 | 5/ 5 | 437111.076(005) | 0.001 | | | 1.20E+03 | 0.03 |

Table A.2: DCN $v_2 = 1$ transitions - continued

| $J'$ | $F'$ | $J''$ | $F''$ | Frequency [MHz][a] | o.-c. [MHz] | $I_{abs,lin}$ | $I_{rel,lin}$ | $I_{abs,sat}$ | $I_{rel,sat}$ |
|---|---|---|---|---|---|---|---|---|---|
| 6 | 5/ 5 | 5 | 5/ 4 | 437111.076(005) | 0.001 | | | 1.10E+03 | 0.03 |
| 6 | 5 | 5 | 5 | 437111.992(010) | −0.004 | 2.30E+01 | 0.46 | 5.40E+02 | 0.01 |
| 7 | ← | 6 | (e) | 507336.0498(0020) | | | | | |
| 7 | 7/ 8 | 6 | 7/ 7 | 507335.253(010) | −0.009 | | | 8.20E+02 | 0.01 |
| 7 | 7/ 7 | 6 | 7/ 6 | 507335.253(010) | −0.009 | | | 8.80E+02 | 0.01 |
| 7 | 7 | 6 | 6 | 507336.054(003) | 0.026 | 1.30E+03 | 16.33 | 1.70E+06 | 16.17 |
| 7 | 6 | 6 | 5 | 507336.054(003) | 0.02 | 1.10E+03 | 14.1 | 1.30E+06 | 12.06 |
| 7 | 8 | 6 | 7 | 507336.054(003) | −0.026 | 1.50E+03 | 18.89 | 2.30E+06 | 21.64 |
| 7 | 7/ 6 | 6 | 6/ 6 | 507336.900(010) | 0.014 | | | 3.90E+02 | 0 |
| 7 | 6/ 6 | 6 | 6/ 5 | 507336.900(010) | 0.014 | | | 3.40E+02 | 0 |
| 7 | ← | 6 | (f) | 509939.7034(0020) | | | | | |
| 7 | 7/ 8 | 6 | 7/ 7 | 509938.845(010) | −0.011 | | | 6.10E+03 | 0.06 |
| 7 | 7/ 7 | 6 | 7/ 6 | 509938.845(010) | −0.011 | | | 6.10E+03 | 0.06 |
| 7 | 7 | 6 | 6 | 509939.700(010) | 0.019 | 1.30E+03 | 16.33 | 1.70E+06 | 16.17 |
| 7 | 6 | 6 | 5 | 509939.700(010) | 0.015 | 1.10E+03 | 14.1 | 1.30E+06 | 12.06 |
| 7 | 8 | 6 | 7 | 509939.700(010) | −0.035 | 1.50E+03 | 18.89 | 2.30E+06 | 21.64 |
| 7 | 7/ 6 | 6 | 6/ 6 | 509940.619(010) | 0.01 | | | 4.50E+03 | 0.04 |
| 7 | 6/ 6 | 6 | 6/ 5 | 509940.619(010) | 0.01 | | | 4.00E+03 | 0.04 |
| 8 | ← | 7 | (e) | 579784.4432(0025) | | | | | |
| 8 | 8/ 9 | 7 | 8/ 8 | 579783.628(010) | −0.005 | | | 3.10E+03 | 0.01 |
| 8 | 8/ 8 | 7 | 8/ 7 | 579783.628(010) | −0.005 | | | 3.10E+03 | 0.01 |
| 8 | 7 | 7 | 6 | 579784.448(005) | 0.02 | 1.70E+03 | 14.44 | 3.00E+06 | 12.61 |
| 8 | 8 | 7 | 7 | 579784.448(005) | 0.02 | 2.00E+03 | 16.41 | 3.90E+06 | 16.27 |
| 8 | 9 | 7 | 8 | 579784.448(005) | −0.021 | 2.20E+03 | 18.63 | 5.00E+06 | 20.98 |
| 8 | 8/ 7 | 7 | 7/ 7 | 579785.295(010) | 0.01 | | | 2.00E+03 | 0.01 |
| 8 | 7/ 7 | 7 | 7/ 6 | 579785.295(010) | 0.01 | | | 1.70E+03 | 0.01 |
| 8 | ← | 7 | (f) | 582758.9941(0025) | | | | | |
| 8 | 8/ 9 | 7 | 8/ 8 | 582758.120(005) | −0.003 | | | 1.50E+04 | 0.06 |
| 8 | 8/ 8 | 7 | 8/ 7 | 582758.120(005) | −0.003 | | | 1.40E+04 | 0.06 |
| 8 | 7 | 7 | 6 | 582758.991(005) | 0.013 | 1.70E+03 | 14.44 | 3.00E+06 | 12.61 |
| 8 | 8 | 7 | 7 | 582758.991(005) | 0.012 | 2.00E+03 | 16.41 | 3.90E+06 | 16.27 |
| 8 | 9 | 7 | 8 | 582758.991(005) | −0.029 | 2.20E+03 | 18.63 | 5.00E+06 | 20.98 |
| 8 | 8/ 7 | 7 | 7/ 7 | 582759.910(005) | 0.005 | | | 1.30E+04 | 0.05 |
| 8 | 7/ 7 | 7 | 7/ 6 | 582759.910(005) | 0.005 | | | 1.10E+04 | 0.05 |
| 9 | ← | 8 | (e) | 652221.5649(0032) | | | | | |
| 9 | 9/10 | 8 | 9/ 9 | 652220.735(005) | −0.002 | | | 8.60E+03 | 0.02 |
| 9 | 9/ 9 | 8 | 9/ 8 | 652220.735(005) | −0.002 | | | 8.40E+03 | 0.02 |
| 9 | 8 | 8 | 7 | 652221.566(005) | 0.015 | 2.50E+03 | 14.71 | 6.40E+06 | 13.04 |
| 9 | 9 | 8 | 8 | 652221.566(005) | 0.012 | 2.80E+03 | 16.46 | 8.00E+06 | 16.34 |
| 9 | 10 | 8 | 9 | 652221.566(005) | −0.021 | 3.20E+03 | 18.42 | 1.00E+07 | 20.46 |
| 9 | 9/ 8 | 8 | 8/ 8 | 652222.413(005) | 0.004 | | | 6.70E+03 | 0.01 |
| 9 | 8/ 8 | 8 | 8/ 7 | 652222.413(005) | 0.004 | | | 5.90E+03 | 0.01 |
| 9 | 8 | 8 | 8 | 652223.269(005) | 0.004 | 3.50E+01 | 0.21 | 1.30E+03 | 0 |
| 9 | ← | 8 | (f) | 655566.5929(0032) | | | | | |
| 9 | 9 | 8 | 9 | 655564.821(020) | 0.013 | 3.50E+01 | 0.21 | 1.30E+03 | 0 |
| 9 | 9/10 | 8 | 9/ 9 | 655565.707(005) | 0.003 | | | 3.10E+04 | 0.06 |
| 9 | 9/ 9 | 8 | 9/ 8 | 655565.707(005) | 0.003 | | | 3.00E+04 | 0.06 |
| 9 | 8 | 8 | 7 | 655566.592(005) | 0.014 | 2.50E+03 | 14.71 | 6.40E+06 | 13.04 |
| 9 | 9 | 8 | 8 | 655566.592(005) | 0.01 | 2.80E+03 | 16.46 | 8.00E+06 | 16.34 |
| 9 | 10 | 8 | 9 | 655566.592(005) | −0.023 | 3.20E+03 | 18.42 | 1.00E+07 | 20.46 |
| 9 | 9/ 8 | 8 | 8/ 8 | 655567.501(005) | −0.004 | | | 2.90E+04 | 0.06 |
| 9 | 8/ 8 | 8 | 8/ 7 | 655567.501(005) | −0.004 | | | 2.60E+04 | 0.05 |
| 9 | 8 | 8 | 8 | 655568.411(020) | −0.02 | 3.50E+01 | 0.21 | 1.30E+03 | 0 |
| 10 | ← | 9 | (e) | 724646.0071(0040) | | | | | |
| 10 | 10/11 | 9 | 10/10 | 724645.165(010) | 0.001 | | | 2.00E+04 | 0.02 |
| 10 | 10/10 | 9 | 10/ 9 | 724645.165(010) | 0.001 | | | 1.90E+04 | 0.02 |
| 10 | 9 | 9 | 8 | 724646.016(003) | 0.021 | 3.50E+03 | 14.91 | 1.20E+07 | 13.39 |
| 10 | 10 | 9 | 9 | 724646.016(003) | 0.017 | 3.90E+03 | 16.5 | 1.50E+07 | 16.39 |
| 10 | 11 | 9 | 10 | 724646.016(003) | −0.011 | 4.30E+03 | 18.25 | 1.90E+07 | 20.06 |
| 10 | 10/ 9 | 9 | 9/ 9 | 724646.854(010) | 0.003 | | | 1.80E+04 | 0.02 |

Table A.2: DCN $v_2 = 1$ transitions - continued

| $J'$ | $F'$ | $J''$ | $F''$ | Frequency [MHz][a] | o.-c. [MHz] | $I_{abs,lin}$ | $I_{rel,lin}$ | $I_{abs,sat}$ | $I_{rel,sat}$ |
|---|---|---|---|---|---|---|---|---|---|
| 10 | 9/ 9 | 9 | 9/ 8 | 724646.854(010) | 0.003 | | | 1.60E+04 | 0.02 |
| 10 | ← | 9 | (f) | 728361.0404(0040) | | | | | |
| 10 | 10/11 | 9 | 10/10 | 728360.140(010) | 0.004 | | | 5.80E+04 | 0.06 |
| 10 | 10/10 | 9 | 10/ 9 | 728360.140(010) | 0.004 | | | 5.50E+04 | 0.06 |
| 10 | 9 | 9 | 8 | 728361.040(003) | 0.013 | 3.50E+03 | 14.91 | 1.20E+07 | 13.39 |
| 10 | 10 | 9 | 9 | 728361.040(003) | 0.008 | 3.90E+03 | 16.5 | 1.50E+07 | 16.39 |
| 10 | 11 | 9 | 10 | 728361.040(003) | −0.02 | 4.30E+03 | 18.25 | 1.90E+07 | 20.06 |
| 10 | 10/ 9 | 9 | 9/ 9 | 728361.947(010) | −0.006 | | | 5.60E+04 | 0.06 |
| 10 | 9/ 9 | 9 | 9/ 8 | 728361.947(010) | −0.006 | | | 5.10E+04 | 0.05 |
| 12 | ← | 11 | (e) | 869451.2255(0062) | | | | | |
| 12 | 11 | 11 | 10 | 869451.229(010) | 0.014 | 6.30E+03 | 15.22 | 3.90E+07 | 13.91 |
| 12 | 12 | 11 | 11 | 869451.229(010) | 0.009 | 6.80E+03 | 16.55 | 4.60E+07 | 16.46 |
| 12 | 13 | 11 | 12 | 869451.229(010) | −0.013 | 7.40E+03 | 18 | 5.50E+07 | 19.47 |
| 12 | ← | 11 | (f) | 873904.6485(0062) | | | | | |
| 12 | 11 | 11 | 10 | 873904.644(010) | 0.007 | 6.30E+03 | 15.22 | 3.90E+07 | 13.91 |
| 12 | 12 | 11 | 11 | 873904.644(010) | 0.001 | 6.80E+03 | 16.55 | 4.60E+07 | 16.46 |
| 12 | 13 | 11 | 12 | 873904.644(010) | −0.021 | 7.40E+03 | 18 | 5.50E+07 | 19.47 |
| 13 | ← | 12 | (e) | 941829.1893(0076) | | | | | |
| 13 | 12 | 12 | 11 | 941829.188(010) | 0.009 | 8.00E+03 | 15.33 | 6.40E+07 | 14.12 |
| 13 | 13 | 12 | 12 | 941829.188(010) | 0.003 | 8.70E+03 | 16.57 | 7.50E+07 | 16.48 |
| 13 | 14 | 12 | 13 | 941829.188(010) | −0.017 | 9.40E+03 | 17.9 | 8.80E+07 | 19.24 |
| 13 | ← | 12 | (f) | 946650.8945(0076) | | | | | |
| 13 | 12 | 12 | 11 | 946650.894(010) | 0.01 | 8.00E+03 | 15.33 | 6.40E+07 | 14.12 |
| 13 | 13 | 12 | 12 | 946650.894(010) | 0.004 | 8.70E+03 | 16.57 | 7.50E+07 | 16.48 |
| 13 | 14 | 12 | 13 | 946650.894(010) | −0.016 | 9.40E+03 | 17.9 | 8.80E+07 | 19.24 |
| 26 | ← | 25 | (e) | 1880566.6355(0708) | | | | | |
| 26 | 26 | 25 | 26 | 1880566.580(050) | 1.926 | 1.00E+02 | 0.02 | 1.10E+04 | 0 |
| 26 | 25 | 25 | 24 | 1880566.580(050) | −0.046 | 6.70E+04 | 16.01 | 4.50E+09 | 15.38 |
| 26 | 26 | 25 | 25 | 1880566.580(050) | −0.049 | 7.00E+04 | 16.64 | 4.90E+09 | 16.61 |
| 26 | 27 | 25 | 26 | 1880566.580(050) | −0.064 | 7.30E+04 | 17.3 | 5.30E+09 | 17.94 |
| 26 | 25 | 25 | 25 | 1880566.580(050) | −1.683 | 1.00E+02 | 0.02 | 1.10E+04 | 0 |
| 26 | ← | 25 | (f) | 1890096.7719(0708) | | | | | |
| 26 | 26 | 25 | 26 | 1890096.785(050) | 2.119 | 1.00E+02 | 0.02 | 1.10E+04 | 0 |
| 26 | 25 | 25 | 24 | 1890096.785(050) | 0.019 | 6.70E+04 | 16.01 | 4.50E+09 | 15.38 |
| 26 | 26 | 25 | 25 | 1890096.785(050) | 0.017 | 7.00E+04 | 16.64 | 4.90E+09 | 16.61 |
| 26 | 27 | 25 | 26 | 1890096.785(050) | 0.001 | 7.30E+04 | 17.3 | 5.30E+09 | 17.94 |
| 26 | 25 | 25 | 25 | 1890096.785(050) | −1.75 | 1.00E+02 | 0.02 | 1.10E+04 | 0 |
| 27 | ← | 26 | (e) | 1952560.8553(0816) | | | | | |
| 27 | 27 | 26 | 27 | 1952560.822(050) | 1.966 | 1.10E+02 | 0.02 | 1.20E+04 | 0 |
| 27 | 26 | 26 | 25 | 1952560.822(050) | −0.023 | 7.60E+04 | 16.04 | 5.70E+09 | 15.42 |
| 27 | 27 | 26 | 26 | 1952560.822(050) | −0.025 | 7.80E+04 | 16.64 | 6.20E+09 | 16.61 |
| 27 | 28 | 26 | 27 | 1952560.822(050) | −0.041 | 8.10E+04 | 17.27 | 6.60E+09 | 17.89 |
| 27 | 26 | 26 | 26 | 1952560.822(050) | −1.658 | 1.10E+02 | 0.02 | 1.20E+04 | 0 |
| 27 | ← | 26 | (f) | 1962445.4406(0816) | | | | | |
| 27 | 27 | 26 | 27 | 1962445.400(050) | 2.081 | 1.10E+02 | 0.02 | 1.20E+04 | 0 |
| 27 | 26 | 26 | 25 | 1962445.400(050) | −0.035 | 7.60E+04 | 16.04 | 5.70E+09 | 15.42 |
| 27 | 27 | 26 | 26 | 1962445.400(050) | −0.037 | 7.80E+04 | 16.64 | 6.20E+09 | 16.61 |
| 27 | 28 | 26 | 27 | 1962445.400(050) | −0.053 | 8.10E+04 | 17.27 | 6.60E+09 | 17.89 |
| 27 | 26 | 26 | 26 | 1962445.400(050) | −1.801 | 1.10E+02 | 0.02 | 1.20E+04 | 0 |

Table A.3: Table of the experimental direct $\ell$-type transitions in the first excited bending state of DCN used in the fit. For each transition a calculated hyperfine-free rotational frequency is given followed by the measured hyperfine lines. Please note that the hyperfine structure has not been resolved experimentally. Intensities were calculated for the linear and saturation experiment in absolute (given is the dimensionless intrinsic line strength) and relative units.

| $J'$ | $F'$ | $J''$ | $F''$ | Frequency [MHz][a] | o.-c. | $I_{abs,lin}$ | $I_{rel,lin}$ | $I_{abs,sat}$ | $I_{rel,sat}$ |
|---|---|---|---|---|---|---|---|---|---|
| $\ell = 1^f$ | | $\ell = 1^e$ | | | [MHz] | | | | |
| 5 | ← | 5 | | 5583.7408(0011) | | | | | |
| 5 | 5 | 5 | 5 | 5583.658(010)$c$ | 0.003 | 6.60E+02 | 31.15 | 4.35E+05 | 31.02 |
| 5 | 6 | 5 | 6 | 5583.776(010)$c$ | 0.002 | 8.11E+02 | 38.3 | 6.58E+05 | 46.9 |
| 5 | 4 | 5 | 4 | 5583.806(010)$c$ | 0.007 | 5.54E+02 | 26.18 | 3.07E+05 | 21.92 |
| 6 | ← | 6 | | 7816.1292(0016) | | | | | |
| 6 | 6 | 6 | 6 | 7816.048(010)$c$ | 0.005 | 1.10E+03 | 31.76 | 1.22E+06 | 31.7 |
| 6 | 7 | 6 | 7 | 7816.166(010)$c$ | 0.002 | 1.31E+03 | 37.68 | 1.72E+06 | 44.6 |
| 6 | 5 | 6 | 5 | 7816.190(010)$c$ | 0.006 | 9.53E+02 | 27.42 | 9.09E+05 | 23.62 |
| 7 | ← | 7 | | 10419.7828(0023) | | | | | |
| 7 | 7 | 7 | 7 | 10419.703(010)$c$ | 0.006 | 1.71E+03 | 32.15 | 2.92E+06 | 32.12 |
| 7 | 8 | 7 | 8 | 10419.825(010)$c$ | 0.006 | 1.98E+03 | 37.19 | 3.91E+06 | 42.96 |
| 7 | 6 | 7 | 6 | 10419.841(010)$c$ | 0.005 | 1.50E+03 | 28.3 | 2.26E+06 | 24.88 |
| 8 | ← | 8 | | 13394.3336(0031) | | | | | |
| 8 | 8 | 8 | 8 | 13394.253(010)$c$ | 0.005 | 2.50E+03 | 32.41 | 6.24E+06 | 32.39 |
| 8 | 9 | 8 | 9 | 13394.385(010)$c$ | 0.015 | 2.84E+03 | 36.79 | 8.04E+06 | 41.74 |
| 8 | 7 | 8 | 7 | 13394.385(010)$c$ | −0.001 | 2.23E+03 | 28.95 | 4.98E+06 | 25.84 |
| 9 | ← | 9 | | 16739.3616(0041) | | | | | |
| 9 | 9 | 9 | 9 | 16739.278(010)$c$ | 0.002 | 3.49E+03 | 32.6 | 1.22E+07 | 32.58 |
| 9 | 10 | 9 | 10 | 16739.416(010)$c$ | 0.017 | 3.91E+03 | 36.47 | 1.53E+07 | 40.79 |
| 9 | 8 | 9 | 8 | 16739.416(010)$c$ | 0.003 | 3.16E+03 | 29.46 | 9.97E+06 | 26.61 |
| 10 | ← | 10 | | 20454.3950(0053) | | | | | |
| 10 | 10 | 10 | 10 | 20454.400(050)$d$ | 0.091 | 4.72E+03 | 32.73 | 2.23E+07 | 32.72 |
| 10 | 11 | 10 | 11 | 20454.400(050)$d$ | −0.033 | 5.23E+03 | 36.21 | 2.73E+07 | 40.04 |
| 10 | 9 | 10 | 9 | 20454.400(050)$d$ | −0.045 | 4.31E+03 | 29.86 | 1.86E+07 | 27.23 |
| 11 | ← | 11 | | 24538.9103(0067) | | | | | |
| 11 | 11 | 11 | 11 | 24538.920(050)$e$ | 0.096 | 6.21E+03 | 32.83 | 3.85E+07 | 32.82 |
| 11 | 12 | 11 | 12 | 24538.920(050)$e$ | −0.028 | 6.80E+03 | 35.98 | 4.63E+07 | 39.42 |
| 11 | 10 | 11 | 10 | 24538.920(050)$e$ | −0.04 | 5.71E+03 | 30.18 | 3.26E+07 | 27.74 |
| 12 | ← | 12 | | 28992.3332(0085) | | | | | |
| 12 | 12 | 12 | 12 | 28992.370(040)$e$ | 0.123 | 7.97E+03 | 32.91 | 6.36E+07 | 32.9 |
| 12 | 13 | 12 | 13 | 28992.370(040)$e$ | −0.002 | 8.67E+03 | 35.79 | 7.52E+07 | 38.91 |
| 12 | 11 | 12 | 11 | 28992.370(040)$e$ | −0.012 | 7.38E+03 | 30.45 | 5.45E+07 | 28.18 |
| 13 | ← | 13 | | 33814.0384(0106) | | | | | |
| 13 | 13 | 13 | 13 | 33814.030(050)$e$ | 0.078 | 1.00E+04 | 32.97 | 1.01E+08 | 32.96 |
| 13 | 14 | 13 | 14 | 33814.030(050)$e$ | −0.047 | 1.09E+04 | 35.62 | 1.18E+08 | 38.48 |
| 13 | 12 | 13 | 12 | 33814.030(050)$e$ | −0.056 | 9.35E+03 | 30.68 | 8.74E+07 | 28.55 |
| 14 | ← | 14 | | 39003.3501(0131) | | | | | |
| 14 | 14 | 14 | 14 | 39003.360(050)$e$ | 0.097 | 1.24E+04 | 33.02 | 1.55E+08 | 33.01 |
| 14 | 15 | 14 | 15 | 39003.360(050)$e$ | −0.028 | 1.34E+04 | 35.47 | 1.79E+08 | 38.11 |
| 14 | 13 | 14 | 13 | 39003.360(050)$e$ | −0.037 | 1.16E+04 | 30.88 | 1.35E+08 | 28.87 |
| 15 | ← | 15 | | 44559.5425(0161) | | | | | |
| 15 | 15 | 15 | 15 | 44559.550(050)$e$ | 0.095 | 1.52E+04 | 33.06 | 2.31E+08 | 33.05 |
| 15 | 16 | 15 | 16 | 44559.550(050)$e$ | −0.031 | 1.62E+04 | 35.35 | 2.64E+08 | 37.79 |
| 15 | 14 | 15 | 14 | 44559.550(050)$e$ | −0.039 | 1.43E+04 | 31.04 | 2.03E+08 | 29.15 |
| 16 | ← | 16 | | 50481.8401(0195) | | | | | |
| 16 | 16 | 16 | 16 | 50481.790(080)$e$ | 0.038 | 1.83E+04 | 33.09 | 3.35E+08 | 33.09 |
| 16 | 17 | 16 | 17 | 50481.790(080)$e$ | −0.088 | 1.95E+04 | 35.23 | 3.80E+08 | 37.51 |
| 16 | 15 | 16 | 15 | 50481.790(080)$e$ | −0.096 | 1.73E+04 | 31.19 | 2.98E+08 | 29.4 |

Table A.3: DCN direct $\ell$-type transitions - continued

| $J'$ | $F'$ | $J''$ | $F''$ | Frequency [MHz][a] | o.-c. | $I_{abs,lin}$ | $I_{rel,lin}$ | $I_{abs,sat}$ | $I_{rel,sat}$ |
|---|---|---|---|---|---|---|---|---|---|
| $\ell = 1^f$ | | $\ell = 1^e$ | | | [MHz] | | | | |
| 17 | ← | 17 | | 56769.4181(0236) | | | | | |
| 17 | 17 | 17 | 17 | 56769.320(080)$e$ | −0.01 | 2.18E+04 | 33.12 | 4.77E+08 | 33.11 |
| 17 | 18 | 17 | 18 | 56769.320(080)$e$ | −0.136 | 2.32E+04 | 35.13 | 5.37E+08 | 37.26 |
| 17 | 16 | 17 | 16 | 56769.320(080)$e$ | −0.143 | 2.07E+04 | 31.32 | 4.27E+08 | 29.62 |
| 18 | ← | 18 | | 63421.4033(0283) | | | | | |
| 18 | 18 | 18 | 18 | 63421.280(080)$e$ | −0.035 | 2.58E+04 | 33.14 | 6.65E+08 | 33.14 |
| 18 | 19 | 18 | 19 | 63421.280(080)$e$ | −0.161 | 2.73E+04 | 35.04 | 7.43E+08 | 37.04 |
| 18 | 17 | 18 | 17 | 63421.280(080)$e$ | −0.168 | 2.45E+04 | 31.43 | 5.98E+08 | 29.82 |
| 19 | ← | 19 | | 70436.8739(0338) | | | | | |
| 19 | 19 | 19 | 19 | 70436.843(050) | 0.058 | 3.02E+04 | 33.16 | 9.11E+08 | 33.16 |
| 19 | 20 | 19 | 20 | 70436.843(050) | −0.068 | 3.18E+04 | 34.96 | 1.01E+09 | 36.85 |
| 19 | 18 | 19 | 18 | 70436.843(050) | −0.075 | 2.87E+04 | 31.54 | 8.24E+08 | 29.99 |
| 20 | ← | 20 | | 77814.8607(0401) | | | | | |
| 20 | 20 | 20 | 20 | 77814.839(050) | 0.067 | 3.51E+04 | 33.17 | 1.23E+09 | 33.17 |
| 20 | 21 | 20 | 21 | 77814.839(050) | −0.059 | 3.69E+04 | 34.88 | 1.36E+09 | 36.67 |
| 20 | 19 | 20 | 19 | 77814.839(050) | −0.066 | 3.34E+04 | 31.63 | 1.12E+09 | 30.15 |
| 22 | ← | 22 | | 93654.2709(0556) | | | | | |
| 22 | 22 | 22 | 22 | 93654.257(050) | 0.074 | 4.63E+04 | 33.2 | 2.14E+09 | 33.2 |
| 22 | 23 | 22 | 23 | 93654.257(050) | −0.052 | 4.85E+04 | 34.75 | 2.35E+09 | 36.37 |
| 22 | 21 | 22 | 21 | 93654.257(050) | −0.058 | 4.43E+04 | 31.79 | 1.97E+09 | 30.43 |
| 23 | ← | 23 | | 102113.5228(0651) | | | | | |
| 23 | 22 | 23 | 22 | 102113.517(050) | −0.051 | 5.06E+04 | 31.85 | 2.56E+09 | 30.55 |
| 23 | 23 | 23 | 23 | 102113.517(050) | 0.081 | 5.27E+04 | 33.21 | 2.78E+09 | 33.21 |
| 23 | 24 | 23 | 24 | 102113.517(050) | −0.045 | 5.51E+04 | 34.69 | 3.03E+09 | 36.24 |
| 24 | ← | 24 | | 110930.9492(0759) | | | | | |
| 24 | 23 | 24 | 23 | 110930.983(050) | −0.013 | 5.74E+04 | 31.92 | 3.29E+09 | 30.66 |
| 24 | 24 | 24 | 24 | 110930.983(050) | 0.119 | 5.97E+04 | 33.22 | 3.57E+09 | 33.22 |
| 24 | 25 | 24 | 25 | 110930.983(050) | −0.007 | 6.23E+04 | 34.64 | 3.88E+09 | 36.11 |

## A.2 $D^{13}CN$

Table A.4: Rotational spectrum of $D^{13}CN$ in the vibrational ground state. For each transition a calculated hyperfine-free rotational frequency is given followed by the measured hyperfine lines. Please refer to the text as to which lines where measured in sub-Doppler and which in Doppler resolution. Intensities were calculated for the linear and saturation experiment in absolute (given is the dimensionless intrinsic line strength) and relative units.

| $J'$ | $F'$ | $J''$ | $F''$ | Frequency [MHz][a] | o.-c. | $I_{abs,lin}$ | $I_{rel,lin}$ | $I_{abs,sat}$ | $I_{rel,sat}$ |
|---|---|---|---|---|---|---|---|---|---|
| | | | | | [MHz] | | | | |
| 1 | ← | 0 | | 71175.0667(0002) | | | | | |
| 1 | 1 | 0 | 1 | 71173.890(010) | 0.001 | 1.00E+00 | 33.33 | 1.00E+00 | 25.71 |
| 1 | 2 | 0 | 1 | 71175.318(010) | 0.006 | 1.67E+00 | 55.56 | 2.78E+00 | 71.43 |
| 1 | 0 | 0 | 1 | 71177.411(010) | 0.008 | 3.33E-01 | 11.11 | 1.11E-01 | 2.86 |
| 2 | ← | 1 | | 142348.7996(0005) | | | | | |
| 2 | 2 | 1 | 2 | 142347.540(030)$f$ | 0.157 | 5.00E-01 | 8.33 | 2.50E-01 | 2.27 |
| 2 | 1 | 1 | 0 | 142347.540(030)$f$ | −0.085 | 6.67E-01 | 11.11 | 4.44E-01 | 4.03 |
| 2 | 2 | 1 | 1 | 142348.883(030)$f$ | 0.077 | 1.50E+00 | 25.00 | 2.25E+00 | 20.39 |
| 2 | 3 | 1 | 2 | 142348.883(030)$f$ | −0.031 | 2.80E+00 | 46.67 | 7.84E+00 | 71.04 |
| 2 | 1 | 1 | 1 | 142351.129(030)$f$ | −0.010 | 5.00E-01 | 8.33 | 2.50E-01 | 2.27 |

Table A.4: D$^{13}$CN $v_2 = 0$ transitions - continued

| $J'$ | $F'$ | $J''$ | $F''$ | Frequency [MHz][a] | o.-c. [MHz] | $I_{abs,lin}$ | $I_{rel,lin}$ | $I_{abs,sat}$ | $I_{rel,sat}$ |
|---|---|---|---|---|---|---|---|---|---|
| 3 | ← | 2 | | 213519.8648(0008) | | | | | |
| 3 | 3 | 2 | 3 | 213518.338(005) | −0.005 | 3.33E-01 | 3.70 | 1.11E-01 | 0.44 |
| 3 | 2 | 2 | 1 | 213519.622(005) | −0.010 | 1.80E+00 | 20.00 | 3.24E+00 | 12.73 |
| 3 | 3 | 2 | 2 | 213519.865(010) | −0.009 | 2.67E+00 | 29.63 | 7.11E+00 | 27.93 |
| 3 | 4 | 2 | 3 | 213519.936(005) | −0.001 | 3.86E+00 | 42.86 | 1.49E+01 | 58.43 |
| 3 | 2 | 2 | 2 | 213521.965(005) | −0.001 | 3.33E-01 | 3.70 | 1.11E-01 | 0.44 |
| 4 | ← | 3 | | 284686.9284(0011) | | | | | |
| 4 | 3 | 3 | 2 | 284686.822(005) | −0.011 | 2.86E+00 | 23.81 | 8.16E+00 | 17.64 |
| 4 | 4 | 3 | 3 | 284686.935(010) | −0.005 | 3.75E+00 | 31.25 | 1.41E+01 | 30.39 |
| 4 | 5 | 3 | 4 | 284686.977(005) | −0.007 | 4.89E+00 | 40.74 | 2.39E+01 | 51.66 |
| 5 | ← | 4 | | 355848.6571(0015) | | | | | |
| 5 | 5 | 4 | 5 | 355847.038(003) | 0.004 | 2.00E-01 | 1.33 | 4.00E-02 | 0.05 |
| 5 | 5/6 | 4 | 5/5 | 355847.858(005) | 0.003 | | | 4.07E-03 | 0.01 |
| 5 | 5/5 | 4 | 5/4 | 355847.858(005) | 0.003 | | | 4.11E-03 | 0.01 |
| 5 | 4 | 4 | 3 | 355848.612(005) | 0.002 | 3.89E+00 | 25.93 | 1.51E+01 | 20.66 |
| 5 | 5 | 4 | 4 | 355848.703(010) | 0.031 | 4.80E+00 | 32.00 | 2.30E+01 | 31.48 |
| 5 | 6 | 4 | 5 | 355848.703(010) | −0.001 | 5.91E+00 | 39.39 | 3.49E+01 | 47.71 |
| 5 | 4 | 4 | 4 | 355850.600(003) | 0.005 | 2.00E-01 | 1.33 | 4.00E-02 | 0.05 |
| 6 | ← | 5 | | 427003.7172(0020) | | | | | |
| 6 | 6 | 5 | 6 | 427002.064(005) | 0.000 | 1.67E-01 | 0.93 | 2.78E-02 | 0.03 |
| 6 | 6/7 | 5 | 6/6 | 427002.908(005) | 0.007 | | | 1.99E-02 | 0.02 |
| 6 | 6/6 | 5 | 6/5 | 427002.908(005) | 0.007 | | | 1.89E-02 | 0.02 |
| 6 | 5 | 5 | 4 | 427003.737(020) | 0.044 | 4.91E+00 | 27.27 | 2.41E+01 | 22.70 |
| 6 | 6 | 5 | 5 | 427003.737(020) | 0.003 | 5.83E+00 | 32.41 | 3.40E+01 | 32.05 |
| 6 | 7 | 5 | 6 | 427003.737(020) | −0.024 | 6.92E+00 | 38.46 | 4.79E+01 | 45.14 |
| 6 | 6/5 | 5 | 5/5 | 427004.675(020) | 0.009 | | | 6.50E-03 | 0.01 |
| 6 | 5/5 | 5 | 5/4 | 427004.675(020) | 0.009 | | | 4.38E-03 | 0.00 |
| 6 | 5 | 5 | 5 | 427005.616(005) | 0.000 | 1.67E-01 | 0.93 | 2.78E-02 | 0.03 |
| 7 | ← | 6 | | 498150.7756(0026) | | | | | |
| 7 | 7 | 6 | 7 | 498149.097(005) | −0.002 | 1.43E-01 | 0.68 | 2.04E-02 | 0.01 |
| 7 | 7/8 | 6 | 7/7 | 498149.953(010) | 0.005 | | | 5.30E-02 | 0.04 |
| 7 | 7/7 | 6 | 7/6 | 498149.953(010) | 0.005 | | | 4.95E-02 | 0.03 |
| 7 | 6 | 6 | 5 | 498150.799(010) | 0.034 | 5.92E+00 | 28.21 | 3.51E+01 | 24.15 |
| 7 | 7 | 6 | 6 | 498150.799(010) | 0.004 | 6.86E+00 | 32.65 | 4.70E+01 | 32.37 |
| 7 | 8 | 6 | 7 | 498150.799(010) | −0.019 | 7.93E+00 | 37.78 | 6.29E+01 | 43.33 |
| 7 | 7/6 | 6 | 6/6 | 498151.720(010) | 0.006 | | | 2.78E-02 | 0.02 |
| 7 | 6/6 | 6 | 6/5 | 498151.720(010) | 0.006 | | | 2.14E-02 | 0.01 |
| 7 | 6 | 6 | 6 | 498152.643(005) | −0.004 | 1.43E-01 | 0.68 | 2.04E-02 | 0.01 |
| 8 | ← | 7 | | 569288.4994(0033) | | | | | |
| 8 | 8 | 7 | 8 | 569286.800(005) | −0.003 | 1.25E-01 | 0.52 | 1.56E-02 | 0.01 |
| 8 | 8/9 | 7 | 8/8 | 569287.662(005) | −0.001 | | | 1.02E-01 | 0.05 |
| 8 | 8/8 | 7 | 8/7 | 569287.662(005) | −0.001 | | | 9.44E-02 | 0.05 |
| 8 | 7 | 7 | 6 | 569288.519(005) | 0.021 | 6.93E+00 | 28.89 | 4.81E+01 | 25.25 |
| 8 | 8 | 7 | 7 | 569288.519(005) | −0.003 | 7.88E+00 | 32.81 | 6.20E+01 | 32.57 |
| 8 | 9 | 7 | 8 | 569288.519(005) | −0.022 | 8.94E+00 | 37.25 | 7.99E+01 | 41.99 |
| 8 | 8/7 | 7 | 7/7 | 569289.435(005) | 0.005 | | | 6.90E-02 | 0.04 |
| 8 | 7/7 | 7 | 7/6 | 569289.435(005) | 0.005 | | | 5.67E-02 | 0.03 |
| 8 | 7 | 7 | 7 | 569290.339(005) | −0.010 | 1.25E-01 | 0.52 | 1.56E-02 | 0.01 |
| 9 | ← | 8 | | 640415.5559(0042) | | | | | |
| 9 | 9 | 8 | 9 | 640413.840(010) | −0.002 | 1.11E-01 | 0.41 | 1.23E-02 | 0.01 |
| 9 | 9/10 | 8 | 9/ 9 | 640414.713(005) | 0.001 | | | 1.60E-01 | 0.07 |
| 9 | 9/9 | 8 | 9/8 | 640414.713(005) | 0.001 | | | 1.49E-01 | 0.06 |
| 9 | 8 | 8 | 7 | 640415.587(005) | 0.026 | 7.94E+00 | 29.41 | 6.31E+01 | 26.10 |
| 9 | 9 | 8 | 8 | 640415.587(005) | 0.006 | 8.89E+00 | 32.92 | 7.90E+01 | 32.70 |
| 9 | 10 | 8 | 9 | 640415.587(005) | −0.011 | 9.95E+00 | 36.84 | 9.90E+01 | 40.96 |
| 9 | 9/8 | 8 | 8/8 | 640416.482(005) | 0.002 | | | 1.26E-01 | 0.05 |
| 9 | 8/8 | 8 | 8/7 | 640416.482(005) | 0.002 | | | 1.08E-01 | 0.04 |
| 9 | 8 | 8 | 8 | 640417.378(010) | −0.011 | 1.11E-01 | 0.41 | 1.23E-02 | 0.01 |
| 10 | ← | 9 | | 711530.6130(0053) | | | | | |
| 10 | 10/11 | 9 | 10/10 | 711529.756(020) | −0.007 | | | 2.22E-01 | 0.07 |

Table A.4: $D^{13}CN$ $v_2 = 0$ transitions - continued

| $J'$ | $F'$ | $J''$ | $F''$ | Frequency [MHz][a] | o.-c. [MHz] | $I_{abs,lin}$ | $I_{rel,lin}$ | $I_{abs,sat}$ | $I_{rel,sat}$ |
|---|---|---|---|---|---|---|---|---|---|
| 10 | 10/10 | 9 | 10/ 9 | 711529.756(020) | −0.007 | | | 2.07E-01 | 0.07 |
| 10 | 9 | 9 | 8 | 711530.641(005) | 0.017 | 8.95E+00 | 29.82 | 8.01E+01 | 26.79 |
| 10 | 10 | 9 | 9 | 711530.641(005) | 0.001 | 9.90E+00 | 33.00 | 9.80E+01 | 32.80 |
| 10 | 11 | 9 | 10 | 711530.641(005) | −0.015 | 1.10E+01 | 36.51 | 1.20E+02 | 40.14 |
| 10 | 9/10 | 9 | 9/ 9 | 711531.535(020) | 0.003 | | | 1.93E-01 | 0.06 |
| 10 | 9/9 | 9 | 9/8 | 711531.535(020) | 0.003 | | | 1.69E-01 | 0.06 |
| 11 | ← | 10 | | 782632.3387(0065) | | | | | |
| 11 | 11/12 | 10 | 11/11 | 782631.477(020) | −0.006 | | | 2.85E-01 | 0.08 |
| 11 | 11/11 | 10 | 11/10 | 782631.477(020) | −0.006 | | | 2.66E-01 | 0.07 |
| 11 | 10 | 10 | 9 | 782632.367(005) | 0.013 | 9.95E+00 | 30.16 | 9.90E+01 | 27.36 |
| 11 | 11 | 10 | 10 | 782632.367(005) | −0.001 | 1.09E+01 | 33.06 | 1.19E+02 | 32.87 |
| 11 | 12 | 10 | 11 | 782632.367(005) | −0.016 | 1.20E+01 | 36.23 | 1.43E+02 | 39.48 |
| 11 | 11/10 | 10 | 10/10 | 782633.249(020) | −0.004 | | | 2.62E-01 | 0.07 |
| 11 | 10/10 | 10 | 10/ 9 | 782633.249(020) | −0.004 | | | 2.34E-01 | 0.06 |
| 12 | ← | 11 | | 853719.4017(0081) | | | | | |
| 12 | 11 | 11 | 10 | 853719.433(020) | 0.013 | 1.10E+01 | 30.43 | 1.20E+02 | 27.83 |
| 12 | 12 | 11 | 11 | 853719.433(020) | 0.000 | 1.19E+01 | 33.10 | 1.42E+02 | 32.92 |
| 12 | 13 | 11 | 12 | 853719.433(020) | −0.014 | 1.30E+01 | 36.00 | 1.68E+02 | 38.94 |
| 13 | ← | 12 | | 924790.4711(0099) | | | | | |
| 13 | 12 | 12 | 11 | 924790.489(020) | −0.004 | 1.20E+01 | 30.67 | 1.43E+02 | 28.24 |
| 13 | 13 | 12 | 12 | 924790.489(020) | −0.015 | 1.29E+01 | 33.14 | 1.67E+02 | 32.97 |
| 13 | 14 | 12 | 13 | 924790.489(020) | −0.029 | 1.40E+01 | 35.80 | 1.95E+02 | 38.49 |
| 27 | ← | 26 | | 1917362.3932(1018) | | | | | |
| 27 | 27 | 26 | 27 | 1917362.532(100) | 2.057 | 3.70E-02 | 0.05 | 1.37E-03 | 0.00 |
| 27 | 26 | 26 | 25 | 1917362.532(100) | 0.079 | 2.60E+01 | 32.08 | 6.75E+02 | 30.85 |
| 27 | 27 | 26 | 26 | 1917362.532(100) | 0.075 | 2.70E+01 | 33.29 | 7.27E+02 | 33.22 |
| 27 | 28 | 26 | 27 | 1917362.532(100) | 0.062 | 2.80E+01 | 34.55 | 7.83E+02 | 35.78 |
| 27 | 26 | 26 | 26 | 1917362.532(100) | −1.593 | 3.70E-02 | 0.05 | 1.37E-03 | 0.00 |
| 28 | ← | 27 | | 1988034.3301(1169) | | | | | |
| 28 | 28 | 27 | 28 | 1988034.420(100) | 2.016 | 3.57E-02 | 0.04 | 1.28E-03 | 0.00 |
| 28 | 27 | 27 | 26 | 1988034.420(100) | 0.025 | 2.70E+01 | 32.12 | 7.28E+02 | 30.94 |
| 28 | 28 | 27 | 27 | 1988034.420(100) | 0.021 | 2.80E+01 | 33.29 | 7.82E+02 | 33.23 |
| 28 | 29 | 27 | 28 | 1988034.420(100) | 0.008 | 2.90E+01 | 34.50 | 8.40E+02 | 35.70 |
| 28 | 27 | 27 | 27 | 1988034.420(100) | −1.643 | 3.57E-02 | 0.04 | 1.28E-03 | 0.00 |

Table A.5: Rotational spectrum of $D^{13}CN$ in the first excited vibrational state $v_2 = 1^{e,f}$. For each transition a calculated hyperfine-free rotational frequency is given followed by the measured hyperfine lines. Please refer to the text as to which lines were measured in sub-Doppler and which in Doppler resolution. Intensities were calculated for the linear and saturation experiment in absolute (given is the dimensionless intrinsic line strength) and relative units.

| $J'$ | $F'$ | $J''$ | $F''$ | Frequency [MHz][a] | o.-c. [MHz] | $I_{abs,lin}$ | $I_{rel,lin}$ | $I_{abs,sat}$ | $I_{rel,sat}$ |
|---|---|---|---|---|---|---|---|---|---|
| 2 | ← | 1 | (e) | 142462.2686(0006) | | | | | |
| 2 | 2 | 1 | 1 | 142462.267(020)$g$ | 1.196 | 1.70E+01 | 12.5 | 2.80E+02 | 10.13 |
| 2 | 2 | 1 | 2 | 142462.267(020)$g$ | 0.443 | 5.60E+00 | 4.17 | 3.20E+01 | 1.13 |
| 2 | 1 | 1 | 1 | 142462.267(020)$g$ | 0.098 | 5.60E+00 | 4.17 | 3.20E+01 | 1.13 |
| 2 | 3 | 1 | 2 | 142462.267(020)$g$ | −0.292 | 3.20E+01 | 23.33 | 9.90E+02 | 35.31 |
| 2 | 1 | 1 | 0 | 142462.267(020)$g$ | −1.825 | 7.50E+00 | 5.56 | 5.60E+01 | 2 |
| 2 | ← | 1 | (f) | 143191.3791(0006) | | | | | |
| 2 | 2 | 1 | 1 | 143191.390(020)$g$ | 1.208 | 1.70E+01 | 12.5 | 2.80E+02 | 10.13 |
| 2 | 2 | 1 | 2 | 143191.390(020)$g$ | 0.555 | 5.60E+00 | 4.17 | 3.20E+01 | 1.13 |
| 2 | 1 | 1 | 1 | 143191.390(020)$g$ | −0.056 | 5.60E+00 | 4.17 | 3.20E+01 | 1.13 |
| 2 | 3 | 1 | 2 | 143191.390(020)$g$ | −0.287 | 3.20E+01 | 23.33 | 9.90E+02 | 35.31 |

Table A.5: $D^{13}CN$ $v_2 = 1$ transitions - continued

| $J'$ | $F'$ | $J''$ | $F''$ | Frequency [MHz][a] | o.-c. [MHz] | $I_{abs,lin}$ | $I_{rel,lin}$ | $I_{abs,sat}$ | $I_{rel,sat}$ |
|---|---|---|---|---|---|---|---|---|---|
| 2 | 1 | 1 | 0 | 143191.390(020)g | −1.73 | 7.50E+00 | 5.56 | 5.60E+01 | 2 |
| 3 | ← | 2 | (e) | 213690.0172(0009) | | | | | |
| 3 | 3 | 2 | 3 | 213688.977(010) | −0.002 | 1.00E+01 | 1.85 | 1.10E+02 | 0.22 |
| 3 | 3/ 3 | 2 | 3/ 2 | 213689.347(020) | 0.001 | | | 1.80E+00 | 0 |
| 3 | 3 | 2 | 2 | 213689.713(010) | −0.001 | 8.30E+01 | 14.81 | 6.90E+03 | 13.9 |
| 3 | 2 | 2 | 1 | 213690.145(010) | 0.011 | 5.60E+01 | 10 | 3.10E+03 | 6.33 |
| 3 | 4 | 2 | 3 | 213690.145(010) | −0.001 | 1.20E+02 | 21.43 | 1.40E+04 | 29.08 |
| 3 | 2 | 2 | 2 | 213691.234(010) | 0.003 | 1.00E+01 | 1.85 | 1.10E+02 | 0.22 |
| 3 | ← | 2 | (f) | 214783.5584(0009) | | | | | |
| 3 | 3 | 2 | 3 | 214782.412(010) | −0.001 | 1.00E+01 | 1.85 | 1.10E+02 | 0.22 |
| 3 | 3 | 2 | 2 | 214783.256(010) | 0.001 | 8.30E+01 | 14.81 | 6.90E+03 | 13.9 |
| 3 | 2 | 2 | 1 | 214783.683(010) | 0.024 | 5.60E+01 | 10 | 3.10E+03 | 6.33 |
| 3 | 4 | 2 | 3 | 214783.683(010) | −0.008 | 1.20E+02 | 21.43 | 1.40E+04 | 29.08 |
| 3 | 2 | 2 | 2 | 214784.925(010) | 0.002 | 1.00E+01 | 1.85 | 1.10E+02 | 0.22 |
| 4 | ← | 3 | (e) | 284913.7030(0013) | | | | | |
| 4 | 4 | 3 | 4 | 284912.411(005) | 0.001 | 1.50E+01 | 1.04 | 2.20E+02 | 0.07 |
| 4 | 4 | 3 | 3 | 284913.565(005) | −0.012 | 2.20E+02 | 15.62 | 4.90E+04 | 15.18 |
| 4 | 3 | 3 | 2 | 284913.699(005) | −0.004 | 1.70E+02 | 11.9 | 2.80E+04 | 8.81 |
| 4 | 5 | 3 | 4 | 284913.768(005) | −0.006 | 2.90E+02 | 20.37 | 8.30E+04 | 25.8 |
| 4 | 3 | 3 | 3 | 284915.221(005) | 0.001 | 1.50E+01 | 1.04 | 2.20E+02 | 0.07 |
| 4 | ← | 3 | (f) | 286371.5254(0013) | | | | | |
| 4 | 4 | 3 | 4 | 286370.117(005) | −0.005 | 1.50E+01 | 1.04 | 2.20E+02 | 0.07 |
| 4 | 4 | 3 | 3 | 286371.385(005) | −0.015 | 2.20E+02 | 15.62 | 4.90E+04 | 15.18 |
| 4 | 3 | 3 | 2 | 286371.513(005) | −0.005 | 1.70E+02 | 11.9 | 2.80E+04 | 8.81 |
| 4 | 5 | 3 | 4 | 286371.591(005) | −0.008 | 2.90E+02 | 20.37 | 8.30E+04 | 25.8 |
| 4 | 3 | 3 | 3 | 286373.179(005) | −0.007 | 1.50E+01 | 1.04 | 2.20E+02 | 0.07 |
| 5 | ← | 4 | (e) | 356131.9719(0018) | | | | | |
| 5 | 5 | 4 | 5 | 356130.537(003) | −0.003 | 1.90E+01 | 0.67 | 3.60E+02 | 0.03 |
| 5 | 5/ 6 | 4 | 5/ 5 | 356131.239(100) | −0.014 | | | 1.40E+01 | 0 |
| 5 | 5/ 5 | 4 | 5/ 4 | 356131.239(100) | −0.014 | | | 2.60E+01 | 0 |
| 5 | 5 | 4 | 4 | 356131.906(020) | 0.002 | 4.60E+02 | 16 | 2.10E+05 | 15.73 |
| 5 | 4 | 4 | 3 | 356131.906(020) | −0.045 | 3.70E+02 | 12.96 | 1.40E+05 | 10.32 |
| 5 | 6 | 4 | 5 | 356131.990(020) | −0.025 | 5.60E+02 | 19.7 | 3.20E+05 | 23.83 |
| 5 | 5/ 4 | 4 | 4/ 4 | 356132.752(005) | −0.008 | | | 1.20E+00 | 0 |
| 5 | 4/ 4 | 4 | 4/ 3 | 356132.752(005) | −0.008 | | | 1.30E+00 | 0 |
| 5 | 4 | 4 | 4 | 356133.587(003) | −0.007 | 1.90E+01 | 0.67 | 3.60E+02 | 0.03 |
| 5 | ← | 4 | (f) | 357953.8766(0018) | | | | | |
| 5 | 5 | 4 | 5 | 357952.340(003) | 0.008 | 1.90E+01 | 0.67 | 3.60E+02 | 0.03 |
| 5 | 5/ 6 | 4 | 5/ 5 | 357953.106(005) | 0.004 | | | 4.50E+02 | 0.03 |
| 5 | 5/ 5 | 4 | 5/ 4 | 357953.106(005) | 0.004 | | | 6.10E+02 | 0.05 |
| 5 | 5 | 4 | 4 | 357953.847(020) | 0.038 | 4.60E+02 | 16 | 2.10E+05 | 15.73 |
| 5 | 4 | 4 | 3 | 357953.847(020) | −0.006 | 3.70E+02 | 12.96 | 1.40E+05 | 10.32 |
| 5 | 6 | 4 | 5 | 357953.925(020) | 0.003 | 5.60E+02 | 19.7 | 3.20E+05 | 23.83 |
| 5 | 5/ 4 | 4 | 4/ 4 | 357954.733(005) | 0 | | | 1.40E+02 | 0.01 |
| 5 | 4/ 4 | 4 | 4/ 3 | 357954.733(005) | 0 | | | 1.60E+02 | 0.01 |
| 5 | 4 | 4 | 4 | 357955.643(003) | 0.005 | 1.90E+01 | 0.67 | 3.60E+02 | 0.03 |
| 6 | ← | 5 | (e) | 427343.4702(0023) | | | | | |
| 6 | 6 | 5 | 6 | 427341.952(005) | 0 | 2.30E+01 | 0.46 | 5.40E+02 | 0.01 |
| 6 | 6/ 7 | 5 | 6/ 6 | 427342.707(005) | −0.001 | | | 1.50E+02 | 0 |
| 6 | 6/ 6 | 5 | 6/ 5 | 427342.707(005) | −0.001 | | | 1.90E+02 | 0 |
| 6 | 6 | 5 | 5 | 427343.448(020) | 0.022 | 8.10E+02 | 16.2 | 6.60E+05 | 16.01 |
| 6 | 5 | 5 | 4 | 427343.448(020) | 0.003 | 6.80E+02 | 13.64 | 4.70E+05 | 11.34 |
| 6 | 7 | 5 | 6 | 427343.505(020) | 0.007 | 9.60E+02 | 19.23 | 9.30E+05 | 22.55 |
| 6 | 6/ 5 | 5 | 5/ 5 | 427344.293(005) | 0.008 | | | 3.60E+01 | 0 |
| 6 | 5/ 5 | 5 | 5/ 4 | 427344.293(005) | 0.008 | | | 3.20E+01 | 0 |
| 6 | 5 | 5 | 5 | 427345.135(005) | 0 | 2.30E+01 | 0.46 | 5.40E+02 | 0.01 |
| 6 | ← | 5 | (f) | 429529.2085(0023) | | | | | |
| 6 | 6 | 5 | 6 | 429527.580(005) | 0.005 | 2.30E+01 | 0.46 | 5.40E+02 | 0.01 |
| 6 | 6/ 7 | 5 | 6/ 6 | 429528.389(005) | −0.001 | | | 1.90E+03 | 0.05 |

Table A.5: $D^{13}CN$ $v_2 = 1$ transitions - continued

| $J'$ | $F'$ | $J''$ | $F''$ | Frequency [MHz][a] | o.-c. [MHz] | $I_{abs,lin}$ | $I_{rel,lin}$ | $I_{abs,sat}$ | $I_{rel,sat}$ |
|---|---|---|---|---|---|---|---|---|---|
| 6 | 6/ 6 | 5 | 6/ 5 | 429528.389(005) | −0.001 | | | 2.10E+03 | 0.05 |
| 6 | 6 | 5 | 5 | 429529.182(020) | 0.017 | 8.10E+02 | 16.2 | 6.60E+05 | 16.01 |
| 6 | 5 | 5 | 4 | 429529.182(020) | 0.001 | 6.80E+02 | 13.64 | 4.70E+05 | 11.34 |
| 6 | 7 | 5 | 6 | 429529.237(020) | −0.001 | 9.60E+02 | 19.23 | 9.30E+05 | 22.55 |
| 6 | 6/ 5 | 5 | 5/ 5 | 429530.100(005) | 0.009 | | | 9.90E+02 | 0.02 |
| 6 | 5/ 5 | 5 | 5/ 4 | 429530.100(005) | 0.009 | | | 9.20E+02 | 0.02 |
| 6 | 5 | 5 | 5 | 429531.017(005) | 0.007 | 2.30E+01 | 0.46 | 5.40E+02 | 0.01 |
| 7 | ← | 6 | (e) | 498546.8441(0030) | | | | | |
| 7 | 7 | 6 | 6 | 498546.835(010) | 0.024 | 1.30E+03 | 16.33 | 1.70E+06 | 16.17 |
| 7 | 6 | 6 | 5 | 498546.835(010) | 0.018 | 1.10E+03 | 14.1 | 1.30E+06 | 12.06 |
| 7 | 8 | 6 | 7 | 498546.835(010) | −0.027 | 1.50E+03 | 18.89 | 2.30E+06 | 21.64 |
| 7 | ← | 6 | (f) | 501096.1179(0030) | | | | | |
| 7 | 7 | 6 | 6 | 501096.095(020) | 0.009 | 1.30E+03 | 16.33 | 1.70E+06 | 16.17 |
| 7 | 6 | 6 | 5 | 501096.095(020) | 0.005 | 1.10E+03 | 14.1 | 1.30E+06 | 12.06 |
| 7 | 8 | 6 | 7 | 501096.149(020) | 0.012 | 1.50E+03 | 18.89 | 2.30E+06 | 21.64 |
| 8 | 8/ 9 | 7 | 8/ 8 | 569739.916(005) | −0.008 | | | 3.10E+03 | 0.01 |
| 8 | 8/ 8 | 7 | 8/ 7 | 569739.916(005) | −0.008 | | | 3.10E+03 | 0.01 |
| 8 | ← | 7 | (e) | 569740.7404(0038) | | | | | |
| 8 | 8 | 7 | 7 | 569740.729(010) | 0.016 | 2.00E+03 | 16.41 | 3.90E+06 | 16.27 |
| 8 | 7 | 7 | 6 | 569740.729(010) | 0.016 | 1.70E+03 | 14.44 | 3.00E+06 | 12.61 |
| 8 | 9 | 7 | 8 | 569740.729(010) | −0.022 | 2.20E+03 | 18.63 | 5.00E+06 | 20.98 |
| 8 | 8/ 7 | 7 | 7/ 7 | 569741.580(005) | 0.01 | | | 1.80E+03 | 0.01 |
| 8 | 7/ 7 | 7 | 7/ 6 | 569741.580(005) | 0.01 | | | 1.60E+03 | 0.01 |
| 8 | ← | 7 | (f) | 572653.2024(0038) | | | | | |
| 8 | 8 | 7 | 8 | 572651.460(020) | −0.001 | 3.10E+01 | 0.26 | 9.80E+02 | 0 |
| 8 | 8/ 9 | 7 | 8/ 8 | 572652.327(005) | −0.001 | | | 1.50E+04 | 0.06 |
| 8 | 8/ 8 | 7 | 8/ 7 | 572652.327(005) | −0.001 | | | 1.40E+04 | 0.06 |
| 8 | 8 | 7 | 7 | 572653.200(010) | 0.025 | 2.00E+03 | 16.41 | 3.90E+06 | 16.27 |
| 8 | 7 | 7 | 6 | 572653.200(010) | 0.026 | 1.70E+03 | 14.44 | 3.00E+06 | 12.61 |
| 8 | 9 | 7 | 8 | 572653.200(010) | −0.015 | 2.20E+03 | 18.63 | 5.00E+06 | 20.98 |
| 8 | 8/ 7 | 7 | 7/ 7 | 572654.109(005) | 0.01 | | | 1.20E+04 | 0.05 |
| 8 | 7/ 7 | 7 | 7/ 6 | 572654.109(005) | 0.01 | | | 1.00E+04 | 0.04 |
| 8 | 7 | 7 | 7 | 572655.022(020) | −0.002 | 3.10E+01 | 0.26 | 9.80E+02 | 0 |
| 9 | ← | 8 | (e) | 640923.8060(0047) | | | | | |
| 9 | 9 | 8 | 9 | 640922.143(010) | −0.002 | 3.50E+01 | 0.21 | 1.30E+03 | 0 |
| 9 | 9/10 | 8 | 9/ 9 | 640922.968(005) | −0.003 | | | 8.90E+03 | 0.02 |
| 9 | 9/ 9 | 8 | 9/ 8 | 640922.968(005) | −0.003 | | | 8.60E+03 | 0.02 |
| 9 | 9 | 8 | 8 | 640923.795(010) | 0.015 | 2.80E+03 | 16.46 | 8.00E+06 | 16.34 |
| 9 | 8 | 8 | 7 | 640923.795(010) | 0.017 | 2.50E+03 | 14.71 | 6.40E+06 | 13.04 |
| 9 | 10 | 8 | 9 | 640923.795(010) | −0.016 | 3.20E+03 | 18.42 | 1.00E+07 | 20.47 |
| 9 | 9/ 8 | 8 | 8/ 8 | 640924.640(005) | 0.004 | | | 6.30E+03 | 0.01 |
| 9 | 8/ 8 | 8 | 8/ 7 | 640924.640(005) | 0.004 | | | 5.60E+03 | 0.01 |
| 9 | 8 | 8 | 8 | 640925.484(010) | −0.009 | 3.50E+01 | 0.21 | 1.30E+03 | 0 |
| 9 | ← | 8 | (f) | 644199.0598(0047) | | | | | |
| 9 | 9 | 8 | 9 | 644197.277(005) | −0.004 | 3.50E+01 | 0.21 | 1.30E+03 | 0 |
| 9 | 9/10 | 8 | 9/ 9 | 644198.165(005) | −0.001 | | | 3.10E+04 | 0.06 |
| 9 | 9/ 9 | 8 | 9/ 8 | 644198.165(005) | −0.001 | | | 2.90E+04 | 0.06 |
| 9 | 9 | 8 | 8 | 644199.053(010) | 0.018 | 2.80E+03 | 16.46 | 8.00E+06 | 16.34 |
| 9 | 8 | 8 | 7 | 644199.053(010) | 0.022 | 2.50E+03 | 14.71 | 6.40E+06 | 13.04 |
| 9 | 10 | 8 | 9 | 644199.053(010) | −0.013 | 3.20E+03 | 18.42 | 1.00E+07 | 20.47 |
| 9 | 9/ 8 | 8 | 8/ 8 | 644199.960(005) | 0.003 | | | 2.70E+04 | 0.05 |
| 9 | 8/ 8 | 8 | 8/ 7 | 644199.960(005) | 0.003 | | | 2.40E+04 | 0.05 |
| 9 | 8 | 8 | 8 | 644200.870(005) | −0.01 | 3.50E+01 | 0.21 | 1.30E+03 | 0 |
| 10 | ← | 9 | (e) | 712094.6883(0058) | | | | | |
| 10 | 10/11 | 9 | 10/10 | 712093.833(020) | −0.004 | | | 2.10E+04 | 0.02 |
| 10 | 10/10 | 9 | 10/ 9 | 712093.833(020) | −0.004 | | | 2.00E+04 | 0.02 |
| 10 | 10 | 9 | 9 | 712094.682(005) | 0.019 | 3.90E+03 | 16.5 | 1.50E+07 | 16.39 |
| 10 | 9 | 9 | 8 | 712094.682(005) | 0.023 | 3.50E+03 | 14.91 | 1.20E+07 | 13.39 |
| 10 | 11 | 9 | 10 | 712094.682(005) | −0.007 | 4.30E+03 | 18.25 | 1.90E+07 | 20.06 |
| 10 | 10/ 9 | 9 | 9/ 9 | 712095.518(020) | 0.001 | | | 1.70E+04 | 0.02 |

Table A.5: D$^{13}$CN $v_2 = 1$ transitions - continued

| $J'$ | $F'$ | $J''$ | $F''$ | Frequency [MHz][a] | o.-c. [MHz] | $I_{abs,lin}$ | $I_{rel,lin}$ | $I_{abs,sat}$ | $I_{rel,sat}$ |
|---|---|---|---|---|---|---|---|---|---|
| 10 | 9/ 9 | 9 | 9/ 8 | 712095.518(020) | 0.001 | | | 1.50E+04 | 0.02 |
| 10 | ← | 9 | (f) | 715732.2887(0058) | | | | | |
| 10 | 10/11 | 9 | 10/10 | 715731.370(020) | −0.008 | | | 5.80E+04 | 0.06 |
| 10 | 10/10 | 9 | 10/ 9 | 715731.370(020) | −0.008 | | | 5.50E+04 | 0.06 |
| 10 | 10 | 9 | 9 | 715732.272(005) | 0.008 | 3.90E+03 | 16.5 | 1.50E+07 | 16.39 |
| 10 | 9 | 9 | 8 | 715732.272(005) | 0.013 | 3.50E+03 | 14.91 | 1.20E+07 | 13.39 |
| 10 | 11 | 9 | 10 | 715732.272(005) | −0.018 | 4.30E+03 | 18.25 | 1.90E+07 | 20.06 |
| 10 | 10/ 9 | 9 | 9/ 9 | 715733.175(020) | −0.008 | | | 5.30E+04 | 0.06 |
| 10 | 9/ 9 | 9 | 9/ 8 | 715733.175(020) | −0.008 | | | 4.80E+04 | 0.05 |
| 11 | ← | 10 | (e) | 783252.0351(0072) | | | | | |
| 11 | 11/12 | 10 | 11/11 | 783251.157(020) | −0.012 | | | 4.20E+04 | 0.03 |
| 11 | 11/11 | 10 | 11/10 | 783251.157(020) | −0.012 | | | 4.00E+04 | 0.02 |
| 11 | 10 | 10 | 9 | 783252.022(005) | 0.017 | 4.80E+03 | 15.08 | 2.30E+07 | 13.67 |
| 11 | 11 | 10 | 10 | 783252.022(005) | 0.013 | 5.20E+03 | 16.53 | 2.70E+07 | 16.43 |
| 11 | 12 | 10 | 11 | 783252.022(005) | −0.01 | 5.70E+03 | 18.12 | 3.30E+07 | 19.74 |
| 11 | 11/10 | 10 | 10/10 | 783252.858(020) | −0.002 | | | 3.60E+04 | 0.02 |
| 11 | 10/10 | 10 | 10/ 9 | 783252.858(020) | −0.002 | | | 3.30E+04 | 0.02 |
| 11 | 11/12 | 10 | 11/11 | 787250.560(030) | −0.003 | | | 1.00E+05 | 0.06 |
| 11 | 11/11 | 10 | 11/10 | 787250.560(030) | −0.003 | | | 9.30E+04 | 0.06 |
| 11 | ← | 10 | (f) | 787251.4880(0072) | | | | | |
| 11 | 10 | 10 | 9 | 787251.468(005) | 0.011 | 4.80E+03 | 15.08 | 2.30E+07 | 13.67 |
| 11 | 11 | 10 | 10 | 787251.468(005) | 0.005 | 5.20E+03 | 16.53 | 2.70E+07 | 16.43 |
| 11 | 12 | 10 | 11 | 787251.468(005) | −0.018 | 5.70E+03 | 18.12 | 3.30E+07 | 19.74 |
| 11 | 11/10 | 10 | 10/10 | 787252.370(030) | −0.009 | | | 9.40E+04 | 0.06 |
| 11 | 10/10 | 10 | 10/ 9 | 787252.370(030) | −0.009 | | | 8.60E+04 | 0.05 |
| 12 | ← | 11 | (e) | 854394.4945(0088) | | | | | |
| 12 | 11 | 11 | 10 | 854394.463(010) | 0 | 6.30E+03 | 15.22 | 3.90E+07 | 13.91 |
| 12 | 12 | 11 | 11 | 854394.463(010) | −0.005 | 6.80E+03 | 16.55 | 4.60E+07 | 16.46 |
| 12 | 13 | 11 | 12 | 854394.463(010) | −0.025 | 7.40E+03 | 18 | 5.50E+07 | 19.47 |
| 12 | ← | 11 | (f) | 858755.2578(0088) | | | | | |
| 12 | 11 | 11 | 10 | 858755.234(010) | 0.009 | 6.30E+03 | 15.22 | 3.90E+07 | 13.91 |
| 12 | 12 | 11 | 11 | 858755.234(010) | 0.003 | 6.80E+03 | 16.55 | 4.60E+07 | 16.46 |
| 12 | 13 | 11 | 12 | 858755.234(010) | −0.018 | 7.40E+03 | 18 | 5.50E+07 | 19.47 |
| 13 | ← | 12 | (e) | 925520.7154(0107) | | | | | |
| 13 | 12 | 12 | 11 | 925520.688(010) | 0.006 | 8.00E+03 | 15.33 | 6.40E+07 | 14.12 |
| 13 | 13 | 12 | 12 | 925520.688(010) | 0.001 | 8.70E+03 | 16.57 | 7.50E+07 | 16.48 |
| 13 | 14 | 12 | 13 | 925520.688(010) | −0.017 | 9.40E+03 | 17.9 | 8.80E+07 | 19.24 |
| 13 | ← | 12 | (f) | 930242.1988(0107) | | | | | |
| 13 | 12 | 12 | 11 | 930242.166(010) | 0.001 | 8.00E+03 | 15.33 | 6.40E+07 | 14.12 |
| 13 | 13 | 12 | 12 | 930242.166(010) | −0.004 | 8.70E+03 | 16.57 | 7.50E+07 | 16.48 |
| 13 | 14 | 12 | 13 | 930242.166(010) | −0.023 | 9.40E+03 | 17.9 | 8.80E+07 | 19.24 |
| 27 | ← | 26 | (e) | 1918827.6872(1076) | | | | | |
| 27 | 27 | 26 | 27 | 1918827.613(100) | 1.916 | 1.10E+02 | 0.02 | 1.20E+04 | 0 |
| 27 | 26 | 26 | 25 | 1918827.613(100) | −0.019 | 7.60E+04 | 16.04 | 5.70E+09 | 15.42 |
| 27 | 27 | 26 | 26 | 1918827.613(100) | −0.022 | 7.80E+04 | 16.64 | 6.20E+09 | 16.61 |
| 27 | 28 | 26 | 27 | 1918827.613(100) | −0.035 | 8.10E+04 | 17.27 | 6.60E+09 | 17.89 |
| 27 | 26 | 26 | 26 | 1918827.613(100) | −1.656 | 1.10E+02 | 0.02 | 1.20E+04 | 0 |
| 27 | ← | 26 | (f) | 1928511.2862(1076) | | | | | |
| 27 | 27 | 26 | 27 | 1928511.208(050) | 2.042 | 1.10E+02 | 0.02 | 1.20E+04 | 0 |
| 27 | 26 | 26 | 25 | 1928511.208(050) | −0.016 | 7.60E+04 | 16.04 | 5.70E+09 | 15.42 |
| 27 | 27 | 26 | 26 | 1928511.208(050) | −0.019 | 7.80E+04 | 16.64 | 6.20E+09 | 16.61 |
| 27 | 28 | 26 | 27 | 1928511.208(050) | −0.032 | 8.10E+04 | 17.27 | 6.60E+09 | 17.89 |
| 27 | 26 | 26 | 26 | 1928511.208(050) | −1.78 | 1.10E+02 | 0.02 | 1.20E+04 | 0 |
| 28 | ← | 27 | (e) | 1989548.6727(1235) | | | | | |
| 28 | 28 | 27 | 28 | 1989548.549(100) | 1.879 | 1.10E+02 | 0.02 | 1.30E+04 | 0 |
| 28 | 27 | 27 | 26 | 1989548.549(100) | −0.07 | 8.40E+04 | 16.06 | 7.10E+09 | 15.47 |
| 28 | 28 | 27 | 27 | 1989548.549(100) | −0.072 | 8.80E+04 | 16.65 | 7.70E+09 | 16.62 |

Table A.5: $D^{13}CN$ $v_2 = 1$ transitions - continued

| $J'$ | $F'$ | $J''$ | $F''$ | Frequency [MHz][a] | o.-c. [MHz] | $I_{abs,lin}$ | $I_{rel,lin}$ | $I_{abs,sat}$ | $I_{rel,sat}$ |
|---|---|---|---|---|---|---|---|---|---|
| 28 | 29 | 27 | 28 | 1989548.549(100) | −0.086 | 9.10E+04 | 17.25 | 8.20E+09 | 17.85 |
| 28 | 27 | 27 | 27 | 1989548.549(100) | −1.704 | 1.10E+02 | 0.02 | 1.30E+04 | 0 |
| | | | | | | | | | |
| 28 | ← | 27 | (f) | 1999578.6528(1235) | | | | | |
| 28 | 28 | 27 | 28 | 1999578.690(100) | 2.17 | 1.10E+02 | 0.02 | 1.30E+04 | 0 |
| 28 | 27 | 27 | 26 | 1999578.690(100) | 0.099 | 8.40E+04 | 16.06 | 7.10E+09 | 15.47 |
| 28 | 28 | 27 | 27 | 1999578.690(100) | 0.096 | 8.80E+04 | 16.65 | 7.70E+09 | 16.62 |
| 28 | 29 | 27 | 28 | 1999578.690(100) | 0.083 | 9.10E+04 | 17.25 | 8.20E+09 | 17.85 |
| 28 | 27 | 27 | 27 | 1999578.690(100) | −1.663 | 1.10E+02 | 0.02 | 1.30E+04 | 0 |

Table A.6: Table of the experimental direct $\ell$-type transitions in the first excited bending state of $D^{13}CN$ used in the fit. For each transition a calculated hyperfine-free rotational frequency is given followed by the measured hyperfine lines. Please note that the hyperfine structure has not been resolved experimentally. Intensities were calculated for the linear and saturation experiment in absolute (given is the dimensionless intrinsic line strength) and relative units.

| $J'$ | $F'$ | $J''$ | $F''$ | Frequency [MHz][a] | o.-c. | $I_{abs,lin}$ | $I_{rel,lin}$ | $I_{abs,sat}$ | $I_{rel,sat}$ |
|---|---|---|---|---|---|---|---|---|---|
| $\ell = 1^f$ | | $\ell = 1^e$ | | | [MHz] | | | | |
| 6 | ← | 6 | | 7652.6973(0000) | | | | | |
| 6 | 5 | 6 | 5 | 7652.700(050)$d$ | −0.053 | 9.50E+02 | 27.42 | 9.10E+05 | 23.62 |
| 6 | 6 | 6 | 6 | 7652.700(050)$d$ | 0.084 | 1.10E+03 | 31.76 | 1.20E+06 | 31.70 |
| 6 | 7 | 6 | 7 | 7652.700(050)$d$ | −0.033 | 1.30E+03 | 37.68 | 1.70E+06 | 44.60 |
| | | | | | | | | | |
| 7 | ← | 7 | | 10201.9712(0000) | | | | | |
| 7 | 6 | 7 | 6 | 10201.950(050)$d$ | −0.075 | 1.50E+03 | 28.30 | 2.30E+06 | 24.88 |
| 7 | 7 | 7 | 7 | 10201.950(050)$d$ | 0.059 | 1.70E+03 | 32.15 | 2.90E+06 | 32.12 |
| 7 | 8 | 7 | 8 | 10201.950(050)$d$ | −0.058 | 2.00E+03 | 37.19 | 3.90E+06 | 42.96 |
| | | | | | | | | | |
| 8 | ← | 8 | | 13114.4332(0000) | | | | | |
| 8 | 8 | 8 | 8 | 13114.350(100)$d$ | −0.003 | 2.50E+03 | 32.41 | 6.20E+06 | 32.39 |
| 8 | 9 | 8 | 9 | 13114.350(100)$d$ | −0.122 | 2.80E+03 | 36.79 | 8.00E+06 | 41.74 |
| 8 | 9 | 8 | 8 | 13116.350(100)$d$ | 0.243 | 3.50E+01 | 0.46 | 1.30E+03 | 0.01 |
| | | | | | | | | | |
| 9 | ← | 9 | | 16389.6871(0000) | | | | | |
| 9 | 8 | 9 | 8 | 16389.630(100)$d$ | −0.110 | 3.20E+03 | 29.46 | 1.00E+07 | 26.61 |
| 9 | 9 | 9 | 9 | 16389.630(100)$d$ | 0.022 | 3.50E+03 | 32.60 | 1.20E+07 | 32.58 |
| 9 | 10 | 9 | 10 | 16389.630(100)$d$ | −0.097 | 3.90E+03 | 36.47 | 1.50E+07 | 40.79 |
| | | | | | | | | | |
| 10 | ← | 10 | | 20027.2875(0000) | | | | | |
| 10 | 9 | 10 | 9 | 20027.100(100)$d$ | −0.240 | 4.30E+03 | 29.86 | 1.90E+07 | 27.23 |
| 10 | 10 | 10 | 10 | 20027.100(100)$d$ | −0.109 | 4.70E+03 | 32.73 | 2.20E+07 | 32.72 |
| 10 | 11 | 10 | 11 | 20027.100(100)$d$ | −0.228 | 5.20E+03 | 36.21 | 2.70E+07 | 40.04 |
| | | | | | | | | | |
| 11 | ← | 11 | | 24026.7404(0000) | | | | | |
| 11 | 10 | 11 | 10 | 24026.600(100)$d$ | −0.193 | 5.70E+03 | 30.18 | 3.30E+07 | 27.74 |
| 11 | 11 | 11 | 11 | 24026.600(100)$d$ | −0.062 | 6.20E+03 | 32.83 | 3.90E+07 | 32.82 |
| 11 | 12 | 11 | 12 | 24026.600(100)$d$ | −0.182 | 6.80E+03 | 35.98 | 4.60E+07 | 39.42 |
| | | | | | | | | | |
| 19 | ← | 19 | | 68973.9808(0000) | | | | | |
| 19 | 18 | 19 | 18 | 68973.949(050) | −0.073 | 2.90E+04 | 31.54 | 8.20E+08 | 29.99 |
| 19 | 19 | 19 | 19 | 68973.949(050) | 0.056 | 3.00E+04 | 33.16 | 9.10E+08 | 33.16 |
| 19 | 20 | 19 | 20 | 68973.949(050) | −0.066 | 3.20E+04 | 34.96 | 1.00E+09 | 36.85 |
| | | | | | | | | | |
| 20 | ← | 20 | | 76200.0127(0000) | | | | | |
| 20 | 19 | 20 | 19 | 76199.970(050) | −0.080 | 3.30E+04 | 31.63 | 1.10E+09 | 30.15 |
| 20 | 20 | 20 | 20 | 76199.970(050) | 0.048 | 3.50E+04 | 33.17 | 1.20E+09 | 33.17 |
| 20 | 21 | 20 | 21 | 76199.970(050) | −0.074 | 3.70E+04 | 34.88 | 1.40E+09 | 36.67 |
| | | | | | | | | | |
| 21 | ← | 21 | | 83780.3561(0000) | | | | | |
| 21 | 20 | 21 | 20 | 83780.316(050) | −0.074 | 3.90E+04 | 31.71 | 1.50E+09 | 30.30 |

Table A.6: $D^{13}CN$ direct $\ell$-type transitions - continued

| $J'$ | $F'$ | $J''$ | $F''$ | Frequency [MHz][a] | o.-c. | $I_{abs,lin}$ | $I_{rel,lin}$ | $I_{abs,sat}$ | $I_{rel,sat}$ |
|---|---|---|---|---|---|---|---|---|---|
| $\ell = 1^f$ | | $\ell = 1^e$ | | | [MHz] | | | | |
| 21 | 21 | 21 | 21 | 83780.316(050) | 0.054 | 4.00E+04 | 33.19 | 1.60E+09 | 33.19 |
| 21 | 22 | 21 | 22 | 83780.316(050) | −0.068 | 4.20E+04 | 34.81 | 1.80E+09 | 36.51 |
| | | | | | | | | | |
| 22 | ← | 22 | | 91714.0059(0000) | | | | | |
| 22 | 21 | 22 | 21 | 91713.964(050) | −0.071 | 4.40E+04 | 31.79 | 2.00E+09 | 30.43 |
| 22 | 22 | 22 | 22 | 91713.964(050) | 0.057 | 4.60E+04 | 33.20 | 2.10E+09 | 33.20 |
| 22 | 23 | 22 | 23 | 91713.964(050) | −0.066 | 4.80E+04 | 34.75 | 2.30E+09 | 36.37 |
| | | | | | | | | | |
| 23 | ← | 23 | | 99999.9134(0000) | | | | | |
| 23 | 22 | 23 | 22 | 99999.891(050) | −0.047 | 5.10E+04 | 31.85 | 2.60E+09 | 30.55 |
| 23 | 23 | 23 | 23 | 99999.891(050) | 0.081 | 5.30E+04 | 33.21 | 2.80E+09 | 33.21 |
| 23 | 24 | 23 | 24 | 99999.891(050) | −0.041 | 5.50E+04 | 34.69 | 3.00E+09 | 36.24 |
| | | | | | | | | | |
| 24 | ← | 24 | | 108636.9868(0000) | | | | | |
| 24 | 23 | 24 | 23 | 108636.966(050) | −0.040 | 5.70E+04 | 31.92 | 3.30E+09 | 30.66 |
| 24 | 24 | 24 | 24 | 108636.966(050) | 0.088 | 6.00E+04 | 33.22 | 3.60E+09 | 33.22 |
| 24 | 25 | 24 | 25 | 108636.966(050) | −0.034 | 6.20E+04 | 34.64 | 3.90E+09 | 36.11 |
| | | | | | | | | | |
| 25 | ← | 25 | | 117624.0917(0000) | | | | | |
| 25 | 24 | 25 | 24 | 117624.122(050) | 0.018 | 6.50E+04 | 31.97 | 4.20E+09 | 30.77 |
| 25 | 25 | 25 | 25 | 117624.122(050) | 0.145 | 6.70E+04 | 33.23 | 4.50E+09 | 33.23 |
| 25 | 26 | 25 | 26 | 117624.122(050) | 0.022 | 7.00E+04 | 34.59 | 4.90E+09 | 36.00 |

## A.3 $DC^{15}N$

Table A.7: Rotational spectrum of $DC^{15}N$ in the vibrational ground state (000). Please refer to the text as to which lines were measured in sub-Doppler and which in Doppler resolution.

| $J'$ | $J''$ | Frequency [MHz] | $\Delta\nu$ [MHz] | o.-c. [MHz] |
|---|---|---|---|---|
| 1 | 0 | 70339.382 | 0.010 | 0.004 |
| 2 | 1 | 140677.458$g$ | 0.020 | 0.007 |
| 3 | 2 | 211012.913 | 0.010 | 0.000 |
| 4 | 3 | 281344.465 | 0.010 | 0.006 |
| 5 | 4 | 351670.782 | 0.003 | −0.002 |
| 6 | 5 | 421990.583 | 0.005 | 0.000 |
| 7 | 6 | 492302.551 | 0.005 | 0.000 |
| 9 | 8 | 632897.780 | 0.005 | 0.003 |
| 10 | 9 | 703178.425 | 0.005 | −0.002 |
| 11 | 10 | 773446.033 | 0.005 | 0.003 |
| 12 | 11 | 843699.279 | 0.010 | −0.005 |
| 13 | 12 | 913936.884 | 0.010 | −0.003 |
| 25 | 24 | 1755094.147 | 0.100 | 0.064 |
| 26 | 25 | 1825009.987 | 0.050 | −0.017 |
| 27 | 26 | 1894892.090 | 0.050 | −0.029 |
| 28 | 27 | 1964739.146 | 0.030 | 0.010 |

Table A.8: Rotational spectrum of DC$^{15}$N in the first excited bending state (01$^{e,f}$0). Please refer to the text as to which lines were measured in sub-Doppler and which in Doppler resolution.

| $J'$ | $\ell' = 1$ | $J''$ | $\ell'' = 1$ | Frequency [MHz] | $\Delta\nu$ [MHz] | o.-c. [MHz] |
|---|---|---|---|---|---|---|
| 5 | f | 5 | e | 5280.6200$c$ | 0.010 | 0.002 |
| 6 | f | 6 | e | 7391.8550$c$ | 0.010 | 0.004 |
| 7 | f | 7 | e | 9854.2310$c$ | 0.010 | 0.004 |
| 8 | f | 8 | e | 12667.4110$c$ | 0.010 | 0.004 |
| 9 | f | 9 | e | 15831.0120$c$ | 0.010 | 0.004 |
| 19 | f | 19 | e | 66622.222 | 0.010 | −0.004 |
| 20 | f | 20 | e | 73601.793 | 0.010 | −0.003 |
| 21 | f | 21 | e | 80923.574 | 0.010 | −0.007 |
| 22 | f | 22 | e | 88586.613 | 0.010 | 0.004 |
| 23 | f | 23 | e | 96589.872 | 0.010 | 0.006 |
| 24 | f | 24 | e | 104932.301 | 0.010 | 0.002 |
| 25 | f | 25 | e | 113612.810 | 0.010 | −0.002 |
| 2 | e | 1 | e | 140825.528$g$ | 0.020 | 0.006 |
| 2 | f | 1 | f | 141529.809$g$ | 0.010 | 0.028 |
| 3 | e | 2 | e | 211234.960 | 0.010 | −0.003 |
| 3 | f | 2 | f | 212291.228 | 0.010 | −0.003 |
| 4 | e | 3 | e | 281640.424 | 0.010 | 0.004 |
| 4 | f | 3 | f | 283048.555 | 0.020 | 0.003 |
| 5 | e | 4 | e | 352040.568 | 0.003 | 0.002 |
| 5 | f | 4 | f | 353800.342 | 0.010 | −0.027 |
| 6 | e | 5 | e | 422434.072 | 0.005 | −0.001 |
| 6 | f | 5 | f | 424545.305 | 0.005 | −0.002 |
| 7 | e | 6 | e | 492819.613 | 0.005 | 0.000 |
| 7 | f | 6 | f | 495281.988 | 0.005 | −0.001 |
| 8 | e | 7 | e | 563195.861 | 0.030 | 0.000 |
| 8 | f | 7 | f | 566009.043 | 0.005 | 0.001 |
| 9 | e | 8 | e | 633561.488 | 0.005 | −0.001 |
| 9 | f | 8 | f | 636725.082 | 0.005 | −0.009 |
| 10 | e | 9 | e | 703915.173 | 0.005 | 0.001 |
| 10 | f | 9 | f | 707428.764 | 0.005 | 0.002 |
| 11 | f | 10 | f | 778118.688 | 0.005 | 0.004 |
| 12 | e | 11 | e | 844581.399 | 0.010 | 0.002 |
| 12 | f | 11 | f | 848793.488 | 0.010 | 0.004 |
| 13 | e | 12 | e | 914891.295 | 0.010 | 0.006 |
| 13 | f | 12 | f | 919451.795 | 0.010 | 0.004 |
| 25 | e | 24 | e | 1756886.865 | 0.100 | −0.024 |
| 25 | f | 24 | f | 1765567.450 | 0.050 | 0.048 |
| 26 | e | 25 | e | 1826869.635 | 0.050 | 0.043 |
| 26 | f | 25 | f | 1835887.046 | 0.005 | −0.004 |
| 27 | e | 26 | e | 1896817.908 | 0.030 | −0.005 |
| 27 | f | 26 | f | 1906171.166 | 0.030 | 0.025 |
| 28 | e | 27 | e | 1966730.627 | 0.050 | 0.087 |
| 28 | f | 27 | f | 1976418.393 | 0.050 | 0.067 |

## A.4 $D^{13}C^{15}N$

Table A.9: Rotational spectrum of $D^{13}C^{15}N$ in the vibrational ground state (000). Please refer to the text as to which lines were measured in Doppler and which in sub-Doppler mode.

| $J'$ | $J''$ | Frequency [MHz] | $\Delta\nu$ [MHz] | o.-c. [MHz] |
|---|---|---|---|---|
| 1 | 0 | 69062.400 | 0.010 | 0.010 |
| 2 | 1 | 138123.535$g$ | 0.020 | 0.009 |
| 3 | 2 | 207182.151 | 0.010 | −0.003 |
| 4 | 3 | 276237.015 | 0.003 | −0.003 |
| 5 | 4 | 345286.885 | 0.010 | 0.019 |
| 6 | 5 | 414330.442 | 0.005 | 0.000 |
| 7 | 6 | 483366.492 | 0.003 | −0.002 |
| 9 | 8 | 621411.010 | 0.005 | −0.001 |
| 10 | 9 | 690416.970 | 0.005 | 0.000 |
| 11 | 10 | 759410.394 | 0.005 | 0.002 |
| 12 | 11 | 828390.031 | 0.010 | 0.005 |
| 13 | 12 | 897354.628 | 0.010 | 0.007 |
| 26 | 25 | 1791957.487 | 0.100 | 0.032 |
| 27 | 26 | 1860580.510 | 0.050 | 0.049 |
| 28 | 27 | 1929169.777 | 0.030 | 0.033 |
| 29 | 28 | 1997724.078 | 0.100 | 0.014 |

Table A.10: Rotational spectrum of $D^{13}C^{15}N$ in the first excited bending state ($01^{e,f}0$). Please refer to the text as to which lines where measured in sub-Doppler and which in Doppler resolution.

| $J'$ | $\ell' = 1$ | $J''$ | $\ell'' = 1$ | Frequency [MHz] | $\Delta\nu$ [MHz] | o.-c. [MHz] |
|---|---|---|---|---|---|---|
| 19 | f | 19 | e | 65105.796 | 0.010 | 0.003 |
| 20 | f | 20 | e | 71927.711 | 0.010 | 0.000 |
| 21 | f | 21 | e | 79084.358 | 0.010 | 0.001 |
| 22 | f | 22 | e | 86574.809 | 0.010 | −0.006 |
| 23 | f | 23 | e | 94398.120 | 0.010 | −0.009 |
| 24 | f | 24 | e | 102553.311 | 0.010 | 0.007 |
| 25 | f | 25 | e | 111039.309 | 0.010 | 0.002 |
| 2 | e | 1 | e | 138239.614$g$ | 0.020 | 0.033 |
| 2 | f | 1 | f | 138927.705$g$ | 0.020 | 0.005 |
| 3 | e | 2 | e | 207356.187 | 0.005 | 0.000 |
| 3 | f | 2 | f | 208388.254 | 0.005 | 0.002 |
| 4 | e | 3 | e | 276468.959 | 0.010 | −0.014 |
| 4 | f | 3 | f | 277844.836 | 0.010 | −0.012 |
| 5 | e | 4 | e | 345576.667 | 0.005 | 0.002 |
| 5 | f | 4 | f | 347296.178 | 0.005 | 0.009 |
| 6 | e | 5 | e | 414677.990 | 0.005 | 0.000 |
| 6 | f | 5 | f | 416740.898 | 0.005 | 0.002 |
| 7 | e | 6 | e | 483771.672 | 0.005 | −0.002 |
| 7 | f | 6 | f | 486177.717 | 0.005 | 0.006 |
| 9 | e | 8 | e | 621931.034 | 0.005 | 0.001 |
| 9 | f | 8 | f | 625022.346 | 0.005 | 0.008 |
| 10 | e | 9 | e | 690994.158 | 0.005 | −0.005 |
| 10 | f | 9 | f | 694427.513 | 0.005 | −0.003 |
| 11 | e | 10 | e | 760044.563 | 0.005 | −0.001 |
| 11 | f | 10 | f | 763819.514 | 0.005 | −0.001 |
| 12 | e | 11 | e | 829080.961 | 0.010 | −0.005 |
| 12 | f | 11 | f | 833197.020 | 0.010 | −0.001 |
| 13 | e | 12 | e | 898102.091 | 0.010 | −0.005 |
| 13 | f | 12 | f | 902558.714 | 0.010 | −0.004 |
| 26 | e | 25 | e | 1793410.161 | 0.050 | −0.014 |
| 26 | f | 25 | f | 1802225.850 | 0.100 | −0.083 |
| 27 | e | 26 | e | 1862084.468 | 0.050 | −0.007 |
| 27 | f | 26 | f | 1871228.921 | 0.050 | 0.042 |
| 28 | e | 27 | e | 1930724.504 | 0.030 | −0.027 |
| 28 | f | 27 | f | 1940196.421 | 0.030 | −0.014 |
| 29 | e | 28 | e | 1999329.046 | 0.100 | −0.043 |

# B

# Experimental Data - Methylene

Table B.1: Compilation of experimental data used in the analysis of $CH_2$. All frequency information are in MHz for the microwave and Terahertz data and in $cm^{-1}$ for the GSCD (ground state combination difference) data.

| $N'_{Ka'Kc'}$ | $J'$ | $F'$ | $N''_{Ka''Kc''}$ | $J''$ | $F''$ | Frequency | $\Delta\nu$ | o-c. | Reference |
|---|---|---|---|---|---|---|---|---|---|
| para-transitions | | | | | | | | | |
| $2_{12}$ | 2 | | $3_{03}$ | 3 | | 439960.991 | 0.030 | 0.047 | [83] |
| $2_{12}$ | 3 | | $3_{03}$ | 4 | | 444825.666 | 0.030 | −0.053 | [83] |
| $2_{12}$ | 1 | | $3_{03}$ | 2 | | 444913.930 | 0.030 | 0.008 | [83] |
| $5_{05}$ | 4 | | $4_{14}$ | 4 | | 581275.290 | 0.030 | −0.005 | this work |
| $5_{05}$ | 6 | | $4_{14}$ | 5 | | 592424.998 | 0.030 | −0.002 | [83] |
| $5_{05}$ | 4 | | $4_{14}$ | 3 | | 593122.087 | 0.030 | 0.013 | [83] |
| $5_{05}$ | 5 | | $4_{14}$ | 4 | | 593662.479 | 0.030 | −0.006 | [83] |
| $1_{10}$ | 1 | | $1_{01}$ | 1 | | 1902654.362 | 0.200 | 0.174 | this work |
| $1_{10}$ | 2 | | $1_{01}$ | 1 | | 1907986.637 | 0.300 | 0.090 | this work |
| $1_{10}$ | 1 | | $1_{01}$ | 2 | | 1912328.935 | 0.200 | 0.009 | this work |
| $1_{10}$ | 0 | | $1_{01}$ | 1 | | 1916348.190 | 0.200 | −0.241 | this work |
| $1_{10}$ | 2 | | $1_{01}$ | 2 | | 1917661.094 | 0.100 | −0.191 | this work |
| $1_{10}$ | 1 | | $1_{01}$ | 0 | | 1925866.221 | 0.200 | 0.787 | this work |
| ortho-transitions | | | | | | | | | |
| $4_{04}$ | 5 | 6 | $3_{13}$ | 4 | 5 | 68371.278 | 0.041 | −0.053 | [82] |
| $4_{04}$ | 5 | 5 | $3_{13}$ | 4 | 4 | 68375.875 | 0.039 | 0.001 | [82] |
| $4_{04}$ | 5 | 4 | $3_{13}$ | 4 | 3 | 68380.873 | 0.041 | 0.019 | [82] |
| $4_{04}$ | 3 | 2 | $3_{13}$ | 2 | 1 | 69007.179 | 0.074 | −0.027 | [82] |
| $4_{04}$ | 3 | 3 | $3_{13}$ | 2 | 2 | 69014.202 | 0.037 | −0.005 | [82] |
| $4_{04}$ | 3 | 4 | $3_{13}$ | 2 | 3 | 69019.187 | 0.044 | −0.005 | [82] |
| $4_{04}$ | 4 | 3 | $3_{13}$ | 3 | 2 | 70678.633 | 0.042 | 0.020 | [82] |
| $4_{04}$ | 4 | 4 | $3_{13}$ | 3 | 3 | 70679.543 | 0.045 | −0.006 | [82] |
| $4_{04}$ | 4 | 5 | $3_{13}$ | 3 | 4 | 70680.720 | 0.038 | 0.026 | [82] |
| $1_{11}$ | 1 | 2 | $2_{02}$ | 2 | 3 | 931423.714 | 0.100 | 0.160 | [84] |
| $1_{11}$ | 1 | 1 | $2_{02}$ | 2 | 2 | 931462.528 | 0.100 | −0.355 | [84] |
| $1_{11}$ | 1 | 0 | $2_{02}$ | 2 | 1 | 931483.535 | 0.100 | 0.261 | [84] |

Table B.1: $CH_2$ - continued

| $N'_{Ka'Kc'}$ | $J'$ | $F'$ | $N''_{Ka''Kc''}$ | $J''$ | $F''$ | Frequency | $\Delta\nu$ | o-c. | Reference |
|---|---|---|---|---|---|---|---|---|---|
| $1_{11}$ | 2 | 1 | $2_{02}$ | 3 | 2 | 945812.507 | 0.100 | 0.307 | [84] |
| $1_{11}$ | 2 | 2 | $2_{02}$ | 3 | 3 | 945825.283 | 0.100 | −0.008 | [84] |
| $1_{11}$ | 2 | 3 | $2_{02}$ | 3 | 4 | 945839.334 | 0.100 | −0.110 | [84] |
| $1_{11}$ | 0 | 1 | $2_{02}$ | 1 | 2 | 956661.048 | 0.100 | −0.279 | [84] |
| $1_{11}$ | 0 | 1 | $2_{02}$ | 1 | 1 | 956714.349 | 0.100 | 0.018 | [84] |
| $2_{11}$ | 1 | 1 | $2_{02}$ | 2 | 2 | 1942878.947 | 0.200 | −0.032 | this work |
| $2_{11}$ | 1 | 2 | $2_{02}$ | 2 | 3 | 1942910.487 | 0.200 | −0.754 | this work |
| $2_{11}$ | 3 | 4 | $2_{02}$ | 2 | 3 | 1944411.017 | 0.200 | −0.112 | this work |
| $2_{11}$ | 3 | 3 | $2_{02}$ | 2 | 2 | 1944448.270 | 0.300 | −0.177 | this work |
| $2_{11}$ | 3 | 2 | $2_{02}$ | 2 | 1 | 1944476.330 | 0.300 | 0.079 | this work |
| $2_{11}$ | 2 | 3 | $2_{02}$ | 2 | 3 | 1949051.376 | [a] | | this work |
| $2_{11}$ | 2 | 2 | $2_{02}$ | 2 | 2 | 1949058.720 | [a] | | this work |
| $2_{11}$ | 2 | 1 | $2_{02}$ | 2 | 1 | 1949063.340 | [a] | | this work |
| $2_{11}$ | 3 | 2 | $2_{02}$ | 3 | 2 | 1954910.784 | 0.500 | −0.558 | this work |
| $2_{11}$ | 3 | 3 | $2_{02}$ | 3 | 3 | 1954917.270 | 0.500 | −0.048 | this work |
| $2_{11}$ | 3 | 4 | $2_{02}$ | 3 | 4 | 1954925.038 | 0.500 | −0.297 | this work |
| $2_{11}$ | 3 | 2 | $2_{02}$ | 3 | 3 | 1954943.129 | 0.500 | 0.393 | this work |
| $2_{11}$ | 3 | 3 | $2_{02}$ | 3 | 4 | 1954959.111 | 0.500 | −0.047 | this work |
| $2_{11}$ | 1 | 1 | $2_{02}$ | 1 | 2 | 1958077.452 | 0.500 | 0.160 | this work |
| $2_{11}$ | 1 | 0 | $2_{02}$ | 1 | 1 | 1958112.867 | 0.300 | −0.054 | this work |
| $2_{11}$ | 1 | 2 | $2_{02}$ | 1 | 2 | [b] | | | this work |
| $2_{11}$ | 1 | 1 | $2_{02}$ | 1 | 1 | 1958130.100 | 0.500 | −0.195 | this work |
| $2_{11}$ | 1 | 1 | $2_{02}$ | 1 | 0 | 1958156.446 | 0.500 | −0.336 | this work |
| $2_{11}$ | 1 | 2 | $2_{02}$ | 1 | 1 | 1958165.435 | 0.500 | −0.616 | this work |
| $2_{11}$ | 2 | 1 | $2_{02}$ | 3 | 2 | 1959496.844 | 0.300 | 0.755 | this work |
| $2_{11}$ | 2 | 2 | $2_{02}$ | 3 | 3 | 1959526.242 | 0.300 | 0.623 | this work |
| $2_{11}$ | 2 | 3 | $2_{02}$ | 3 | 4 | 1959564.919 | 0.200 | 0.455 | this work |
| $2_{11}$ | 2 | 3 | $2_{02}$ | 1 | 2 | 1964253.432 | 0.500 | 0.927 | this work |
| $2_{11}$ | 2 | 2 | $2_{02}$ | 1 | 2 | [b] | | | this work |
| GSCD and IR data | | | | | | | | | |
| para-transitions | | | | | | | | | |
| $4_{23}$ | 3 | | $3_{21}$ | 2 | | 62.6936 | 0.003 | −0.0002 | [96] |
| $4_{23}$ | 5 | | $3_{21}$ | 4 | | 62.7207 | 0.003 | 0.0012 | [96] |
| $4_{23}$ | 4 | | $3_{21}$ | 3 | | 62.8660 | 0.003 | −0.0018 | [96] |
| $4_{32}$ | 3 | | $3_{30}$ | 2 | | 63.0078 | 0.003 | −0.0046 | [96] |
| $4_{32}$ | 5 | | $3_{30}$ | 4 | | 63.1109 | 0.003 | −0.0017 | [96] |
| $4_{32}$ | 4 | | $3_{30}$ | 3 | | 63.4257 | 0.003 | −0.0004 | [96] |
| $6_{16}$ | 7 | | $5_{14}$ | 6 | | 72.3054 | 0.003 | 0.0017 | [96] |
| $6_{16}$ | 5 | | $5_{14}$ | 4 | | 72.3079 | 0.003 | 0.0027 | [96] |
| $3_{03}$ | 4 | | $1_{01}$ | 2 | | 77.9934 | 0.003 | −0.0020 | [96] |
| $3_{03}$ | 3 | | $1_{01}$ | 1 | | 78.0396 | 0.003 | −0.0001 | [96] |
| $5_{32}$ | 4 | | $4_{32}$ | 3 | | 78.8736 | 0.003 | 0.0017 | [96] |
| $5_{32}$ | 6 | | $4_{32}$ | 5 | | 78.8971 | 0.003 | −0.0004 | [96] |
| $5_{32}$ | 5 | | $4_{32}$ | 4 | | 79.0651 | 0.003 | 0.0034 | [96] |

Table B.1: $CH_2$ - continued

| $N'_{Ka'Kc'}$ | $J'$ | $F'$ | $N''_{Ka''Kc''}$ | $J''$ | $F''$ | Frequency | $\Delta\nu$ | o-c. | Reference |
|---|---|---|---|---|---|---|---|---|---|
| $5_{05}$ | 6 | | $3_{03}$ | 4 | | 139.9194 | 0.003 | −0.0016 | [96] |
| $5_{05}$ | 4 | | $3_{03}$ | 2 | | 139.9827 | 0.003 | −0.0029 | [96] |
| $2_{21}$ | 3 | | $3_{03}$ | 4 | | 182.7725 | 0.003 | 0.0009 | [96] |
| $2_{21}$ | 1 | | $3_{03}$ | 2 | | 183.0503 | 0.003 | 0.0010 | [96] |
| $9_{18}$ | 10 | | $8_{18}$ | 9 | | 186.6883 | 0.003 | 0.0025 | [96] |
| $9_{18}$ | 8 | | $8_{18}$ | 7 | | 186.7128 | 0.003 | −0.0018 | [96] |
| $3_{21}$ | 3 | | $3_{03}$ | 3 | | 229.5982 | 0.003 | 0.0042 | [96] |
| $3_{21}$ | 4 | | $3_{03}$ | 4 | | 229.9493 | 0.003 | −0.0001 | [96] |
| $3_{21}$ | 2 | | $3_{03}$ | 2 | | 230.0598 | 0.003 | −0.0008 | [96] |
| $5_{23}$ | 6 | | $5_{05}$ | 6 | | 231.7726 | 0.002 | −0.0013 | [96] |
| $5_{23}$ | 4 | | $5_{05}$ | 4 | | 231.7983 | 0.002 | −0.0003 | [96] |
| $2_{21}$ | 3 | | $1_{01}$ | 2 | | 260.7659 | 0.003 | −0.0010 | [96] |
| $4_{23}$ | 4 | | $3_{03}$ | 3 | | 292.4642 | 0.003 | 0.0025 | [96] |
| $4_{23}$ | 5 | | $3_{03}$ | 4 | | 292.6700 | 0.003 | 0.0011 | [96] |
| $4_{23}$ | 3 | | $3_{03}$ | 2 | | 292.7534 | 0.003 | −0.0010 | [96] |
| $5_{23}$ | 6 | | $3_{03}$ | 4 | | 371.6922 | 0.003 | −0.0027 | [96] |
| $5_{23}$ | 4 | | $3_{03}$ | 2 | | 371.7826 | 0.003 | −0.0017 | [96] |
| $5_4$ | 5 | | $4_3$ | 4 | | 382.3709 | 0.001 | −0.0032 | [97] [c] |
| $5_4$ | 6 | | $4_3$ | 5 | | 382.4631 | 0.001 | 0.0015 | [97] [c] |
| $5_4$ | 4 | | $4_3$ | 3 | | 382.4745 | 0.001 | 0.0019 | [97] [c] |
| $6_{43}$ | 6 | | $5_{32}$ | 5 | | 398.5056 | 0.001 | −0.0006 | [97] |
| $6_{43}$ | 7 | | $5_{32}$ | 6 | | 398.5908 | 0.001 | −0.0005 | [97] |
| $6_{43}$ | 5 | | $5_{32}$ | 4 | | 398.6071 | 0.001 | −0.0009 | [97] |
| $7_{43}$ | 7 | | $6_{34}$ | 6 | | 414.6628 | 0.001 | 0.0022 | [97] |
| $7_{43}$ | 8 | | $6_{34}$ | 7 | | 414.7376 | 0.001 | −0.0010 | [97] |
| $7_{43}$ | 6 | | $6_{34}$ | 5 | | 414.7534 | 0.001 | 0.0008 | [97] |
| ortho-transitions | | | | | | | | | |
| $4_{31}$ | 3 | | $3_{31}$ | 2 | | 63.0148 | 0.003 | 0.0011 | [96] |
| $4_{22}$ | 3 | | $3_{22}$ | 2 | | 63.0283 | 0.003 | −0.0009 | [96] |
| $4_{22}$ | 5 | | $3_{22}$ | 4 | | 63.0542 | 0.003 | 0.0006 | [96] |
| $4_{31}$ | 5 | | $3_{31}$ | 4 | | 63.1176 | 0.003 | 0.0038 | [96] |
| $4_{22}$ | 4 | | $3_{22}$ | 3 | | 63.1983 | 0.003 | −0.0003 | [96] |
| $4_{31}$ | 4 | | $3_{31}$ | 3 | | 63.4336 | 0.003 | 0.0062 | [96] |
| $5_{24}$ | 6 | | $4_{22}$ | 5 | | 78.2012 | 0.003 | 0.0028 | [96] |
| $5_{24}$ | 4 | | $4_{22}$ | 3 | | 78.2000 | 0.003 | −0.0004 | [96] |
| $5_{24}$ | 5 | | $4_{22}$ | 4 | | 78.2771 | 0.003 | −0.0027 | [96] |
| $5_{33}$ | 4 | | $4_{31}$ | 3 | | 78.8634 | 0.003 | −0.0031 | [96] |
| $5_{33}$ | 6 | | $4_{31}$ | 5 | | 78.8913 | 0.003 | −0.0007 | [96] |
| $5_{33}$ | 5 | | $4_{31}$ | 4 | | 79.0547 | 0.003 | −0.0065 | [96] |
| $7_{17}$ | 8 | | $6_{15}$ | 7 | | 80.1670 | 0.003 | −0.0007 | [96] |
| $7_{17}$ | 6 | | $6_{15}$ | 5 | | 80.1679 | 0.003 | 0.0001 | [96] |
| $7_{17}$ | 7 | | $6_{15}$ | 6 | | 80.2360 | 0.003 | 0.0006 | [96] |
| $7_{26}$ | 6 | | $8_{08}$ | 7 | | 110.7374 | 0.003 | −0.0001 | [96] |
| $7_{26}$ | 8 | | $8_{08}$ | 9 | | 110.7452 | 0.003 | 0.0015 | [96] |

Table B.1: $CH_2$ - continued

| $N'_{Ka'Kc'}$ | $J'$ | $F'$ | $N''_{Ka''Kc''}$ | $J''$ | $F''$ | Frequency | $\Delta\nu$ | o-c. | Reference |
|---|---|---|---|---|---|---|---|---|---|
| $8_{17}$ | 9 | | $7_{17}$ | 8 | | 161.7859 | 0.003 | 0.0006 | [96] |
| $8_{17}$ | 7 | | $7_{17}$ | 6 | | 161.8146 | 0.003 | −0.0007 | [96] |
| $10_{19}$ | 11 | | $9_{19}$ | 10 | | 212.4727 | 0.003 | 0.0012 | [96] |
| $10_{19}$ | 9 | | $9_{19}$ | 8 | | 212.4985 | 0.003 | −0.0011 | [96] |
| $3_{22}$ | 4 | | $2_{02}$ | 3 | | 276.6446 | 0.002 | −0.0017 | [96] |
| $3_{22}$ | 2 | | $2_{02}$ | 1 | | 276.8303 | 0.002 | 0.0014 | [96] |
| $4_{22}$ | 5 | | $2_{02}$ | 3 | | 339.6980 | 0.003 | −0.0018 | [96] |
| $4_{22}$ | 3 | | $2_{02}$ | 1 | | 339.8604 | 0.003 | 0.0023 | [96] |
| $5_4$ | 5 | | $4_3$ | 4 | | 382.3709 | 0.001 | −0.0032 | [97] [c] |
| $5_4$ | 6 | | $4_3$ | 5 | | 382.4631 | 0.001 | 0.0015 | [97] [c] |
| $5_4$ | 4 | | $4_3$ | 3 | | 382.4745 | 0.001 | 0.0019 | [97] [c] |
| $6_{42}$ | 6 | | $5_{33}$ | 5 | | 398.5111 | 0.001 | 0.0006 | [97] |
| $6_{42}$ | 7 | | $5_{33}$ | 6 | | 398.5965 | 0.001 | 0.0007 | [97] |
| $6_{42}$ | 5 | | $5_{33}$ | 4 | | 398.6128 | 0.001 | −0.0004 | [97] |
| $7_{44}$ | 8 | | $6_{33}$ | 7 | | 414.7215 | 0.001 | −0.0019 | [97] |
| $7_{44}$ | 6 | | $6_{33}$ | 5 | | 414.7376 | 0.001 | −0.0010 | [97] |

[a] These lines were not included in the fit. The assignment is ambiguous due to their small frequency spacing and different Zeeman splitting.

[b] Line is blended with the one above. The o.-c. value is that of the intensity weighted line position.

[c] $K$ doubling was not resolved for this transition.

Table B.2: Transition frequency predictions for $CH_2$ calculated for $J \leq 6$ and $K_a = 0, 1$. Transition intensities $I$ are given for a temperature of 300 K. Einstein $A$ coefficients are also stated, as well as the lower energy level $E_{lower}$ of the transition.

| Frequency [MHz] | $\Delta\nu$ [MHz] | log$I$ [nm$^2$MHz] | $A$ [s$^{-1}$] | $E_{lower}$ [cm$^{-1}$] | $N'_{Ka',Kc'}$ | $J'$ | $F'$ | $N''_{Ka'',Kc''}$ | $J''$ | $F''$ |
|---|---|---|---|---|---|---|---|---|---|---|
| para-$CH_2$ | | | | | | | | | | |
| 433821.829 | 0.236 | −4.249 | 3.375E-07 | 93.937 | $2_{1,2}$ | 3 | | $3_{0,3}$ | 3 | |
| 439960.944 | 0.025 | −3.327 | 4.062E-06 | 93.937 | $2_{1,2}$ | 2 | | $3_{0,3}$ | 3 | |
| 444825.720 | 0.025 | −3.153 | 4.418E-06 | 93.570 | $2_{1,2}$ | 3 | | $3_{0,3}$ | 4 | |
| 444913.922 | 0.026 | −3.484 | 4.813E-06 | 93.484 | $2_{1,2}$ | 1 | | $3_{0,3}$ | 2 | |
| 447412.902 | 0.254 | −5.738 | 1.161E-08 | 93.484 | $2_{1,2}$ | 3 | | $3_{0,3}$ | 2 | |
| 453552.018 | 0.096 | −4.190 | 5.897E-07 | 93.484 | $2_{1,2}$ | 2 | | $3_{0,3}$ | 2 | |
| 581275.290 | 0.030 | −4.356 | 6.553E-07 | 214.080 | $5_{0,5}$ | 4 | | $4_{1,4}$ | 4 | |
| 591775.204 | 0.616 | −6.325 | 7.281E-09 | 213.730 | $5_{0,5}$ | 4 | | $4_{1,4}$ | 5 | |
| 592425.000 | 0.028 | −2.874 | 1.426E-05 | 213.730 | $5_{0,5}$ | 6 | | $4_{1,4}$ | 5 | |
| 593122.074 | 0.029 | −3.055 | 1.362E-05 | 213.685 | $5_{0,5}$ | 4 | | $4_{1,4}$ | 3 | |
| 593662.485 | 0.028 | −2.964 | 1.378E-05 | 214.080 | $5_{0,5}$ | 5 | | $4_{1,4}$ | 4 | |
| 604162.399 | 0.614 | −4.334 | 6.082E-07 | 213.730 | $5_{0,5}$ | 5 | | $4_{1,4}$ | 5 | |
| 1902654.188 | 0.148 | −2.346 | 8.332E-04 | 15.898 | $1_{1,0}$ | 1 | | $1_{0,1}$ | 1 | |
| 1907986.547 | 0.135 | −2.118 | 8.502E-04 | 15.898 | $1_{1,0}$ | 2 | | $1_{0,1}$ | 1 | |
| 1912328.926 | 0.107 | −2.110 | 1.445E-03 | 15.575 | $1_{1,0}$ | 1 | | $1_{0,1}$ | 2 | |
| 1916348.431 | 0.121 | −2.204 | 3.512E-03 | 15.898 | $1_{1,0}$ | 0 | | $1_{0,1}$ | 1 | |
| 1917661.285 | 0.083 | −1.627 | 2.655E-03 | 15.575 | $1_{1,0}$ | 2 | | $1_{0,1}$ | 2 | |
| 1925865.434 | 0.146 | −2.188 | 1.224E-03 | 15.123 | $1_{1,0}$ | 1 | | $1_{0,1}$ | 0 | |
| 2000539.865 | 0.343 | −2.591 | 4.570E-04 | 93.937 | $3_{1,2}$ | 2 | | $3_{0,3}$ | 3 | |
| 2001934.529 | 0.399 | −2.597 | 2.505E-04 | 93.937 | $3_{1,2}$ | 4 | | $3_{0,3}$ | 3 | |
| 2009466.079 | 0.357 | −1.570 | 3.457E-03 | 93.937 | $3_{1,2}$ | 3 | | $3_{0,3}$ | 3 | |
| 2012938.420 | 0.399 | −1.411 | 3.885E-03 | 93.570 | $3_{1,2}$ | 4 | | $3_{0,3}$ | 4 | |

Table B.2: $CH_2$ transition frequency predictions - continued

| Frequency [MHz] | $\Delta\nu$ [MHz] | log$I$ [nm$^2$MHz] | $A$ [s$^{-1}$] | $E_{lower}$ [cm$^{-1}$] | $N'_{Ka',Kc'}$ | $J'$ | $F'$ | $N''_{Ka'',Kc''}$ | $J''$ | $F''$ |
|---|---|---|---|---|---|---|---|---|---|---|
| 2014130.938 | 0.355 | −1.690 | 3.681E-03 | 93.484 | $3_{1,2}$ | 2 | | $3_{0,3}$ | 2 | |
| 2020469.970 | 0.378 | −2.590 | 3.331E-04 | 93.570 | $3_{1,2}$ | 3 | | $3_{0,3}$ | 4 | |
| 2023057.152 | 0.360 | −2.582 | 3.399E-04 | 93.484 | $3_{1,2}$ | 3 | | $3_{0,3}$ | 2 | |
| 2173606.586 | 7.811 | −7.487 | 5.250E-09 | 160.966 | $5_{0,5}$ | 4 | | $3_{1,2}$ | 3 | |
| 2181509.444 | 3.134 | −3.024 | 2.177E-04 | 233.883 | $5_{1,4}$ | 4 | | $5_{0,5}$ | 5 | |
| 2181707.278 | 3.219 | −3.031 | 1.483E-04 | 233.883 | $5_{1,4}$ | 6 | | $5_{0,5}$ | 5 | |
| 2191442.272 | 3.143 | −1.570 | 5.122E-03 | 233.883 | $5_{1,4}$ | 5 | | $5_{0,5}$ | 5 | |
| 2193444.676 | 3.163 | −1.478 | 5.348E-03 | 233.491 | $5_{1,4}$ | 6 | | $5_{0,5}$ | 6 | |
| 2193525.332 | 7.817 | −7.591 | 3.437E-09 | 160.715 | $5_{0,5}$ | 5 | | $3_{1,2}$ | 4 | |
| 2193896.639 | 3.133 | −1.644 | 5.281E-03 | 233.470 | $5_{1,4}$ | 4 | | $5_{0,5}$ | 4 | |
| 2203179.670 | 3.172 | −3.023 | 1.820E-04 | 233.491 | $5_{1,4}$ | 5 | | $5_{0,5}$ | 6 | |
| 2203829.467 | 3.143 | −3.016 | 1.851E-04 | 233.470 | $5_{1,4}$ | 5 | | $5_{0,5}$ | 4 | |
| 2770895.142 | 1.560 | −2.026 | 3.693E-03 | 15.898 | $2_{1,2}$ | 1 | | $1_{0,1}$ | 1 | |
| 2779533.237 | 1.547 | −1.553 | 6.615E-03 | 15.898 | $2_{1,2}$ | 2 | | $1_{0,1}$ | 1 | |
| 2780569.880 | 1.562 | −3.176 | 2.626E-04 | 15.575 | $2_{1,2}$ | 1 | | $1_{0,1}$ | 2 | |
| 2783068.860 | 1.550 | −1.284 | 8.785E-03 | 15.575 | $2_{1,2}$ | 3 | | $1_{0,1}$ | 2 | |
| 2789207.976 | 1.550 | −2.040 | 2.169E-03 | 15.575 | $2_{1,2}$ | 2 | | $1_{0,1}$ | 2 | |
| 2794106.388 | 1.545 | −1.915 | 4.831E-03 | 15.123 | $2_{1,2}$ | 1 | | $1_{0,1}$ | 0 | |
| 3589950.592 | 7.866 | −2.366 | 1.763E-03 | 93.937 | $4_{1,4}$ | 3 | | $3_{0,3}$ | 3 | |
| 3600954.483 | 7.871 | −4.142 | 2.967E-05 | 93.570 | $4_{1,4}$ | 3 | | $3_{0,3}$ | 4 | |
| 3601797.376 | 7.865 | −1.195 | 2.048E-02 | 93.937 | $4_{1,4}$ | 4 | | $3_{0,3}$ | 3 | |
| 3602301.353 | 7.878 | −1.079 | 2.183E-02 | 93.570 | $4_{1,4}$ | 5 | | $3_{0,3}$ | 4 | |
| 3603541.665 | 7.861 | −1.313 | 2.004E-02 | 93.484 | $4_{1,4}$ | 3 | | $3_{0,3}$ | 2 | |
| 3612801.267 | 7.870 | −2.376 | 1.356E-03 | 93.570 | $4_{1,4}$ | 4 | | $3_{0,3}$ | 4 | |
| 3749250.837 | 7.868 | −7.529 | 1.102E-08 | 108.408 | $5_{0,5}$ | 4 | | $2_{1,2}$ | 3 | |
| 4340112.158 | 1.628 | −6.724 | 1.089E-07 | 15.898 | $3_{1,2}$ | 2 | | $1_{0,1}$ | 1 | |
| 4349164.510 | 26.642 | −2.709 | 1.464E-03 | 233.883 | $6_{1,6}$ | 5 | | $5_{0,5}$ | 5 | |
| 4349786.896 | 1.628 | −7.281 | 3.027E-08 | 15.575 | $3_{1,2}$ | 2 | | $1_{0,1}$ | 2 | |
| 4358713.110 | 1.636 | −6.853 | 5.824E-08 | 15.575 | $3_{1,2}$ | 3 | | $1_{0,1}$ | 2 | |
| 4360901.908 | 26.650 | −4.841 | 1.084E-05 | 233.491 | $6_{1,6}$ | 5 | | $5_{0,5}$ | 6 | |
| 4361223.654 | 26.643 | −1.168 | 4.325E-02 | 233.883 | $6_{1,6}$ | 6 | | $5_{0,5}$ | 5 | |
| 4361551.705 | 26.642 | −1.243 | 4.300E-02 | 233.470 | $6_{1,6}$ | 5 | | $5_{0,5}$ | 4 | |
| 4372961.052 | 26.651 | −2.715 | 1.231E-03 | 233.491 | $6_{1,6}$ | 6 | | $5_{0,5}$ | 6 | |
| ortho-$CH_2$ | | | | | | | | | | |
| 68371.331 | 0.030 | −4.655 | 2.356E-09 | 153.556 | $4_{0,4}$ | 5 | 6 | $3_{1,3}$ | 4 | 5 |
| 68375.876 | 0.020 | −4.746 | 2.262E-09 | 153.557 | $4_{0,4}$ | 5 | 5 | $3_{1,3}$ | 4 | 4 |
| 68380.855 | 0.030 | −4.837 | 2.240E-09 | 153.558 | $4_{0,4}$ | 5 | 4 | $3_{1,3}$ | 4 | 3 |
| 68409.569 | 0.099 | −6.124 | 1.157E-10 | 153.557 | $4_{0,4}$ | 5 | 4 | $3_{1,3}$ | 4 | 4 |
| 68974.985 | 0.100 | −5.906 | 2.496E-10 | 153.488 | $4_{0,4}$ | 3 | 3 | $3_{1,3}$ | 2 | 3 |
| 68981.078 | 0.068 | −5.907 | 3.493E-10 | 153.487 | $4_{0,4}$ | 3 | 2 | $3_{1,3}$ | 2 | 2 |
| 69007.207 | 0.037 | −5.175 | 1.885E-09 | 153.486 | $4_{0,4}$ | 3 | 2 | $3_{1,3}$ | 2 | 1 |
| 69014.207 | 0.024 | −5.004 | 1.995E-09 | 153.487 | $4_{0,4}$ | 3 | 3 | $3_{1,3}$ | 2 | 2 |
| 69019.181 | 0.031 | −4.844 | 2.245E-09 | 153.488 | $4_{0,4}$ | 3 | 4 | $3_{1,3}$ | 2 | 3 |
| 70678.113 | 0.040 | −6.023 | 2.010E-10 | 153.860 | $4_{0,4}$ | 4 | 3 | $3_{1,3}$ | 3 | 3 |
| 70678.613 | 0.028 | −4.962 | 2.309E-09 | 153.860 | $4_{0,4}$ | 4 | 3 | $3_{1,3}$ | 3 | 2 |
| 70678.954 | 0.057 | −6.023 | 1.561E-10 | 153.860 | $4_{0,4}$ | 4 | 4 | $3_{1,3}$ | 3 | 4 |
| 70679.549 | 0.020 | −4.844 | 2.358E-09 | 153.860 | $4_{0,4}$ | 4 | 4 | $3_{1,3}$ | 3 | 3 |
| 70680.694 | 0.026 | −4.729 | 2.514E-09 | 153.860 | $4_{0,4}$ | 4 | 5 | $3_{1,3}$ | 3 | 4 |
| 79741.541 | 0.401 | −6.029 | 2.515E-10 | 153.558 | $4_{0,4}$ | 4 | 3 | $3_{1,3}$ | 4 | 3 |
| 79771.691 | 0.388 | −5.937 | 2.420E-10 | 153.557 | $4_{0,4}$ | 4 | 4 | $3_{1,3}$ | 4 | 4 |
| 79809.300 | 0.391 | −5.824 | 2.571E-10 | 153.556 | $4_{0,4}$ | 4 | 5 | $3_{1,3}$ | 4 | 5 |
| 931423.554 | 0.084 | −2.841 | 4.454E-05 | 47.139 | $1_{1,1}$ | 1 | 2 | $2_{0,2}$ | 2 | 3 |
| 931427.048 | 0.097 | −3.585 | 8.027E-06 | 47.139 | $1_{1,1}$ | 1 | 2 | $2_{0,2}$ | 2 | 2 |
| 931429.434 | 0.144 | −4.758 | 5.385E-07 | 47.139 | $1_{1,1}$ | 1 | 2 | $2_{0,2}$ | 2 | 1 |
| 931462.883 | 0.057 | −3.111 | 3.984E-05 | 47.139 | $1_{1,1}$ | 1 | 1 | $2_{0,2}$ | 2 | 2 |
| 931465.270 | 0.088 | −3.585 | 1.336E-05 | 47.139 | $1_{1,1}$ | 1 | 1 | $2_{0,2}$ | 2 | 1 |
| 931483.274 | 0.081 | −3.462 | 5.326E-05 | 47.139 | $1_{1,1}$ | 1 | 0 | $2_{0,2}$ | 2 | 1 |
| 935325.239 | 0.173 | −3.368 | 9.531E-06 | 47.139 | $1_{1,1}$ | 2 | 3 | $2_{0,2}$ | 2 | 3 |
| 935328.733 | 0.214 | −4.271 | 1.189E-06 | 47.139 | $1_{1,1}$ | 2 | 3 | $2_{0,2}$ | 2 | 2 |
| 935352.926 | 0.206 | −4.238 | 1.798E-06 | 47.139 | $1_{1,1}$ | 2 | 2 | $2_{0,2}$ | 2 | 3 |
| 935356.420 | 0.172 | −3.626 | 7.359E-06 | 47.139 | $1_{1,1}$ | 2 | 2 | $2_{0,2}$ | 2 | 2 |
| 935358.806 | 0.175 | −4.289 | 1.598E-06 | 47.139 | $1_{1,1}$ | 2 | 2 | $2_{0,2}$ | 2 | 1 |
| 935374.722 | 0.221 | −4.267 | 2.805E-06 | 47.139 | $1_{1,1}$ | 2 | 1 | $2_{0,2}$ | 2 | 2 |
| 935377.109 | 0.195 | −3.813 | 7.968E-06 | 47.139 | $1_{1,1}$ | 2 | 1 | $2_{0,2}$ | 2 | 1 |
| 941463.015 | 0.138 | −8.043 | 4.763E-10 | 47.139 | $1_{1,1}$ | 0 | 1 | $2_{0,2}$ | 2 | 2 |
| 941465.402 | 0.164 | −8.523 | 1.576E-10 | 47.139 | $1_{1,1}$ | 0 | 1 | $2_{0,2}$ | 2 | 1 |

Table B.2: $CH_2$ transition frequency predictions - continued

| Frequency [MHz] | $\Delta\nu$ [MHz] | log$I$ [nm$^2$MHz] | $A$ [s$^{-1}$] | $E_{lower}$ [cm$^{-1}$] | $N'_{Ka',Kc'}$ | $J'$ | $F'$ | $N''_{Ka'',Kc''}$ | $J''$ | $F''$ |
|---|---|---|---|---|---|---|---|---|---|---|
| 941864.525 | 0.263 | −7.962 | 3.440E-10 | 46.791 | $1_{1,1}$ | 1 | 2 | $2_{0,2}$ | 3 | 2 |
| 941895.919 | 0.201 | −7.059 | 2.751E-09 | 46.790 | $1_{1,1}$ | 1 | 2 | $2_{0,2}$ | 3 | 3 |
| 941900.361 | 0.215 | −7.481 | 1.735E-09 | 46.791 | $1_{1,1}$ | 1 | 1 | $2_{0,2}$ | 3 | 2 |
| 945766.211 | 0.258 | −5.183 | 1.487E-07 | 46.791 | $1_{1,1}$ | 2 | 3 | $2_{0,2}$ | 3 | 2 |
| 945793.897 | 0.105 | −3.641 | 7.263E-06 | 46.791 | $1_{1,1}$ | 2 | 2 | $2_{0,2}$ | 3 | 2 |
| 945797.604 | 0.162 | −3.640 | 5.194E-06 | 46.790 | $1_{1,1}$ | 2 | 3 | $2_{0,2}$ | 3 | 3 |
| 945812.200 | 0.067 | −2.909 | 6.522E-05 | 46.791 | $1_{1,1}$ | 2 | 1 | $2_{0,2}$ | 3 | 2 |
| 945825.291 | 0.054 | −2.739 | 5.799E-05 | 46.790 | $1_{1,1}$ | 2 | 2 | $2_{0,2}$ | 3 | 3 |
| 945839.445 | 0.067 | −2.578 | 5.994E-05 | 46.788 | $1_{1,1}$ | 2 | 3 | $2_{0,2}$ | 3 | 4 |
| 946625.360 | 0.153 | −3.328 | 1.492E-05 | 46.632 | $1_{1,1}$ | 1 | 2 | $2_{0,2}$ | 1 | 2 |
| 946661.195 | 0.132 | −3.813 | 8.151E-06 | 46.632 | $1_{1,1}$ | 1 | 1 | $2_{0,2}$ | 1 | 2 |
| 946678.363 | 0.135 | −3.804 | 4.995E-06 | 46.630 | $1_{1,1}$ | 1 | 2 | $2_{0,2}$ | 1 | 1 |
| 946714.199 | 0.142 | −4.024 | 5.017E-06 | 46.630 | $1_{1,1}$ | 1 | 1 | $2_{0,2}$ | 1 | 1 |
| 946732.203 | 0.163 | −3.905 | 1.980E-05 | 46.630 | $1_{1,1}$ | 1 | 0 | $2_{0,2}$ | 1 | 1 |
| 946740.686 | 0.168 | −3.900 | 6.668E-06 | 46.629 | $1_{1,1}$ | 1 | 1 | $2_{0,2}$ | 1 | 0 |
| 950527.045 | 0.230 | −4.440 | 8.304E-07 | 46.632 | $1_{1,1}$ | 2 | 3 | $2_{0,2}$ | 1 | 2 |
| 950554.732 | 0.194 | −5.156 | 2.237E-07 | 46.632 | $1_{1,1}$ | 2 | 2 | $2_{0,2}$ | 1 | 2 |
| 950573.034 | 0.240 | −6.312 | 2.607E-08 | 46.632 | $1_{1,1}$ | 2 | 1 | $2_{0,2}$ | 1 | 2 |
| 950607.735 | 0.217 | −4.726 | 6.020E-07 | 46.630 | $1_{1,1}$ | 2 | 2 | $2_{0,2}$ | 1 | 1 |
| 950626.038 | 0.282 | −5.181 | 3.522E-07 | 46.630 | $1_{1,1}$ | 2 | 1 | $2_{0,2}$ | 1 | 1 |
| 950652.525 | 0.312 | −5.080 | 4.440E-07 | 46.629 | $1_{1,1}$ | 2 | 1 | $2_{0,2}$ | 1 | 0 |
| 956661.327 | 0.083 | −3.072 | 4.586E-05 | 46.632 | $1_{1,1}$ | 0 | 1 | $2_{0,2}$ | 1 | 2 |
| 956714.331 | 0.082 | −3.295 | 2.745E-05 | 46.630 | $1_{1,1}$ | 0 | 1 | $2_{0,2}$ | 1 | 1 |
| 956740.818 | 0.116 | −3.773 | 9.137E-06 | 46.629 | $1_{1,1}$ | 0 | 1 | $2_{0,2}$ | 1 | 0 |
| 1113781.327 | 0.381 | −5.502 | 2.465E-07 | 289.260 | $6_{0,6}$ | 5 | 4 | $5_{1,5}$ | 5 | 5 |
| 1113782.374 | 0.389 | −4.122 | 5.913E-06 | 289.260 | $6_{0,6}$ | 5 | 4 | $5_{1,5}$ | 5 | 4 |
| 1113814.941 | 0.364 | −5.499 | 2.029E-07 | 289.260 | $6_{0,6}$ | 5 | 5 | $5_{1,5}$ | 5 | 6 |
| 1113816.153 | 0.369 | −4.045 | 5.773E-06 | 289.260 | $6_{0,6}$ | 5 | 5 | $5_{1,5}$ | 5 | 5 |
| 1113817.200 | 0.375 | −5.503 | 2.014E-07 | 289.260 | $6_{0,6}$ | 5 | 5 | $5_{1,5}$ | 5 | 4 |
| 1113856.756 | 0.375 | −3.954 | 6.026E-06 | 289.260 | $6_{0,6}$ | 5 | 6 | $5_{1,5}$ | 5 | 6 |
| 1113857.968 | 0.376 | −5.500 | 1.714E-07 | 289.260 | $6_{0,6}$ | 5 | 6 | $5_{1,5}$ | 5 | 5 |
| 1125077.633 | 1.070 | −6.236 | 4.627E-08 | 288.883 | $6_{0,6}$ | 5 | 4 | $5_{1,5}$ | 6 | 5 |
| 1125112.459 | 1.057 | −7.857 | 9.063E-10 | 288.883 | $6_{0,6}$ | 5 | 5 | $5_{1,5}$ | 6 | 5 |
| 1125144.026 | 1.047 | −6.159 | 4.523E-08 | 288.882 | $6_{0,6}$ | 5 | 5 | $5_{1,5}$ | 6 | 6 |
| 1125185.841 | 1.048 | −7.922 | 6.614E-10 | 288.882 | $6_{0,6}$ | 5 | 6 | $5_{1,5}$ | 6 | 6 |
| 1125199.833 | 0.347 | −2.465 | 1.892E-04 | 288.883 | $6_{0,6}$ | 7 | 6 | $5_{1,5}$ | 6 | 5 |
| 1125231.400 | 0.353 | −4.082 | 4.574E-06 | 288.882 | $6_{0,6}$ | 7 | 6 | $5_{1,5}$ | 6 | 6 |
| 1125788.466 | 0.397 | −5.933 | 9.319E-08 | 288.859 | $6_{0,6}$ | 5 | 4 | $5_{1,5}$ | 4 | 5 |
| 1125823.291 | 0.367 | −3.938 | 7.531E-06 | 288.859 | $6_{0,6}$ | 5 | 5 | $5_{1,5}$ | 4 | 5 |
| 1125827.667 | 0.362 | −3.938 | 9.200E-06 | 288.858 | $6_{0,6}$ | 5 | 4 | $5_{1,5}$ | 4 | 4 |
| 1125859.011 | 0.354 | −2.650 | 1.785E-04 | 288.857 | $6_{0,6}$ | 5 | 4 | $5_{1,5}$ | 4 | 3 |
| 1125862.493 | 0.352 | −2.559 | 1.803E-04 | 288.858 | $6_{0,6}$ | 5 | 5 | $5_{1,5}$ | 4 | 4 |
| 1125865.107 | 0.352 | −2.469 | 1.878E-04 | 288.859 | $6_{0,6}$ | 5 | 6 | $5_{1,5}$ | 4 | 5 |
| 1125896.486 | 0.344 | −6.184 | 4.287E-08 | 289.260 | $6_{0,6}$ | 6 | 5 | $5_{1,5}$ | 5 | 6 |
| 1125897.520 | 0.343 | −4.026 | 5.213E-06 | 289.260 | $6_{0,6}$ | 6 | 6 | $5_{1,5}$ | 5 | 6 |
| 1125897.698 | 0.344 | −4.026 | 6.165E-06 | 289.260 | $6_{0,6}$ | 6 | 5 | $5_{1,5}$ | 5 | 5 |
| 1125898.732 | 0.345 | −2.480 | 1.835E-04 | 289.260 | $6_{0,6}$ | 6 | 6 | $5_{1,5}$ | 5 | 5 |
| 1125898.746 | 0.347 | −2.555 | 1.825E-04 | 289.260 | $6_{0,6}$ | 6 | 5 | $5_{1,5}$ | 5 | 4 |
| 1137194.005 | 1.010 | −4.091 | 5.409E-06 | 288.883 | $6_{0,6}$ | 6 | 5 | $5_{1,5}$ | 6 | 5 |
| 1137195.039 | 1.014 | −5.634 | 1.310E-07 | 288.883 | $6_{0,6}$ | 6 | 6 | $5_{1,5}$ | 6 | 5 |
| 1137225.571 | 1.002 | −5.636 | 1.542E-07 | 288.882 | $6_{0,6}$ | 6 | 5 | $5_{1,5}$ | 6 | 6 |
| 1137226.605 | 1.005 | −4.028 | 5.292E-06 | 288.882 | $6_{0,6}$ | 6 | 6 | $5_{1,5}$ | 6 | 6 |
| 1308155.867 | 3.738 | −7.631 | 1.944E-09 | 112.153 | $4_{0,4}$ | 3 | 2 | $2_{1,1}$ | 2 | 1 |
| 1308157.732 | 3.738 | −8.362 | 3.609E-10 | 112.153 | $4_{0,4}$ | 3 | 2 | $2_{1,1}$ | 2 | 2 |
| 1308190.860 | 3.739 | −7.461 | 2.052E-09 | 112.153 | $4_{0,4}$ | 3 | 3 | $2_{1,1}$ | 2 | 2 |
| 1308193.856 | 3.742 | −8.363 | 2.576E-10 | 112.152 | $4_{0,4}$ | 3 | 3 | $2_{1,1}$ | 2 | 3 |
| 1308238.052 | 3.747 | −7.302 | 2.304E-09 | 112.152 | $4_{0,4}$ | 3 | 4 | $2_{1,1}$ | 2 | 3 |
| 1325622.500 | 3.736 | −7.791 | 9.857E-10 | 112.000 | $4_{0,4}$ | 4 | 3 | $2_{1,1}$ | 3 | 2 |
| 1325649.354 | 3.741 | −7.671 | 1.011E-09 | 111.999 | $4_{0,4}$ | 4 | 4 | $2_{1,1}$ | 3 | 3 |
| 1325684.918 | 3.749 | −7.553 | 1.086E-09 | 111.998 | $4_{0,4}$ | 4 | 5 | $2_{1,1}$ | 3 | 4 |
| 1942863.520 | 0.198 | −2.856 | 9.350E-04 | 47.139 | $2_{1,1}$ | 1 | 0 | $2_{0,2}$ | 2 | 1 |
| 1942878.980 | 0.127 | −2.501 | 7.052E-04 | 47.139 | $2_{1,1}$ | 1 | 1 | $2_{0,2}$ | 2 | 2 |
| 1942881.367 | 0.168 | −2.984 | 2.319E-04 | 47.139 | $2_{1,1}$ | 1 | 1 | $2_{0,2}$ | 2 | 1 |
| 1942911.241 | 0.135 | −2.228 | 7.933E-04 | 47.139 | $2_{1,1}$ | 1 | 2 | $2_{0,2}$ | 2 | 3 |
| 1942914.735 | 0.108 | −2.986 | 1.388E-04 | 47.139 | $2_{1,1}$ | 1 | 2 | $2_{0,2}$ | 2 | 2 |
| 1942917.122 | 0.130 | −4.168 | 9.121E-06 | 47.139 | $2_{1,1}$ | 1 | 2 | $2_{0,2}$ | 2 | 1 |

Table B.2: $CH_2$ transition frequency predictions - continued

| Frequency [MHz] | $\Delta\nu$ [MHz] | log$I$ [nm$^2$MHz] | $A$ [s$^{-1}$] | $E_{lower}$ [cm$^{-1}$] | $N'_{Ka',Kc'}$ | $J'$ | $F'$ | $N''_{Ka'',Kc''}$ | $J''$ | $F''$ |
|---|---|---|---|---|---|---|---|---|---|---|
| 1944411.130 | 0.137 | −2.268 | 4.026E-04 | 47.139 | $2_{1,1}$ | 3 | 4 | $2_{0,2}$ | 2 | 3 |
| 1944444.953 | 0.159 | −3.344 | 4.352E-05 | 47.139 | $2_{1,1}$ | 3 | 3 | $2_{0,2}$ | 2 | 3 |
| 1944448.447 | 0.129 | −2.426 | 3.600E-04 | 47.139 | $2_{1,1}$ | 3 | 3 | $2_{0,2}$ | 2 | 2 |
| 1944470.371 | 0.226 | −4.896 | 1.707E-06 | 47.139 | $2_{1,1}$ | 3 | 2 | $2_{0,2}$ | 2 | 3 |
| 1944473.865 | 0.164 | −3.338 | 6.170E-05 | 47.139 | $2_{1,1}$ | 3 | 2 | $2_{0,2}$ | 2 | 2 |
| 1944476.251 | 0.144 | −2.596 | 3.408E-04 | 47.139 | $2_{1,1}$ | 3 | 2 | $2_{0,2}$ | 2 | 1 |
| 1949050.258 | 0.146 | −1.624 | 2.294E-03 | 47.139 | $2_{1,1}$ | 2 | 3 | $2_{0,2}$ | 2 | 3 |
| 1949053.253 | 0.166 | −2.533 | 3.955E-04 | 47.139 | $2_{1,1}$ | 2 | 2 | $2_{0,2}$ | 2 | 3 |
| 1949053.752 | 0.165 | −2.533 | 2.829E-04 | 47.139 | $2_{1,1}$ | 2 | 3 | $2_{0,2}$ | 2 | 2 |
| 1949056.747 | 0.145 | −1.876 | 1.798E-03 | 47.139 | $2_{1,1}$ | 2 | 2 | $2_{0,2}$ | 2 | 2 |
| 1949058.612 | 0.151 | −2.547 | 6.395E-04 | 47.139 | $2_{1,1}$ | 2 | 1 | $2_{0,2}$ | 2 | 2 |
| 1949059.134 | 0.163 | −2.546 | 3.841E-04 | 47.139 | $2_{1,1}$ | 2 | 2 | $2_{0,2}$ | 2 | 1 |
| 1949060.998 | 0.151 | −2.065 | 1.938E-03 | 47.139 | $2_{1,1}$ | 2 | 1 | $2_{0,2}$ | 2 | 1 |
| 1953316.457 | 0.258 | −7.395 | 9.093E-09 | 46.791 | $2_{1,1}$ | 1 | 1 | $2_{0,2}$ | 3 | 2 |
| 1953352.213 | 0.214 | −7.902 | 1.699E-09 | 46.791 | $2_{1,1}$ | 1 | 2 | $2_{0,2}$ | 3 | 2 |
| 1953383.607 | 0.171 | −6.960 | 1.486E-08 | 46.790 | $2_{1,1}$ | 1 | 2 | $2_{0,2}$ | 3 | 3 |
| 1954883.495 | 0.202 | −2.556 | 2.096E-04 | 46.790 | $2_{1,1}$ | 3 | 4 | $2_{0,2}$ | 3 | 3 |
| 1954885.924 | 0.188 | −2.562 | 2.659E-04 | 46.791 | $2_{1,1}$ | 3 | 3 | $2_{0,2}$ | 3 | 2 |
| 1954911.342 | 0.153 | −1.660 | 2.969E-03 | 46.791 | $2_{1,1}$ | 3 | 2 | $2_{0,2}$ | 3 | 2 |
| 1954917.318 | 0.144 | −1.538 | 2.807E-03 | 46.790 | $2_{1,1}$ | 3 | 3 | $2_{0,2}$ | 3 | 3 |
| 1954925.335 | 0.149 | −1.381 | 3.135E-03 | 46.788 | $2_{1,1}$ | 3 | 4 | $2_{0,2}$ | 3 | 4 |
| 1954942.736 | 0.163 | −2.560 | 3.739E-04 | 46.790 | $2_{1,1}$ | 3 | 2 | $2_{0,2}$ | 3 | 3 |
| 1954959.158 | 0.183 | −2.553 | 2.712E-04 | 46.788 | $2_{1,1}$ | 3 | 3 | $2_{0,2}$ | 3 | 4 |
| 1958077.292 | 0.160 | −2.286 | 1.174E-03 | 46.632 | $2_{1,1}$ | 1 | 1 | $2_{0,2}$ | 1 | 2 |
| 1958112.449 | 0.158 | −2.383 | 2.815E-03 | 46.630 | $2_{1,1}$ | 1 | 0 | $2_{0,2}$ | 1 | 1 |
| 1958113.048 | 0.146 | −1.811 | 2.102E-03 | 46.632 | $2_{1,1}$ | 1 | 2 | $2_{0,2}$ | 1 | 2 |
| 1958130.296 | 0.147 | −2.511 | 6.994E-04 | 46.630 | $2_{1,1}$ | 1 | 1 | $2_{0,2}$ | 1 | 1 |
| 1958156.782 | 0.162 | −2.382 | 9.404E-04 | 46.629 | $2_{1,1}$ | 1 | 1 | $2_{0,2}$ | 1 | 0 |
| 1958166.051 | 0.158 | −2.284 | 7.071E-04 | 46.630 | $2_{1,1}$ | 1 | 2 | $2_{0,2}$ | 1 | 1 |
| 1959491.230 | 0.228 | −4.841 | 1.403E-06 | 46.791 | $2_{1,1}$ | 2 | 3 | $2_{0,2}$ | 3 | 2 |
| 1959494.225 | 0.171 | −3.314 | 6.622E-05 | 46.791 | $2_{1,1}$ | 2 | 2 | $2_{0,2}$ | 3 | 2 |
| 1959496.089 | 0.143 | −2.592 | 5.812E-04 | 46.791 | $2_{1,1}$ | 2 | 1 | $2_{0,2}$ | 3 | 2 |
| 1959522.623 | 0.150 | −3.310 | 4.768E-05 | 46.790 | $2_{1,1}$ | 2 | 3 | $2_{0,2}$ | 3 | 3 |
| 1959525.619 | 0.117 | −2.423 | 5.142E-04 | 46.790 | $2_{1,1}$ | 2 | 2 | $2_{0,2}$ | 3 | 3 |
| 1959564.463 | 0.124 | −2.264 | 5.303E-04 | 46.788 | $2_{1,1}$ | 2 | 3 | $2_{0,2}$ | 3 | 4 |
| 1959646.759 | 0.177 | −6.891 | 1.249E-08 | 46.632 | $2_{1,1}$ | 3 | 3 | $2_{0,2}$ | 1 | 2 |
| 1959672.177 | 0.205 | −7.764 | 2.346E-09 | 46.632 | $2_{1,1}$ | 3 | 2 | $2_{0,2}$ | 1 | 2 |
| 1959725.181 | 0.239 | −7.328 | 6.401E-09 | 46.630 | $2_{1,1}$ | 3 | 2 | $2_{0,2}$ | 1 | 1 |
| 1964252.064 | 0.154 | −2.222 | 5.868E-04 | 46.632 | $2_{1,1}$ | 2 | 3 | $2_{0,2}$ | 1 | 2 |
| 1964255.060 | 0.134 | −2.963 | 1.490E-04 | 46.632 | $2_{1,1}$ | 2 | 2 | $2_{0,2}$ | 1 | 2 |
| 1964256.924 | 0.141 | −4.135 | 1.672E-05 | 46.632 | $2_{1,1}$ | 2 | 1 | $2_{0,2}$ | 1 | 2 |
| 1964308.063 | 0.151 | −2.497 | 4.356E-04 | 46.630 | $2_{1,1}$ | 2 | 2 | $2_{0,2}$ | 1 | 1 |
| 1964309.927 | 0.173 | −2.970 | 2.445E-04 | 46.630 | $2_{1,1}$ | 2 | 1 | $2_{0,2}$ | 1 | 1 |
| 1964336.414 | 0.204 | −2.850 | 3.219E-04 | 46.629 | $2_{1,1}$ | 2 | 1 | $2_{0,2}$ | 1 | 0 |
| 2079888.684 | 1.206 | −2.951 | 2.903E-04 | 156.218 | $4_{1,3}$ | 3 | 2 | $4_{0,4}$ | 4 | 3 |
| 2079916.537 | 1.202 | −2.832 | 2.730E-04 | 156.218 | $4_{1,3}$ | 3 | 3 | $4_{0,4}$ | 4 | 4 |
| 2079917.972 | 1.204 | −4.013 | 1.799E-05 | 156.218 | $4_{1,3}$ | 3 | 3 | $4_{0,4}$ | 4 | 3 |
| 2079953.877 | 1.206 | −2.715 | 2.779E-04 | 156.218 | $4_{1,3}$ | 3 | 4 | $4_{0,4}$ | 4 | 5 |
| 2079955.617 | 1.205 | −4.013 | 1.401E-05 | 156.218 | $4_{1,3}$ | 3 | 4 | $4_{0,4}$ | 4 | 4 |
| 2079957.053 | 1.205 | −5.818 | 2.193E-07 | 156.218 | $4_{1,3}$ | 3 | 4 | $4_{0,4}$ | 4 | 3 |
| 2080677.882 | 1.275 | −2.739 | 1.821E-04 | 156.218 | $4_{1,3}$ | 5 | 6 | $4_{0,4}$ | 4 | 5 |
| 2080714.211 | 1.276 | −4.215 | 7.205E-06 | 156.218 | $4_{1,3}$ | 5 | 5 | $4_{0,4}$ | 4 | 5 |
| 2080715.951 | 1.274 | −2.828 | 1.754E-04 | 156.218 | $4_{1,3}$ | 5 | 5 | $4_{0,4}$ | 4 | 4 |
| 2080744.504 | 1.283 | −6.213 | 8.841E-08 | 156.218 | $4_{1,3}$ | 5 | 4 | $4_{0,4}$ | 4 | 5 |
| 2080746.244 | 1.278 | −4.213 | 8.847E-06 | 156.218 | $4_{1,3}$ | 5 | 4 | $4_{0,4}$ | 4 | 4 |
| 2080747.680 | 1.276 | −2.919 | 1.740E-04 | 156.218 | $4_{1,3}$ | 5 | 4 | $4_{0,4}$ | 4 | 3 |
| 2089618.556 | 1.211 | −2.851 | 2.053E-04 | 156.218 | $4_{1,3}$ | 4 | 4 | $4_{0,4}$ | 4 | 5 |
| 2089619.419 | 1.211 | −2.852 | 2.629E-04 | 156.218 | $4_{1,3}$ | 4 | 3 | $4_{0,4}$ | 4 | 4 |
| 2089619.587 | 1.211 | −1.467 | 4.060E-03 | 156.218 | $4_{1,3}$ | 4 | 5 | $4_{0,4}$ | 4 | 5 |
| 2089620.296 | 1.211 | −1.581 | 3.819E-03 | 156.218 | $4_{1,3}$ | 4 | 4 | $4_{0,4}$ | 4 | 4 |
| 2089620.855 | 1.210 | −1.674 | 3.966E-03 | 156.218 | $4_{1,3}$ | 4 | 3 | $4_{0,4}$ | 4 | 3 |
| 2089621.327 | 1.211 | −2.851 | 1.680E-04 | 156.218 | $4_{1,3}$ | 4 | 5 | $4_{0,4}$ | 4 | 4 |
| 2089621.732 | 1.211 | −2.852 | 2.045E-04 | 156.218 | $4_{1,3}$ | 4 | 4 | $4_{0,4}$ | 4 | 3 |
| 2091278.659 | 1.261 | −7.997 | 1.883E-09 | 155.839 | $4_{1,3}$ | 3 | 3 | $4_{0,4}$ | 5 | 4 |
| 2091351.433 | 1.252 | −7.780 | 2.418E-09 | 155.838 | $4_{1,3}$ | 3 | 4 | $4_{0,4}$ | 5 | 5 |
| 2092075.438 | 1.248 | −2.904 | 1.259E-04 | 155.838 | $4_{1,3}$ | 5 | 6 | $4_{0,4}$ | 5 | 5 |

Table B.2: $CH_2$ transition frequency predictions - continued

| Frequency [MHz] | $\Delta\nu$ [MHz] | log$I$ [nm$^2$MHz] | $A$ [s$^{-1}$] | $E_{lower}$ [cm$^{-1}$] | $N'_{Ka',Kc'}$ | $J'$ | $F'$ | $N''_{Ka'',Kc''}$ | $J''$ | $F''$ |
|---|---|---|---|---|---|---|---|---|---|---|
| 2092078.073 | 1.249 | −2.905 | 1.482E-04 | 155.839 | $4_{1,3}$ | 5 | 5 | $4_{0,4}$ | 5 | 4 |
| 2092108.366 | 1.244 | −1.526 | 4.338E-03 | 155.839 | $4_{1,3}$ | 5 | 4 | $4_{0,4}$ | 5 | 4 |
| 2092111.766 | 1.242 | −1.451 | 4.223E-03 | 155.838 | $4_{1,3}$ | 5 | 5 | $4_{0,4}$ | 5 | 5 |
| 2092115.851 | 1.241 | −1.361 | 4.394E-03 | 155.836 | $4_{1,3}$ | 5 | 6 | $4_{0,4}$ | 5 | 6 |
| 2092142.059 | 1.244 | −2.905 | 1.813E-04 | 155.838 | $4_{1,3}$ | 5 | 4 | $4_{0,4}$ | 5 | 5 |
| 2092152.180 | 1.244 | −2.903 | 1.489E-04 | 155.836 | $4_{1,3}$ | 5 | 5 | $4_{0,4}$ | 5 | 6 |
| 2092722.533 | 1.207 | −2.722 | 3.556E-04 | 155.791 | $4_{1,3}$ | 3 | 3 | $4_{0,4}$ | 3 | 4 |
| 2092737.442 | 1.204 | −2.727 | 4.913E-04 | 155.789 | $4_{1,3}$ | 3 | 2 | $4_{0,4}$ | 3 | 3 |
| 2092761.614 | 1.207 | −1.547 | 4.136E-03 | 155.791 | $4_{1,3}$ | 3 | 4 | $4_{0,4}$ | 3 | 4 |
| 2092766.730 | 1.204 | −1.704 | 3.707E-03 | 155.789 | $4_{1,3}$ | 3 | 3 | $4_{0,4}$ | 3 | 3 |
| 2092770.570 | 1.204 | −1.825 | 3.923E-03 | 155.788 | $4_{1,3}$ | 3 | 2 | $4_{0,4}$ | 3 | 2 |
| 2092799.858 | 1.207 | −2.727 | 3.512E-04 | 155.788 | $4_{1,3}$ | 3 | 3 | $4_{0,4}$ | 3 | 2 |
| 2092805.811 | 1.208 | −2.721 | 2.768E-04 | 155.789 | $4_{1,3}$ | 3 | 4 | $4_{0,4}$ | 3 | 3 |
| 2093521.948 | 1.272 | −7.799 | 1.894E-09 | 155.791 | $4_{1,3}$ | 5 | 5 | $4_{0,4}$ | 3 | 4 |
| 2093552.241 | 1.274 | −9.092 | 1.180E-10 | 155.791 | $4_{1,3}$ | 5 | 4 | $4_{0,4}$ | 3 | 4 |
| 2093596.438 | 1.277 | −8.019 | 1.397E-09 | 155.789 | $4_{1,3}$ | 5 | 4 | $4_{0,4}$ | 3 | 3 |
| 2100981.541 | 1.244 | −2.911 | 2.319E-04 | 155.839 | $4_{1,3}$ | 4 | 3 | $4_{0,4}$ | 5 | 4 |
| 2100982.418 | 1.247 | −4.194 | 9.389E-06 | 155.839 | $4_{1,3}$ | 4 | 4 | $4_{0,4}$ | 5 | 4 |
| 2100983.449 | 1.252 | −6.183 | 7.888E-08 | 155.839 | $4_{1,3}$ | 4 | 5 | $4_{0,4}$ | 5 | 4 |
| 2101016.111 | 1.240 | −2.820 | 2.221E-04 | 155.838 | $4_{1,3}$ | 4 | 4 | $4_{0,4}$ | 5 | 5 |
| 2101017.142 | 1.242 | −4.194 | 7.688E-06 | 155.838 | $4_{1,3}$ | 4 | 5 | $4_{0,4}$ | 5 | 5 |
| 2101057.556 | 1.240 | −2.731 | 2.232E-04 | 155.836 | $4_{1,3}$ | 4 | 5 | $4_{0,4}$ | 5 | 6 |
| 2102425.416 | 1.211 | −5.788 | 3.083E-07 | 155.791 | $4_{1,3}$ | 4 | 3 | $4_{0,4}$ | 3 | 4 |
| 2102426.293 | 1.212 | −3.992 | 1.497E-05 | 155.791 | $4_{1,3}$ | 4 | 4 | $4_{0,4}$ | 3 | 4 |
| 2102427.324 | 1.214 | −2.707 | 2.365E-04 | 155.791 | $4_{1,3}$ | 4 | 5 | $4_{0,4}$ | 3 | 4 |
| 2102469.613 | 1.212 | −3.995 | 1.911E-05 | 155.789 | $4_{1,3}$ | 4 | 3 | $4_{0,4}$ | 3 | 3 |
| 2102470.490 | 1.211 | −2.824 | 2.207E-04 | 155.789 | $4_{1,3}$ | 4 | 4 | $4_{0,4}$ | 3 | 3 |
| 2102502.741 | 1.217 | −2.943 | 2.156E-04 | 155.788 | $4_{1,3}$ | 4 | 3 | $4_{0,4}$ | 3 | 2 |
| 2306192.662 | 6.840 | −4.958 | 3.062E-06 | 326.816 | $6_{1,5}$ | 7 | 6 | $6_{0,6}$ | 6 | 6 |
| 2306193.696 | 6.839 | −3.337 | 1.279E-04 | 326.816 | $6_{1,5}$ | 7 | 6 | $6_{0,6}$ | 6 | 5 |
| 2306444.018 | 6.730 | −3.348 | 1.804E-04 | 326.816 | $6_{1,5}$ | 5 | 4 | $6_{0,6}$ | 6 | 5 |
| 2306475.139 | 6.732 | −3.272 | 1.760E-04 | 326.816 | $6_{1,5}$ | 5 | 5 | $6_{0,6}$ | 6 | 6 |
| 2306476.173 | 6.732 | −4.821 | 4.964E-06 | 326.816 | $6_{1,5}$ | 5 | 5 | $6_{0,6}$ | 6 | 5 |
| 2306513.750 | 6.735 | −4.821 | 4.205E-06 | 326.816 | $6_{1,5}$ | 5 | 6 | $6_{0,6}$ | 6 | 6 |
| 2306514.784 | 6.735 | −6.978 | 2.926E-08 | 326.816 | $6_{1,5}$ | 5 | 6 | $6_{0,6}$ | 6 | 5 |
| 2316460.531 | 6.746 | −3.283 | 1.731E-04 | 326.816 | $6_{1,5}$ | 6 | 5 | $6_{0,6}$ | 6 | 6 |
| 2316461.480 | 6.746 | −1.672 | 5.970E-03 | 326.816 | $6_{1,5}$ | 6 | 6 | $6_{0,6}$ | 6 | 6 |
| 2316461.565 | 6.746 | −1.736 | 6.090E-03 | 326.816 | $6_{1,5}$ | 6 | 5 | $6_{0,6}$ | 6 | 5 |
| 2316462.514 | 6.745 | −3.282 | 1.465E-04 | 326.816 | $6_{1,5}$ | 6 | 6 | $6_{0,6}$ | 6 | 5 |
| 2318187.868 | 6.760 | −1.647 | 6.324E-03 | 326.416 | $6_{1,5}$ | 7 | 6 | $6_{0,6}$ | 7 | 6 |
| 2318233.426 | 6.851 | −8.380 | 1.170E-09 | 326.414 | $6_{1,5}$ | 7 | 6 | $6_{0,6}$ | 5 | 6 |
| 2318275.242 | 6.851 | −8.460 | 9.737E-10 | 326.413 | $6_{1,5}$ | 7 | 6 | $6_{0,6}$ | 5 | 5 |
| 2318470.344 | 6.791 | −8.637 | 7.657E-10 | 326.416 | $6_{1,5}$ | 5 | 5 | $6_{0,6}$ | 7 | 6 |
| 2318508.955 | 6.793 | −8.153 | 1.973E-09 | 326.416 | $6_{1,5}$ | 5 | 6 | $6_{0,6}$ | 7 | 6 |
| 2318515.903 | 6.732 | −3.197 | 2.109E-04 | 326.414 | $6_{1,5}$ | 5 | 5 | $6_{0,6}$ | 5 | 6 |
| 2318525.563 | 6.730 | −3.198 | 2.569E-04 | 326.413 | $6_{1,5}$ | 5 | 4 | $6_{0,6}$ | 5 | 5 |
| 2318554.514 | 6.734 | −1.654 | 6.229E-03 | 326.414 | $6_{1,5}$ | 5 | 6 | $6_{0,6}$ | 5 | 6 |
| 2318557.718 | 6.732 | −1.744 | 5.987E-03 | 326.413 | $6_{1,5}$ | 5 | 5 | $6_{0,6}$ | 5 | 5 |
| 2318560.389 | 6.731 | −1.819 | 6.152E-03 | 326.412 | $6_{1,5}$ | 5 | 4 | $6_{0,6}$ | 5 | 4 |
| 2318592.544 | 6.733 | −3.198 | 2.103E-04 | 326.412 | $6_{1,5}$ | 5 | 5 | $6_{0,6}$ | 5 | 4 |
| 2318596.329 | 6.735 | −3.196 | 1.786E-04 | 326.413 | $6_{1,5}$ | 5 | 6 | $6_{0,6}$ | 5 | 5 |
| 2321839.757 | 3.754 | −7.863 | 3.056E-09 | 78.340 | $4_{0,4}$ | 3 | 2 | $1_{1,1}$ | 2 | 1 |
| 2321858.059 | 3.755 | −8.593 | 5.683E-10 | 78.339 | $4_{0,4}$ | 3 | 2 | $1_{1,1}$ | 2 | 2 |
| 2321891.188 | 3.756 | −7.691 | 3.237E-09 | 78.339 | $4_{0,4}$ | 3 | 3 | $1_{1,1}$ | 2 | 2 |
| 2321918.874 | 3.766 | −8.592 | 4.073E-10 | 78.338 | $4_{0,4}$ | 3 | 3 | $1_{1,1}$ | 2 | 3 |
| 2321963.071 | 3.772 | −7.530 | 3.650E-09 | 78.338 | $4_{0,4}$ | 3 | 4 | $1_{1,1}$ | 2 | 3 |
| 2328455.736 | 6.773 | −3.329 | 1.570E-04 | 326.416 | $6_{1,5}$ | 6 | 5 | $6_{0,6}$ | 7 | 6 |
| 2328456.685 | 6.773 | −4.943 | 3.228E-06 | 326.416 | $6_{1,5}$ | 6 | 6 | $6_{0,6}$ | 7 | 6 |
| 2328501.295 | 6.751 | −6.975 | 3.544E-08 | 326.414 | $6_{1,5}$ | 6 | 5 | $6_{0,6}$ | 5 | 6 |
| 2328502.244 | 6.751 | −4.800 | 4.490E-06 | 326.414 | $6_{1,5}$ | 6 | 6 | $6_{0,6}$ | 5 | 6 |
| 2328543.110 | 6.751 | −4.802 | 5.272E-06 | 326.413 | $6_{1,5}$ | 6 | 5 | $6_{0,6}$ | 5 | 5 |
| 2328544.059 | 6.751 | −3.264 | 1.543E-04 | 326.413 | $6_{1,5}$ | 6 | 6 | $6_{0,6}$ | 5 | 5 |
| 2328577.936 | 6.753 | −3.340 | 1.530E-04 | 326.412 | $6_{1,5}$ | 6 | 5 | $6_{0,6}$ | 5 | 4 |
| 2344681.627 | 0.528 | −2.096 | 1.251E-03 | −0.002 | $1_{1,1}$ | 1 | 2 | $0_{0,0}$ | 1 | 1 |
| 2344694.486 | 0.546 | −2.189 | 1.681E-03 | −0.001 | $1_{1,1}$ | 1 | 1 | $0_{0,0}$ | 1 | 0 |
| 2344717.463 | 0.524 | −2.305 | 1.288E-03 | −0.002 | $1_{1,1}$ | 1 | 1 | $0_{0,0}$ | 1 | 1 |

Table B.2: $CH_2$ transition frequency predictions - continued

| Frequency [MHz] | $\Delta\nu$ [MHz] | log$I$ [nm$^2$MHz] | $A$ [s$^{-1}$] | $E_{lower}$ [cm$^{-1}$] | $N'_{Ka',Kc'}$ | $J'$ | $F'$ | $N''_{Ka'',Kc''}$ | $J''$ | $F''$ |
|---|---|---|---|---|---|---|---|---|---|---|
| 2344727.580 | 0.532 | −1.607 | 3.859E-03 | −0.004 | $1_{1,1}$ | 1 | 2 | $0_{0,0}$ | 1 | 2 |
| 2344735.467 | 0.527 | −2.184 | 5.110E-03 | −0.002 | $1_{1,1}$ | 1 | 0 | $0_{0,0}$ | 1 | 1 |
| 2344763.416 | 0.554 | −2.084 | 2.142E-03 | −0.004 | $1_{1,1}$ | 1 | 1 | $0_{0,0}$ | 1 | 2 |
| 2348606.325 | 0.515 | −1.960 | 2.858E-03 | −0.001 | $1_{1,1}$ | 2 | 1 | $0_{0,0}$ | 1 | 0 |
| 2348610.999 | 0.512 | −1.608 | 3.858E-03 | −0.002 | $1_{1,1}$ | 2 | 2 | $0_{0,0}$ | 1 | 1 |
| 2348629.266 | 0.513 | −1.340 | 5.109E-03 | −0.004 | $1_{1,1}$ | 2 | 3 | $0_{0,0}$ | 1 | 2 |
| 2348629.302 | 0.524 | −2.091 | 2.114E-03 | −0.002 | $1_{1,1}$ | 2 | 1 | $0_{0,0}$ | 1 | 1 |
| 2348656.952 | 0.558 | −2.097 | 1.251E-03 | −0.004 | $1_{1,1}$ | 2 | 2 | $0_{0,0}$ | 1 | 2 |
| 2348675.255 | 0.611 | −3.279 | 1.370E-04 | −0.004 | $1_{1,1}$ | 2 | 1 | $0_{0,0}$ | 1 | 2 |
| 2354694.619 | 0.574 | −2.662 | 5.709E-04 | −0.001 | $1_{1,1}$ | 0 | 1 | $0_{0,0}$ | 1 | 0 |
| 2354717.595 | 0.547 | −2.186 | 1.708E-03 | −0.002 | $1_{1,1}$ | 0 | 1 | $0_{0,0}$ | 1 | 1 |
| 2354763.548 | 0.564 | −1.967 | 2.831E-03 | −0.004 | $1_{1,1}$ | 0 | 1 | $0_{0,0}$ | 1 | 2 |
| 3012666.249 | 14.902 | −9.052 | 3.751E-10 | 225.920 | $6_{0,6}$ | 5 | 4 | $4_{1,3}$ | 4 | 4 |
| 3012667.126 | 14.902 | −7.765 | 7.261E-09 | 225.920 | $6_{0,6}$ | 5 | 4 | $4_{1,3}$ | 4 | 3 |
| 3012700.044 | 14.904 | −9.053 | 3.061E-10 | 225.920 | $6_{0,6}$ | 5 | 5 | $4_{1,3}$ | 4 | 5 |
| 3012701.075 | 14.903 | −7.675 | 7.307E-09 | 225.920 | $6_{0,6}$ | 5 | 5 | $4_{1,3}$ | 4 | 4 |
| 3012741.859 | 14.906 | −7.587 | 7.579E-09 | 225.920 | $6_{0,6}$ | 5 | 6 | $4_{1,3}$ | 4 | 5 |
| 3033656.672 | 14.910 | −7.749 | 6.235E-09 | 225.624 | $6_{0,6}$ | 6 | 5 | $4_{1,3}$ | 5 | 4 |
| 3033686.965 | 14.912 | −9.219 | 2.115E-10 | 225.623 | $6_{0,6}$ | 6 | 5 | $4_{1,3}$ | 5 | 5 |
| 3033687.999 | 14.912 | −7.672 | 6.302E-09 | 225.623 | $6_{0,6}$ | 6 | 6 | $4_{1,3}$ | 5 | 5 |
| 3033724.328 | 14.915 | −9.217 | 1.799E-10 | 225.622 | $6_{0,6}$ | 6 | 6 | $4_{1,3}$ | 5 | 6 |
| 3188207.272 | 3.734 | −3.034 | 5.573E-04 | 47.139 | $3_{1,3}$ | 2 | 1 | $2_{0,2}$ | 2 | 2 |
| 3188209.659 | 3.732 | −2.557 | 1.670E-03 | 47.139 | $3_{1,3}$ | 2 | 1 | $2_{0,2}$ | 2 | 1 |
| 3188229.907 | 3.739 | −3.016 | 3.481E-04 | 47.139 | $3_{1,3}$ | 2 | 2 | $2_{0,2}$ | 2 | 3 |
| 3188233.401 | 3.734 | −2.367 | 1.551E-03 | 47.139 | $3_{1,3}$ | 2 | 2 | $2_{0,2}$ | 2 | 2 |
| 3188235.788 | 3.732 | −3.034 | 3.339E-04 | 47.139 | $3_{1,3}$ | 2 | 2 | $2_{0,2}$ | 2 | 1 |
| 3188269.129 | 3.743 | −2.112 | 1.994E-03 | 47.139 | $3_{1,3}$ | 2 | 3 | $2_{0,2}$ | 2 | 3 |
| 3188272.623 | 3.737 | −3.017 | 2.481E-04 | 47.139 | $3_{1,3}$ | 2 | 3 | $2_{0,2}$ | 2 | 2 |
| 3190322.616 | 3.754 | −8.190 | 1.298E-09 | 47.139 | $3_{1,3}$ | 4 | 4 | $2_{0,2}$ | 2 | 3 |
| 3190351.330 | 3.763 | −9.406 | 1.014E-10 | 47.139 | $3_{1,3}$ | 4 | 3 | $2_{0,2}$ | 2 | 3 |
| 3190354.824 | 3.754 | −8.455 | 9.076E-10 | 47.139 | $3_{1,3}$ | 4 | 3 | $2_{0,2}$ | 2 | 2 |
| 3198644.750 | 3.740 | −3.948 | 6.822E-05 | 46.791 | $3_{1,3}$ | 2 | 1 | $2_{0,2}$ | 3 | 2 |
| 3198670.878 | 3.738 | −4.714 | 7.025E-06 | 46.791 | $3_{1,3}$ | 2 | 2 | $2_{0,2}$ | 3 | 2 |
| 3198702.272 | 3.740 | −3.775 | 6.096E-05 | 46.790 | $3_{1,3}$ | 2 | 2 | $2_{0,2}$ | 3 | 3 |
| 3198710.100 | 3.738 | −6.308 | 1.277E-07 | 46.791 | $3_{1,3}$ | 2 | 3 | $2_{0,2}$ | 3 | 2 |
| 3198741.494 | 3.742 | −4.728 | 4.849E-06 | 46.790 | $3_{1,3}$ | 2 | 3 | $2_{0,2}$ | 3 | 3 |
| 3198783.334 | 3.751 | −3.617 | 6.266E-05 | 46.788 | $3_{1,3}$ | 2 | 3 | $2_{0,2}$ | 3 | 4 |
| 3199414.258 | 3.741 | −3.815 | 5.578E-05 | 47.139 | $3_{1,3}$ | 3 | 2 | $2_{0,2}$ | 2 | 3 |
| 3199414.758 | 3.737 | −2.268 | 1.402E-03 | 47.139 | $3_{1,3}$ | 3 | 3 | $2_{0,2}$ | 2 | 3 |
| 3199415.353 | 3.732 | −1.202 | 1.270E-02 | 47.139 | $3_{1,3}$ | 3 | 4 | $2_{0,2}$ | 2 | 3 |
| 3199417.752 | 3.734 | −2.267 | 1.967E-03 | 47.139 | $3_{1,3}$ | 3 | 2 | $2_{0,2}$ | 2 | 2 |
| 3199418.252 | 3.731 | −1.362 | 1.130E-02 | 47.139 | $3_{1,3}$ | 3 | 3 | $2_{0,2}$ | 2 | 2 |
| 3199420.139 | 3.731 | −1.533 | 1.067E-02 | 47.139 | $3_{1,3}$ | 3 | 2 | $2_{0,2}$ | 2 | 1 |
| 3200792.302 | 3.741 | −1.297 | 1.310E-02 | 46.791 | $3_{1,3}$ | 4 | 3 | $2_{0,2}$ | 3 | 2 |
| 3200794.981 | 3.741 | −1.179 | 1.337E-02 | 46.790 | $3_{1,3}$ | 4 | 4 | $2_{0,2}$ | 3 | 3 |
| 3200800.953 | 3.741 | −1.064 | 1.427E-02 | 46.788 | $3_{1,3}$ | 4 | 5 | $2_{0,2}$ | 3 | 4 |
| 3200823.695 | 3.748 | −2.354 | 1.150E-03 | 46.790 | $3_{1,3}$ | 4 | 3 | $2_{0,2}$ | 3 | 3 |
| 3200836.821 | 3.750 | −2.354 | 8.949E-04 | 46.788 | $3_{1,3}$ | 4 | 4 | $2_{0,2}$ | 3 | 4 |
| 3200865.536 | 3.760 | −4.152 | 1.832E-05 | 46.788 | $3_{1,3}$ | 4 | 3 | $2_{0,2}$ | 3 | 4 |
| 3203405.585 | 3.727 | −3.259 | 3.339E-04 | 46.632 | $3_{1,3}$ | 2 | 1 | $2_{0,2}$ | 1 | 2 |
| 3203431.713 | 3.727 | −2.084 | 2.999E-03 | 46.632 | $3_{1,3}$ | 2 | 2 | $2_{0,2}$ | 1 | 2 |
| 3203458.588 | 3.727 | −2.085 | 4.993E-03 | 46.630 | $3_{1,3}$ | 2 | 1 | $2_{0,2}$ | 1 | 1 |
| 3203470.935 | 3.729 | −1.337 | 1.196E-02 | 46.632 | $3_{1,3}$ | 2 | 3 | $2_{0,2}$ | 1 | 2 |
| 3203484.717 | 3.728 | −1.608 | 8.969E-03 | 46.630 | $3_{1,3}$ | 2 | 2 | $2_{0,2}$ | 1 | 1 |
| 3203485.075 | 3.728 | −1.960 | 6.646E-03 | 46.629 | $3_{1,3}$ | 2 | 1 | $2_{0,2}$ | 1 | 0 |
| 3209855.230 | 3.736 | −2.417 | 1.401E-03 | 46.791 | $3_{1,3}$ | 3 | 2 | $2_{0,2}$ | 3 | 2 |
| 3209855.730 | 3.733 | −3.317 | 1.258E-04 | 46.791 | $3_{1,3}$ | 3 | 3 | $2_{0,2}$ | 3 | 2 |
| 3209886.624 | 3.739 | −3.321 | 1.745E-04 | 46.790 | $3_{1,3}$ | 3 | 2 | $2_{0,2}$ | 3 | 3 |
| 3209887.123 | 3.736 | −2.296 | 1.321E-03 | 46.790 | $3_{1,3}$ | 3 | 3 | $2_{0,2}$ | 3 | 3 |
| 3209887.718 | 3.732 | −3.312 | 9.909E-05 | 46.790 | $3_{1,3}$ | 3 | 4 | $2_{0,2}$ | 3 | 3 |
| 3209928.964 | 3.744 | −3.317 | 1.259E-04 | 46.788 | $3_{1,3}$ | 3 | 3 | $2_{0,2}$ | 3 | 4 |
| 3209929.559 | 3.739 | −2.141 | 1.470E-03 | 46.788 | $3_{1,3}$ | 3 | 4 | $2_{0,2}$ | 3 | 4 |
| 3214616.564 | 3.725 | −8.671 | 5.591E-10 | 46.632 | $3_{1,3}$ | 3 | 3 | $2_{0,2}$ | 1 | 2 |
| 3214669.068 | 3.731 | −9.102 | 2.898E-10 | 46.630 | $3_{1,3}$ | 3 | 2 | $2_{0,2}$ | 1 | 1 |
| 3356110.583 | 0.572 | −6.769 | 9.059E-08 | −0.001 | $2_{1,1}$ | 1 | 1 | $0_{0,0}$ | 1 | 0 |
| 3356115.713 | 0.544 | −6.769 | 2.718E-07 | −0.002 | $2_{1,1}$ | 1 | 0 | $0_{0,0}$ | 1 | 1 |

Table B.2: $CH_2$ transition frequency predictions - continued

| Frequency [MHz] | $\Delta\nu$ [MHz] | log$I$ [nm$^2$MHz] | $A$ [s$^{-1}$] | $E_{lower}$ [cm$^{-1}$] | $N'_{Ka',Kc'}$ | $J'$ | $F'$ | $N''_{Ka'',Kc''}$ | $J''$ | $F''$ |
|---|---|---|---|---|---|---|---|---|---|---|
| 3356133.559 | 0.538 | −6.897 | 6.745E-08 | −0.002 | $2_{1,1}$ | 1 | 1 | $0_{0,0}$ | 1 | 1 |
| 3356169.315 | 0.535 | −6.670 | 6.824E-08 | −0.002 | $2_{1,1}$ | 1 | 2 | $0_{0,0}$ | 1 | 1 |
| 3356179.513 | 0.540 | −6.671 | 1.137E-07 | −0.004 | $2_{1,1}$ | 1 | 1 | $0_{0,0}$ | 1 | 2 |
| 3356215.268 | 0.563 | −6.196 | 2.034E-07 | −0.004 | $2_{1,1}$ | 1 | 2 | $0_{0,0}$ | 1 | 2 |
| 3362290.215 | 0.542 | −7.195 | 3.411E-08 | −0.001 | $2_{1,1}$ | 2 | 1 | $0_{0,0}$ | 1 | 0 |
| 3362311.327 | 0.532 | −6.841 | 4.624E-08 | −0.002 | $2_{1,1}$ | 2 | 2 | $0_{0,0}$ | 1 | 1 |
| 3362313.191 | 0.530 | −7.315 | 2.590E-08 | −0.002 | $2_{1,1}$ | 2 | 1 | $0_{0,0}$ | 1 | 1 |
| 3362354.285 | 0.544 | −6.564 | 6.245E-08 | −0.004 | $2_{1,1}$ | 2 | 3 | $0_{0,0}$ | 1 | 2 |
| 3362357.280 | 0.562 | −7.307 | 1.581E-08 | −0.004 | $2_{1,1}$ | 2 | 2 | $0_{0,0}$ | 1 | 2 |
| 3362359.144 | 0.578 | −8.480 | 1.770E-09 | −0.004 | $2_{1,1}$ | 2 | 1 | $0_{0,0}$ | 1 | 2 |
| 3976427.534 | 15.040 | −3.844 | 9.717E-05 | 156.218 | $5_{1,5}$ | 4 | 3 | $4_{0,4}$ | 4 | 4 |
| 3976428.970 | 15.040 | −2.668 | 1.457E-03 | 156.218 | $5_{1,5}$ | 4 | 3 | $4_{0,4}$ | 4 | 3 |
| 3976457.137 | 15.042 | −3.840 | 7.624E-05 | 156.218 | $5_{1,5}$ | 4 | 4 | $4_{0,4}$ | 4 | 5 |
| 3976458.878 | 15.041 | −2.574 | 1.406E-03 | 156.218 | $5_{1,5}$ | 4 | 4 | $4_{0,4}$ | 4 | 4 |
| 3976460.314 | 15.040 | −3.842 | 7.587E-05 | 156.218 | $5_{1,5}$ | 4 | 4 | $4_{0,4}$ | 4 | 3 |
| 3976496.339 | 15.043 | −2.458 | 1.501E-03 | 156.218 | $5_{1,5}$ | 4 | 5 | $4_{0,4}$ | 4 | 5 |
| 3976498.079 | 15.042 | −3.838 | 6.268E-05 | 156.218 | $5_{1,5}$ | 4 | 5 | $4_{0,4}$ | 4 | 4 |
| 3987789.656 | 15.045 | −4.608 | 1.676E-05 | 155.839 | $5_{1,5}$ | 4 | 3 | $4_{0,4}$ | 5 | 4 |
| 3987821.000 | 15.045 | −5.995 | 5.353E-07 | 155.839 | $5_{1,5}$ | 4 | 4 | $4_{0,4}$ | 5 | 4 |
| 3987854.693 | 15.046 | −4.515 | 1.617E-05 | 155.838 | $5_{1,5}$ | 4 | 4 | $4_{0,4}$ | 5 | 5 |
| 3987860.202 | 15.046 | −8.103 | 3.413E-09 | 155.839 | $5_{1,5}$ | 4 | 5 | $4_{0,4}$ | 5 | 4 |
| 3987893.895 | 15.047 | −6.021 | 4.124E-07 | 155.838 | $5_{1,5}$ | 4 | 5 | $4_{0,4}$ | 5 | 5 |
| 3987934.308 | 15.050 | −4.427 | 1.621E-05 | 155.836 | $5_{1,5}$ | 4 | 5 | $4_{0,4}$ | 5 | 6 |
| 3988502.430 | 15.045 | −4.551 | 1.492E-05 | 156.218 | $5_{1,5}$ | 5 | 4 | $4_{0,4}$ | 4 | 5 |
| 3988503.478 | 15.044 | −2.553 | 1.214E-03 | 156.218 | $5_{1,5}$ | 5 | 5 | $4_{0,4}$ | 4 | 5 |
| 3988504.171 | 15.044 | −2.553 | 1.485E-03 | 156.218 | $5_{1,5}$ | 5 | 4 | $4_{0,4}$ | 4 | 4 |
| 3988504.690 | 15.043 | −1.080 | 3.052E-02 | 156.218 | $5_{1,5}$ | 5 | 6 | $4_{0,4}$ | 4 | 5 |
| 3988505.218 | 15.043 | −1.170 | 2.931E-02 | 156.218 | $5_{1,5}$ | 5 | 5 | $4_{0,4}$ | 4 | 4 |
| 3988505.607 | 15.043 | −1.262 | 2.901E-02 | 156.218 | $5_{1,5}$ | 5 | 4 | $4_{0,4}$ | 4 | 3 |
| 3988571.034 | 15.056 | −1.149 | 3.072E-02 | 155.839 | $5_{1,5}$ | 6 | 5 | $4_{0,4}$ | 5 | 4 |
| 3988573.160 | 15.056 | −1.074 | 3.089E-02 | 155.838 | $5_{1,5}$ | 6 | 6 | $4_{0,4}$ | 5 | 5 |
| 3988604.727 | 15.059 | −2.617 | 1.045E-03 | 155.838 | $5_{1,5}$ | 6 | 5 | $4_{0,4}$ | 5 | 5 |
| 3988613.574 | 15.059 | −2.617 | 8.850E-04 | 155.836 | $5_{1,5}$ | 6 | 6 | $4_{0,4}$ | 5 | 6 |
| 3988645.140 | 15.062 | −4.772 | 7.330E-06 | 155.836 | $5_{1,5}$ | 6 | 5 | $4_{0,4}$ | 5 | 6 |
| 3989233.531 | 15.039 | −4.245 | 3.872E-05 | 155.791 | $5_{1,5}$ | 4 | 3 | $4_{0,4}$ | 3 | 4 |
| 3989264.875 | 15.039 | −2.447 | 1.893E-03 | 155.791 | $5_{1,5}$ | 4 | 4 | $4_{0,4}$ | 3 | 4 |
| 3989277.728 | 15.039 | −2.447 | 2.432E-03 | 155.789 | $5_{1,5}$ | 4 | 3 | $4_{0,4}$ | 3 | 3 |
| 3989304.076 | 15.040 | −1.157 | 3.019E-02 | 155.791 | $5_{1,5}$ | 4 | 5 | $4_{0,4}$ | 3 | 4 |
| 3989309.071 | 15.040 | −1.272 | 2.831E-02 | 155.789 | $5_{1,5}$ | 4 | 4 | $4_{0,4}$ | 3 | 3 |
| 3989310.856 | 15.040 | −1.390 | 2.773E-02 | 155.788 | $5_{1,5}$ | 4 | 3 | $4_{0,4}$ | 3 | 2 |
| 3999866.293 | 15.048 | −2.641 | 1.218E-03 | 155.839 | $5_{1,5}$ | 5 | 4 | $4_{0,4}$ | 5 | 4 |
| 3999867.340 | 15.047 | −4.022 | 4.145E-05 | 155.839 | $5_{1,5}$ | 5 | 5 | $4_{0,4}$ | 5 | 4 |
| 3999899.986 | 15.049 | −4.022 | 5.062E-05 | 155.838 | $5_{1,5}$ | 5 | 4 | $4_{0,4}$ | 5 | 5 |
| 3999901.033 | 15.048 | −2.566 | 1.183E-03 | 155.838 | $5_{1,5}$ | 5 | 5 | $4_{0,4}$ | 5 | 5 |
| 3999902.245 | 15.047 | −4.021 | 3.510E-05 | 155.838 | $5_{1,5}$ | 5 | 6 | $4_{0,4}$ | 5 | 5 |
| 3999941.447 | 15.051 | −4.022 | 4.144E-05 | 155.836 | $5_{1,5}$ | 5 | 5 | $4_{0,4}$ | 5 | 6 |
| 3999942.658 | 15.050 | −2.477 | 1.228E-03 | 155.836 | $5_{1,5}$ | 5 | 6 | $4_{0,4}$ | 5 | 6 |
| 4001311.215 | 15.041 | −9.457 | 1.520E-10 | 155.791 | $5_{1,5}$ | 5 | 5 | $4_{0,4}$ | 3 | 4 |
| 4001354.364 | 15.043 | −9.662 | 1.161E-10 | 155.789 | $5_{1,5}$ | 5 | 4 | $4_{0,4}$ | 3 | 3 |
| 4601438.876 | 4.193 | −6.612 | 2.447E-07 | −0.001 | $3_{1,3}$ | 2 | 1 | $0_{0,0}$ | 1 | 0 |
| 4601461.852 | 4.193 | −6.735 | 1.842E-07 | −0.002 | $3_{1,3}$ | 2 | 1 | $0_{0,0}$ | 1 | 1 |
| 4601487.980 | 4.193 | −6.259 | 3.307E-07 | −0.002 | $3_{1,3}$ | 2 | 2 | $0_{0,0}$ | 1 | 1 |
| 4601507.805 | 4.203 | −7.908 | 1.237E-08 | −0.004 | $3_{1,3}$ | 2 | 1 | $0_{0,0}$ | 1 | 2 |
| 4601533.933 | 4.205 | −6.733 | 1.110E-07 | −0.004 | $3_{1,3}$ | 2 | 2 | $0_{0,0}$ | 1 | 2 |
| 4601573.155 | 4.211 | −5.987 | 4.425E-07 | −0.004 | $3_{1,3}$ | 2 | 3 | $0_{0,0}$ | 1 | 2 |

# C

# Experimental Data - Water

## C.1 $D_2O$

Table C.1: Rotational transitions of $D_2O$ in the ground and first excited bending mode. Next to the at Cologne, Kiel and at the JPL newly measured lines, all to date available high-resolution microwave data is given. Not included in this compilation is FIR and IR Fourier Transform data.

| $N'_{Ka'Kc'}$ | $N''_{Ka'',Kc''}$ | Frequency [MHz][a] | o.-c. [MHz] | Reference |
|---|---|---|---|---|
| | | $v_2 = 0$ | | |
| $3_{1,3}$ | $2_{2,0}$ | 10919.422(7) | −0.015 | This work, Kiel |
| $4_{4,1}$ | $5_{3,2}$ | 10947.134(4) | −0.004 | This work, Kiel |
| $8_{7,2}$ | $9_{6,3}$ | 30182.490(50) | −0.087 | [150] |
| $8_{7,1}$ | $9_{6,4}$ | 30778.500(50) | −0.105 | [150] |
| $4_{2,3}$ | $3_{3,0}$ | 43414.560(50) | 0.018 | [150] |
| $4_{4,0}$ | $5_{3,3}$ | 55482.320(50) | −0.107 | [150] |
| $8_{5,4}$ | $7_{6,1}$ | 70240.630(50) | −0.002 | [150] |
| $8_{5,3}$ | $7_{6,2}$ | 74471.690(50) | −0.018 | [150] |
| $6_{1,6}$ | $5_{2,3}$ | 93350.060(50) | −0.120 | [150] |
| $9_{8,2}$ | $10_{7,3}$ | 103076.400(50) | −0.103 | [150] |
| $9_{8,1}$ | $10_{7,4}$ | 103152.890(50) | −0.124 | [150] |
| $6_{2,4}$ | $7_{1,7}$ | 104875.710(50) | −0.006 | [150] |
| $11_{2,10}$ | $10_{3,7}$ | 120183.280(50) | 0.063 | [150] |
| $10_{9,2}$ | $11_{8,3}$ | 145134.800(50) | 0.175 | [150] |
| $10_{9,1}$ | $11_{8,4}$ | 145143.820(50) | −0.051 | [150] |
| $4_{1,4}$ | $3_{2,1}$ | 151710.400(50) | 0.018 | [150] |
| $5_{5,1}$ | $6_{4,2}$ | 180171.220(50) | 0.123 | [150] |
| $5_{1,5}$ | $4_{2,2}$ | 181833.020(50) | −0.150 | [150] |
| $5_{5,0}$ | $6_{4,3}$ | 187633.100(50) | −0.096 | [150] |
| $7_{4,4}$ | $6_{5,1}$ | 192519.440(50) | −0.084 | [150] |
| $12_{8,5}$ | $11_{9,2}$ | 215689.010(50) | 0.027 | [150] |

Table C.1: $D_2O$ - continued

| $N'_{Ka'Kc'}$ | $N''_{Ka'',Kc''}$ | Frequency [MHz][a] | o.-c. [MHz] | Reference |
|---|---|---|---|---|
| $12_{8,4}$ | $11_{9,3}$ | 215731.730(50) | −0.010 | [150] |
| $7_{4,3}$ | $6_{5,2}$ | 218442.500(50) | 0.014 | [150] |
| $4_{2,2}$ | $3_{3,1}$ | 227010.500(50) | −0.113 | [150] |
| $11_{3,8}$ | $12_{2,11}$ | 254484.270(50) | −0.036 | [150] |
| $11_{7,5}$ | $10_{8,2}$ | 265060.070(50) | −0.021 | [150] |
| $11_{7,4}$ | $10_{8,3}$ | 265381.300(50) | −0.199 | [150] |
| $6_{6,1}$ | $7_{5,2}$ | 307107.530(50) | 0.067 | [150] |
| $6_{3,4}$ | $5_{4,1}$ | 307743.140(50) | 0.005 | [150] |
| $6_{6,0}$ | $7_{5,3}$ | 308133.650(50) | 0.296 | [150] |
| $1_{1,0}$ | $1_{0,1}$ | 316799.810(50) | −0.025 | [150] |
| $5_{2,4}$ | $4_{3,1}$ | 339035.260(50) | 0.134 | [150] |
| $10_{6,5}$ | $9_{7,2}$ | 345039.170(50) | 0.103 | [150] |
| $10_{6,4}$ | $9_{7,3}$ | 347278.230(50) | −0.020 | [150] |
| $7_{2,5}$ | $8_{1,8}$ | 393332.820(50) | 0.073 | [150] |
| $7_{7,1}$ | $8_{6,2}$ | 403251.620(50) | −0.050 | [150] |
| $7_{7,0}$ | $8_{6,3}$ | 403377.360(50) | −0.024 | [150] |
| $2_{1,1}$ | $2_{0,2}$ | 403561.820(50) | −0.173 | [150] |
| $10_{2,9}$ | $9_{3,6}$ | 428706.470(50) | 0.107 | [150] |
| $6_{3,3}$ | $5_{4,2}$ | 430949.260(50) | 0.051 | [150] |
| $9_{5,5}$ | $8_{6,2}$ | 452326.480(50) | −0.048 | [150] |
| $3_{1,2}$ | $2_{2,1}$ | 458531.450(50) | 0.046 | [150] |
| $9_{5,4}$ | $8_{6,3}$ | 466238.740(50) | −0.030 | [150] |
| $2_{0,2}$ | $1_{1,1}$ | 468246.570(50) | 0.006 | [150] |
| $8_{8,1}$ | $9_{7,2}$ | 469619.170(50) | −0.040 | [150] |
| $8_{8,0}$ | $9_{7,3}$ | 469633.530(50) | −0.027 | [150] |
| $14_{9,6}$ | $13_{10,3}$ | 550640.596(50) | 0.037 | This work, JPL |
| $14_{9,5}$ | $13_{10,4}$ | 550663.224(50) | 0.089 | This work, JPL |
| $3_{1,2}$ | $3_{0,3}$ | 555330.278(37) | −0.008 | [149] |
| $3_{1,2}$ | $3_{0,3}$ | 555330.360(50) | 0.074 | [150] |
| $8_{4,5}$ | $7_{5,2}$ | 571220.050(40) | 0.005 | [149] |
| $8_{4,5}$ | $7_{5,2}$ | 571220.050(50) | 0.005 | [150] |
| $6_{2,5}$ | $5_{3,2}$ | 572114.814(36) | −0.067 | [149] |
| $6_{2,5}$ | $5_{3,2}$ | 572114.910(50) | 0.029 | [150] |
| $13_{8,6}$ | $12_{9,3}$ | 577398.123(50) | −0.075 | This work, JPL |
| $13_{8,5}$ | $12_{9,4}$ | 577562.917(50) | −0.088 | This work, JPL |
| $1_{1,1}$ | $0_{0,0}$ | 607349.449(36) | 0.037 | [149] |
| $1_{1,1}$ | $0_{0,0}$ | 607349.600(50) | 0.188 | [150] |
| $12_{7,6}$ | $11_{8,3}$ | 635578.084(50) | 0.054 | This work, JPL |
| $12_{7,5}$ | $11_{8,4}$ | 636708.108(50) | 0.015 | This work, JPL |
| $9_{2,8}$ | $8_{3,5}$ | 642615.950(50) | −0.042 | [150] |
| $8_{4,4}$ | $7_{5,3}$ | 643247.288(37) | −0.036 | [149] |
| $8_{4,4}$ | $7_{5,3}$ | 643247.420(50) | 0.096 | [150] |
| $7_{3,5}$ | $6_{4,2}$ | 649560.254(41) | −0.100 | [149] |
| $7_{3,5}$ | $6_{4,2}$ | 649560.460(50) | 0.106 | [150] |

Table C.1: $D_2O$ - continued

| $N'_{Ka'Kc'}$ | $N''_{Ka'',Kc''}$ | Frequency [MHz][a] | o.-c. [MHz] | Reference |
|---|---|---|---|---|
| $12_{5,8}$ | $13_{2,11}$ | 657391.609(50) | 0.014 | This work, JPL |
| $12_{3,9}$ | $13_{2,12}$ | 663187.094(50) | 0.139 | This work, JPL |
| $13_{5,9}$ | $14_{2,12}$ | 675156.496(50) | −0.008 | This work, JPL |
| $4_{2,2}$ | $4_{1,3}$ | 692243.579(36) | 0.004 | [149] |
| $4_{2,2}$ | $4_{1,3}$ | 692243.600(50) | 0.025 | [150] |
| $3_{2,1}$ | $3_{1,2}$ | 697922.720(50) | −0.018 | This work, Cologne |
| $3_{2,1}$ | $3_{1,2}$ | 697922.831(36) | 0.093 | [149] |
| $7_{2,6}$ | $6_{3,3}$ | 714087.250(50) | −0.081 | [150] |
| $7_{2,6}$ | $6_{3,3}$ | 714087.313(36) | −0.018 | [149] |
| $14_{3,12}$ | $13_{4,9}$ | 722576.782(80) | −0.265 | This work, Cologne |
| $5_{2,3}$ | $4_{3,2}$ | 722669.850(50) | −0.044 | [150] |
| $5_{2,3}$ | $4_{3,2}$ | 722669.979(36) | 0.085 | [149] |
| $11_{6,6}$ | $10_{7,3}$ | 724368.662(50) | 0.088 | This work, Cologne |
| $11_{5,7}$ | $12_{2,10}$ | 726149.933(50) | −0.043 | This work, Cologne |
| $11_{6,5}$ | $10_{7,4}$ | 731439.719(50) | 0.018 | This work, Cologne |
| $8_{2,7}$ | $7_{3,4}$ | 740648.830(54) | −0.020 | [149] |
| $8_{2,7}$ | $7_{3,4}$ | 740648.840(50) | −0.010 | [150] |
| $2_{2,0}$ | $2_{1,1}$ | 743563.430(50) | −0.019 | [150] |
| $2_{2,0}$ | $2_{1,1}$ | 743563.526(36) | 0.077 | [149] |
| $8_{2,6}$ | $9_{1,9}$ | 745537.939(50) | 0.127 | This work, Cologne |
| $13_{6,8}$ | $14_{3,11}$ | 745996.368(100) | 0.253 | This work, Cologne |
| $5_{2,3}$ | $5_{1,4}$ | 751110.615(36) | 0.040 | [149] |
| $5_{2,3}$ | $5_{1,4}$ | 751110.670(50) | 0.095 | [150] |
| $14_{5,10}$ | $15_{2,13}$ | 765073.407(100) | −0.035 | This work, Cologne |
| $4_{1,3}$ | $4_{0,4}$ | 782470.880(50) | −0.051 | [150] |
| $4_{1,3}$ | $4_{0,4}$ | 782470.894(36) | −0.037 | [149] |
| $4_{1,3}$ | $4_{0,4}$ | 782470.921(150) | −0.010 | This work, JPL |
| $10_{5,6}$ | $9_{6,3}$ | 836330.269(150) | −0.012 | This work, JPL |
| $10_{5,6}$ | $9_{6,3}$ | 836330.300(80) | 0.019 | This work, Cologne |
| $3_{0,3}$ | $2_{1,2}$ | 850757.500(150) | −0.099 | This work, JPL |
| $3_{0,3}$ | $2_{1,2}$ | 850757.646(36) | 0.047 | [149] |
| $3_{0,3}$ | $2_{1,2}$ | 850757.720(50) | 0.121 | [150] |
| $10_{5,5}$ | $9_{6,4}$ | 874888.637(30) | −0.037 | This work, Cologne |
| $10_{5,5}$ | $9_{6,4}$ | 874888.670(150) | −0.004 | This work, JPL |
| $6_{2,4}$ | $6_{1,5}$ | 890396.080(50) | −0.088 | [150] |
| $6_{2,4}$ | $6_{1,5}$ | 890396.169(36) | 0.001 | [149] |
| $6_{2,4}$ | $6_{1,5}$ | 890396.190(150) | 0.022 | This work, JPL |
| $6_{2,4}$ | $6_{1,5}$ | 890396.194(50) | 0.026 | This work, Cologne |
| $9_{4,6}$ | $10_{1,9}$ | 892841.028(50) | 0.004 | This work, Cologne |
| $9_{4,6}$ | $10_{1,9}$ | 892841.059(150) | 0.035 | This work, JPL |
| $10_{5,6}$ | $11_{2,9}$ | 894248.995(150) | −0.148 | This work, JPL |
| $10_{5,6}$ | $11_{2,9}$ | 894249.111(100) | −0.032 | This work, Cologne |
| $2_{1,2}$ | $1_{0,1}$ | 897947.107(36) | −0.022 | [149] |
| $2_{1,2}$ | $1_{0,1}$ | 897947.110(50) | −0.019 | [150] |

Table C.1: $D_2O$ - continued

| $N'_{Ka'Kc'}$ | $N''_{Ka'',Kc''}$ | Frequency [MHz][a] | o.-c. [MHz] | Reference |
|---|---|---|---|---|
| $2_{1,2}$ | $1_{0,1}$ | 897947.126(100) | −0.003 | This work, Cologne |
| $15_{9,6}$ | $14_{10,5}$ | 904181.624(300) | −0.346 | This work, Cologne |
| $15_{9,7}$ | $14_{10,4}$ | 904185.657 [b] | | This work, Cologne |
| $15_{5,11}$ | $16_{2,14}$ | 912728.825(200) | −0.271 | This work, Cologne |
| $8_{4,5}$ | $9_{1,8}$ | 913288.967(50) | −0.017 | This work, Cologne |
| $7_{3,4}$ | $6_{4,3}$ | 922666.516(50) | 0.023 | This work, Cologne |
| $7_{3,4}$ | $6_{4,3}$ | 922666.552(54) | 0.059 | [149] |
| $4_{1,3}$ | $3_{2,2}$ | 930942.470(50) | −0.067 | [150] |
| $4_{1,3}$ | $3_{2,2}$ | 930942.494(36) | −0.043 | [149] |
| $4_{1,3}$ | $3_{2,2}$ | 930942.504(50) | −0.033 | This work, Cologne |
| $9_{4,6}$ | $8_{5,3}$ | 940346.368(80) | −0.025 | This work, Cologne |
| $14_{8,7}$ | $13_{9,4}$ | 940463.848(100) | −0.029 | This work, Cologne |
| $14_{8,6}$ | $13_{9,5}$ | 941013.823(100) | −0.082 | This work, Cologne |
| $2_{2,1}$ | $2_{1,2}$ | 947556.517(42) | 0.036 | [149] |
| $2_{2,1}$ | $2_{1,2}$ | 947556.570(50) | 0.089 | [150] |
| $8_{3,6}$ | $7_{4,3}$ | 951194.083(38) | −0.058 | [149] |
| $7_{4,4}$ | $8_{1,7}$ | 1025247.592(75) | −0.013 | [149] |
| $7_{3,4}$ | $7_{2,5}$ | 1043212.727(36) | 0.034 | [149] |
| $5_{3,3}$ | $6_{0,6}$ | 1049534.487(40) | −0.019 | [149] |
| $3_{2,2}$ | $3_{1,3}$ | 1065096.947(150) | −0.007 | This work, JPL |
| $3_{2,2}$ | $3_{1,3}$ | 1065096.951(36) | −0.003 | [149] |
| $3_{2,2}$ | $3_{1,3}$ | 1065097.240(50) | 0.286 | [150] |
| $8_{3,5}$ | $8_{2,6}$ | 1074239.913(150) | −0.074 | This work, JPL |
| $8_{3,5}$ | $8_{2,6}$ | 1074239.946(36) | −0.041 | [149] |
| $13_{3,10}$ | $14_{2,13}$ | 1075343.286(150) | −0.014 | This work, JPL |
| $6_{3,4}$ | $7_{0,7}$ | 1076067.817(36) | −0.029 | [149] |
| $6_{3,4}$ | $7_{0,7}$ | 1076067.821(150) | −0.025 | This work, JPL |
| $5_{1,4}$ | $5_{0,5}$ | 1076226.486(36) | −0.101 | [149] |
| $11_{4,8}$ | $12_{1,11}$ | 1078323.909(150) | −0.171 | This work, JPL |
| $6_{3,3}$ | $6_{2,4}$ | 1084697.772(36) | −0.023 | [149] |
| $12_{6,7}$ | $13_{3,10}$ | 1085862.882(150) | −0.140 | This work, JPL |
| $4_{3,2}$ | $5_{0,5}$ | 1104667.270(39) | 0.002 | [149] |
| $7_{2,5}$ | $7_{1,6}$ | 1115694.317(36) | −0.044 | [149] |
| $3_{1,3}$ | $2_{0,2}$ | 1158044.885(36) | 0.007 | [149] |
| $5_{3,2}$ | $5_{2,3}$ | 1169734.995(36) | −0.004 | [149] |
| $7_{3,5}$ | $8_{0,8}$ | 1174586.218(36) | 0.028 | [149] |
| $4_{0,4}$ | $3_{1,3}$ | 1213568.563(36) | 0.003 | [149] |
| $4_{2,3}$ | $4_{1,4}$ | 1223121.625(36) | −0.061 | [149] |
| $6_{4,3}$ | $7_{1,6}$ | 1236240.541(40) | −0.020 | [149] |
| $3_{3,1}$ | $4_{0,4}$ | 1247703.885(37) | −0.009 | [149] |
| $6_{2,4}$ | $5_{3,3}$ | 1251173.516(54) | −0.001 | [149] |
| $4_{3,1}$ | $4_{2,2}$ | 1262090.454(36) | −0.028 | [149] |
| $3_{3,0}$ | $3_{2,1}$ | 1331417.531(36) | 0.005 | [149] |
| $3_{3,1}$ | $3_{2,2}$ | 1396175.485(38) | −0.014 | [149] |

Table C.1: $D_2O$ - continued

| $N'_{Ka'Kc'}$ | $N''_{Ka'',Kc''}$ | Frequency [MHz][a] | o.-c. [MHz] | Reference |
|---|---|---|---|---|
| $3_{3,1}$ | $3_{2,2}$ | 1396175.673(100) | 0.173 | Thiw work, Cologne |
| $5_{1,4}$ | $4_{2,3}$ | 1403825.537(36) | 0.003 | [149] |
| $4_{1,4}$ | $3_{0,3}$ | 1404963.376(41) | −0.030 | [149] |
| $6_{1,5}$ | $6_{0,6}$ | 1410311.882(225) | 0.026 | [149] |
| $8_{2,6}$ | $8_{1,7}$ | 1415793.386(36) | −0.117 | [149] |
| $5_{2,4}$ | $5_{1,5}$ | 1419292.416(40) | −0.022 | [149] |
| $4_{3,2}$ | $4_{2,3}$ | 1432266.246(36) | 0.031 | [149] |
| $8_{3,5}$ | $7_{4,4}$ | 1464785.824(36) | −0.061 | [149] |
| $5_{3,3}$ | $5_{2,4}$ | 1497312.256(37) | 0.010 | [149] |
| $2_{2,1}$ | $1_{1,0}$ | 1528703.708(36) | −0.067 | [149] |
| $5_{4,2}$ | $6_{1,5}$ | 1544144.781(40) | 0.026 | [149] |
| $5_{0,5}$ | $4_{1,4}$ | 1550720.750(37) | 0.117 | [149] |
| $8_{4,4}$ | $8_{3,5}$ | 1580060.751(38) | −0.017 | [149] |
| $6_{3,4}$ | $6_{2,5}$ | 1597742.538(38) | −0.012 | [149] |
| $2_{2,0}$ | $1_{1,1}$ | 1615372.081(43) | 0.076 | [149] |
| $6_{2,5}$ | $6_{1,6}$ | 1648499.608(43) | −0.092 | [149] |
| $5_{1,5}$ | $4_{0,4}$ | 1656547.715(40) | 0.039 | [149] |
| $7_{4,3}$ | $7_{3,4}$ | 1703425.922(37) | −0.015 | [149] |
| $7_{3,5}$ | $7_{2,6}$ | 1736774.264(36) | 0.024 | [149] |
| $15_{5,10}$ | $15_{4,11}$ | 1749822.272 [b] | | Thsi work, Cologne |
| $7_{1,6}$ | $7_{0,7}$ | 1755338.631(300) | −0.070 | This work, Cologne |
| $7_{1,6}$ | $7_{0,7}$ | 1755338.658(36) | −0.043 | [149] |
| $9_{2,7}$ | $9_{1,8}$ | 1763000.712(50) | −0.056 | This work, Cologne |
| $15_{7,9}$ | $14_{8,6}$ | 1763237.529(300) | 0.537 | This work, Cologne |
| $10_{3,8}$ | $11_{0,11}$ | 1783780.771(200) | 0.102 | This work, Cologne |
| $15_{7,8}$ | $14_{8,7}$ | 1786332.747(500) | 0.394 | This work, Cologne |
| $12_{5,7}$ | $11_{6,6}$ | 1787308.010(50) | 0.082 | This work, Cologne |
| $12_{5,7}$ | $11_{6,6}$ | 1787308.208(150) | 0.280 | This work, JPL |
| $7_{2,5}$ | $6_{3,4}$ | 1794965.199(42) | −0.016 | [149] |
| $7_{2,5}$ | $6_{3,4}$ | 1794965.200(100) | −0.015 | This work, Cologne |
| $6_{4,2}$ | $6_{3,3}$ | 1801301.096(100) | −0.121 | This work, Cologne |
| $6_{4,2}$ | $6_{3,3}$ | 1801301.264(86) | 0.047 | [149] |
| $3_{2,2}$ | $2_{1,1}$ | 1819579.775(30) | −0.065 | This work, Cologne |
| $3_{2,2}$ | $2_{1,1}$ | 1819579.805(36) | −0.035 | [149] |
| $12_{4,9}$ | $11_{5,6}$ | 1834264.176(50) | 0.043 | This work, Cologne |
| $15_{3,12}$ | $16_{2,15}$ | 1835649.609(200) | −0.308 | This work, Cologne |
| $12_{5,7}$ | $12_{4,8}$ | 1840056.425(50) | 0.032 | This work, Cologne |
| $6_{1,5}$ | $5_{2,4}$ | 1858089.462(200) | −0.133 | This work, Cologne |
| $6_{1,5}$ | $5_{2,4}$ | 1858089.610(41) | 0.015 | [149] |
| $5_{4,1}$ | $5_{3,2}$ | 1862114.253(45) | −0.043 | [149] |
| $5_{4,1}$ | $5_{3,2}$ | 1862114.377(300) | 0.081 | This work, Cologne |
| $6_{0,6}$ | $5_{1,5}$ | 1867070.057(300) | −0.121 | This work, Cologne |
| $6_{0,6}$ | $5_{1,5}$ | 1867070.394(171) | 0.216 | [149] |
| $14_{6,9}$ | $13_{7,6}$ | 1870230.665(300) | 0.290 | This work, Cologne |

Table C.1: $D_2O$ - continued

| $N'_{Ka'Kc'}$ | $N''_{Ka'',Kc''}$ | Frequency [MHz][a] | o.-c. [MHz] | Reference |
|---|---|---|---|---|
| $4_{4,0}$ | $4_{3,1}$ | 1891829.820(36) | 0.022 | [149] |
| $11_{2,9}$ | $12_{1,12}$ | 1892814.477(300) | −0.218 | This work, Cologne |
| $4_{4,1}$ | $4_{3,2}$ | 1903352.039(200) | 0.008 | This work, Cologne |
| $7_{2,6}$ | $7_{1,7}$ | 1903660.752(100) | −0.090 | This work, Cologne |
| $7_{2,6}$ | $7_{1,7}$ | 1903660.786(59) | −0.056 | [149] |
| $5_{4,2}$ | $5_{3,3}$ | 1904922.080(37) | −0.024 | [149] |
| $8_{3,6}$ | $8_{2,7}$ | 1913971.130(50) | −0.098 | This work, Cologne |
| $8_{3,6}$ | $8_{2,7}$ | 1913971.246(55) | 0.018 | [149] |
| $6_{4,3}$ | $6_{3,4}$ | 1915511.337(100) | −0.078 | This work, Cologne |
| $6_{4,3}$ | $6_{3,4}$ | 1915511.368(88) | −0.047 | [149] |
| $6_{1,6}$ | $5_{0,5}$ | 1920687.348(50) | 0.006 | This work, Cologne |
| $6_{1,6}$ | $5_{0,5}$ | 1920687.354(39) | 0.012 | [149] |
| $4_{4,1}$ | $5_{1,4}$ | 1931792.769(54) | 0.057 | [149] |
| $7_{4,4}$ | $7_{3,5}$ | 1943341.397(100) | −0.109 | This work, Cologne |
| $7_{4,4}$ | $7_{3,5}$ | 1943341.484(37) | −0.022 | [149] |
| $14_{4,10}$ | $14_{3,11}$ | 1954181.445(50) | −0.129 | This work, Cologne |
| $14_{6,8}$ | $13_{7,7}$ | 1975478.994(200) | 0.327 | This work, Cologne |
| $13_{4,10}$ | $12_{5,7}$ | 1985234.152(100) | −0.165 | This work, Cologne |
| $11_{5,6}$ | $11_{4,7}$ | 1986803.459(100) | −0.016 | This work, Cologne |
| $8_{4,5}$ | $8_{3,6}$ | 1996904.485(36) | 0.008 | [149] |
| $7_{5,3}$ | $8_{2,6}$ | 2011053.447(44) | 0.016 | [149] |
| $4_{2,3}$ | $3_{1,2}$ | 2072754.810(39) | 0.004 | [149] |
| $8_{1,7}$ | $8_{0,8}$ | 2092680.133(41) | 0.043 | [149] |
| $3_{2,1}$ | $2_{1,2}$ | 2104010.651(42) | 0.028 | [149] |
| $7_{0,7}$ | $6_{1,6}$ | 2170174.279(41) | −0.126 | [149] |
| $8_{2,7}$ | $8_{1,8}$ | 2177194.243(41) | −0.047 | [149] |
| $7_{1,6}$ | $6_{2,5}$ | 2277013.478(38) | 0.073 | [149] |
| $5_{2,4}$ | $4_{1,3}$ | 2293369.151(44) | −0.032 | [149] |
| $8_{5,3}$ | $8_{4,4}$ | 2330851.127(38) | 0.036 | [149] |
| $8_{2,6}$ | $7_{3,5}$ | 2333887.194(100) | −0.210 | This work, Cologne |
| $8_{2,6}$ | $7_{3,5}$ | 2333887.400(36) | −0.004 | [149] |
| $7_{5,2}$ | $7_{4,3}$ | 2376878.361(300) | −0.212 | This work, Cologne |
| $7_{5,2}$ | $7_{4,3}$ | 2376878.544(40) | −0.029 | [149] |
| $8_{5,4}$ | $8_{4,5}$ | 2397641.676(41) | −0.012 | [149] |
| $6_{5,1}$ | $6_{4,2}$ | 2400382.322(40) | −0.014 | [149] |
| $7_{5,3}$ | $7_{4,4}$ | 2401599.350(38) | 0.021 | [149] |
| $6_{5,2}$ | $6_{4,3}$ | 2407649.965(37) | 0.021 | [149] |
| $5_{5,0}$ | $5_{4,1}$ | 2410887.788(38) | 0.041 | [149] |
| $5_{5,1}$ | $5_{4,2}$ | 2412421.601(51) | 0.079 | [149] |
| $8_{0,8}$ | $7_{1,7}$ | 2465848.800(120) | −0.093 | [149] |
| $3_{3,1}$ | $2_{2,0}$ | 2472191.939(39) | 0.048 | [149] |
| $8_{1,8}$ | $7_{0,7}$ | 2477700.224(36) | −0.090 | [149] |
| $3_{3,0}$ | $2_{2,1}$ | 2487871.584(58) | −0.084 | [149] |
| $6_{2,5}$ | $5_{1,4}$ | 2492960.465(37) | 0.010 | [149] |

Table C.1: $D_2O$ - continued

| $N'_{Ka'Kc'}$ | $N''_{Ka'',Kc''}$ | Frequency [MHz][a] | o.-c. [MHz] | Reference |
|---|---|---|---|---|
| $6_{5,2}$ | $7_{2,5}$ | 2528196.099(44) | −0.045 | [149] |
| $3_{3,0}$ | $3_{0,3}$ | 2584670.452(36) | −0.098 | [149] |
| $8_{1,7}$ | $7_{2,6}$ | 2654868.110(67) | −0.031 | [149] |
| $4_{2,2}$ | $3_{1,3}$ | 2688283.075(71) | 0.009 | [149] |
| $7_{2,6}$ | $6_{1,5}$ | 2689181.271(37) | −0.023 | [149] |
| $4_{3,1}$ | $4_{0,4}$ | 2736804.981(38) | −0.008 | [149] |
| $4_{3,2}$ | $3_{2,1}$ | 2807098.229(92) | −0.054 | [149] |
| $4_{3,1}$ | $3_{2,2}$ | 2885276.612(180) | 0.018 | [149] |
| $8_{6,2}$ | $8_{5,3}$ | 2889555.699(56) | −0.008 | [149] |
| $8_{6,3}$ | $8_{5,4}$ | 2893642.415(45) | −0.003 | [149] |
| $7_{6,1}$ | $7_{5,2}$ | 2898621.125(42) | 0.024 | [149] |
| $8_{2,7}$ | $7_{1,6}$ | 2899555.915(37) | 0.011 | [149] |
| $7_{6,2}$ | $7_{5,3}$ | 2899626.742(73) | 0.034 | [149] |
| $6_{6,0}$ | $6_{5,1}$ | 2902252.230(49) | 0.023 | [149] |
| $6_{6,1}$ | $6_{5,2}$ | 2902428.470(65) | −0.052 | [149] |
| $5_{3,2}$ | $5_{0,5}$ | 2997072.252(44) | 0.091 | [149] |
| $5_{3,3}$ | $4_{2,2}$ | 3098437.767(37) | −0.087 | [149] |
| $5_{3,2}$ | $4_{2,3}$ | 3324671.327(71) | 0.218 | [149] |
| $6_{3,4}$ | $5_{2,3}$ | 3339592.524(36) | 0.093 | [149] |
| $7_{7,0}$ | $7_{6,1}$ | 3367260.520(59) | 0.087 | [149] |
| $7_{7,1}$ | $7_{6,2}$ | 3367279.110(40) | 0.025 | [149] |
| $8_{7,1}$ | $8_{6,2}$ | 3367685.512(59) | −0.029 | [149] |
| $8_{7,2}$ | $8_{6,3}$ | 3367809.159(40) | −0.072 | [149] |
| $5_{2,3}$ | $4_{1,4}$ | 3378057.828(38) | 0.033 | [149] |
| $4_{4,1}$ | $3_{3,0}$ | 3379032.803(38) | 0.015 | [149] |
| $4_{4,0}$ | $3_{3,1}$ | 3380930.919(49) | 0.026 | [149] |
| $6_{3,3}$ | $6_{0,6}$ | 3385405.730(59) | −0.089 | [149] |
| $7_{3,5}$ | $6_{2,4}$ | 3535559.341(120) | −0.025 | [149] |
| $3_{3,1}$ | $2_{0,2}$ | 3619317.293(47) | −0.039 | [149] |
| $8_{3,6}$ | $7_{2,5}$ | 3697832.834(97) | 0.063 | [149] |
| $5_{4,2}$ | $4_{3,1}$ | 3741269.401(38) | −0.075 | [149] |
| $5_{4,1}$ | $4_{3,2}$ | 3754519.171(37) | −0.019 | [149] |
| $6_{4,2}$ | $6_{1,5}$ | 3776395.270(38) | 0.090 | [149] |
| $5_{4,1}$ | $5_{1,4}$ | 3782959.825(64) | −0.045 | [149] |
| $6_{3,3}$ | $5_{2,4}$ | 3833183.610(50) | 0.052 | [149] |
| $4_{4,0}$ | $4_{1,3}$ | 3846163.892(59) | 0.037 | [149] |
| $7_{4,3}$ | $7_{1,6}$ | 3862332.991(36) | −0.000 | [149] |
| $7_{3,4}$ | $7_{0,7}$ | 3914245.631(61) | −0.124 | [149] |
| $4_{3,2}$ | $3_{0,3}$ | 4060351.346(109) | 0.039 | [149] |
| $8_{4,4}$ | $8_{1,7}$ | 4070094.342(88) | 0.084 | [149] |
| $6_{4,3}$ | $5_{3,2}$ | 4085368.747(52) | −0.100 | [149] |
| $6_{4,2}$ | $5_{3,3}$ | 4137172.519(62) | −0.010 | [149] |
| $5_{5,1}$ | $4_{4,0}$ | 4261861.286(52) | 0.086 | [149] |
| $5_{5,0}$ | $4_{4,1}$ | 4262055.007(90) | 0.101 | [149] |

Table C.1: $D_2O$ - continued

| $N'_{Ka'Kc'}$ | $N''_{Ka'',Kc''}$ | Frequency [MHz][a] | o.-c. [MHz] | Reference |
|---|---|---|---|---|
| $7_{4,4}$ | $6_{3,3}$ | 4394203.184(120) | 0.107 | [149] |
| $7_{3,4}$ | $6_{2,5}$ | 4435920.495(95) | 0.036 | [149] |
| $8_{3,5}$ | $8_{0,8}$ | 4582713.451(58) | −0.129 | [149] |
| $6_{5,2}$ | $5_{4,1}$ | 4630904.565(36) | 0.070 | [149] |
| $6_{5,1}$ | $5_{4,2}$ | 4632632.725(45) | −0.036 | [149] |
| $8_{4,5}$ | $7_{3,4}$ | 4651524.577(56) | 0.021 | [149] |
| $5_{4,2}$ | $5_{1,5}$ | 4821526.699(106) | −0.089 | [149] |
| $8_{5,3}$ | $8_{2,6}$ | 4985151.759(48) | −0.087 | [149] |
| $8_{4,4}$ | $7_{3,5}$ | 4988188.093(171) | −0.066 | [149] |
| $7_{5,3}$ | $6_{4,2}$ | 4994501.210(49) | 0.021 | [149] |
| $7_{5,2}$ | $6_{4,3}$ | 5002971.123(63) | 0.120 | [149] |
| $6_{6,1}$ | $5_{5,0}$ | 5122445.287(450) | 0.017 | [149] |
| $6_{6,0}$ | $5_{5,1}$ | 5122463.195(189) | −0.251 | [149] |
| $8_{3,5}$ | $7_{2,6}$ | 5144901.449(225) | −0.182 | [149] |
| | | $v_2 = 1$ | | |
| $4_{1,4}$ | $3_{2,1}$ | 29695.580(50) | −0.036 | [150] |
| $5_{2,3}$ | $6_{1,6}$ | 50538.860(50) | 0.034 | [150] |
| $5_{1,5}$ | $4_{2,2}$ | 51436.540(50) | −0.067 | [150] |
| $4_{2,2}$ | $3_{3,1}$ | 54216.530(50) | 0.008 | [150] |
| $6_{5,2}$ | $7_{4,3}$ | 66958.410(50) | −0.068 | [150] |
| $6_{3,4}$ | $5_{4,1}$ | 79170.080(50) | −0.098 | [150] |
| $2_{2,0}$ | $3_{1,3}$ | 105236.444(50) | 0.013 | This work, JPL |
| $5_{2,4}$ | $4_{3,1}$ | 169894.010(50) | −0.148 | [150] |
| $6_{3,3}$ | $5_{4,2}$ | 193023.090(50) | −0.070 | [150] |
| $4_{4,1}$ | $5_{3,2}$ | 244879.030(50) | −0.056 | [150] |
| $6_{2,4}$ | $7_{1,7}$ | 269656.050(50) | −0.059 | [150] |
| $4_{4,0}$ | $5_{3,3}$ | 285640.480(50) | −0.037 | [150] |
| $8_{4,5}$ | $7_{5,2}$ | 290261.310(50) | −0.133 | [150] |
| $8_{4,4}$ | $7_{5,3}$ | 352239.570(50) | 0.057 | [150] |
| $1_{1,0}$ | $1_{0,1}$ | 354717.830(50) | 0.021 | [150] |
| $3_{1,2}$ | $2_{2,1}$ | 363629.650(50) | 0.103 | [150] |
| $6_{2,5}$ | $5_{3,2}$ | 406703.030(50) | −0.073 | [150] |
| $7_{3,5}$ | $6_{4,2}$ | 424737.310(50) | 0.057 | [150] |
| $2_{0,2}$ | $1_{1,1}$ | 434820.730(50) | 0.155 | [150] |
| $2_{1,1}$ | $2_{0,2}$ | 444777.950(50) | 0.020 | [150] |
| $5_{5,1}$ | $6_{4,2}$ | 462565.690(50) | 0.036 | [151] |
| $5_{5,0}$ | $6_{4,3}$ | 468907.360(50) | 0.002 | [151] |
| $10_{5,5}$ | $9_{6,4}$ | 541721.381(50) | 0.034 | This work, JPL |
| $5_{2,3}$ | $4_{3,2}$ | 552878.214(50) | 0.068 | This work, JPL |
| $8_{2,7}$ | $7_{3,4}$ | 587361.951(50) | 0.087 | This work, JPL |
| $7_{2,5}$ | $8_{1,8}$ | 587929.458(50) | −0.062 | This work, JPL |
| $3_{1,2}$ | $3_{0,3}$ | 601404.710(50) | −0.027 | [150] |
| $6_{6,1}$ | $7_{5,2}$ | 629280.200(50) | −0.095 | This work, JPL |

Table C.1: $D_2O$ - continued

| $N'_{Ka'Kc'}$ | $N''_{Ka'',Kc''}$ | Frequency [MHz][a] | o.-c. [MHz] | Reference |
|---|---|---|---|---|
| $6_{6,0}$ | $7_{5,3}$ | 630094.957(50) | −0.013 | This work, JPL |
| $1_{1,1}$ | $0_{0,0}$ | 641981.990(50) | 0.005 | [150] |
| $9_{4,6}$ | $8_{5,3}$ | 662165.673(50) | 0.031 | This work, JPL |
| $7_{3,4}$ | $6_{4,3}$ | 680516.602(50) | −0.050 | This work, JPL |
| $8_{3,6}$ | $7_{4,3}$ | 733611.402(100) | 0.107 | This work, Cologne |
| $12_{6,7}$ | $11_{7,4}$ | 745285.130(300) | −0.139 | This work, Cologne |
| $7_{7,1}$ | $8_{6,2}$ | 756029.994(100) | 0.158 | This work, Cologne |
| $7_{7,0}$ | $8_{6,3}$ | 756123.799(100) | 0.154 | This work, Cologne |
| $12_{6,6}$ | $11_{7,5}$ | 759923.667(100) | −0.047 | This work, Cologne |
| $4_{2,2}$ | $4_{1,3}$ | 778853.769(150) | −0.056 | This work, JPL |
| $4_{2,2}$ | $4_{1,3}$ | 778853.818(50) | −0.007 | This work, Cologne |
| $3_{2,1}$ | $3_{1,2}$ | 792727.656(150) | −0.018 | This work, JPL |
| $9_{4,5}$ | $8_{5,4}$ | 808662.796(150) | 0.171 | This work, JPL |
| $3_{0,3}$ | $2_{1,2}$ | 821975.947(150) | 0.097 | This work, JPL |
| $5_{2,3}$ | $5_{1,4}$ | 829096.253(150) | −0.030 | This work, JPL |
| $4_{1,3}$ | $4_{0,4}$ | 836450.963(50) | −0.002 | This work, Cologne |
| $4_{1,3}$ | $4_{0,4}$ | 836450.977(150) | 0.012 | This work, JPL |
| $4_{1,3}$ | $3_{2,2}$ | 844357.620(150) | 0.055 | This work, JPL |
| $4_{1,3}$ | $3_{2,2}$ | 844357.669(50) | 0.104 | This work, Cologne |
| $2_{2,0}$ | $2_{1,1}$ | 844695.608(50) | 0.006 | This work, Cologne |
| $2_{2,0}$ | $2_{1,1}$ | 844695.615(150) | 0.013 | This work, JPL |
| $11_{5,7}$ | $10_{6,4}$ | 892862.721(100) | −0.126 | This work, Cologne |
| $2_{1,2}$ | $1_{0,1}$ | 929330.974(50) | 0.060 | This work, Cologne |
| $6_{3,4}$ | $6_{2,5}$ | 1770261.588(100) | −0.049 | This work, Cologne |
| $11_{3,8}$ | $11_{2,9}$ | 1772461.456(200) | −0.384 | This work, Cologne |
| $13_{4,10}$ | $12_{5,7}$ | 1773779.475(150) | −0.113 | This work, Cologne |
| $6_{2,5}$ | $6_{1,6}$ | 1795193.053(200) | −0.241 | This work, Cologne |
| $6_{1,5}$ | $5_{2,4}$ | 1797743.227(50) | −0.104 | This work, Cologne |
| $9_{3,6}$ | $8_{4,5}$ | 1806824.671(200) | 0.171 | This work, Cologne |
| $8_{4,4}$ | $8_{3,5}$ | 1816986.883(50) | −0.067 | This work, Cologne |
| $9_{2,7}$ | $9_{1,8}$ | 1848385.676(50) | 0.033 | This work, Cologne |
| $6_{0,6}$ | $5_{1,5}$ | 1851780.365(100) | −0.123 | This work, Cologne |
| $7_{1,6}$ | $7_{0,7}$ | 1873204.916(500) | −0.163 | This work, Cologne |
| $3_{2,2}$ | $2_{1,1}$ | 1922132.425(50) | 0.001 | This work, Cologne |
| $6_{1,6}$ | $5_{0,5}$ | 1922568.555(100) | −0.110 | This work, Cologne |
| $7_{4,3}$ | $7_{3,4}$ | 1944488.727(200) | −0.084 | This work, Cologne |

[a] Numbers in parentheses give the experimental uncertainty in units of the last digits.

[b] These lines have been omitted from the fit. Presumably they are blended.

## C.2 HDO

Table C.2: Pure rotational transitions of HDO in the ground and first excited bending mode. Next to the at Cologne, Kiel and at the JPL newly measured lines, all to date available high-resolution microwave, and millimeter- and submillimeter wavelength data with microwave accuracy is given. Not included in this compilation is FIR and IR Fourier Transform data.

| $N'_{Ka'Kc'}$ | $N''_{Ka''Kc''}$ | Frequency [MHz][a] | o.-c. [MHz] | Reference |
|---|---|---|---|---|
| | | $v_2 = 0$ | | |
| $6_{4,2}$ | $6_{4,3}$ | 2394.560(50) | −0.001 | [150] |
| $9_{5,4}$ | $9_{5,5}$ | 3044.710(100) | −0.092 | [150] |
| $4_{3,1}$ | $4_{3,2}$ | 5702.780(50) | −0.049 | [150] |
| $7_{4,3}$ | $7_{4,4}$ | 8577.8113(2) | 0.0000 | This work, Kiel |
| $10_{5,5}$ | $10_{5,6}$ | 8837.2144(2) | −0.0001 | This work, Kiel |
| $2_{2,0}$ | $2_{2,1}$ | 10278.2455(10) | −0.0006 | [150] |
| $14_{6,8}$ | $14_{6,9}$ | 18392.7867(11) | −0.0001 | This work, Kiel |
| $11_{5,6}$ | $11_{5,7}$ | 22581.4395(11) | 0.0014 | This work, Kiel |
| $8_{4,4}$ | $8_{4,5}$ | 24884.7672(11) | −0.0019 | This work, Kiel |
| $7_{1,7}$ | $6_{2,4}$ | 26880.380(50) | −0.005 | [150] |
| $11_{7,5}$ | $12_{6,6}$ | 28668.340(50) | −0.022 | [150] |
| $11_{7,4}$ | $12_{6,7}$ | 31670.430(50) | −0.042 | [150] |
| $13_{2,12}$ | $12_{3,9}$ | 45902.540(40) | −0.037 | [150] |
| $3_{2,1}$ | $3_{2,2}$ | 50236.300(50) | −0.051 | [150] |
| $12_{5,7}$ | $12_{5,8}$ | 51917.870(50) | 0.033 | [150] |
| $4_{3,1}$ | $5_{2,4}$ | 61185.950(50) | −0.016 | [150] |
| $9_{4,5}$ | $9_{4,6}$ | 61704.590(50) | 0.017 | [150] |
| $6_{3,3}$ | $6_{3,4}$ | 64427.340(50) | 0.022 | [150] |
| $6_{0,6}$ | $5_{2,3}$ | 69550.580(50) | −0.020 | [150] |
| $1_{1,0}$ | $1_{1,1}$ | 80578.295(20) | 0.001 | [150] |
| $7_{3,5}$ | $6_{4,2}$ | 87962.810(14) | −0.002 | [150] |
| $13_{5,8}$ | $13_{5,9}$ | 108897.100(50) | −0.021 | This work, JPL |
| $5_{1,5}$ | $4_{2,2}$ | 120778.190(14) | −0.062 | [150] |
| $14_{7,8}$ | $13_{8,5}$ | 132669.198(50) | 0.010 | This work, JPL |
| $14_{7,7}$ | $13_{8,6}$ | 133642.552(50) | −0.020 | This work, JPL |
| $10_{4,6}$ | $10_{4,7}$ | 134770.220(50) | −0.123 | [150] |
| $6_{1,6}$ | $5_{2,3}$ | 138530.570(50) | 0.003 | [150] |
| $4_{2,2}$ | $4_{2,3}$ | 143727.210(50) | −0.117 | [150] |
| $7_{3,4}$ | $7_{3,5}$ | 151616.190(50) | 0.018 | [150] |
| $9_{6,4}$ | $10_{5,5}$ | 160329.460(50) | −0.001 | [150] |
| $9_{6,3}$ | $10_{5,6}$ | 169246.050(50) | −0.008 | [150] |
| $3_{2,1}$ | $4_{0,4}$ | 207110.650(50) | −0.132 | [150] |
| $7_{2,5}$ | $8_{1,8}$ | 207345.710(50) | −0.176 | [150] |
| $14_{5,9}$ | $14_{5,10}$ | 210133.925(100) | −0.080 | This work, JPL |
| $9_{4,6}$ | $8_{5,3}$ | 210310.650(50) | −0.016 | [150] |
| $3_{1,2}$ | $2_{2,1}$ | 225896.720(50) | 0.010 | [150] |

Table C.2: HDO - continued

| $N'_{Ka'Kc'}$ | $N''_{Ka''Kc''}$ | Frequency [MHz][a] | o.-c. [MHz] | Reference |
|---|---|---|---|---|
| $7_{2,5}$ | $8_{0,8}$ | 228072.391(100) | −0.031 | This work, JPL |
| $8_{4,4}$ | $9_{2,7}$ | 232312.291(100) | −0.149 | This work, JPL |
| $2_{1,1}$ | $2_{1,2}$ | 241561.550(50) | −0.046 | [150] |
| $7_{3,4}$ | $6_{4,3}$ | 241973.570(50) | 0.025 | [150] |
| $5_{2,3}$ | $4_{3,2}$ | 255050.234(50) | −0.089 | This work, JPL |
| $5_{2,3}$ | $4_{3,2}$ | 255050.260(50) | −0.063 | [184] |
| $7_{5,3}$ | $8_{4,4}$ | 258223.760(50) | −0.083 | [150] |
| $2_{2,0}$ | $3_{1,3}$ | 266161.070(50) | −0.025 | [150] |
| $9_{4,5}$ | $8_{5,4}$ | 272907.540(50) | −0.014 | [150] |
| $7_{5,2}$ | $8_{4,5}$ | 283318.590(50) | 0.062 | [150] |
| $8_{3,5}$ | $8_{3,6}$ | 305038.550(50) | 0.018 | [150] |
| $5_{2,3}$ | $5_{2,4}$ | 310533.290(50) | −0.170 | [150] |
| $6_{2,5}$ | $5_{3,2}$ | 313750.620(50) | −0.012 | [150] |
| $5_{4,2}$ | $6_{3,3}$ | 317151.250(50) | 0.031 | [150] |
| $11_{5,7}$ | $10_{6,4}$ | 332949.590(50) | 0.003 | [150] |
| $3_{3,1}$ | $4_{2,2}$ | 335395.500(26) | 0.021 | [150] |
| $11_{5,6}$ | $10_{6,5}$ | 355841.380(50) | −0.055 | [150] |
| $5_{3,2}$ | $6_{1,5}$ | 356835.850(50) | −0.312 | [150] |
| $12_{8,5}$ | $13_{7,6}$ | 365047.315(50) | 0.029 | This work, JPL |
| $12_{8,4}$ | $13_{7,7}$ | 365382.948(50) | −0.003 | This work, JPL |
| $5_{4,1}$ | $6_{3,4}$ | 382065.100(50) | 0.036 | [150] |
| $13_{3,10}$ | $14_{2,13}$ | 429811.772(100) | −0.363 | This work, JPL |
| $12_{2,11}$ | $11_{3,8}$ | 443173.868(100) | 0.022 | This work, JPL |
| $1_{0,1}$ | $0_{0,0}$ | 464924.520(50) | 0.016 | [150] |
| $3_{3,0}$ | $4_{2,3}$ | 479947.370(50) | −0.104 | [150] |
| $3_{1,2}$ | $3_{1,3}$ | 481779.500(50) | −0.059 | [150] |
| $2_{0,2}$ | $1_{1,1}$ | 490596.640(50) | 0.023 | [150] |
| $1_{1,0}$ | $1_{0,1}$ | 509292.420(100) | −0.071 | [150] |
| $10_{7,4}$ | $11_{6,5}$ | 528958.354(100) | 0.057 | [150] |
| $10_{7,3}$ | $11_{6,6}$ | 529990.765(100) | −0.032 | [150] |
| $2_{2,0}$ | $3_{0,3}$ | 537792.507(50) | −0.055 | This work, JPL |
| $8_{3,6}$ | $7_{4,3}$ | 539935.900(100) | −0.079 | [150] |
| $9_{3,6}$ | $9_{3,7}$ | 540374.264(100) | 0.073 | [150] |
| $8_{2,6}$ | $9_{1,9}$ | 548555.008(100) | −0.081 | [150] |
| $6_{2,4}$ | $6_{2,5}$ | 559816.148(50) | −0.145 | This work, JPL |
| $6_{2,4}$ | $6_{2,5}$ | 559816.740(500) | 0.447 | [184] |
| $2_{1,1}$ | $2_{0,2}$ | 599926.710(100) | 0.051 | [150] |
| $7_{2,6}$ | $6_{3,3}$ | 622482.571(100) | −0.031 | [150] |
| $8_{6,3}$ | $9_{5,4}$ | 663044.560(100) | −0.024 | [150] |
| $8_{6,3}$ | $9_{5,4}$ | 663044.565(50) | −0.019 | This work, JPL |
| $8_{6,2}$ | $9_{5,5}$ | 666105.695(100) | 0.143 | [150] |
| $10_{4,7}$ | $9_{5,4}$ | 700845.589(100) | 0.106 | [150] |
| $9_{1,8}$ | $8_{3,5}$ | 717695.816(100) | −0.238 | This work, JPL |
| $11_{2,10}$ | $10_{3,7}$ | 736164.076(50) | −0.064 | This work, Cologne |

Table C.2: HDO - continued

| $N'_{Ka'Kc'}$ | $N''_{Ka''Kc''}$ | Frequency [MHz][a] | o.-c. [MHz] | Reference |
|---|---|---|---|---|
| $3_{1,2}$ | $3_{0,3}$ | 753411.063(50) | 0.037 | This work, Cologne |
| $3_{1,2}$ | $3_{0,3}$ | 753411.150(100) | 0.124 | [150] |
| $6_{5,2}$ | $7_{4,3}$ | 766165.655(100) | −0.120 | [150] |
| $6_{5,2}$ | $7_{4,3}$ | 766165.795(50) | 0.020 | This work, Cologne |
| $10_{1,9}$ | $9_{3,6}$ | 769629.209(150) | −0.474 | This work, JPL |
| $6_{5,1}$ | $7_{4,4}$ | 774779.016(100) | −0.060 | [150] |
| $6_{5,1}$ | $7_{4,4}$ | 774779.095(50) | 0.019 | This work, Cologne |
| $6_{5,1}$ | $7_{4,4}$ | 774779.139(150) | 0.063 | This work, JPL |
| $4_{1,3}$ | $4_{1,4}$ | 797487.016(100) | −0.038 | [150] |
| $4_{1,3}$ | $3_{2,2}$ | 827263.389(100) | −0.026 | [150] |
| $4_{1,3}$ | $3_{2,2}$ | 827263.430(150) | 0.015 | This work, JPL |
| $4_{4,1}$ | $5_{3,2}$ | 836994.625(100) | −0.064 | [150] |
| $4_{4,1}$ | $5_{3,2}$ | 836994.638(150) | −0.051 | This work, JPL |
| $12_{5,8}$ | $11_{6,5}$ | 838579.285(100) | −0.088 | This work, JPL |
| $12_{5,8}$ | $11_{6,5}$ | 838579.340(200) | −0.033 | This work, Cologne |
| $10_{4,6}$ | $9_{5,5}$ | 838660.607(150) | −0.022 | This work, JPL |
| $10_{4,6}$ | $9_{5,5}$ | 838660.610(100) | −0.019 | This work, Cologne |
| $10_{4,6}$ | $9_{5,5}$ | 838660.821(100) | 0.192 | [150] |
| $8_{2,7}$ | $7_{3,4}$ | 838953.225(50) | 0.010 | This work, Cologne |
| $8_{2,7}$ | $7_{3,4}$ | 838953.267(150) | 0.052 | This work, JPL |
| $8_{2,7}$ | $7_{3,4}$ | 838953.288(100) | 0.073 | [150] |
| $2_{1,2}$ | $1_{1,1}$ | 848961.688(150) | 0.008 | This work, JPL |
| $2_{1,2}$ | $1_{1,1}$ | 848961.843(100) | 0.163 | [150] |
| $8_{3,5}$ | $7_{4,4}$ | 853552.362(100) | 0.040 | [150] |
| $8_{3,5}$ | $7_{4,4}$ | 853552.407(150) | 0.085 | This work, JPL |
| $8_{3,5}$ | $7_{4,4}$ | 853552.442(100) | 0.120 | This work, Cologne |
| $11_{8,4}$ | $12_{7,5}$ | 859038.087(150) | 0.012 | This work, JPL |
| $11_{8,3}$ | $12_{7,6}$ | 859141.711(150) | −0.008 | This work, JPL |
| $11_{8,3}$ | $12_{7,6}$ | 859141.739(200) | 0.020 | This work, Cologne |
| $4_{4,0}$ | $5_{3,3}$ | 859356.727(150) | −0.084 | This work, JPL |
| $4_{4,0}$ | $5_{3,3}$ | 859356.762(50) | −0.049 | This work, Cologne |
| $10_{3,7}$ | $10_{3,8}$ | 862657.796(150) | −0.054 | This work, JPL |
| $7_{2,5}$ | $7_{2,6}$ | 890267.278(150) | −0.193 | This work, JPL |
| $12_{5,7}$ | $11_{6,6}$ | 891523.164(150) | −0.215 | This work, JPL |
| $12_{5,7}$ | $11_{6,6}$ | 891523.213(150) | −0.166 | This work, Cologne |
| $1_{1,1}$ | $0_{0,0}$ | 893638.568(150) | −0.133 | This work, JPL |
| $1_{1,1}$ | $0_{0,0}$ | 893638.666(100) | −0.035 | [150] |
| $1_{1,1}$ | $0_{0,0}$ | 893638.703(100) | 0.002 | This work, Cologne |
| $6_{2,4}$ | $5_{3,3}$ | 895874.293(150) | −0.136 | This work, JPL |
| $6_{2,4}$ | $5_{3,3}$ | 895874.360(100) | −0.069 | [150] |
| $6_{2,4}$ | $5_{3,3}$ | 895874.371(20) | −0.058 | This work, Cologne |
| $10_{2,9}$ | $9_{3,6}$ | 904870.954(50) | −0.092 | This work, Cologne |
| $4_{3,1}$ | $5_{1,4}$ | 912605.132(200) | 0.020 | This work, Cologne |
| $7_{4,3}$ | $8_{2,6}$ | 915003.785(200) | −0.170 | This work, Cologne |

Table C.2: HDO - continued

| $N'_{Ka'Kc'}$ | $N''_{Ka''Kc''}$ | Frequency [MHz][a] | o.-c. [MHz] | Reference |
|---|---|---|---|---|
| $2_{0,2}$ | $1_{0,1}$ | 919310.885(100) | 0.070 | This work, Cologne |
| $11_{2,9}$ | $10_{4,6}$ | 927314.545(100) | −0.217 | This work, Cologne |
| $9_{2,8}$ | $8_{3,5}$ | 938410.259(100) | −0.015 | This work, Cologne |
| $14_{3,11}$ | $15_{2,14}$ | 954429.407(200) | 0.538 | This work, Cologne |
| $9_{3,7}$ | $8_{4,4}$ | 958569.027(30) | −0.002 | This work, Cologne |
| $10_{5,5}$ | $11_{3,8}$ | 969367.029(300) | −0.333 | This work, Cologne |
| $4_{1,3}$ | $4_{0,4}$ | 984137.828(100) | −0.018 | [150] |
| $3_{0,3}$ | $2_{1,2}$ | 995411.501(100) | 0.040 | [150] |
| $2_{1,1}$ | $1_{1,0}$ | 1009944.697(100) | −0.286 | [150] |
| $11_{4,8}$ | $10_{5,5}$ | 1179651.358(150) | 0.286 | This work, JPL |
| $5_{1,4}$ | $5_{1,5}$ | 1180323.574(150) | 0.063 | This work, JPL |
| $9_{3,6}$ | $9_{2,7}$ | 1731255.730(150) | 0.071 | This work, JPL |
| $8_{3,5}$ | $8_{2,6}$ | 1759978.347(100) | −0.120 | This work, Cologne |
| $4_{0,4}$ | $3_{0,3}$ | 1763558.514(100) | 0.138 | This work, Cologne |
| $10_{3,7}$ | $10_{2,8}$ | 1790300.120(150) | −0.018 | This work, JPL |
| $10_{3,7}$ | $10_{2,8}$ | 1790300.142(150) | 0.004 | This work, Cologne |
| $10_{4,7}$ | $11_{1,10}$ | 1792459.576(500) | −0.299 | This work, Cologne |
| $4_{2,3}$ | $4_{1,4}$ | 1818529.655(100) | 0.104 | This work, Cologne |
| $14_{5,10}$ | $13_{6,7}$ | 1841900.874(500) | −1.161 | This work, Cologne |
| $13_{3,11}$ | $12_{4,8}$ | 1852724.177(200) | 0.275 | This work, Cologne |
| $7_{3,4}$ | $7_{2,5}$ | 1853872.637(100) | −0.209 | This work, Cologne |
| $4_{3,2}$ | $3_{3,1}$ | 1872608.586(50) | 0.020 | This work, Cologne |
| $4_{3,1}$ | $3_{3,0}$ | 1877486.797(50) | 0.069 | This work, Cologne |
| $2_{2,1}$ | $2_{0,2}$ | 1881290.837(50) | −0.003 | This work, Cologne |
| $3_{2,2}$ | $3_{0,3}$ | 1920432.785(200) | −0.022 | This work, Cologne |
| $6_{3,4}$ | $7_{0,7}$ | 1929254.905(100) | −0.161 | This work, Cologne |
| $7_{3,5}$ | $8_{0,8}$ | 1930328.813(100) | −0.283 | This work, Cologne |
| $9_{4,6}$ | $10_{1,9}$ | 1934042.618(500) | −0.120 | This work, Cologne |
| $5_{3,3}$ | $6_{1,6}$ | 1950154.435(500) | −0.002 | This work, Cologne |
| $4_{1,4}$ | $3_{0,3}$ | 1950209.102(50) | −0.066 | This work, Cologne |
| $4_{1,4}$ | $3_{0,3}$ | 1950209.230(300) | 0.062 | This work, JPL |
| $11_{3,8}$ | $11_{2,9}$ | 1950538.690(300) | −0.074 | This work, JPL |
| $11_{3,8}$ | $11_{2,9}$ | 1950538.691(50) | −0.073 | This work, Cologne |
| $5_{0,5}$ | $4_{1,4}$ | 1965553.683(50) | 0.001 | This work, Cologne |
| $9_{2,7}$ | $9_{1,8}$ | 1975899.649(50) | −0.274 | This work, Cologne |
| $11_{2,9}$ | $12_{1,12}$ | 1976507.451(100) | 0.091 | This work, Cologne |
| $6_{3,3}$ | $6_{2,4}$ | 1982064.052(50) | −0.233 | This work, Cologne |
| $7_{7,1}$ | $8_{6,2}$ | 1994453.774(200) | 0.250 | This work, Cologne |
| $7_{7,0}$ | $8_{6,3}$ | 1994469.633(200) | −0.068 | This work, Cologne |
| $4_{3,2}$ | $4_{2,3}$ | 2351731.338(200) | −0.034 | This work, Cologne |
| $6_{3,4}$ | $6_{2,5}$ | 2477452.945(150) | −0.315 | [178] |
| $8_{1,7}$ | $8_{0,8}$ | 2579630.342(150) | −0.617 | This work, JPL |
| $10_{4,6}$ | $10_{3,7}$ | 2583945.090(150) | −0.927 | This work, JPL |

Table C.2: HDO - continued

| $N'_{Ka'Kc'}$ | $N''_{Ka''Kc''}$ | Frequency [MHz][a] | o.-c. [MHz] | Reference |
|---|---|---|---|---|
| | | $v_2 = 1 \leftarrow 0$ | | |
| $5_{2,4}$ | $5_{1,5}$ | 44372102.9700(20) | 0.0003 | [179] |
| | | $v_2 = 1$ | | |
| $2_{2,0}$ | $2_{2,1}$ | 10557.1615(17) | −0.0089 | This work, Kiel |
| $4_{3,2}$ | $5_{2,3}$ | 19173.575(6) | 0.012 | This work, Kiel |
| $11_{5,6}$ | $11_{5,7}$ | 20005.382(13) | 0.039 | This work, Kiel |
| $5_{3,2}$ | $5_{3,3}$ | 21820.0359(13) | 0.0031 | This work, Kiel |
| $8_{4,4}$ | $8_{4,5}$ | 23168.304(4) | −0.014 | This work, Kiel |
| $6_{2,5}$ | $5_{3,2}$ | 27892.290(50) | −0.134 | [150] |
| $3_{2,1}$ | $3_{2,2}$ | 51675.470(50) | 0.147 | [150] |
| $6_{3,3}$ | $6_{3,4}$ | 63155.550(50) | 0.405 | [150] |
| $3_{1,2}$ | $2_{2,1}$ | 67153.040(50) | 0.114 | [150] |
| $12_{2,11}$ | $11_{3,8}$ | 82646.889(50) | −0.042 | This work, JPL |
| $1_{1,0}$ | $1_{1,1}$ | 86935.382(50) | 0.026 | This work, JPL |
| $13_{5,8}$ | $13_{5,9}$ | 96864.427(50) | 0.001 | This work, JPL |
| $6_{4,3}$ | $7_{3,4}$ | 131666.991(50) | −0.104 | This work, JPL |
| $4_{2,2}$ | $4_{2,3}$ | 148307.286(50) | −0.092 | This work, JPL |
| $7_{3,4}$ | $7_{3,5}$ | 149231.142(50) | 0.027 | This work, JPL |
| $8_{3,6}$ | $7_{4,3}$ | 172840.350(50) | 0.092 | This work, JPL |
| $3_{2,1}$ | $4_{1,4}$ | 230427.340(50) | −0.343 | [151] |
| $6_{2,4}$ | $7_{1,7}$ | 263019.642(50) | −0.003 | This work, JPL |
| $6_{4,2}$ | $7_{3,5}$ | 283126.075(50) | −0.045 | This work, JPL |
| $5_{2,3}$ | $5_{2,4}$ | 321887.048(50) | −0.014 | This work, JPL |
| $7_{2,6}$ | $6_{3,3}$ | 335139.518(50) | −0.088 | This work, JPL |
| $4_{3,1}$ | $5_{2,4}$ | 346634.044(50) | −0.058 | This work, JPL |
| $2_{0,2}$ | $1_{1,1}$ | 434517.710(50) | −0.238 | [150] |
| $2_{0,2}$ | $1_{1,1}$ | 434517.764(100) | −0.184 | This work, JPL |
| $1_{0,1}$ | $0_{0,0}$ | 466402.000(50) | −0.023 | [150] |
| $3_{1,2}$ | $3_{1,3}$ | 519750.317(50) | 0.274 | This work, JPL |
| $7_{2,5}$ | $8_{1,8}$ | 542836.093(50) | 0.021 | This work, JPL |
| $8_{2,7}$ | $7_{3,4}$ | 548428.153(50) | 0.191 | This work, JPL |
| $1_{1,0}$ | $1_{0,1}$ | 574366.714(50) | 0.108 | This work, JPL |
| $6_{2,4}$ | $6_{2,5}$ | 583238.334(50) | 0.074 | This work, JPL |
| $9_{3,7}$ | $8_{4,4}$ | 596647.522(50) | −0.047 | This work, JPL |
| $3_{3,1}$ | $4_{2,2}$ | 616666.473(50) | −0.251 | This work, JPL |
| $6_{2,4}$ | $5_{3,3}$ | 632950.684(50) | −0.032 | This work, JPL |
| $9_{2,8}$ | $8_{3,5}$ | 641527.584(50) | 0.074 | This work, JPL |
| $2_{1,1}$ | $2_{0,2}$ | 671641.716(100) | 0.042 | This work, JPL |
| $2_{1,1}$ | $2_{0,2}$ | 671641.750(50) | 0.076 | [150] |
| $4_{1,3}$ | $3_{2,2}$ | 681865.479(50) | 0.280 | This work, JPL |
| $5_{4,2}$ | $6_{3,3}$ | 692660.880(100) | −0.016 | This work, Cologne |
| $7_{5,2}$ | $8_{4,5}$ | 731061.968(200) | −0.243 | This work, Cologne |
| $11_{4,8}$ | $10_{5,5}$ | 744424.666(200) | 0.018 | This work, Cologne |

Table C.2: HDO - continued

| $N'_{Ka'Kc'}$ | $N''_{Ka''Kc''}$ | Frequency [MHz][a] | o.-c. [MHz] | Reference |
|---|---|---|---|---|
| $5_{4,1}$ | $6_{3,4}$ | 756268.955(100) | 0.042 | This work, Cologne |
| $3_{3,0}$ | $4_{2,3}$ | 765779.635(100) | −0.328 | This work, Cologne |
| $3_{1,2}$ | $3_{0,3}$ | 835662.436(150) | −0.046 | This work, JPL |
| $2_{1,2}$ | $1_{1,1}$ | 845564.717(150) | −0.393 | This work, JPL |
| $4_{1,3}$ | $4_{1,4}$ | 860617.831(200) | 0.272 | This work, JPL |
| $2_{0,2}$ | $1_{0,1}$ | 921949.145(200) | −0.052 | This work, Cologne |
| $7_{2,5}$ | $7_{2,6}$ | 932070.192(300) | 0.235 | This work, Cologne |
| $3_{0,3}$ | $2_{1,2}$ | 945851.583(30) | 0.005 | This work, Cologne |
| $1_{1,1}$ | $0_{0,0}$ | 953833.328(30) | 0.056 | This work, Cologne |
| $10_{3,8}$ | $9_{4,5}$ | 968603.636(300) | −0.303 | This work, Cologne |
| $4_{0,4}$ | $3_{0,3}$ | 1765957.476(200) | −0.099 | This work, Cologne |
| $6_{1,5}$ | $6_{0,6}$ | 1833290.171(200) | 0.324 | This work, Cologne |
| $3_{2,2}$ | $3_{1,3}$ | 1849939.330(300) | 0.002 | This work, Cologne |
| $4_{2,3}$ | $3_{2,2}$ | 1853954.920(300) | −0.264 | This work, Cologne |
| $4_{3,2}$ | $3_{3,1}$ | 1879007.160(200) | 0.250 | This work, Cologne |
| $4_{3,1}$ | $3_{3,0}$ | 1883774.302(300) | −0.223 | This work, Cologne |
| $5_{0,5}$ | $4_{1,4}$ | 1930965.563(300) | 0.499 | This work, Cologne |
| $9_{3,6}$ | $9_{2,7}$ | 1948102.143(100) | 0.471 | This work, Cologne |
| $4_{2,2}$ | $3_{2,1}$ | 1950586.997(50) | −0.241 | This work, Cologne |
| $6_{1,5}$ | $5_{2,4}$ | 1953579.903(300) | 0.985 | This work, Cologne |
| $4_{1,4}$ | $3_{0,3}$ | 1987098.706(500) | −0.701 | This work, Cologne |
| $10_{3,7}$ | $10_{2,8}$ | 1987282.661(300) | −0.654 | This work, Cologne |
| $8_{3,5}$ | $8_{2,6}$ | 1997617.234(100) | −0.341 | This work, Cologne |

[a] Numbers in parentheses give the experimental uncertainty in units of the last digits.

Table C.3: Rotational transitions of HDO in the ground vibrational state with partially resolved hyperfine structure. The two newly measured transitions are compiled together with earlier beam maser data.

| $J'_{Ka'Kc'}$ | $F'_1$ | $F'$ | $J''_{Ka''Kc''}$ | $F''_1$ | $F''$ | Frequency [MHz][a] | o.-c. [MHz] | Reference |
|---|---|---|---|---|---|---|---|---|
| $5_{4,1}$ | 5 | 5 | $5_{4,2}$ | 4 | 4 | 486.44967(33) | 0.00027 | [180] |
| $5_{4,1}$ | 5 | 6 | $5_{4,2}$ | 4 | 5 | [b] | | |
| $5_{4,1}$ | 5 | 6 | $5_{4,2}$ | 6 | 7 | 486.48697(25) | 0.00001 | [180] |
| $5_{4,1}$ | 5 | 5 | $5_{4,2}$ | 6 | 6 | [b] | | |
| $5_{4,1}$ | 4 | 5 | $5_{4,2}$ | 4 | 5 | 486.52800(200) | −0.00010 | [180] |
| $5_{4,1}$ | 6 | 6 | $5_{4,2}$ | 5 | 5 | 486.56877(29) | −0.00010 | [180] |
| $5_{4,1}$ | 6 | 7 | $5_{4,2}$ | 5 | 6 | [b] | | |
| $5_{4,1}$ | 4 | 5 | $5_{4,2}$ | 5 | 6 | 486.60641(27) | −0.00011 | [180] |
| $5_{4,1}$ | 4 | 4 | $5_{4,2}$ | 5 | 5 | [b] | | |
| $3_{3,0}$ | 3 | 4 | $3_{3,1}$ | 2 | 3 | 824.47545(65) | −0.00006 | [180] |
| $3_{3,0}$ | 4 | 5 | $3_{3,1}$ | 4 | 4 | 824.50735(71) | −0.00008 | [180] |
| $3_{3,0}$ | 3 | 3 | $3_{3,1}$ | 4 | 4 | 824.52469(57) | −0.00124 | [180] |
| $3_{3,0}$ | 2 | 3 | $3_{3,1}$ | 2 | 2 | 824.54869(77) | −0.00059 | [180] |

Table C.3: HDO hyperfine structure - continued

| $J'_{Ka'Kc'}$ | $F'_1$ | $F'$ | $J''_{Ka''Kc''}$ | $F''_1$ | $F''$ | Frequency [MHz][a] | o.-c. [MHz] | Reference |
|---|---|---|---|---|---|---|---|---|
| $3_{3,0}$ | 3 | 4 | $3_{3,1}$ | 3 | 3 | [b] | | |
| $3_{3,0}$ | 3 | 4 | $3_{3,1}$ | 4 | 5 | 824.56853(63) | 0.00008 | [180] |
| $3_{3,0}$ | 2 | 3 | $3_{3,1}$ | 4 | 4 | 824.60421(59) | 0.00199 | [180] |
| $3_{3,0}$ | 2 | 3 | $3_{3,1}$ | 2 | 3 | 824.67060(200) | 0.00338 | [180] |
| $3_{3,0}$ | 4 | 4 | $3_{3,1}$ | 2 | 3 | 824.74195(96) | 0.00052 | [180] |
| $3_{3,0}$ | 4 | 5 | $3_{3,1}$ | 3 | 4 | 824.77303(85) | 0.00001 | [180] |
| $3_{3,0}$ | 3 | 3 | $3_{3,1}$ | 3 | 4 | 824.79043(88) | −0.00004 | [180] |
| $3_{3,0}$ | 2 | 2 | $3_{3,1}$ | 2 | 3 | [b] | | |
| $3_{3,0}$ | 4 | 4 | $3_{3,1}$ | 3 | 3 | 824.81355(91) | −0.00021 | [180] |
| $3_{3,0}$ | 4 | 4 | $3_{3,1}$ | 4 | 5 | 824.83413(120) | 0.00021 | [180] |
| $3_{3,0}$ | 2 | 3 | $3_{3,1}$ | 3 | 4 | 824.86373(98) | −0.00100 | [180] |
| $4_{3,1}$ | 4 | 4 | $4_{3,2}$ | 5 | 5 | 5702.8120(10) | 0.0014 | [182] |
| $4_{3,1}$ | 4 | 5 | $4_{3,2}$ | 5 | 6 | [b] | | |
| $4_{3,1}$ | 4 | 4 | $4_{3,2}$ | 4 | 4 | 5702.8300(10) | 0.0007 | [182] |
| $4_{3,1}$ | 5 | 5 | $4_{3,2}$ | 5 | 5 | [b] | | |
| $4_{3,1}$ | 3 | 3 | $4_{3,2}$ | 3 | 3 | [b] | | |
| $4_{3,1}$ | 4 | 5 | $4_{3,2}$ | 4 | 5 | [b] | | |
| $4_{3,1}$ | 5 | 6 | $4_{3,2}$ | 5 | 6 | [b] | | |
| $4_{3,1}$ | 3 | 4 | $4_{3,2}$ | 3 | 4 | [b] | | |
| $4_{3,1}$ | 5 | 5 | $4_{3,2}$ | 4 | 4 | 5702.8496(10) | 0.0018 | [182] |
| $4_{3,1}$ | 5 | 6 | $4_{3,2}$ | 4 | 5 | [b] | | |
| $2_{2,0}$ | 2 | 3 | $2_{2,1}$ | 3 | 3 | 10278.0599(5) | −0.0010 | [181] |
| $2_{2,0}$ | 2 | 2 | $2_{2,1}$ | 1 | 1 | 10278.0806(5) | −0.0002 | [181] |
| $2_{2,0}$ | 2 | 3 | $2_{2,1}$ | 1 | 2 | [b] | | |
| $2_{2,0}$ | 2 | 2 | $2_{2,1}$ | 3 | 3 | 10278.1361(5) | −0.0016 | [181] |
| $2_{2,0}$ | 3 | 4 | $2_{2,1}$ | 3 | 3 | [b] | | |
| $2_{2,0}$ | 2 | 3 | $2_{2,1}$ | 3 | 4 | 10278.1683(5) | −0.0010 | [181] |
| $2_{2,0}$ | 2 | 3 | $2_{2,1}$ | 2 | 2 | [b] | | |
| $2_{2,0}$ | 1 | 2 | $2_{2,1}$ | 3 | 3 | 10278.2261(5) | −0.0004 | [181] |
| $2_{2,0}$ | 3 | 3 | $2_{2,1}$ | 3 | 3 | 10278.2459(5) | −0.0001 | [181] |
| $2_{2,0}$ | 2 | 2 | $2_{2,1}$ | 2 | 2 | [b] | | |
| $2_{2,0}$ | 1 | 1 | $2_{2,1}$ | 1 | 1 | [b] | | |
| $2_{2,0}$ | 2 | 3 | $2_{2,1}$ | 2 | 3 | [b] | | |
| $2_{2,0}$ | 1 | 2 | $2_{2,1}$ | 1 | 2 | [b] | | |
| $2_{2,0}$ | 3 | 4 | $2_{2,1}$ | 3 | 4 | [b] | | |
| $2_{2,0}$ | 3 | 3 | $2_{2,1}$ | 1 | 2 | 10278.2655(5) | 0.0006 | [181] |
| $2_{2,0}$ | 2 | 2 | $2_{2,1}$ | 2 | 3 | 10278.3246(5) | 0.0007 | [181] |
| $2_{2,0}$ | 3 | 4 | $2_{2,1}$ | 2 | 3 | [b] | | |
| $2_{2,0}$ | 3 | 3 | $2_{2,1}$ | 3 | 4 | 10278.3541(5) | 0.0007 | [181] |
| $2_{2,0}$ | 3 | 3 | $2_{2,1}$ | 2 | 2 | [b] | | |
| $2_{2,0}$ | 1 | 1 | $2_{2,1}$ | 2 | 2 | 10278.4121(5) | 0.0003 | [181] |
| $2_{2,0}$ | 1 | 2 | $2_{2,1}$ | 2 | 3 | [b] | | |
| $2_{2,0}$ | 3 | 3 | $2_{2,1}$ | 2 | 3 | [b] | | |
| $6_{2,4}$ | 6 | 6 | $7_{0,7}$ | 7 | 7 | 11618.0583(55) | 0.0055 | This work, Kiel |

Table C.3: HDO hyperfine structure - continued

| $J'_{Ka'Kc'}$ | $F'_1$ | $F'$ | $J''_{Ka''Kc''}$ | $F''_1$ | $F''$ | Frequency [MHz][a] | o.-c. [MHz] | Reference |
|---|---|---|---|---|---|---|---|---|
| $6_{2,4}$ | 6 | 7 | $7_{0,7}$ | 8 | 8 | 11618.0796(43) | −0.0087 | This work, Kiel |
| $6_{2,4}$ | 5 | 5 | $7_{0,7}$ | 6 | 6 | [b] | | |
| $6_{2,4}$ | 7 | 7 | $7_{0,7}$ | 8 | 8 | [b] | | |
| $6_{2,4}$ | 7 | 7 | $7_{0,7}$ | 7 | 8 | [b] | | |
| $6_{2,4}$ | 7 | 8 | $7_{0,7}$ | 8 | 9 | 11618.1410(14) | −0.0002 | This work, Kiel |
| $6_{2,4}$ | 5 | 6 | $7_{0,7}$ | 6 | 7 | [b] | | |
| $3_{2,1}$ | 4 | 5 | $4_{1,4}$ | 4 | 5 | 20459.9043(10) | −0.0004 | [182] |
| $3_{2,1}$ | 4 | 4 | $4_{1,4}$ | 4 | 4 | 20459.9138(10) | −0.0004 | [182] |
| $3_{2,1}$ | 3 | 4 | $4_{1,4}$ | 4 | 5 | [b] | | |
| $3_{2,1}$ | 3 | 3 | $4_{1,4}$ | 4 | 4 | 20459.9219(10) | −0.0005 | [182] |
| $3_{2,1}$ | 3 | 4 | $4_{1,4}$ | 5 | 5 | 20459.9455(10) | 0.0012 | [182] |
| $3_{2,1}$ | 4 | 4 | $4_{1,4}$ | 4 | 5 | 20460.0009(10) | −0.0011 | [182] |
| $3_{2,1}$ | 3 | 3 | $4_{1,4}$ | 3 | 3 | 20460.0214(10) | 0.0007 | [182] |
| $3_{2,1}$ | 4 | 5 | $4_{1,4}$ | 5 | 6 | [b] | | |
| $3_{2,1}$ | 2 | 2 | $4_{1,4}$ | 3 | 3 | 20460.0316(10) | −0.0002 | [182] |
| $3_{2,1}$ | 4 | 4 | $4_{1,4}$ | 5 | 5 | [b] | | |
| $3_{2,1}$ | 2 | 3 | $4_{1,4}$ | 3 | 4 | 20460.0377(10) | 0.0006 | [182] |
| $13_{1,12}$ | 13 | 14 | $12_{3,9}$ | 13 | 13 | 20767.1527(268) | 0.0036 | This work, Kiel |
| $13_{1,12}$ | 12 | 13 | $12_{3,9}$ | 11 | 12 | [b] | | |
| $13_{1,12}$ | 14 | 15 | $12_{3,9}$ | 13 | 14 | [b] | | |
| $13_{1,12}$ | 13 | 14 | $12_{3,9}$ | 12 | 13 | [b] | | |
| $13_{1,12}$ | 12 | 12 | $12_{3,9}$ | 11 | 11 | 20767.2431(328) | −0.0001 | This work, Kiel |
| $13_{1,12}$ | 14 | 14 | $12_{3,9}$ | 13 | 13 | [b] | | |
| $13_{1,12}$ | 13 | 13 | $12_{3,9}$ | 12 | 12 | [b] | | |
| $5_{3,2}$ | 5 | 6 | $5_{3,3}$ | 5 | 5 | 22307.3629(40) | 0.0035 | [182] |
| $5_{3,2}$ | 6 | 7 | $5_{3,3}$ | 6 | 6 | [b] | | |
| $5_{3,2}$ | 6 | 6 | $5_{3,3}$ | 5 | 5 | 22307.4827(40) | 0.0061 | [182] |
| $5_{3,2}$ | 6 | 7 | $5_{3,3}$ | 5 | 6 | [b] | | |
| $5_{3,2}$ | 5 | 5 | $5_{3,3}$ | 5 | 5 | 22307.5105(40) | 0.0068 | [182] |
| $5_{3,2}$ | 6 | 6 | $5_{3,3}$ | 6 | 6 | [b] | | |
| $5_{3,2}$ | 4 | 4 | $5_{3,3}$ | 4 | 4 | [b] | | |
| $5_{3,2}$ | 5 | 6 | $5_{3,3}$ | 5 | 6 | [b] | | |
| $5_{3,2}$ | 6 | 7 | $5_{3,3}$ | 6 | 7 | [b] | | |
| $5_{3,2}$ | 4 | 5 | $5_{3,3}$ | 4 | 5 | [b] | | |
| $5_{3,2}$ | 5 | 5 | $5_{3,3}$ | 6 | 6 | 22307.5370(40) | 0.0069 | [182] |
| $5_{3,2}$ | 5 | 6 | $5_{3,3}$ | 6 | 7 | [b] | | |
| $5_{3,2}$ | 6 | 6 | $5_{3,3}$ | 6 | 7 | 22307.6587(40) | 0.0110 | [182] |
| $5_{3,2}$ | 5 | 5 | $5_{3,3}$ | 5 | 6 | [b] | | [182] |

[a] Numbers in parentheses give the experimental uncertainty in units of the last digits.

[b] These lines are blended with those written above. They were intensity weighted in the fit.

# Bibliography


[1] H. M. Pickett, J. C. Pearson, and C. E. Miller. Use of Euler Series to Fit spectra with Application to Water. *J. Mol. Spectrosc.*, submitted, 2005.

[2] S. Weinreb, A. H. Barrett, M. L. Meeks, and J. C. Henry. Radio Observations of OH in the Interstellar Medium. *Nature*, 200:829, 1963.

[3] G. Winnewisser, A. F. Krupnov, M. Y. Tretyakov, M. Liedtke, F. Lewen, A. H. Saleck, R. Schieder, A. P. Shkaev, and S. V. Volokhov. Precision broadband Spectroscopy in the Terahertz Region. *J. Mol. Spectrosc.*, 165:294–300, 1994.

[4] G. Winnewisser. Spectroscopy in the Terahertz region. *Vib. Spectrosc.*, 8:241, 1995.

[5] F. Maiwald, F. Lewen, V. Ahrens, M. Beaky, R. Gendriesch, A. N. Koroliev, A. A. Negirev, D. G. Paveljev, B. Vowinkel, and G. Winnewisser. Pure Rotational Spectrum of HCN in the Terahertz Region: Use of a New Planar Schottky Diode Multiplier. *J. Mol. Spectrosc.*, 202:166–168, 2000.

[6] F. Lewen, E. Michael, R. Gendriesch, J. Stutzki, and G. Winnewisser. Terahertz Laser Sideband Spectroscopy with Backward Wave Oscillators. *J. Mol. Spectrosc.*, 183:207–209, 1997.

[7] R. Gendriesch. *Präzisionsbreitband-Spektroskpie bei 2 Terahertz*. PhD thesis, Universität zu Köln, 2000.

[8] L. E. Snyder and D. Buhl. Observations of Radio Emission from Interstellar Hydrogen Cyanide. *ApJL*, 163:L47, 1971.

[9] J. Cernicharo, M. J. Barlow, E. Gonzalez-Alfonso, P. Cox, P. E. Clegg, Nguyen-Q-Rieu, A. Omont, M. Guelin, and X.-W. Liu *et al.* The ISO/LWS far infrared spectrum of IRC+10 216. *A&A*, 315:L201–L204, 1996.

[10] H. Roberts, E. Herbst, and T. J. Millar. The chemistry of multiply deuterated species in cold, dense interstellar cores. *A&A*, 424:905–917, 2004.

[11] E. Gonzalez-Alfonso and J. Cernicharo. HCN hyperfine anomalies in dark clouds. *A&A*, 279:506–520, 1993.

[12] J. M. Hollis, P. R. Jewell, and F. J. Lovas. Confirmation of interstellar methylene. *ApJ*, 438:259–264, 1995.

[13] D. P. Ruffle and E. Herbst. New models of interstellar gas-grain chemistry - II. Surface photochemistry in quiescent cores. *Mon. Not. R. Astron. Soc.*, 322:770–778, 2001.

[14] E. Polehampton, K. M. Menten, S. Brünken, G. Winnewisser, and J.-P. Baluteau. Far-Infrared detection of methylene. *A&A*, 431:203–213, 2005.

[15] T. de Graauw. Heterodyne Instrument for the Far Infrared (HIFI)for the Herschel Space Observatory. *American Astronomical Society Meeting Abstracts*, 204, 2004.

[16] D. A. Neufeld and G. J. Melnick. $H_2O$ line emission from shocked gas. *ApJ*, 322:266–274, 1987.

[17] K. M. Menten and G. J. Melnick. Hot water around late-type stars - Detection of two millimeter-wave emission lines from the $\nu_2$ vibrationally excited state. *ApJL*, 341:L91–L94, 1989.

[18] P. Bernath. The Spectroscopy of Water Vapour: Experiment, Theory and Applications. *Phys. Chem. Chem. Phys*, 4:1501–1509, 2002.

[19] L. H. Coudert, O. Pirali, M. Vervloet, R. Lanquetin, and C. Camy-Peyret. The eight first vibrational states of the water molecule: measurements and analysis. *J. Mol. Spectrosc.*, 228:471–498, 2004.

[20] L. Ajili, G. Scalari, J. Faist, H. Beere, E. Linfield, D. Ritchie, and G. Davies. High power quantum cascade lasers operating at $\lambda = 87$ and $130$ $\mu$m. *Applied Physics Letters*, 85:3986–3988, 2004.

[21] W. E. Lamb. Theory of an Optical Maser. *Phys. Rev.*, 134:1429–1450, 1964.

[22] W. Demtröder. *Laserspektroskopie*. Springer Verlag, Berlin, 1991.

[23] P. F. Bernath. *Spectra of Atoms and Molecules*. Oxford University Press, New York, 1995.

[24] G. Klapper, F. Lewen, R. Gendriesch, S. P. Belov, and G. Winnewisser. Sub-Doppler Measurements of the Rotational Spectrum of $^{13}C^{16}O$. *J. Mol. Spectrosc.*, 201:124–127, 2000.

[25] G. Winnewisser, S. P. Belov, T. Klaus, and R. Schieder. Sub-Doppler Measurements on the Rotational Transitions of Carbon Monoxide. *J. Mol. Spectrosc.*, 184:468–472, 1997.

[26] V. S. Letokhov and V. P. Chebotayev. *Nonlinear Laser Spectroscopy*. Springer Series in Opt. Science, Vol. 4, 1977.

[27] A. Maestrini, J. Ward, J. Ward, G. Chattopadhyay, F. Maiwald, K. Ellis, H. Javadi, and I. Mehdi. A Planar-Diode Frequency Tripler at 1.9 THz. In *2003 IEEE MTT-S International Microwave Symposium Digest*, Philadelphia, 2003.

[28] E. A. Michael. *Aufbau und Charakterisierung eines kompakten optisch gepumpten Ferninfrarot-Ringlasers mit offenem Resonator und variabler Auskopplung*. PhD thesis, Universität zu Köln, 1995.

[29] E. Michael, F. Lewen, R. Gendriesch, J. Stutzki, and G. Winnewisser. Frequency lock of an optically pumped FIR ring laser at 803 and 1626 GHz. *Int. J. Infrared Millimeter Waves*, 20:1073–1083, 1999.

[30] H. M. Pickett, R. L. Poynter, E. A. Cohen, M. L. Delitsky, J. C. Pearson, and H. S. P. Müller. Submillimeter, Millimeter, and Microwave Spectral Line Catalog. *J. Quant. Spectrosc. Radiat. Transfer*, 60:11865–11875, 1999.

[31] W. Gordy and R. L. Cook. *Microwave Molecular Spectra*. John Wiley & Sons, New York, 1984.

[32] H. Klein, F. Lewen, R. Schieder, J. Stutzki, and G. Winnewisser. Precise Laboratory Observation of the $^3P_2 \leftarrow ^3P_1$ Fine-Structure Transitions of $^{12}C$ and $^{13}C$. *ApJL*, 494:L125, 1998.

[33] K. Sarka, D. Papousek, J. Demaison, H. Mäder, and H. Harder. *Advanced Series in Physical Chemisry: Vibration-Rotational Spectroscopy and Molecular Dynamics*. World Scientific, 1997.

[34] J. Ekkers and W. H. Flygare. Pulsed microwave fourier-transform spectrometer. *Rev. Sci. Instrum.*, 47:448, 1976.

[35] V. Meyer, W. Jäger, R. Schwarz, and H. Dreizler. A Microwave Fourier Transform Spectrometer in the Range from 18 to 26.4 GHz with Increased Sensitivity Using Circular Waveguides. Measurements of Isotopomers of Carbonylsulfide and of Methane. *Z. Naturforsch. A*, 46:445–449, 1991.

[36] J. M. Brown, J. T. Hougen, K. P. Huber, J. W. C. Johns, I. Kop, H. Lefebvre-Brion, A. J. Merer, D. A. Ramsey, J. Rostas, and R. N. Zare. The labeling of parity doublet levels in linear molecules. *J. Mol. Spectrosc.*, 55:500, 1975.

[37] K. Yamada. Effect of phase-choices in rovibrational wavefunctions on the labeling of $k$-type and $\ell$-type doubling in molecular-energy levels. *Z. Naturforsch. A*, 38:821–834, 1983.

[38] C. H. Townes and A. L. Schawlow. *Microwave Spectroscopy*. Dover Publications, Inc., New York, 1955.

[39] J. K. G. Watson. Determination of centrifugal-distortion coefficients of asymmetric-top molecules. *J. Chem. Phys*, 46:1935–1949, 1967.

[40] J. K. G. Watson. Aspects of quartic and sextic centrifugal effects on rotational energy levels. In J. R. Durig, editor, *Vibrational Spectra and Structure*, Amsterdam, 1977. Elsevier, 1977.

[41] R. Gendriesch, F. Lewen, G. Winnewisser, and H. S. P. Müller. Far-infrared laser-sideband measurements of the amidogen radical, $NH_2$, near 2 THz with microwave accuracy. *J. Mol. Struct.*, 599:293–304, 2001.

[42] H. S. P. Müller and S. Brünken. Accurate rotational spectroscopy of sulfur dioxide, $So_2$, in its ground vibrational and first excited bending states, $v_2 = 0$, 1, up to 2 THz. *J. Mol. Spectrosc.*, accepted, 2005.

[43] T. J. Sears, P. R. Bunker, A. R. W. McKellar, K. M. Evenson, D. A. Jennings, and J. M. Brown. The rotational spectrum and hyperfine structure of the methylene radical $CH_2$ studied by far-infrared laser magnetic resonance spectroscopy. *J. Chem. Phys.*, 77:5348–5362, 1982.

[44] J. M. Brown and T. J. Sears. A reduced form of the spin-rotation Hamiltonian for asymmetric-top molecules, with applications to $HO_2$ and $NH_2$. *J. Mol. Spectrosc.*, 75:111–133, 1979.

[45] J. Verhoeven and A. Dynamus. Magnetic Properties and Molecular Quadrupole Tensor of the Water Molecule by Beam-Maser Zeeman Spectroscopy. *J. Chem. Phys.*, 52:3222–3233, 1970.

[46] K. B. Jefferts, A. A. Penzias, and R. W. Wilson. Deuterium in the Orion Nebula. *ApJL*, 179:L57–L59, 1973.

[47] R. W. Wilson, A. A. Penzias, K. B. Jefferts, and P. M. Solomon. Interstellar Deuterium: the Hyperfine Structure of DCN. *ApJL*, 179:L107–L110, 1973.

[48] S. D. Rodgers and T. J. Millar. The chemistry of deuterium in hot molecular cores. *Mon. Not. R. Astron. Soc.*, 280:1046–1054, 1996.

[49] H. Roberts, G. A. Fuller, T. J. Millar, J. Hatchell, and J. V. Buckle. A survey of [HDCO]/[$H_2$CO] and [DCN]/[HCN] ratios towards low-mass protostellar cores. *A&A*, 381:1026–1038, 2002.

[50] J. Hatchell, T. J. Millar, and S. D. Rodgers. The DCN/HCN abundance ratio in hot molecular cores. *A&A*, 332:695–702, 1998.

[51] D. C. Lis, E. Roueff, M. Gerin, T. G. Phillips, L. H. Coudert, F. F. S. van der Tak, and P. Schilke. Detection of Triply Deuterated Ammonia in the Barnard 1 Cloud. *ApJL*, 571:L55–L58, 2002.

[52] F. Bensch, I. Pak, J. G. A. Wouterloot, G. Klapper, and G. Winnewisser. Detection of $^{13}C^{17}O$ and Observations of Rare CO Isotopomers toward the $\rho$ Ophiuchi Molecular Cloud. *ApJL*, 562:L185–L188, 2001.

[53] A. M. S. Boonman, R. Stark, F. F. S. van der Tak, E. F. van Dishoeck, P. B. van der Wal, F. Schäfer, G. de Lange, and W. M. Laauwen. Highly Abundant HCN in the Inner Hot Envelope of GL 2591: Probing the Birth of a Hot Core? *ApJL*, 553:L63–L67, 2001.

[54] S. Thorwirth, F. Wyrowski, P. Schilke, K. M. Menten, S. Brünken, H. S. P. Müller, and G. Winnewisser. Detection of HCN Direct *l*-type transitions Probing Hot Molecular Gas in the Proto-Planetary Nebula CRL 618. *ApJ*, 586:338–343, 2003.

[55] J. W. Simmons, W. E. Anderson, and W. Gordy. Microwave Spectrum and Molecular Constants of Hydrogen Cyanide. *Physical Review*, 77:77–79, 1950.

[56] A. Miyahara, H. Hirakawa, and K. Shimoda. $\ell$-Type Doubling Spectra of HCN and DCN in the SHF Region. *J. Phys. Soc. Japan*, 11:335, 1956.

[57] H. Hirakawa, T. Oka, and K. Shimoda. $\ell$-Type Doubling Spectra of HCN and DCN. *J. Phys. Soc. Japan*, 11:1208, 1956.

[58] T. Törring. $\ell$-Typ-Dubletts der isotopen HCN-Molekeln. *Z. Physik*, 161:179, 1961.

[59] A. G. Maki and D. R. Lide. Microwave and Infrared Measurements on HCN and DCN: Observations on $\ell$-Type Resonance Doublets. *J. Chem. Phys.*, 47:3206, 1967.

[60] M. Winnewisser and J. Vogt. $\ell$-Type Doublet Transitions of the Rare Staable Isotopic Species of Hydrogen Cyanide, HCN. *Z. Naturforsch.*, 33a:1323–1327, 1978.

[61] E. Fliege, H. Dreizler, A. P. Cox, and S. D. Hubbard. Quadrupole Hyperfine Structure of the Direct $\ell$-Type Doubling Spectrum of Hydrogen Cyanide by Microwave Fourier Transform spectroscopy. *Z. Naturforsch.*, 39a:1104–1107, 1984.

[62] A. G. Maki. Microwave Spectra of Molecules of Astrophysical Interest - VI. Carbonyl Sulfide and Hydrogen Cyanide. *J. Phys. Chem. Ref. Data*, 3:221–244, 1974.

[63] N. V. Thanh and I. Rossi. Line Parameters for the 1-200 GHz Spectral Range of HCN and DCN. *J. Mol. Spectrosc.*, 157:68–83, 1993.

[64] J. Preusser and A. G. Maki. Millimeter-Wave Measurements of Vibrationally Excited States of the HCN Isotopomers $H^{13}C^{14}N$, $H^{12}C^{15}N$, $H^{13}C^{15}N$, $D^{12}C^{14}N$, $D^{13}C^{14}N$, $D^{12}C^{15}N$, and $D^{13}C^{15}N$. *J. Mol. Spectrosc.*, 162:484–497, 1993.

[65] F. De Lucia and W. Gordy. Molecular-beam maser for shorter-millimeter wave regions. Spectral constants of HCN and DCN. *Phys. Rev.*, 187:58–65, 1969.

[66] V. Ahrens, F. Lewen, S. Takano, G. Winnewisser, Š. Urban, A. A. Negirev, and A. N. Koroliev. Sub-Doppler Saturation Spectroscopy of HCN up to 1 THz and Detection of $J = 3 \rightarrow 2(4 \rightarrow 3)$ Emission from TMC1. *Z. Naturforsch*, 57a:669–681, 2002.

[67] S. Thorwirth, H. S. P. Müller, F. Lewen, S. Brünken, V. Ahrens, and G. Winnewisser. A concise New Look at the *l*-type Spectrum of $H^{12}C^{14}N$. *ApJ*, 585:L163–L165, 2003.

[68] Z. Zelinger, T. Amano, V. Ahrens, S. Brünken, F. Lewen, H. S. P. Müller, and G. Winnewisser. Submillimeter-wave spectroscopy of HCN in excited vibrational states. *J. Mol. Spectrosc.*, 220:223–233, 2003.

[69] U. Fuchs, S. Brünken, G. Fuchs, S. Thorwirth, V. Ahrens, F. Lewen, S. Urban, T. Giesen, and G. Winnewisser. High Resolution Spectroscopy of HCN Isotopomers: $H^{13}CN$, $HC^{15}N$, and $H^{13}C^{15}N$ in the Ground and First Excited Bending Vibrational State. *Z. Naturforsch.*, 59:861–872, 2004.

[70] C. M. King and E. R. Nixon. Matrix-Isolation Study of the Hydrogen Cyanide Dimer. *J. Chem. Phys.*, 48:1685–1695, 1968.

[71] E. F. Pearson, R. A. Creswell, M. Winnewisser, and G. Winnewisser. Molecular-structures of HNC and HCN derived from 8 stable isotopic species. *Z. Naturforsch.*, 31a:1394–1397, 1976.

[72] R. M. Garvey and F. C. De Lucia. Nuclear shielding and magnetic hyperfine structure of hydrogen cyanide. *J. Mol. Spectrosc.*, 50:38–44, 1974.

[73] G. Cazzoli and L. Dore. Observation of crossing resonances in the hyperfine structure of the J = 1 ← 0 transition of $DC^{15}N$. *J. Mol. Spectrosc.*, 143:231–236, 1990.

[74] W. Quapp, M. Hirsch, G. C. Mellau, S. Klee, M. Winnewisser, and A. Maki. Climbing the Bending Vibrational Ladder in $D^{13}C^{15}N$ by Hot Gas Emission Spectroscopy. *J. Mol. Spectrosc.*, 195:284–298, 1999.

[75] E. Möllmann, A. G. Maki, M. Winnewisser, B. P. Winnewisser, and W. Quapp. High-Temperature Infrared Emission Spectra of $D^{12}C^{14}N$ and $D^{13}C^{14}N$. *J. Mol. Spectrosc.*, 212:22–31, 2002.

[76] G. Winnewisser, A. G. Maki, and D. R. Johnson. Rotational constants for HCN and DCN. *J. Mol. Spectrosc.*, 39:149–158, 1971.

[77] G. Tomasevich. PhD thesis, Harvard University, 1970.

[78] H.-H. Lee, R. P. A. Bettens, and E. Herbst. Fractional abundances of molecules in dense interstellar clouds: A compendium of recent model results. *A&A*, 119:111–114, 1996.

[79] E. F. van Dishoeck and J. H. Black. Comprehensive models of diffuse interstellar clouds - Physical conditions and molecular abundances. *ApJS*, 62:109–145, 1986.

[80] L. Vejby-Christensen, L. H. Andersen, O. Heber, D. Kella, H. B. Pedersen, H. T. Schmidt, and D. Zajfman. Complete Branching Ratios for the Dissociative Recombination of $H_2O^+$, $H_3O^+$, and $CH_3^+$. *ApJ*, 483:531, 1997.

[81] E. Herbst. The chemistry of interstellar space. *Chem. Soc. Rev.*, 30:168, 2001.

[82] F. J. Lovas, R. D. Suenram, and K. M. Evenson. Laboratory measurement of the $4_{04} - 3_{13}$ 70 GHz transition of ground-state methylene ($CH_2$). *ApJL*, 267:L131–L133, 1983.

[83] H. Ozeki and S. Saito. Laboratory Submillimeter-Wave Spectroscopy of the $CH_2$ ($^3B_1$) Radical. *ApJL*, 451:L97–L99, 1995.

[84] E. A. Michael, F. Lewen, G. Winnewisser, H. Ozeki, H. Habara, and E. Herbst. Laboratory Spectrum of the $1_{11}-2_{02}$ Rotational Transition of $CH_2$. *ApJ*, 596:1356–1362, 2003.

[85] S. Brünken, E. A. Michael, F. Lewen, Th. Giesen, H. Ozeki, G. Winnewisser, P. Jensen, and E. Herbst. High-resolution terahertz spectrum of $CH_2$ - Low J rotational transitions near 2 THz. *Can. J. Chem.*, 82:676–683, 2004.

[86] G. Herzberg and J. Shoosmith. Spectrum and Structure of the Free Methylene Radical. *Nature*, 183:1801, 1959.

[87] G. Herzberg and J. W. C. Johns. On the Structure of $CH_2$ in its Triplet Ground State. *J. Chem. Phys.*, 54:2276, 1971.

[88] P. Jensen and P. R. Bunker. The potential surface and stretching frequencies of X $^3B_1$ methylene ($CH_2$) determined from experiment using the Morse oscillator-rigid bender internal dynamics Hamiltonian. *J. Chem. Phys.*, 89:1327–1332, 1988.

[89] T. J. Sears, P. R. Bunker, and A. R. W. McKellar. Observation of the $\nu_2$ band of $CH_2$ by laser magnetic resonance. *J. Chem. Phys.*, 75:4731–4732, 1981.

[90] T. S. Sears, P. R. Bunker, and A. R. McKellar. The laser magnetic resonance spectrum of the $\nu_2$ band of the methylene radical $CH_2$. *J. Chem. Phys.*, 77:5363–5369, 1982.

[91] J. P. Gu, G. Hirsch, R. J. Buenker, M. Brumm, G. Osmann, P. R. Bunker, and P. Jensen. A theoretical study of the absorption spectrum of singlet $CH_2$. *J. Mol. Struct.*, 517:247–264, 2000.

[92] T. J. Sears, A. R. W. McKellar, P. R. Bunker, K. M. Evenson, and J. M. Brown. Infrared and far-infrared transition frequencies for the $CH_2$ radical. *ApJ*, 276:399–402, 1984.

[93] P. Jensen, P. R. Bunker, and A. R. Hoy. The equilibrium geometry, potential function, and rotation-vibration energies of CH2 in the X$^3B_1$ ground state. *J. Chem. Phys.*, 77:5370–5374, 1982.

[94] P. R. Bunker and P. Jensen. A refined potential surface for the X $^3B_1$ electronic state of methylene $CH_2$. *J. Chem. Phys.*, 79:1224–1228, 1983.

[95] P. R. Bunker, P. Jensen, W. P. Kraemer, and R. Beardsworth. The potential surface of X $^3B_1$ methylene ($CH_2$) and the singlet-triplet splitting. *J. Chem. Phys.*, 85:3724–3731, 1986.

[96] M. D. Marshall and A. R. W. McKellar. The $\nu_2$ fundamental band of triplet $CH_2$. *J. Chem. Phys.*, 85:3716–3723, 1986.

[97] T. J. Sears. Infrared rotational transitions in $CH_2$ X $^3B_1$ observed by diode laser absorption. *J. Chem. Phys.*, 85:3711–3715, 1986.

[98] P. R. and S. R. Langhoff. Ab initio rotation-vibration transition moments for $CH_2$ in the $\tilde{X}^3$ $B_1$ and $\tilde{a}^1A_1$ electronic states. *J. Mol. Spectrosc.*, 102:204–211, 1983.

[99] L. Margules, F. Lewen, G. Winnewisser, P. Botschwina, and H. S. P. Müller. The Rotational Spectrum up to 1 THz and the Molecular Structure of Thiomethylium, $HCS^+$. *Phys. Chem. Chem. Phys.*, 5:2770–2773, 2003.

[100] W. Braun, A. M. Bass, and M. Pilling. Flash Photolysis of Ketene and Diazomethane: The Production and Reaction Kinetics of Triplet and Singlet Methylene. *J. Chem. Phys.*, 52:5131–5143, 1970.

[101] P. E. Clegg, P. A. R. Ade, and C. Armand *et al.* The ISO Long-Wavelength Spectrometer. *A&A*, 315:L38–L42, 1996.

[102] E. A. Bergin, E. Lellouch, M. Harwit, M. A. Gurwell, G. J. Melnick, M. L. N. Ashby, and G. Chin *et al.* Submillimeter Wave Astronomy Satellite Observations of Jupiter and Saturn: Detection of 557 GHZ Water Emission from the Upper Atmosphere. *ApJL*, 539:L147–L150, 2000.

[103] M. A. Gurwell, E. A. Bergin, G. J. Melnick, M. L. N. Ashby, G. Chin, N. R. Erickson, and P. F. Goldsmith *et al.* Submillimeter Wave Astronomy Satellite Observations of the Martian Atmosphere: Temperature and Vertical Distribution of Water Vapor. *ApJL*, 539:L143–L146, 2000.

[104] C. de Bergh, B. Bezard, D. Crisp, J. P. Maillard, T. Owen, J. Pollack, and D. Grinspoon. Water in the deep atmosphere of Venus from high-resolution spectra of the night side. *Advances in Space Research*, 15:79–88, 1995.

[105] A. Lecacheux, N. Biver, J. Crovisier, D. Bockelée-Morvan, P. Baron, R. S. Booth, P. Encrenaz, H.-G. Florén, U. Frisk, Å. Hjalmarson, and S. Kwok *et al.* Observations of water in comets with Odin. *A&A*, 402:L55–L58, 2003.

[106] D. A. Neufeld, M. L. N. Ashby, E. A. Bergin, G. Chin, N. R. Erickson, P. F. Goldsmith, M. Harwit, J. E. Howe, and S. C. Kleiner. *et al.* Observations of Absorption by Water Vapor toward Sagittarius B2. *ApJL*, 539:L111–L113, 2000.

[107] R. L. Snell, J. E. Howe, M. L. N. Ashby, E. A. Bergin, G. Chin, N. R. Erickson, P. F. Goldsmith, M. Harwit, S. C. Kleiner, and D. G. Koch *et al.* Water Abundance in Molecular Cloud Cores. *ApJL*, 539:L101–L105, 2000.

[108] D. A. Neufeld, H. Feuchtgruber, M. Harwit, and G. J. Melnick. Infrared Space Observatory Observations of Far-Infrared Rotational Emission Lines of Water Vapor toward the Supergiant Star VY Canis Majoris. *ApJL*, 517:L147–L150, 1999.

[109] T. Tsuji. Water in Emission in the Infrared Space Observatory Spectrum of the Early M Supergiant Star $\mu$ Cephei. *ApJL*, 540:L99–L102, 2000.

[110] O. L. Polyansky, N. F. Zobov, S. Viti, J. Tennyson, P. F. Bernath, and L. Wallace. High-Temperature Rotational Transitions of Water in Sunspot and Laboratory Spectra. *J. Mol. Spectrosc.*, 186:422–447, 1997.

[111] G. J. Melnick, D. A. Neufeld, K. E. S. Ford, D. J. Hollenbach, and M. L. N. Ashby. Discovery of water vapour around IRC+10216 as evidence for comets orbiting another star. *Nature*, 412:160–163, 2001.

[112] M. J. Claussen, G. M. Heiligman, and K. Y. Lo. Water-vapor maser emission from galactic nuclei. *Nature*, 310:298–300, 1984.

[113] R. Meier, T. C. Owen, H. E. Matthews, D. C. Jewitt, D. Bockelee-Morvan, N. Biver, J. Crovisier, and D. Gautier. A Determination of the HDO/$H_2O$ Ratio in Comet C/1995 O1 (Hale-Bopp). *Science*, 279:842–844, 1998.

[114] T. Encrenaz, E. Lellouch, G. Paubert, and S. Gulkis. The water vapor vertical distribution on mars from millimeter transitions of HDO and $H_2^{18}O$. *Planetary and Space Science*, 49:731–741, 2001.

[115] T. Encrenaz, E. Lellouch, G. Paubert, and S. Gulkis. First detection of HDO in the atmosphere of Venus at radio wavelengths - an estimate of the $H_2O$ vertical distribution. *A&A*, 246:L63–L66, 1991.

[116] C. Ceccarelli, C. Vastel, A. G. G. M. Tielens, A. Castets, A. C. A. Boogert, L. Loinard, and E. Caux. The puzzling detection of $D_2CO$ in the molecular cloud L1689N. *A&A*, 381:L17–L20, 2002.

[117] P. Caselli, F. F. S. van der Tak, C. Ceccarelli, and A. Bacmann. Abundant $H_2D^+$ in the pre-stellar core L1544. *A&A*, 403:L37–L41, 2003.

[118] F. F. S. van der Tak, P. Schilke, H. S. P. Müller, D. C. Lis, T. G. Phillips, M. Gerin, and E. Roueff. Triply deuterated ammonia in NGC 1333. *A&A*, 388:L53–L56, 2002.

[119] B. Parise, A. Castets, E. Herbst, E. Caux, C. Ceccarelli, I. Mukhopadhyay, and A. G. G. M. Tielens. First detection of triply-deuterated methanol. *A&A*, 416:159–163, 2004.

[120] J. E. Beckman, G. D. Watt, G. J. White, J. P. Phillips, R. L. Frost, and J. H. Davis. Detection of the $2_{1,1}$ - $2_{1,2}$ rotational emission line of HDO in the Orion Molecular Cloud. *Mon. Not. R. Astron. Soc.*, 201:357–364, 1982.

[121] H. Olofsson. Deuterated water in Orion-KL and W51M. *A&A*, 134:36–44, 1984.

[122] T. Jacq, C. M. Walmsley, C. Henkel, A. Baudry, R. Mauersberger, and P. R. Jewell. Deuterated water and ammonia in hot cores. *A&A*, 228:447–470, 1990.

[123] J. R. Pardo, J. Cernicharo, F. Herpin, J. Kawamura, J. Kooi, and T. G. Phillips. Deuterium Enhancement in Water toward Orion IRc2 Deduced from HDO Lines above 800 GHz. *ApJ*, 562:799–803, 2001.

[124] C. Henkel, R. Mauersberger, T. L. Wilson, L. E. Snyder, K. M. Menten, and J. G. A. Wouterloot. Deuterated water in Orion-KL and NGC7538. *A&A*, 182:299–304, 1987.

[125] B. Parise, E. Caux, A. Castets, C. Ceccarelli, L. Loinard, A. G. G. M. Tielens, A. Bacmann, S. Cazaux, C. Comito, F. Helmich, C. Kahane, P. Schilke, E. van Dishoeck, V. Wakelam, and A. Walters. HDO abundance in the envelope of the solar-type protostar IRAS 16293-2422. *A&A*, 431:547–554, 2005.

[126] A. V. Burenin, T. M. Fevral'Skikh, E. N. Karyakin, O. L. Polyansky, and S. M. Shapin. Effective Padé Hamiltonian operator and its application for treatment of $H_2{}^{16}O$ rotational spectrum in the ground state. *J. Mol. Spectrosc.*, 100:182–192, 1983.

[127] S. P. Belov, I. N. Kozin, O. L. Polyansky, M. Y. Tret'yakov, and N. F. Zobov. Rotational spectrum of the $H_2^{16}O$ molecule in the (010) excited vibrational state. *J. Mol. Spectrosc.*, 126:113–117, 1987.

[128] V. G. Tyuterev. The generating function approach to the formulation of the effective rotational Hamiltonian. A simple closed form model describing strong centrifugal distortion in water-type nonrigid molecules. *J. Mol. Spectrosc.*, 151:97–129, 1992.

[129] O. L. Polyansky, P. Jensen, and J. Tennyson. A spectroscopically determined potential energy surface for the ground state of $H_2{}^{16}O$: A new level of accuracy. *J. Chem. Phys.*, 101:7651–7657, 1994.

[130] O. L. Polyansky, P. Jensen, and J. Tennyson. The potential energy surface of $H_2{}^{16}O$. *J. Chem. Phys.*, 105:6490–6497, 1996.

[131] L. H. Coudert. Analysis of the rotational levels of water. *J. Mol. Spectrosc.*, 154:427–442, 1992.

[132] L. H. Coudert. Analysis of the Rotational Levels of Water and Determination of the Potential Energy Function for the Bending $\nu_2$ Mode. *J. Mol. Spectrosc.*, 165:406–425, 1994.

[133] L. H. Coudert. Analysis of the Line Positions and Line Intensities in the $\nu_2$ Band of the Water Molecule. *J. Mol. Spectrosc.*, 181:246–273, 1997.

[134] H. Partridge and D. W. Schwenke. The determination of an accurate isotope dependent potential energy surface for water from extensive ab initio calculations and experimental data. *J. Chem. Phys.*, 106:4618–4639, 1997.

[135] D. W. Schwenke. First principles prediction of isotopic shifts in $H_2O$. *J. Chem. Phys.*, 118:6898–6904, 2003.

[136] P. Jensen. The potential energy surface for the electronic ground state of the water molecule determined from experimental data using a variational approach. *J. Mol. Spectrosc.*, 133:438–460, 1989.

[137] N. Papineau, J.-M. Flaud, C. Camy-Peyret, and G. Guelachvili. The $2\nu_2$, $\nu_1$ and $\nu_3$ bands of $D_2{}^{16}O$. The ground state (000) and the triad of interacting states ((020), (100), (001)). *J. Mol. Spectrosc.*, 87:219–232, 1981.

[138] S. A. Clough, Y. Beers, G. P. Klein, and L. S. Rothman. Dipole moment of water from Stark measurements of $H_2O$, HDO, and $D_2O$. *J. Phys. Chem.*, 59:2254–2259, 1973.

[139] R. A. Toth. HDO and $D_2O$ Low Pressure, Long Path Spectra in the 600-3100 $cm^{-1}$ Region. II. $D_2O$ Line Positions and Strengths. *J. Mol. Spectrosc.*, 195:98–122, 1999.

[140] S. Hu, O. N. Ulenikov, E. S. Bekhtereva, G. A. Onopenko, S. He, H. Lin, J. Cheng, and Q. Zhu. High-Resolution Fourier-Transform Intracavity Laser Absorption Spectroscopy of $D_2O$ in the Region of the 4 $\nu_1$+$\nu_3$ Band. *J. Mol. Spectrosc.*, 212:89–95, 2002.

[141] S. He, O. N. Ulenikov, G. A. Onopenko, E. S. Bekhtereva, X. Wang, S. Hu, H. Lin, and Q. Zhu. High-Resolution Fourier Transform Spectrum of the $D_2O$ Molecule in the Region of the Second Triad of Interacting Vibrational States. *J. Mol. Spectrosc.*, 200:34–39, 2000.

[142] A. Bykov, O. Naumenko, L. Sinitsa, B. Voronin, and B. P. Winnewisser. The $3\nu_2$ Band of $D_2{}^{16}O$. *J. Mol. Spectrosc.*, 199:158–165, 2000.

[143] S. V. Shirin, N. F. Zobov, O. L. Polyansky, J. Tennyson, T. Parekunnel, and P. F. Bernath. Analysis of hot $D_2O$ emission using spectroscopically determined potentials. *J. Chem. Phys.*, 120:206–210, 2004.

[144] X. Wang, O. N. Ulenikov, G. A. Onopenko, E. S. Bekhtereva, S. He, S. Hu, H. Lin, and Q. Zhu. High-Resolution Study of the First Hexad of $D_2O$. *J. Mol. Spectrosc.*, 200:25–33, 2000.

[145] P. S. Ormsby, K. N. Rao, M. Winnewisser, B. P. Winnewisser, O. V. Naumenko, A. D. Bykov, and L. N. Sinitsa. The $3\nu_2$ + $\nu_3$, $\nu_1$ + $\nu_2$ + $\nu_3$, $\nu_1$ + $3\nu_2$, $2\nu_1$ + $\nu_2$, and $\nu_2$ + $2\nu_3$ Bands of $D_2{}^{16}O$: The Second Hexade of Interacting States. *J. Mol. Spectrosc.*, 158:109–130, 1993.

[146] O. N. Ulenikov, S. He, G. A. Onopenko, E. S. Bekhtereva, X. Wang, S. Hu, H. Lin, and Q. Zhu. High-Resolution Study of the ($v_1$ + 1/2$v_2$ + $v_3$ = 3) Polyad of Strongly Interacting Vibrational Bands of $D_2O$. *J. Mol. Spectrosc.*, 204:216–225, 2000.

[147] A. D. Bykov, O. V. Naumenko, L. N. Sinitsa, B. P. Winnewisser, M. Winnewisser, P. S. Ormsby, and K. N. Rao. The Hot Band $\nu_1$ + $2\nu_2$ + $\nu_3$ - $\nu_2$ of $D_2{}^{16}O$. *J. Mol. Spectrosc.*, 166:169–175, 1994.

[148] O. N. Ulenikov, S. Hu, E. S. Bekhtereva, G. A. Onopenko, S. He, X. Wang, J. Zheng, and Q. Zhu. High-Resolution Fourier Transform Spectrum of $D_2O$ in the Region Near 0.97 $\mu$m. *J. Mol. Spectrosc.*, 210:18–27, 2001.

[149] F. Matsushima, M. Matsunaga, G. Qian, Y. Ohtaki, R. Wang, and K. Takagi. Frequency Measurement of Pure Rotational Transitions of $D_2O$ from 0.5 to 5 THz. *J. Mol. Spectrosc.*, 206:41–46, 2001.

[150] J. K. Messer, F. C. De Lucia, and P. Helminger. Submillimeter spectroscopy of the major isotopes of water. *J. Mol. Spectrosc.*, 105:139–155, 1984.

[151] O. I. Baskakov, V. A. Alekseev, E. A. Alekseev, and B. I. Polevoi. New Submillimeter Rotational Lines of Water and its Isotopes. *Optika I Spektroskopiya*, 63:1016–1018, 1987.

[152] C. Camy-Peyret, J. M. Flaud, A. Mahmoudi, F. Guelachvili, and J. W. C. Johns. Line positions and intensities in the $\nu_2$ band of $D_2O$: improved pumped $D_2O$ laser frequencies. *Int. J. Infrared Millimeter Waves*, 6:199–233, 1985.

[153] G. Mellau, S. N. Mikhailenko, E. N. Starikova, S. A. Tashkun, H. Over, and V. G. Tyuterev. Rotational levels of the (000) and (010) states of $D_2{}^{16}O$ from hot emission spectra in the 320-860cm$^{-1}$ region. *J. Mol. Spectrosc.*, 224:32–60, 2004.

[154] J. W. C. Johns. High-Resolution far-infrared (20-350 cm$^{-1}$) spectra of several istopic-species of $H_2O$. *Journal of the Optical Society of America B*, 2:1340–1354, 1985.

[155] R. Paso and V. M. Horneman. High-resolution rotational absorption spectra of $H_2{}^{16}O$, $HD^{16}O$, and $D_2{}^{16}O$ between 110 and 500 cm$^{-1}$. *Journal of the Optical Society of America B*, 12:1813–1838, 1995.

[156] O. L. Polyansky, S. V. Csazar, S. V. Shirin, N. F. Zobov, J. Barletta, D. D. Tennyson, D. W. Schwenke, and P. J. Knowles. High-Accuracy ab Initio Rotation-Vibration Transitions for Water. *Science*, 299:539–542, 2003.

[157] H. Bluyssen, J. Verhoeven, and A. Dynamus. Hyperfine Structure of HDO and $D_2O$ by Beam Maser Spectroscopy. *Physics Letters*, 25A:214–215, 1967.

[158] J. Verhoeven, H. Bluyssen, and A. Dynamus. Hyperfine Structure of HDO and $D_2O$ by Beam Maser Spectroscopy. *Physics Letters*, 26A:424–425, 1968.

[159] S. G. Kukolich. Measurement of the Molecular $g$ Values in $H_2O$ and $D_2O$ and Hyperfine Structure in $H_2O$*. *J. Chem. Phys.*, 50:3751–3755, 1969.

[160] R. Bhattacharjee, J. S. Muenter, and M. D. Marshall. Nuclear quadrupole coupling in $D_2O$. *J. Mol. Spectrosc.*, 145:302–307, 1991.

[161] J.-M. Flaud, C. Camy-Peyret, A. Mahmoudi, and G. Guelachvili. The $\nu_2$ band of $HD^{16}O$. *Int. J. Infrared Millimeter Waves*, 7:1063–1090, 1986.

[162] P. Thaddeus, L. C. Krisher, and J. H. N. Loubser. Hyperfine Structure in the Microwave Spectrum of HDO, HDS, $CH_2O$, and CHDO: Beam-Maser Spectroscopy on Asymmetric-Top Molecules. *J. Chem. Phys.*, 40:257–273, 1964.

[163] S. L. Shostak and J. S. Muenter. The dipole moment of water. II. Analysis of the vibrational dependence of the dipole moment in terms of a dipole moment function. *J. Chem. Phys.*, 94:5883–5890, 1991.

[164] E. Bertseva, O. Naumenko, and A. Campargue. The $5\nu_{OH}$ Overtone Transition of HDO. *J. Mol. Spectrosc.*, 203:28–36, 2000.

[165] A. Campargue, E. Bertseva, and O. Naumenko. The Absorption Spectrum of HDO in the 16 300-16 670 and 18 000-18 350 cm$^{-1}$ Spectral Regions. *J. Mol. Spectrosc.*, 204:94–105, 2000.

[166] O. Naumenko, E. Bertseva, and A. Campargue. The $4\nu_{OH}$ Absorption Spectrum of HDO. *J. Mol. Spectrosc.*, 197:122–132, 1999.

[167] O. Naumenko, E. Bertseva, A. Campargue, and D. W. Schwenke. Experimental and Ab Initio Studies of the HDO Absorption Spectrum in the 13165-13500 $cm^{-1}$ Spectral Region. *J. Mol. Spectrosc.*, 201:297–309, 2000.

[168] O. Naumenko and A. Campargue. High-Order Resonance Interactions in HDO: Analysis of the Absorption Spectrum in the 14980-15350 $cm^{-1}$ Spectral Region. *J. Mol. Spectrosc.*, 199:59–72, 2000.

[169] O. V. Naumenko, S. Voronina, and S.-M. Hu. High resolution Fourier transform spectrum of HDO in the 7500-8200$cm^{-1}$ region: revisited. *J. Mol. Spectrosc.*, 227:151–157, 2004.

[170] R. A. Toth. Measurements of HDO between 4719 and 5843 $cm^{-1}$. *J. Mol. Spectrosc.*, 186:276–292, 1997.

[171] R. A. Toth. Line Positions and Strengths of HDO between 6000 and 7700 $cm^{-1}$. *J. Mol. Spectrosc.*, 186:66–89, 1997.

[172] A. Janca, K. Tereszchuk, P. F. Bernath, N. F. Zobov, S. V. Shirin, O. L. Polyansky, and J. Tennyson. Emission spectrum of hot HDO below 4000 $cm^{-1}$. *J. Mol. Spectrosc.*, 219:132–135, 2003.

[173] S. Hu, O. N. Ulenikov, G. A. Onopenko, E. S. Bekhtereva, S. He, X. Wang, H. Lin, and Q. Zhu. High-Resolution Study of Strongly Interacting Vibrational Bands of HDO in the Region 7600-8100 $cm^{-1}$. *J. Mol. Spectrosc.*, 203:228–234, 2000.

[174] S. Hu, S. He, J. Zheng, X. Wang, Y. Ding, and Q. Zhu. High-resolution analysis of the $\nu_2$+2$\nu_3$ band of HDO. *Chinese Physics*, 10:1021–1027, 2001.

[175] R. A. Toth. HDO and $D_2O$ Low Pressure, Long Path Spectra in the 600-3100 $cm^{-1}$ Region I. HDO Line Positions and Strengths. *J. Mol. Spectrosc.*, 195:73–97, 1999.

[176] T. Parekunnel, P. F. Bernath, N. F. Zobov, S. V. Shirin, O. L. Polyansky, and J. Tennyson. Emission Spectrum of Hot HDO in the 380-2190 $cm^{-1}$ Region. *J. Mol. Spectrosc.*, 210:28–40, 2001.

[177] G. I. Guelachvili. Experimental Doppler-limited spectra of the $\upsilon_2$ bands of $H_2{}^{16}O$, $H_2{}^{17}O$, $H_2{}^{18}O$, and HDO by Fourier-transform between 1066 and 2296 $cm^{-1}$. *Journal of the Optical Society of America*, 73:137–150, 1983.

[178] F. Matsushima, H. Odashima, T. Iwasaki, S. Tsunekawa, and K. Takagi. Frequency measurement of pure rotational transitions of $H_2O$ from 0.5 to 5 THz. *J. Mol. Struct.*, 352:371–378, 1995.

[179] K. J. Siemsen, J. E. Bernard, A. A. Madej, and L. Marmet. Absolute Frequency Measurement of an HDO Absorption Line near 1480 $cm^{-1}$. *J. Mol. Spectrosc.*, 199:144–145, 2000.

[180] E. B. Treacy and Y. Beers. Hyperfine Structure of the Rotational Spectrum of HDO. *J. Chem. Phys.*, 36:14773–1480, 1962.

[181] S. G. Kukolich. Beam maser double resonance measurements on HDO. *J. Chem. Phys.*, 66:4345–4348, 1977.

[182] H. A. Fry and S. G. Kukolich. Beam maser measurements of HDO hyperfine structure. *J. Chem. Phys.*, 76:4387–4391, 1982.

[183] L. Olsen, O. Christiansen, L. Hemmingsen, S. P. A. Sauer, and K. V. Mikkelsen. Electric field gradients of water: A systematic investigation of basis set, electron correlation, and rovibrational effects. *J. Chem. Phys.*, 116:1424–1434, 2002.

[184] F. C. De Lucia, R. L. Cook, P. Helminger, and W. Gordy. Millimeter and submillimeter wave rotational spectrum and centrifugal distortion effects of HDO. *J. Chem. Phys.*, 55:5334–5339, 1971.

# Acknowledgements - Danksagung

An erster Stelle möchte ich mich bei Priv. Doz. Dr. Thomas Giesen dafür bedanken, daß er die Betreuung dieser Arbeit übernommen hat. Die zahlreichen fachlichen und mitunter philosophischen Diskussionen über allerlei spektroskopische Fragestellungen haben mir sehr viel Freude bereitet und mich viel gelehrt.

Ich möchte Herrn Prof. Jan Jolie und Herrn Prof. Per Jensen danken für ihre Bereitschaft, als Begutachter dieser Arbeit zu fungieren; sowie Herrn Prof. Michael Kerschgens für die Übernahme des Vorsitzes in der Disputations-Prüfung.

Einen riesigen Dank möchte ich Dr. Frank Lewen aussprechen, für seine vielfältige Hilfe bei allen Problemen, die einem bei der täglichen Laborarbeit über den Weg laufen, für seine ausführlichen Einweisungen in die Geheimnisse der Elektronik und Terahertz-Spektroskopie, dafür, daß er immer noch ein Hebelchen kennt, mit dem man das Spektrometer noch ein wenig besser “tunen” kann und vor allem für seinen unverwüstlichen Optimismus, der einen jede Krise meistern hilft.

Herr Prof. Gisbert Winnewisser sei herzlichst gedankt für sein Vertrauen in und sein Interesse an meiner Arbeit.

Ein ganz großes Dankeschön geht an Dr. Holger S. P. Müller für die enthusiastische Hilfe bei größeren und kleineren Fitproblemen, die ihn oft an die Grenzen seiner Geduld trieben. Obwohl, es steht natürlich alles in der Dokumentation. Vielen Dank außerdem für die Vielzahl an Ideen und Anregungen, was Projekte, Messungen und die Wahl des richtigen Weins zum Abendessen angeht!

Der jetzigen und ehemaligen Besatzung des Zimmer 317 - Dr. Ute Berndt, Dr. Ulrike Fuchs, Dr. Guido Fuchs, Dr. Patrick Pütz, Christian Endres und Katharina Rettenbacher - sei herzlich gedankt für die gute Arbeitsatmosphäre und vor allem die schöne und unterhaltsame Zeit, wenn gerade mal nicht gearbeitet wurde. Ohne Patrick wäre ich so manchen Abend im Labor oder vor dem Computer verhungert, und sein beruhigender Einfluß bei Panikattacken am Teleskop oder anderen Gelegenheiten war sehr wertvoll.

Vielen Dank an die gesamte Speki-Truppe für die schöne Zeit! Ganz besonderen Dank an Michael Caris für gemeinsames Helium-Füllen, Dr. Sven Thorwirth für “Alles wird gut!”, Dr. Ralf Gendriesch für die Einweisung an COSSTA, Simone Esser und Jan Suhr für die Chemie, Christian Endres für Wassermessungen jenseits 2 THz, Dr. Ulrike Fuchs für stundenlanges gemeinsames Lamb-Dippen, Dr. Ernest Michael für viel Hilfe bei der Justage des Lasers, und Petra Neubauer-Guenther für so vieles.

I would like to thank Dr. John Pearson and Dr. Brian Drouin from the spectroscopy group at the JPL for supplying me with additional water data and interesting discussions. Thanks to Dr. Herb Pickett for explaining to me several details of his fabulous spfit and spcat program suite. I would like to thank Dr. Frank Maiwald and the detector group at JPL for allowing me to perform spectroscopy with their HIFI tripler. Thanks also to Dr. Daniel Matthes, now at the Universität Mainz, for getting me started with the transformation procedure.

A big thank you to Prof. Karl Menten, Dr. Friedrich Wyrowski, Dr. Peter Schilke, and Dr. Edward Polehampton for telling me what spectroscopy is good for from an astronomers point of view and how to get the best out of the Effelsberg radio telescope.

Vielen Dank auch an Herrn Prof. Heinrich Mäder für den Crashkurs in FTMW Spektroskopie und die Möglichkeit, in Kiel der Hyperfeinstruktur des HDO auf die Schliche zu kommen.

I am indebted to Prof. Štepan Urban for the calculation of sub-Doppler line intensities. Domo arigato to Dr. Hiroyuki Ozeki for valuable discussions regarding the methylene measurements and thanks to Dr. Trevor Sears for providing me with the results of his $CH_2$ calculations.

Vielen Dank an Holger Müller, Frank Lewen, Petra Neubauer-Guenther und Thomas Giesen für das Korrekturlesen von Teilen dieser Arbeit.

Ich danke meinen Eltern für ihre Unterstützung und ihr Vertrauen.

Matthias, vielen Dank für alles!

# Erklärung

Ich versichere, daß ich die von mir vorgelegte Dissertation selbständig angefertigt, die benutzten Quellen und Hilfsmittel vollständig angegeben und die Stellen der Arbeit - einschließlich Tabellen, Karten und Abbildungen -, die anderen Werken im Wortlaut oder dem Sinn nach entnommen sind, in jedem Einzelfall als Entlehnung kenntlich gemacht habe; daß dieser Dissertation noch keiner anderen Fakultät oder Universität zur Prüfung vorgelegen hat, daß sie abgesehen von unten angegebenen Teilpublikationen noch nicht veröffentlicht worden ist, sowie daß ich eine solche Veröffentlichung vor Abschluß des Promotionsverfahrens nicht vornehmen werde.
Die Bestimmungen der Promotionsordnung sind mir bekannt. Die von mir vorgelegte Dissertation ist von Herrn Privatdozent Dr. T. F. Giesen betreut worden.

# Teilpublikationen

- S. Brünken, H. S. P. Müller, S. Thorwirth, F. Lewen, and G. Winnewisser. The rotational spectra of the ground and first excited bending states of deuterium isocyanide, DNC, up to 2 THz. *J. Mol. Struct.*, accepted.
- H. S. P. Müller and S. Brünken. Accurate Rotational Spectroscopy of Sulfur Dioxide, $SO_2$, in its Ground Vibrational and First Excited Bending States, $v_2 = 0, 1$, up to 2 THz. *J. Mol. Spectrosc.*, 232:201-210, 2005.
- S. Brünken, M. Behnke, S. Thorwirth, K.M.T. Yamada, T. Giesen, J. Hahn, and G. Winnewisser Asymmetric Rotor Analysis of DSOD Spectra up to the ${}^rQ_3$ branch near 653 GHz". *J. Mol. Struct.*, 742:237-242, 2005.
- E. Polehampton, K. M. Menten, S. Brünken, G. Winnewisser, and J.-P. Baluteau. Far-Infrared detection of methylene. *A&A*, 431:203–213, 2005.
- S. Brünken, U. Fuchs, F. Lewen, Š. Urban, T. Giesen, and G. Winnewisser. Sub-Doppler and Doppler spectroscopy of DCN isotopomers in the terahertz region: ground and first excited bending states $(v_1v_2v_3) = (01^{e,f}0)$. *J. Mol. Spectrosc.*, 225:152–161, 2004.
- S. Brünken, E. A. Michael, F. Lewen, Th. Giesen, H. Ozeki, G. Winnewisser, P. Jensen, and E. Herbst. High-resolution terahertz spectrum of $CH_2$ - Low J rotational transitions near 2 THz. *Can. J. Chem.*, 82:676–683, 2004.
- U. Fuchs, S. Brünken, G. Fuchs, S. Thorwirth, V. Ahrens, F. Lewen, S. Urban, T. Giesen, and G. Winnewisser. High Resolution Spectroscopy of HCN Isotopomers: $H^{13}CN$, $HC^{15}N$, and $H^{13}C^{15}N$ in the Ground and First Excited Bending Vibrational State. *Z. Naturforsch.*, 59:861–872, 2004.
- F. Lewen, S. Brünken, G. Winnewisser, M. Simecková and Š. Urban. Doppler-Limited Rotational Spectrum of the NH Radical in the 2 THz Region. *J. Mol. Spectrosc.* 226:113–122, 2004.
- S. Brünken, H. S. P. Müller, F. Lewen, and G. Winnewisser. High Accuracy Measurements on the Ground State Rotational Spectrum of Formaldehyde ($H_2CO$) up to 2 THz. *Phys. Chem. Chem. Phys.*, 5:1515–1518, 2003.
- S. Thorwirth, F. Wyrowski, P. Schilke, K. M. Menten, S. Brünken, H. S. P. Müller, and G. Winnewisser. Detection of HCN Direct *l*-type transitions Probing Hot Molecular Gas in the Proto-Planetary Nebula CRL 618. *ApJ*, 586:338–343, 2003.
- S. Thorwirth, H. S. P. Müller, F. Lewen, S. Brünken, V. Ahrens, and G. Winnewisser. A concise New Look at the *l*-type Spectrum of $H^{12}C^{14}N$. *ApJ*, 585:L163–L165, 2003.

- Z. Zelinger, T. Amano, V. Ahrens, S. Brünken, F. Lewen, H. S. P. Müller, and G. Winnewisser. Submillimeter-wave spectroscopy of HCN in excited vibrational states. *J. Mol. Spectrosc.*, 220:223–233, 2003.
- E. Canè, L. Fusina, H. Bürger, W. Jerzembeck, S. Brünken, F. Lewen, and G. Winnewisser. The Ground State Spectroscopic Parameters and Equilibrium Structure of $PD_3$. *J. Mol. Spectrosc.* 215:1–9, 2002.

# Lebenslauf

Sandra Brünken

| | |
|---|---|
| Geburtsdatum: | 06. Januar 1975 |
| Geburtsort: | Sevelen |
| Staatsangehörigkeit: | deutsch |

## Schulausbildung

| | |
|---|---|
| 1981 – 1985 | Katholische Grundschule in Kevelaer-Twisteden |
| 1985 – 1994 | Kardinal-von-Galen Gymnasium in Kevelaer |
| 06.1994 | Abitur |

## Studium

| | |
|---|---|
| 10.1994 – 05.1996 | Physikstudium an der Rheinischen Friedrich-Wilhelms Universität zu Bonn |
| 05.1996 | Vordiplom in Physik |
| 08.1996 – 05.1997 | Physikstudium an der University of St. Andrews (Schottland, UK) |
| 10.1997 – 07.2000 | Physikstudium an der Technischen Universität Berlin |
| 07.2000 | Diplom in Physik am Institut für Atomare und Analytische Physik der TU Berlin<br>Titel: "Bestimmung von Zerfallswahrscheinlichkeiten atomarer Lochzustände mit Koinzidenzmethoden" |
| 09.2000 – 01.2001 | Forschungsaufenthalt am Institut für Atomare und Analytische Physik der Technischen Universität Berlin |
| 01.2001 | Beginn des Promotionsstudiums Universität zu Köln |